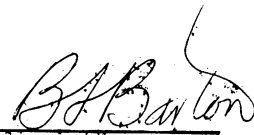


Technical Report No. 146
6137-3-T

IMPEDANCE AND RADIATION CHARACTERISTICS OF A
FERRITE OBSTACLE IN THE APERTURE OF A
RECTANGULAR WAVEGUIDE

by J. C. Palais

Approved by:



B. F. Barton

for

COOLEY ELECTRONICS LABORATORY

Department of Electrical Engineering
The University of Michigan
Ann Arbor

Submitted in partial fulfillment of the requirements for
the degree of Doctor of Philosophy in
The University of Michigan

August 1964

TABLE OF CONTENTS

	<u>Page</u>
ACKNOWLEDGMENTS	iv
LIST OF ILLUSTRATIONS	v
LIST OF SYMBOLS	ix
LIST OF APPENDICES	xvii
ABSTRACT	xviii
CHAPTER I: INTRODUCTION	1
1.1 Statement of the Problem	2
1.2 Scanning Antenna	6
1.3 Single-Pole, Single-Throw Switch	9
1.4 Circulator and Single-Pole, Double-Throw Switch	9
1.5 Summary	10
CHAPTER II: RADIATION FROM A FERRITE CYLINDER	11
2.1 Scattering from an Infinite Ferrite Cylinder with Plane Wave Incidence	11
2.2 Radiation from a Ferrite Cylinder in the Aperture of a Rectangular Waveguide	34
2.3 Conclusions	50
CHAPTER III: REFLECTION COEFFICIENT OF A FERRITE OBSTACLE IN A WAVEGUIDE APERTURE	51
3.1 The Variation Technique	52
3.2 Evaluation of the Reflection Coefficient	63
3.3 Reflection Coefficient for Small Posts	76
3.4 Application to Other Dual Discontinuity Problems	81
3.5 Conclusions	85
CHAPTER IV: DERIVATION OF THE REFLECTION COEFFICIENT USING THE MAGNETIC GREEN'S FUNCTION	86
4.1 The Variational Solution	87
4.2 Conclusions	105
CHAPTER V: EXPERIMENTAL WORK AND CONCLUSIONS	106
5.1 Test Apparatus	106
5.2 Radiation Patterns	109
5.3 Reflection Characteristics	117
5.4 Practical Models	120
5.5 Additional Experiments	138
5.6 Special Applications	143
5.7 Conclusions	149
REFERENCES	187
DISTRIBUTION LIST	189

ACKNOWLEDGMENTS

The author wishes to express sincere appreciation to all the members of the Doctoral Committee for their guidance and helpful criticism on this material. Special thanks is given to the Chairman, Professor John A. M. Lyon, for his helpful counsel and encouragement during this study and to Dr. David K. Adams for direction in the early stages of the investigation.

Special thanks is owed to the author's wife, Sandra, who developed the computer programs required in the study and who checked and otherwise helped with the manuscript at several stages of its development.

The experimental studies were aided considerably by Mr. Wilbur J. Nelson and Mr. David Barkman.

Finally the author wishes to thank Mrs. Lisa Shellman, Mr. Anthony Adaschik, and Mrs. Lillian Thurston who were responsible for the skillful preparation of this manuscript for publication.

The research reported here was supported by the U. S. Army Electronics Materiel Agency, Fort Monmouth, New Jersey.

LIST OF ILLUSTRATIONS

<u>Figure</u>		<u>Page</u>
1. 1	A plane wave incident on an infinitely long, magnetized, ferrite cylinder.	3
1. 2	Beam deflection required for a three port circulator.	4
1. 3	Ferrite scanning antenna.	5
1. 4	Single-pole, single-throw switch.	5
1. 5	Single-pole, double-throw switch.	5
2. 1	Far field scattering patterns, showing variations with internal field.	20
2. 2	Far field scattering patterns showing variations with k_0R (i. e. , variations with radius).	22
2. 3	Far field scattering patterns showing variations with dielectric constant.	24
2. 4	Far field scattering patterns showing variations with saturation magnetization ($4\pi M_S$).	25
2. 5	Beam angle vs. (a) internal field, (b) k_0R , (c) dielectric constant, (d) saturation magnetization ($4\pi M_S$).	26
2. 6	Normalized scattering cross section vs. (a) internal field, (b) k_0R , (c) dielectric constant, (d) saturation magnetization ($4\pi M_S$).	30
2. 7	Ferrite post in aperture of waveguide with infinite ground plane.	35
2. 8	Structures to which the analysis in the text applies.	36
2. 9	Far field scattering patterns showing variations with external field.	42
2. 10	Far field scattering patterns showing variations with k_0R (i. e. , variations with radius).	44
2. 11	Experimental and theoretical curves of beam angle vs. external field.	45
2. 12	Internal and far field distributions.	48
3. 1	Cylindrical ferrite obstacle in a rectangular waveguide. The waveguide is terminated by the open aperture.	52

LIST OF ILLUSTRATIONS (Cont.)

<u>Figure</u>		<u>Page</u>
3. 2	Volume of integration for (3. 11).	56
3. 3	Right cylindrical ferrite obstacle in rectangular waveguide.	65
3. 4	Image points for the rectangular waveguide.	70
3. 5	Impedance of a ferrite post in a matched waveguide as the static external field is varied.	75
3. 6	Impedance of a ferrite post just inside the waveguide, tangent to the aperture, as the static external field is varied.	75
3. 7	Impedance of a small ferrite post near a waveguide aperture.	77
3. 8	Impedance of a small ferrite post near a waveguide aperture.	80
3. 9	T-equivalent circuit.	83
3. 10	Equivalent circuit of a small dielectric post in a matched waveguide.	84
3. 11	Equivalent circuit of a small isotropic permeable post with $\mu > 1$ in a matched waveguide.	84
4. 1	Cylindrical ferrite obstacle in the aperture of a rectangular waveguide.	87
5. 1	Equipment for recording beam patterns.	101
5. 2	Block diagram of the test circuit pictured in Fig. 5. 1.	108
5. 3	Test set-up showing absorbing material around the aperture.	109
5. 4	Experimental beam patterns measured when the applied field is varied.	110
5. 5	VSWR vs. applied field.	115
5. 6	Effect of reversing the applied field.	116
5. 7	Equivalent circuit of the windings of an electromagnet.	117
5. 8	Changes in radiation characteristics for various diameters of the ferrite post.	118
5. 9	Measured impedance of the ferrite scanning antenna as a function of the applied field.	120
5. 10	Components of a practical scanning antenna.	121
5. 11	Assembled scanning antenna.	122
5. 12	Modified practical scanning antenna.	123

LIST OF ILLUSTRATIONS (Cont.)

<u>Figure</u>		<u>Page</u>
5. 13	Beam patterns of the antenna in Fig. 5. 12.	124
5. 14	VSWR vs. applied field for the antenna in Fig. 5. 12.	136
5. 15	Peak magnitude of the beam relative to the peak magnitude obtained when the ferrite is removed.	136
5. 16	Measured beam angle vs. applied field for the antenna in Fig. 5. 12.	137
5. 17	Example of the "redirecting" of energy by a magnetized cylinder.	139
5. 18	Microwave repeater circuit.	140
5. 19	Modulation circuit.	141
5. 20	Experimental beam patterns.	142
5. 21	Waveguide reflection type switch.	144
5. 22	Experimental waveguide switch characteristics.	144
5. 23	Duplexers.	145
5. 24	Diplexers.	145
5. 25	Quadruplexers.	145
5. 26	Quadruplex system.	146
5. 27	Spreading of the microwave spectrum in space.	146
5. 28	Multiquadruplex system.	147
5. 29	Single element of a self-phasing antenna array.	148
5. 30	A self-phasing antenna array using the ferrite scanning antenna.	148
B. 1	An open-ended rectangular waveguide with an infinite flange.	156
C. 1	Magnetization curve.	165
C. 2	Permeability as a function of the internal static field.	166
C. 3	External field vs. internal field for two different demagnetizing factors.	168
C. 4	Permeability as a function of the external static field.	170
C. 5	Geometry for measurement of the applied field.	171

LIST OF ILLUSTRATIONS (Cont.)

<u>Figure</u>		<u>Page</u>
D. 1	Coordinate system for evaluation of terms from Chapter III.	173
E. 1	Cylindrical ferrite obstacle in the aperture of a rectangular waveguide.	177
F. 1	A plane wave incident on an infinitely long, magnetized, plasma cylinder.	183
F. 2	Typical ferrite permeability and plasma permittivity curves.	184
F. 3	Plasma cylinder in the aperture of a rectangular waveguide.	186

LIST OF SYMBOLS

<u>Symbol</u>	<u>Description</u>	<u>First Reference</u>
$\vec{\mu}$	tensor permeability	p. 1
μ	diagonal component of the permeability	p. 1
k	off-diagonal component of the permeability	p. 1
μ_z	a diagonal component of the permeability	p. 1
j	imaginary factor, $\sqrt{-1}$	p. 1
H_z	static magnetic field	Fig. 1. 1
\vec{H}_{inc}	magnetic field	Fig. 1. 1
\vec{E}_{inc}	electric field	Fig. 1. 1
x, y, z	rectangular coordinates	Fig. 1. 1
r, ϕ	polar coordinates	Fig. 1. 1
R	radius of ferrite cylinder	Fig. 1. 1
P(x, y, 0)	point in the (x, y, 0) plane	Fig. 1. 1
a	waveguide width	Fig. 1. 4
b	waveguide height	Fig. 1. 4
ω	radian frequency	p. 11
t	time	p. 11
$\nabla \times$	curl operator	Eq. (2. 1a)
$\nabla \cdot$	divergence operator	Eq. (2. 1c)
\vec{E}	electric field	Eq. (2. 1a)
\vec{H}	magnetic field	Eq. (2. 1a)
\vec{B}	magnetic flux density	Eq. (2. 1a)
μ_0	free space permeability	Eq. (2. 1a)
\vec{D}	electric flux density	Eq. (2. 1b)
ϵ_0	free space permittivity	Eq. (2. 1b)
ϵ	ferrite relative permittivity	Eq. (2. 1b)

LIST OF SYMBOLS (Cont.)

<u>Symbol</u>	<u>Description</u>	<u>First Reference</u>
E_z	z-component of electric field	p. 12
\bar{a}_z	unit vector in z-direction	p. 12
∇	gradient operator	p. 12
H_x	x-component of magnetic field	Eq. (2. 5a)
H_y	y-component of magnetic field	Eq. (2. 5b)
∇^2	Laplacian operator	Eq. (2. 8a)
k_2	ferrite parameter	Eq. (2. 8a)
k_0	free space propagation constant	Eq. (2. 8b)
μ_{eff}	effective permeability	p. 13
H_r	r-component of magnetic field	Eq. (2. 9a)
H_ϕ	ϕ -component of magnetic field	Eq. (2. 9a)
E_z^{inc}	z-component of incident electric field	Eq. (2. 10)
J_n	Bessel function of order n	Eq. (2. 11a)
n	integer	p. 13
\sum	summation operator	Eq. (2. 11a)
H_r^{inc}	r-component of incident magnetic field	Eq. (2. 11b)
H_ϕ^{inc}	ϕ -component of incident magnetic field	Eq. (2. 11c)
J'_n	derivative of J_n with respect to its argument	Eq. (2. 11c)
E_z^{int}	z-component of internal electric field	Eq. (2. 12a)
a_n	unknown coefficient	Eq. (2. 12a)
H_r^{int}	r-component of internal magnetic field	Eq. (2. 12b)
H_ϕ^{int}	ϕ -component of internal magnetic field	Eq. (2. 12c)
E_z^{scat}	z-component of scattered electric field	Eq. (2. 13a)
a_n^s	unknown coefficient	Eq. (2. 13a)
$H_n^{(2)}$	Hankel function of second kind and order n	Eq. (2. 13a)
H_r^{scat}	r-component of scattered magnetic field	Eq. (2. 13b)
H_ϕ^{scat}	ϕ -component of scattered magnetic field	Eq. (2. 13c)
$H_n'^{(2)}$	derivative of $H_n^{(2)}$ with respect to its argument	Eq. (2. 13c)

LIST OF SYMBOLS (Cont.)

<u>Symbol</u>	<u>Description</u>	<u>First Reference</u>
N_n	Neumann function	p. 15
D_n	temporary variable	Eq. (2. 15b)
Z_n	a Bessel, Hankel, or Neumann function	p. 15
σ	scattering cross section	p. 16
\bar{N}	Poynting vector	Eq. (2. 18)
\bar{H}^*	complex conjugate of \bar{H}	Eq. (2. 18)
$\text{Re} ()$	signifies real part of ()	Eq. (2. 18)
\times	cross product operator	Eq. (2. 18)
P_{scat}	scattered power	Eq. (2. 20)
$!$	factorial	Eq. (2. 23b)
$\sigma(\phi)$	differential scattering cross section	Eq. (2. 25)
ℓ	iteration variable, an integer	Eq. (2. 27)
σ_n	normalized cross section	Eq. (2. 30)
β	TE ₁₀ mode propagation factor	Eq. (2. 31)
α	angle	p. 37
λ	free space wavelength	p. 37
λ_c	waveguide cutoff wavelength	p. 37
a_ℓ^{S*}	complex conjugate of a_ℓ^S	Eq. (2. 43)
R_1	reflection coefficient	p. 51
Z	impedance	p. 51
χ_e	electric susceptibility	Eq. (3. 4)
$\vec{\chi}_m$	magnetic susceptibility tensor	Eq. (3. 4)
χ_m	diagonal component of magnetic susceptibility	Eq. (3. 6c)
χ_z	diagonal component of magnetic susceptibility	Eq. (3. 6c)
\bar{J}	fictitious current	Eq. (3. 8)
\vec{G}	dyadic Green's function	Eq. (3. 10)

LIST OF SYMBOLS (Cont.)

<u>Symbol</u>	<u>Description</u>	<u>First Reference</u>
\vec{I}	unit dyadic	Eq. (3. 10)
δ	Dirac delta function	Eq. (3. 10)
\vec{n}	unit vector	p. 55
dv_o	element of volume	Eq. (3. 11)
x_o, y_o	rectangular coordinates	p. 55
r_o	represents (x_o, y_o)	p. 55
\vec{E}_o	electric field	Eq. (3. 11)
$a_z a_z$	denotes third row, third column of the dyadic	p. 56
G_{zz}	component of the Green's function dyadic	p. 56
γ_n	waveguide propagation factor	p. 56
R_{nm}	coupling coefficients	Eq. (3. 12)
R_{nn}	self-reflection coefficients	p. 57
\vec{G}	transpose of \vec{G}	Eq. (3. 13)
\vec{E}_2	electric field	p. 58
\vec{H}_2	magnetic field	p. 58
R_n	reflection and coupling coefficients	Eq. (3. 16)
$\vec{\chi}_{m_2}$	magnetic susceptibility	Eq. (3. 18)
\vec{J}_2	fictitious current	Eq. (3. 19)
$R_1^{(2)}$	reflection coefficient	Eq. (3. 22)
$\delta \vec{J}$	variation of \vec{J}	Eq. (3. 29)
ds	element of surface	Eq. (3. 31)
$v(r)$	temporary variable	Eq. (3. 34)
d	distance from aperture to center of post	p. 65
c	distance from sidewall to ferrite post	p. 65
\vec{a}_r	unit vector in r-direction in cylindrical coordinates	p. 65
E_2^{int}	electric field	Eq. (3. 40b)
$H_{\phi_2}^{int}$	magnetic field	Eq. (3. 40b)

LIST OF SYMBOLS (Cont.)

<u>Symbol</u>	<u>Description</u>	<u>First Reference</u>
$a_n^{(2)}$	unknown coefficient	Eq. (3.41c)
U	solution of two-dimensional source free wave equation	p. 68
e^{jmD}	operator	p. 68
B_n	temporary variable	Eq. (3.46)
$B_n^{(2)}$	temporary variable	Eq. (3.47)
$H_0^{(2)}$	Hankel function of order zero	p. 69
$G_{f.s.}$	free space Green's function	p. 70
G_i	Green's function	p. 70
C_ℓ	temporary variable	Eq. (3.52)
$\delta_{-n\ell}$	Kronecker delta	p. 72
α_n	temporary variable	Eq. (3.57a)
$\alpha_n^{(2)}$	temporary variable	Eq. (3.57b)
$\Gamma_{n\ell}$	temporary variable	Eq. (3.57c)
A	$1/a\gamma_1$	Eq. (3.58)
H_{ext}	external static magnetic field	p. 74
H_{app}	static magnetic field measured	p. 74
γ'	a constant, 1.781	p. 78
δ_{sc}	temporary variable	Eq. (3.64)
X_{sc}	temporary variable	Eq. (3.64)
δ_{oc}	temporary variable	Eq. (3.65)
X_{oc}	temporary variable	Eq. (3.65)
Z_{oc}	open circuit impedance	Eq. (3.66a)
Z_{sc}	short circuit impedance	Eq. (3.66b)
Z_{11}, Z_{12}	impedance elements of equivalent circuit	Fig. 3.9
X_c	capacitive reactance	Fig. 3.10
X_L	inductive reactance	Fig. 3.11
θ_{sc}	angle of short circuit reflection coefficient	p. 89

LIST OF SYMBOLS (Cont.)

<u>Symbol</u>	<u>Description</u>	<u>First Reference</u>
θ_{oc}	angle of open circuit reflection coefficient	p. 85
\bar{J}_m	fictitious current	Eq. (4. 1)
\bar{H}_s	magnetic field	Eq. (4. 5)
\vec{G}_m	magnetic Green's function	p. 88
J_x, J_y	components of fictitious current	Eq. (4. 6)
\bar{a}_x, \bar{a}_y	unit vectors in x and y directions	Eq. (4. 6)
$G_{xx}, G_{xy}, G_{yx}, G_{yy}$	components of Green's function dyadic	Eq. (4. 7)
\vec{G}_{11}	Green's function	p. 90
\vec{G}_{12}	Green's function	p. 90
\vec{G}_{21}	Green's function	p. 90
\vec{G}_{22}	Green's function	p. 90
$\vec{G}_{11}^A, \vec{G}_{11}^B$	Green's functions	Eq. (4. 15)
\vec{G}_1	potential function	Eq. (4. 18)
$G_{n_{xx}}$	temporary variable	p. 94
b_n	unknown coefficient	p. 94
c_n	unknown coefficient	p. 94
Δ	very small distance	p. 95
ϵ_n	constant, 1/2 for $n=0$, 1 for $n \neq 0$	Eq. (4. 27)
E_n	electric field	Eq. (4. 30)
H_x^n, H_y^n	magnetic field components	Eq. (4. 37)
ξ, η	variables of integration	Eq. (4. 37)
r	radial distance	p. 100
\bar{H}_o	magnetic field	Eq. (4. 40b)
H_{ox}, H_{oy}	components of magnetic field	Eq. (4. 41a)
R_{eq}	equivalent coil resistance	Eq. (5. 1)
X_{eq}	equivalent coil reactance	Eq. (5. 1)
R_s	coil series resistance	Eq. (5. 1)

LIST OF SYMBOLS (Cont.)

<u>Symbol</u>	<u>Description</u>	<u>First Reference</u>
R_p	coil parallel resistance	Eq. (5. 1)
L	coil inductance	Eq. (5. 1)
VSWR	voltage standing wave ratio	p. 114
f_1, f_2	frequencies	p. 143
A_o	signal amplitude	p. 147
A_1	attenuation factor	p. 148
\bar{A}	dyadic	p. 152
$A_{xx}, A_{xy}, A_{xz},$		p. 152
$A_{yx}, A_{yy}, A_{yz},$	dyadic components	p. 152
A_{zx}, A_{zy}, A_{zz}		p. 152
\bar{B}	vector	p. 152
B_x, B_y, B_z	vector components	p. 152
$\bar{a}_x, \bar{a}_y, \bar{a}_z$	unit vectors	p. 152
B_{10}	TE ₁₀ mode propagation factor	Eq. (B- 1)
R_{kl}^{10}	reflection and coupling coefficients	Eq. (B- 1)
γ_{kl}	propagation constants	Eq. (B- 1)
$E^{(n)}$	electric field	Eq. (B-2)
$\bar{\pi}^*$	magnetic type Hertzian vector	p. 156
π_y^*	y-component of Hertzian vector	p. 156
E_x, E_y	electric field components	Eq. (B- 5a)
$\Pi_1^{(n)}$	Hertzian vector component in region 1	Eq. (B-6)
$\Pi_2^{(n)}$	Hertzian vector component in region 2	Eq. (B-7)
\sum'_m	summation operator, omitting m = n term	Eq. (B-8)
G_n	temporary variable	Eq. (B- 13)
D_n	temporary variable	Eq. (B- 13)
G	temporary variable	p. 161
ω_o	$-\gamma_e H_{int}$	Eq. (C-2a)
ω_m	$-\gamma_e M_s$	Eq. (C-2a)

LIST OF SYMBOLS (Cont.)

<u>Symbol</u>	<u>Description</u>	<u>First Reference</u>
M_s	saturation magnetization	p. 163
γ_e	gyromagnetic ratio	p. 163
H_{int}	internal static field	p. 163
M	magnetization	Eq. (C-3)
H_{ext}	external static magnetic field	Eq. (C-4)
N_z	demagnetizing factor	Eq. (C-4)
x', y'	rectangular coordinates with origin at center of the ferrite cylinder	p. 172
$\vec{\epsilon}$	tensor permittivity	Eq. (F-1)
$\epsilon_1, \epsilon_2, \epsilon_3$	components of the tensor permittivity	Eq. (F-1)
N	electron density	p. 182
e	electron charge	p. 182
m	electron mass	p. 182
H	static magnetic field	p. 182
ω_0	$\mu_0 eH/m$	p. 182
ω_m	$Ne^2/m\epsilon_0$	p. 182
k_3	plasma parameter	Eq. (F-8)

LIST OF APPENDICES

	<u>Page</u>
APPENDIX A: DYADIC ALGEBRA	152
APPENDIX B: THE REFLECTIONS FROM AN OPEN-ENDED RECTANGULAR WAVEGUIDE	155
APPENDIX C: THE COMPONENTS OF THE FERRITE PERMEABILITY TENSOR	163
APPENDIX D: EVALUATION OF TERMS USED IN CHAPTER III	172
APPENDIX E: REFLECTION COEFFICIENT FOR OBSTACLE PARTLY OUTSIDE OF APERTURE	176
APPENDIX F: PLASMA CYLINDER - FERRITE CYLINDER DUALITY	182

ABSTRACT

A theoretical and experimental investigation is made of a magnetized ferrite obstacle in a rectangular waveguide having an additional discontinuity. The analysis is performed on right cylindrical obstacles (not necessarily circular) together with discontinuities that excite little or no field variations along the cylinder axis. The axis of the obstacle is parallel to the electric field corresponding to the TE_{10} mode of the rectangular waveguide. The main application of the study is to the case where the discontinuity is an aperture (i. e. , the waveguide radiates into free space) and the ferrite obstacle is placed directly in the aperture. This composite antenna structure is shown to be capable of being electronically scanned. The direction of the radiated beam is controlled by the magnitude of the applied magnetic bias field. Scanning over a total range of 60° with good efficiency and reflection characteristics is obtained experimentally at frequencies around 10 Gc/sec. The applied magnetizing fields are less than 300 oersteds for this range of scanning. The antenna has the novel property of being nonreciprocal, the receiving and transmitting beam patterns are mirror images of each other. This is a new antenna and is one of only a few existing types of single element, electronic scanning devices. The small size and weight make it suitable for airborne and mobile equipment. A number of possible applications of this unique antenna are discussed.

It is shown that the theory predicting the radiation patterns applies also to a number of other devices which use cylindrical ferrites, including junction type circulators and switches. The theoretical results substantiate the intuitive explanations of the mechanism of operation of these devices in terms of a field displacement within the material.

The analysis of the impedance of the ferrite and waveguide discontinuity is applicable to a general class of problems that may be called "dual discontinuity" boundary value problems. The method of solution presented uses the variational technique. In addition to the antenna problem, the method is applied to the case of a small post in combination with a

short or open circuit. This geometry is shown to be useful in a measurement technique for permeability or permittivity of either ferrites or dielectrics.

The main contributions of the study can be summarized as follows:

1. A theoretical analysis has been made of the radiation characteristics of a ferrite cylinder in the aperture of a rectangular waveguide. This analysis provides a mathematical basis for the beam shifting property and gives insight into the mechanism involved. This analysis is applied also to junction circulators and switches.
2. A new, single element, electronic scanning antenna has been developed. Experiments confirmed the beam shifting properties predicted in (1). Design of a small, light-weight antenna has proven the practicality of such a device. A number of applications are presented.
3. A mathematical analysis of the reflection coefficient of the structure in (1) has been made. The problem is generalized to include obstacles having any right cylindrical shape placed anywhere within the waveguide or aperture. The solution is valid for the case of any z-independent discontinuity in place of the aperture (including, of course, a matched load). The matched load simplification predicts the behavior of a single-pole, single-throw electronic switch. Extensions of the dual discontinuity method to other problems are discussed.
4. In general, numerical results from the solution of (3) are best obtained using a computer. For small cylinders, however, simple formulas have been derived. Based on these results, a method of measurement of the ferrite properties is described.

CHAPTER I

INTRODUCTION

When an electromagnetic wave encounters a change in the medium through which it is propagating, a change in its characteristics occurs. The wave may be attenuated, shifted in phase, or its direction of propagation may be altered. Any or all of these effects may occur. They depend on either the physical properties of the medium, such as size and shape; or upon such electrical properties as permittivity, permeability, or conductivity. Quantitatively relating these changes in propagation to material properties forms a large part of the science of electromagnetic field theory. In practice, devices based on these interactions find numerous applications in electronics equipment.

A particularly interesting material from the viewpoint of electromagnetic propagation is that called ferrite. A familiar form of ferrite is magnetite, which was the first known magnetic material. Measurements of its properties were performed before this century.¹ However, little use was made of the material until the 1940's. Since that time, ferrite materials have been used extensively in applications such as magnetic cores in coils and transformers where their high permeability is utilized. In these devices the permeability is isotropic, that is, the permeability is independent of the direction of the magnetic and electric fields and can be written as a scalar. Since 1952, a number of ferrite devices have been developed in the microwave region by using the anisotropic properties of ferrites. In the anisotropic case, the permeability is different for different directions of the magnetic field and must be written as a tensor of the form.²

$$\vec{\mu} = \begin{bmatrix} \mu & -jk & 0 \\ jk & \mu & 0 \\ 0 & 0 & \mu_z \end{bmatrix}$$

The anisotropy is brought about by applying a dc magnetic bias field to the ferrite. In the tensor just above, the bias is applied in the z-direction and μ and k are functions of the magnitude of this field. When the static field is reduced to zero, k becomes zero and μ becomes equal to μ_z . For zero bias field the material thus becomes isotropic. The values of μ and k also depend on the frequency of the varying field and on the magnetization.

In particular applications, the ferrite, in conjunction with some waveguiding structure, exhibits such first-order properties as reciprocal or nonreciprocal phase shift, resonance absorption, field displacement, and Faraday rotation which can be traced to the permeability tensor. Examples of microwave devices using these and other ferrite properties are circulators, phase shifters, isolators, limiters, amplifiers, switches, and filters. Ferrites have conductivities on the order of 10^{-6} mho/meter, so that eddy current losses are low even at microwave frequencies. The dielectric constant is a scalar and has a value on the order of 10. Thus, in Maxwell's equations the magnetized material can be treated as a nonconducting body with a scalar dielectric constant and a tensor permeability.

This study is concerned with an example of the interactions between an electromagnetic wave and an anisotropic obstacle in conjunction with some guiding structure. Mainly, ferrites are considered, but the analyses can be extended to other materials.

The sections following state the specific aims of this study, review the history and motivations leading to it, outline the methods of attack, and attempt to convey the particular significance of the results.

1.1 Statement of the Problem

Problems involving tensor properties tend to be very difficult, if not impossible, to solve exactly. Approximate methods must often be used to obtain quantitative results. One problem that can be solved exactly is illustrated in Fig. 1.1. A plane wave is incident on an infinitely long, right circular, ferrite cylinder. The ferrite is magnetized along the z-axis. Analysis of the results shows that the beam patterns depend on the value of the applied static magnetic field, H_z , that is, the direction of the scattered energy can be controlled by the magnetic bias. In addition, the direction of maximum scattering does not have to be 0° or 180° , but can be any value of the angular coordinate ϕ . Indeed, the pattern does not even remain symmetrical. It is apparent that this novel effect might be used in several

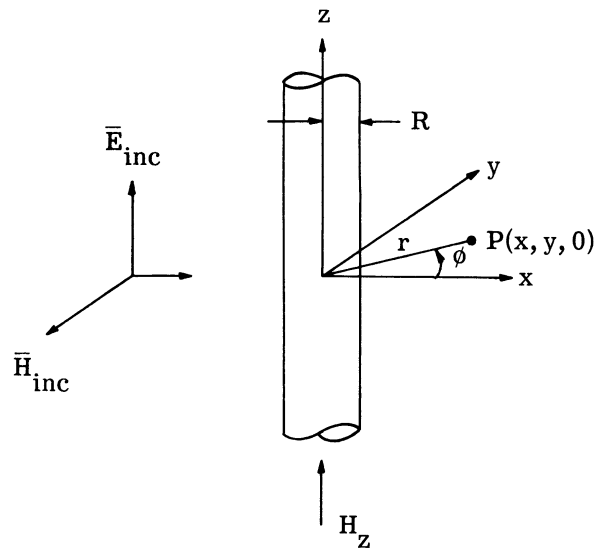


Fig. 1. 1 A plane wave incident on an infinitely long, magnetized, ferrite cylinder.

devices where electronic control of the direction of a propagating wave is desired. A brief, simplified sketch will illustrate several general possibilities.

1. If the applied field is continuously varied, the beam angle will also change directions continuously. This beam shifting property can be used to construct a scanning antenna which transmits the incident wave in any desired direction, or receives from any given direction.
2. At one value of applied field the energy is scattered in the forward direction so that complete transmission of the incident wave occurs. Some other value of applied field causes the energy to be reflected back towards the source and very little transmission takes place. This is a description of a single-pole, single-throw (SPST) switch which can be electronically set to "on" or "off."
3. At one value of applied field (H_1) the incident energy is scattered in the direction ϕ_1 , while for some other value of field (it turns out to be $-H_1$), the energy is scattered in the

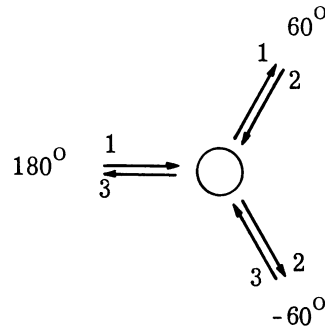


Fig. 1.2 Beam deflection required for a three port circulator.

direction $-\phi_1$. Thus a single-pole, double-throw (SPDT) electronically activated switch can be constructed.

4. The applied field may be adjusted so that the scattered beam angle is 60° . As shown in Fig. 1.2, energy incident at 180° is retransmitted at 60° , energy incident at 60° is retransmitted at -60° , and energy incident at -60° is retransmitted at 180° . This describes a three port circulator (also called a Y-circulator).

The generalizations above leave much to the imagination, particularly with regard to detailed methods of operation and quantitative description of performance. The most immediate questions at this point would seem to be: What can be used in place of the infinite cylinder? What structures can be used for the electromagnetic excitation of the ferrite or for the reception of the energy in the wave deflected by the material? These questions do not have unique answers. The solutions presented here utilize finite ferrite cylinders in conjunction with suitable rectangular waveguide structures. Descriptions of the devices follow:

1. Scanning Antenna. A finite ferrite cylinder is placed in the aperture of a rectangular waveguide as shown in Fig. 1.3. An electromagnet supplies the magnetic bias. The direction of radiation is then controlled by the magnet current.

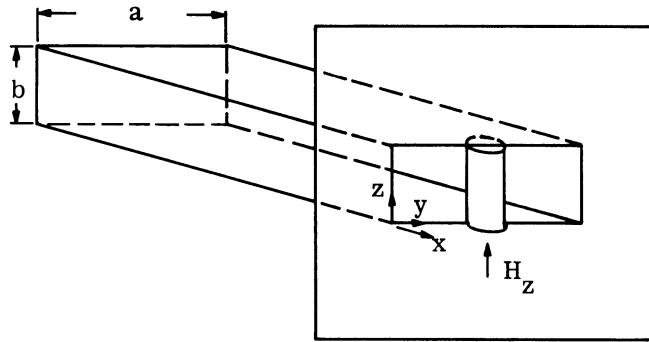


Fig. 1.3 Ferrite scanning antenna.

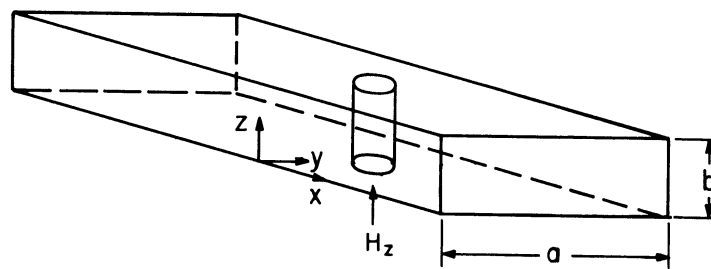


Fig. 1.4 Single-pole, single-throw switch.

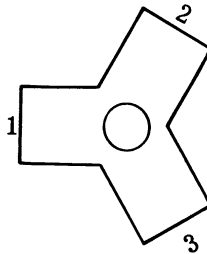


Fig. 1.5 Single-pole, double-throw switch.

2. SPST Switch. A ferrite cylinder is placed inside a waveguide midway between the narrow walls as shown in Fig. 1.4. An electromagnet outside the waveguide is then used to activate the switch.

3. SPDT Switch. A ferrite cylinder is placed in the center of a waveguide y-junction as in Fig. 1.5. The energy incident from port 1 can be transmitted to port 2 or port 3 depending on the magnetic bias.
4. Circulator. The circulator is similar to the SPDT switch described above. In this case, however, the ports must be evenly spaced, 120° apart.

Of course, now that conducting structures have been introduced, modifications in the plane wave theory must be made to account for the changes. Indeed, it must even be ascertained whether we have only modified the plane wave-infinite cylinder situation, or so destroyed the original character of the problem that no relationship exists (with the result that the proposed "devices," based on this relationship, are in fact unrealizable).

Fortunately, as the reader has probably surmised, the devices do work.

This report is mainly concerned with the theoretical and experimental investigation of the scanning antenna. The other devices will be commented on more briefly. The following sections relate the history and relevant literature concerning these devices, and indicate the emphasis given to each one.

1.2 Scanning Antenna

1.2.1 Background Material. The simplest scanning antennas are obtained merely by physically repositioning the antenna. Obvious limitations on the scanning speeds exist because of the high mechanical torques involved. For large antennas, only the slowest movement is possible. In addition, extreme environmental conditions produce problems with the starting motors. The limitations on scanning speed are greatly reduced if electronic means are used to provide the beam steering. A number of methods have been devised to obtain electronic scanning.³ A common procedure is to combine several separate radiators in an array and control the phase of each element of the array by an electronic phase shifter (such as a ferrite phase shifter).

Very few designs exist for single-element electronic scanners. The advantages of size and weight inherent in this type of antenna make it highly desirable in airborne and

space vehicles. Thus, a contribution can be made in development of a practical single-element scanning antenna. Of course, single-element scanners can also be used in arrays if small beam widths are required.

We might first consider a general method of constructing a single-element, electronic-scanning antenna. Some material may be placed in or near the radiating structure and the properties of this material controlled by some electronic means. Several possible materials are:

1. Ferroelectrics. The dielectric constant is controlled by an applied voltage.
2. Plasmas. The values of the components of the tensor permittivity are controlled by a voltage or by a magnetic bias field.
3. Ferrites. The values of the components of the tensor permeability are controlled by the magnitude or direction of the applied magnetic field.

The designs reported to date all use ferrite materials. In 1956, Angelakos and Korman⁴ constructed a rectangular waveguide aperture completely filled with ferrite. By applying various dc magnetic fields, the radiated beam could be changed. The published results showed that relatively high applied fields were required and large reflections were obtained, limiting the efficiency of the device. The amplitude of the radiated wave appeared to drop sharply in the regions where the most beam shift occurred. The radiation patterns of this antenna were studied theoretically by Tyras and Held.⁵ The quasi-TE₁₀ and quasi-TE₂₀ modes were assumed to exist in the aperture and the radiation field was derived from these using the Huygen principle. Another single-element, electronic-scanning antenna was reported by Wheeler.⁶ This antenna consisted of a ferrite sphere in the aperture of a circular waveguide. The basic mode of operation produced a conical scan. Instead of varying the amplitude of the applied magnetic field, its direction was changed. A combination of permanent magnet and electromagnet produced the rotating field. Englebrecht⁷ investigated a related antenna, consisting of a ferrite post biased to ferromagnetic resonance placed just outside a waveguide at the focus of a parabolic reflector. Since the absorption at resonance depends on the direction of circular polarization in the received wave, some

selectivity in the signals reflected by the parabola was obtained. The performance characteristics of this device have not been published. The need for the reflector makes this a much larger antenna than the others described above.

1.2.2 Method of Analysis. The prime objective and accomplishment of this study is the development, design and theoretical treatment of the new antenna proposed in Fig. 1.3. This antenna differs from those described in the preceding section in physical structure, theoretical basis, and performance. Experiments, reported in Chapter V, show that continuous beam shifting using low applied fields can be efficiently obtained. The mathematical analysis of the antenna is divided into two parts: (1) an explanation of the radiation properties and (2) an analysis of the input impedance. In Chapter II, a simplified scattering approach is used to explain how the beam-shifting occurs in terms of the ferrite properties. Predictions of the beam shift are made and compared with experiment. In Chapters III and IV, an analysis of the input impedance is made. This analysis constitutes the major mathematical contribution of the study. The analysis is generalized to the extent that the ferrite cylinder may be anywhere within the waveguide or extending partially out of it and the material need not be circular. The variational technique, an approximate method of solution based on the integral equations which describe the problem, is used to derive the reflection coefficient. In the formulation, the integrations involved are most easily performed for right circular cylinders.

It is informative to discuss the nature of the discontinuity in the waveguide. The reflections may be thought of as resulting from two discontinuities (1) the open aperture and (2) the anisotropic ferrite obstacle. These two discontinuities are superimposed in a complex way, particularly if they are close enough so that the higher order modes excited by each can interact. The solution for the impedance when the ferrite is absent and the aperture alone is considered has been solved previously⁸ and may be considered known. It will be shown that this knowledge can be applied to devise a formulation where the individual effects of the two discontinuities are separated a great deal. The problem is then in a class that might well be termed a "dual discontinuity" boundary value problem. The method of solution presented here may then be used as a model for a number of problems characterized by a "dual discontinuity." For example, the problem of a cylindrical ferrite

or dielectric in a rectangular waveguide terminated in a short or open circuit can be solved easily using this method. This geometry can be used in a method of measurement of ferrite and dielectric properties as outlined in Chapter III. This generalization of the method is suggested as an accomplishment of the study.

1.3 Single-Pole, Single-Throw Switch

Experiments showing the performance of the switch are reported briefly in Chapter V. No great emphasis is placed on the device as other means of achieving the equivalent result are known. The theory of this SPST switch, consisting essentially of finding the reflection coefficient of the magnetized ferrite post in a matched rectangular waveguide, is interesting in itself and not difficult to obtain directly from the analysis described in Section 1.2.2. Several persons have obtained solutions and formulations to various degrees of approximation for the post in a matched rectangular waveguide.

Berk and Epstein⁹ found the reflection coefficient for the case of a thin rod that was not near the waveguide walls. Nikol'skii¹⁰ used an imaging technique and a few terms of the series representation for the fields in the ferrite and in the waveguide to solve for the reflection and transmission coefficients. Hauser¹¹ has obtained a more general formulation than those described above. He derived a variational expression for an obstacle with tensor permeability and permittivity in a matched waveguide. The obstacle had no restriction on size, shape or position in the waveguide. In the paper, no evaluation of the variational expression was made. As will be illustrated in the variational problems in this report, the formulation gives the desired quantity (e. g. , the reflection coefficient) in terms of the ratio of several integrals. These integrals involve the field distributions within the obstacle and are not simple to evaluate explicitly.

In this study, a slightly different and simpler variational expression is derived for the reflection coefficient of a right cylindrical (but not necessarily circular) ferrite obstacle of arbitrary size placed anywhere in the waveguide. The result is then explicitly evaluated for a circular cylinder.

1.4 Circulator and Single-Pole, Double-Throw Switch

The SPDT switch and the three-port circulator are closely allied and may be considered as one device. This device was first introduced several years ago¹² and has

been greatly refined since then using empirical techniques. The theory has been slower in its development. Auld¹³ investigated the general properties of symmetrical junction circulators from the viewpoint of their scattering matrices. What is still needed to complement Auld's study is a theory relating the properties of the material in the junction (the ferrite cylinder for the case of interest here) to the specified performance. A theory both intuitively satisfying and mathematically manageable is desired. Many attempts have been made to derive such a theory,^{*} but the goal has been elusive because of the complexity of the structure. In several of the published theories, assumptions have been made regarding the circulator mechanism and then suitable equations have been derived to verify the mathematical possibility of the original assumptions. The result is that there are now several theories (not necessarily exclusive) that agree (to some extent) with various experiments. The most successful analysis to date appears to be Bosma's investigation of the strip-line version of the Y-circulator.¹⁴ This approximate solution appears to be valid and is applied to UHF circulators. To the author's knowledge, there is as yet no theory equivalent to Bosma's for the waveguide version of the Y-circulator.

Since a complete theory is not yet available, it is reasonable, interesting, and informative, to point out the existing relationship between the junction circulator and the infinite ferrite cylinder problem. An explanation of the circulator mechanism based on this problem is presented in Chapter II.

1.5 Summary

In this study the main concern is the ferrite scanning antenna consisting of a ferrite post in the aperture of a rectangular waveguide. Chapters II through IV deal with the theoretical analysis, while Chapter V presents experiments verifying the practicality of the device. Several other devices using cylindrical ferrites are also considered in the text, including the junction type circulator and an electronic reflection type switch.

* See Bosma¹⁴ for a summary of the papers.

CHAPTER II

RADIATION FROM A FERRITE CYLINDER

The idea for a scanning device utilizing a ferrite cylinder arose from a study of the scattering of plane waves in free space by an infinitely long, ferrite cylinder. In this chapter, we will show the details of the infinite cylinder problem that motivated the scanning antenna application. In addition to finding the radiation patterns by methods found in the works of Nikol'skii¹⁵ and Eggimann,¹⁶ the scattering cross section and differential scattering cross section will be derived. Numerical results will then be presented and analyzed. The original derivation will then be suitably altered to provide an approximate solution for the radiation characteristics of the scanning antenna made up of a magnetized ferrite cylinder placed in the aperture of a rectangular waveguide.

2.1 Scattering from an Infinite Ferrite Cylinder with Plane Wave Incidence

A plane wave is incident on an infinitely long ferrite cylinder as shown in Fig.

1.1. The electric field vector is polarized parallel to the cylinder axis and the wave is incident normal to the axis. Since the plane wave has no z-dependence, none of the scattered fields have a z-dependence and the problem is essentially two dimensional. Due to symmetry, the electric fields have only a z-component.

Wave Equation

Maxwell's equations are (assuming $e^{j\omega t}$ time dependence)

$$\nabla \times \bar{E} = - \frac{\partial \bar{B}}{\partial t} = -j\omega \mu_0 \bar{\mu} \bar{H} \quad (2.1a)$$

$$\nabla \times \bar{H} = \frac{\partial \bar{D}}{\partial t} = j\omega \epsilon_0 \epsilon \bar{E} \quad (2.1b)$$

$$\nabla \cdot \bar{D} = 0 \quad (2.1c)$$

$$\nabla \cdot \bar{B} = 0 \quad (2.1d)$$

where the ferrite permeability tensor* is given by

$$\vec{\mu} = \begin{bmatrix} \mu & -jk & 0 \\ jk & \mu & 0 \\ 0 & 0 & \mu_z \end{bmatrix} \quad (2.2)$$

From (2.1a)

$$\vec{H} = \frac{-1}{j\omega\mu_0} [\vec{\mu}]^{-1} \nabla \times \vec{E} \quad (2.3)$$

where

$$[\vec{\mu}]^{-1} = \frac{1}{\mu^2 - k^2} \begin{bmatrix} \mu & jk & 0 \\ -jk & \mu & 0 \\ 0 & 0 & \frac{\mu^2 - k^2}{\mu_z} \end{bmatrix} \quad (2.4)$$

Since $\vec{E} = E_z \vec{a}_z$, we then obtain from (2.3)

$$\vec{H} = \frac{-1}{j\omega\mu_0(\mu^2 - k^2)} \begin{bmatrix} -jk & \mu \\ -\mu & -jk \end{bmatrix} \nabla E_z, \quad (2.5)$$

or in rectangular coordinates,

$$H_x = \frac{-1}{j\omega\mu_0(\mu^2 - k^2)} \left[\mu \frac{\partial E_z}{\partial y} - jk \frac{\partial E_z}{\partial x} \right] \quad (2.6a)$$

$$H_y = \frac{1}{j\omega\mu_0(\mu^2 - k^2)} \left[jk \frac{\partial E_z}{\partial y} + \mu \frac{\partial E_z}{\partial x} \right] \quad (2.6b)$$

From (2.1b)

$$\frac{\partial H_y}{\partial x} - \frac{\partial H_x}{\partial y} = j\omega\epsilon_0 \epsilon E_z \quad (2.7)$$

*Appendix C gives a discussion of the evaluation of the components μ and k .

In this last equation, put in the quantities H_x and H_y from (2.6a, 2.6b) to obtain the wave equation,

$$\nabla^2 E_z + k_2^2 E_z = 0 \quad \text{inside the material} \quad (2.8a)$$

$$\nabla^2 E_z + k_0^2 E_z = 0 \quad \text{outside the material} \quad (2.8b)$$

where

$$\begin{aligned} k_2^2 &= \omega^2 \mu_o \epsilon_o \epsilon \left(\frac{\mu^2 - k^2}{\mu} \right) \\ &= k_o^2 \mu_{\text{eff}} \end{aligned}$$

$$k_o^2 = \omega^2 \mu_o \epsilon_o$$

$$\nabla^2 = \frac{\partial}{\partial x^2} + \frac{\partial}{\partial y^2},$$

the two dimensional Laplacian operator. This is the equation the electric fields must satisfy. The solution for outward travelling waves is a series of Hankel functions with argument $k_o r$. If (2.3) is expanded in cylindrical coordinates we get,

$$H_r = \frac{1}{\omega \mu_o (\mu^2 - k^2)} \left[k \frac{\partial E_z}{\partial r} + \frac{j\mu}{r} \frac{\partial E_z}{\partial \phi} \right] \quad (2.9a)$$

$$H_\phi = \frac{1}{\omega \mu_o (\mu^2 - k^2)} \left[-j\mu \frac{\partial E_z}{\partial r} + \frac{k}{r} \frac{\partial E_z}{\partial \phi} \right] \quad (2.9b)$$

Incident Fields

The incident plane wave is given by,

$$E_z^{\text{inc}} = e^{j(\omega t - k_o x)} \quad (2.10)$$

This can be expanded in cylindrical coordinates in a series of Bessel functions. Omitting the time dependence

$$E_z^{\text{inc}} = \sum_{n=-\infty}^{\infty} J_n(k_o r) e^{-jn(\phi + \frac{\pi}{2})} \quad (2.11a)$$

Then, substituting (2. 11a) in (2. 9a) and (2. 9b) gives the remaining field components.

$$H_r^{\text{inc}} = \frac{1}{\omega\mu_o} \sum_{n=-\infty}^{\infty} n \frac{J_n(k_o r)}{r} e^{-jn(\phi + \frac{\pi}{2})} \quad (2. 11b)$$

$$H_\phi^{\text{inc}} = \frac{-j}{\omega\mu_o} \sum_{n=-\infty}^{\infty} k_o J_n'(k_o r) e^{-jn(\phi + \frac{\pi}{2})} \quad (2. 11c)$$

The incident electric field satisfies the wave equation (2. 8b) in the region outside the ferrite, where μ and ϵ are both unity.

Internal Fields

The electric field inside the ferrite can be written as a solution to (2. 8a).

$$E_z^{\text{int}} = \sum_{n=-\infty}^{\infty} a_n J_n(k_2 r) e^{-jn(\phi + \frac{\pi}{2})} \quad (2. 12a)$$

Then the magnetic fields are obtained from (2. 9a) and (2. 9b).

$$H_r^{\text{int}} = \frac{1}{\omega\mu_o(\mu^2 - k^2)} \sum_{n=-\infty}^{\infty} a_n \left[k_2 k J_n'(k_2 r) + \frac{n\mu}{r} J_n(k_2 r) \right] e^{-jn(\phi + \frac{\pi}{2})} \quad (2. 12b)$$

$$H_\phi^{\text{int}} = \frac{-j}{\omega\mu_o(\mu^2 - k^2)} \sum_{n=-\infty}^{\infty} a_n \left[\mu k_2 J_n'(k_2 r) + \frac{nk}{r} J_n(k_2 r) \right] e^{-jn(\phi + \frac{\pi}{2})} \quad (2. 12c)$$

Scattered Fields

The scattered electric field representing outward going waves can be written,

$$E_z^{\text{scat}} = \sum_{n=-\infty}^{\infty} a_n^s H_n^{(2)}(k_o r) e^{-jn(\phi + \frac{\pi}{2})} \quad (2. 13a)$$

so that

$$H_r^{\text{scat}} = \frac{1}{\omega\mu_o} \sum_{n=-\infty}^{\infty} a_n^s \frac{n}{r} H_n^{(2)}(k_o r) e^{-jn(\phi + \frac{\pi}{2})} \quad (2. 13b)$$

$$H_\phi^{\text{scat}} = \frac{-j}{\omega\mu_o} \sum_{n=-\infty}^{\infty} a_n^s k_o H_n^{(2)}(k_o r) e^{-jn(\phi + \frac{\pi}{2})} \quad (2. 13c)$$

where

$$H_n^{(2)} = J_n - jN_n, \text{ the Hankel function.}$$

$$N_n \text{ is the Neumann function.}$$

Boundary Conditions

The boundary conditions are continuity of the tangential electric and magnetic fields at the ferrite surface.

$$E_z^{\text{scat}} + E_z^{\text{inc}} = E_z^{\text{int}} \quad \text{at } r = R \quad (2.14a)$$

$$H_\phi^{\text{scat}} + H_\phi^{\text{inc}} = H_\phi^{\text{int}} \quad \text{at } r = R \quad (2.14b)$$

Application of these conditions gives the equations for the unknown coefficients.

$$H_n^{(2)}(k_o R) a_n^S - J_n(k_2 R) a_n = -J_n(k_o R) \quad (2.15a)$$

$$\left[\frac{-k_o}{\omega \mu_o} H_n^{(2)}(k_o R) \right] a_n^S + D_n a_n = \frac{k_o}{\omega \mu_o} J_n'(k_o R) \quad (2.15b)$$

where

$$D_n = \frac{1}{\omega \mu_o (\mu^2 - k^2)} \left[\mu k_2 J_n'(k_2 R) + \frac{nk}{R} J_n(k_2 R) \right]$$

Solving (2.15) for a_n and a_n^S and using the recursion formula

$$Z_n'(z) = \frac{n}{z} Z_n(z) - Z_{n+1}(z)$$

to remove the derivatives of the Bessel functions gives

$$a_n = \frac{\frac{H_{n+1}^{(2)}(k_o R)}{H_n^{(2)}(k_o R)} - \frac{J_{n+1}(k_o R)}{J_n(k_o R)}}{\sqrt{\frac{\epsilon}{\mu_{\text{eff}}}} \left[\frac{n}{k_2 R} \left(1 + \frac{k}{\mu} \right) - \frac{J_{n+1}(k_2 R)}{J_n(k_2 R)} \right] - \frac{n}{k_o R} + \frac{H_{n+1}^{(2)}(k_o R)}{H_n^{(2)}(k_o R)}} \frac{J_n(k_o R)}{J_n(k_2 R)} \quad (2.16a)$$

$$a_n^s = \frac{-\sqrt{\frac{\epsilon}{\mu_{\text{eff}}}} \left[\frac{n}{k_2 R} \left(1 + \frac{k}{\mu}\right) - \frac{J_{n+1}(k_2 R)}{J_n(k_2 R)} \right] - \frac{n}{k_0 R} + \frac{J_{n+1}(k_0 R)}{J_n(k_0 R)}}{\sqrt{\frac{\epsilon}{\mu_{\text{eff}}}} \left[\frac{n}{k_2 R} \left(1 + \frac{k}{\mu}\right) - \frac{J_{n+1}(k_2 R)}{J_n(k_2 R)} \right] - \frac{n}{k_0 R} + \frac{H_{n+1}^{(2)}(k_0 R)}{H_n^{(2)}(k_0 R)}} \frac{J_n(k_0 R)}{H_n^{(2)}(k_0 R)} \quad (2.16b)$$

Far Field Approximations

In the far field we can expand the Hankel function for $k_0 r \gg 1$, $k_0 r \gg |n|$.¹⁷

$$H_n^{(2)}(k_0 r) = \sqrt{\frac{2}{\pi k_0 r}} e^{-jk_0 r + j\frac{n\pi}{2} + j\frac{\pi}{4}}$$

Then the scattered electric field (2.13a) can be written

$$E_z^{\text{scat}} = \sqrt{\frac{2}{\pi k_0 r}} e^{-jk_0 r + j\frac{\pi}{4}} \sum_{n=-\infty}^{\infty} a_n^s e^{-jn\phi} \quad (2.17)$$

This equation is valid only if the series converges quickly enough so that terms with $|n|$ on the order of, or bigger than, $k_0 r$ can be neglected. The rate of convergence of this series depends greatly on the term $k_0 R$, where R is the cylinder radius. In general, more terms are required for large values of $k_0 R$ than for small values. For the data used in this report $k_0 R$ was on the order of one or less and only terms with $|n| \leq 5$ were required.

Scattering Cross Section

To obtain some measure of the total effect of the ferrite on the field a scattering cross section (σ) can be defined:

The cross section is the ratio of the rate of energy scattered to the rate of energy per unit area incident on the object.

For the two dimensional problem the energies are defined as the energy per unit axial length of the cylinder. The geometrical cross section of the cylinder is $2R$.

The Poynting vector

$$\bar{N} = \frac{1}{2} \text{Re}(\bar{E} \times \bar{H}^*) \quad (2.18)$$

gives the time average rate of incident energy per unit area. For the incident plane wave with unit amplitude (2.10) we obtain

$$N_{\text{inc}} = \frac{1}{2} \sqrt{\frac{\epsilon_0}{\mu_0}} \quad (2.19)$$

The total rate of energy scattered by the cylinder is obtained by integrating the Poynting far zone vector involving the scattered fields (2.17) over a surrounding surface.

Thus,

$$P_{\text{scat}} = \int_0^{2\pi} \frac{1}{2} \sqrt{\frac{\epsilon_0}{\mu_0}} \left| E_Z^{\text{scat}} \right|^2 r d\phi \quad (2.20)$$

The cross section is then given by

$$\sigma = \frac{P_{\text{scat}}}{N_{\text{inc}}} = \int_0^{2\pi} \left| E_Z^{\text{scat}} \right|^2 r d\phi \quad (2.21)$$

A value of $\sigma = 2R$ means the scatterer removes energy from an area equal to its own physical dimensions. If $\sigma > 2R$, the scatterer "appears" larger to the incoming wave than its actual size while for $\sigma < 2R$ the scatterer appears smaller. In the far field, (2.17) can be used for E_Z^{scat} . Using orthogonality of the functions $e^{-jn\phi}$ results in

$$\sigma = \frac{4}{k_0} \sum_{n=-\infty}^{\infty} \left| a_n^S \right|^2 \quad (2.22)$$

For the case of a very small cylinder ($k_0 R \ll 1$, $k_2 R \ll 1$), the coefficients a_n^S can be simplified using the power series expansions for the Bessel functions. Only the terms with $n=0$, $n=\pm 1$ are important for this case because a_n^S decreases as $(k_0 R)^{2n}$ for $n \geq 1$ as seen from the values of the coefficients given below.

$$a_0^S \cong \frac{-j\pi(k_0 R)^2}{4} (\epsilon - 1) \quad (2.23a)$$

$$a_{\pm n}^S \cong j \frac{\pi(k_0 R)^{2n}}{n!(n-1)!2^{2n}} \left[\frac{1}{\mu_{\text{eff}}} \left(1 \pm \frac{k}{\mu} \right) - 1 \right] \left[\frac{1}{\mu_{\text{eff}}} \left(1 \pm \frac{k}{\mu} \right) + 1 \right] \quad (2.23b)$$

where n is always positive. Using these coefficients the cross section is found to be

$$\sigma = \frac{\pi^2}{4} (k_0 R)^3 R \left[(\epsilon - 1)^2 + \left(\frac{\mu - k - 1}{\mu - k + 1} \right)^2 + \left(\frac{\mu + k - 1}{\mu + k + 1} \right)^2 \right] \quad (2.24)$$

The cross section varies as the inverse cube of the wavelength. This variation is similar to that for the metal cylinder, where the cross section is¹⁸

$$\sigma = \frac{3\pi^2}{4} (k_0 R)^3 R$$

The differential scattering cross section gives the angular distribution of energy in space. It is defined as

$$\sigma(\phi)d\phi = \lim_{r \rightarrow \infty} \frac{Nr d\phi}{N_{inc}} \quad (2.25)$$

For the present case this gives

$$\sigma(\phi) = \frac{\lim_{r \rightarrow \infty} \frac{1}{2} \sqrt{\frac{\epsilon_0}{\mu_0}} |E_z^{scat}|^2 r}{\frac{1}{2} \sqrt{\frac{\epsilon_0}{\mu_0}}} \quad (2.26)$$

Using (2.17) for $|E_z^{scat}|^2$, gives

$$\sigma(\phi) = \frac{2}{\pi k_0} \sum_{n=-\infty}^{\infty} \sum_{\ell=-\infty}^{\infty} a_n^S a_{\ell}^{S*} e^{-j\phi(n-\ell)} \quad (2.27)$$

For the small cylinder ($k_0 R \ll 1$, $k_2 R \ll 1$), we use the terms through ± 1 and the approximations (2.23) for the coefficients to obtain,

$$\begin{aligned} \sigma(\phi) = & \frac{\pi(k_0 R)^3 R}{8} \left\{ (\epsilon-1)^2 + \left(\frac{\mu-k-1}{\mu-k+1} \right)^2 + \left(\frac{\mu+k-1}{\mu+k+1} \right)^2 \right. \\ & - 2(\epsilon-1) \left(\frac{1-\mu+k}{1+\mu-k} + \frac{1-\mu-k}{1+\mu+k} \right) \cos \phi \\ & \left. + 2 \left(\frac{1-\mu+k}{1+\mu-k} \right) \left(\frac{1-\mu-k}{1+\mu+k} \right) \cos 2\phi \right\} \quad (2.28) \end{aligned}$$

It is noted that for the small cylinder the energy distribution is even in the angle ϕ . That is, the beam pattern is symmetrical. Thus, even though $E_z^{scat}(\phi) \neq E_z^{scat}(-\phi)$ in (2.17), (since $a_{+1}^S \neq a_{-1}^S$), we still have $|E_z^{scat}(\phi)|^2 = |E_z^{scat}(-\phi)|^2$. This is because of the pure imaginary character of a_0^S , $a_{\pm 1}^S$. Thus the asymmetries noted for scattering by a ferrite cylinder

occur only for cylinders where $k_0 R$ and/or $k_2 R$ are not small compared to unity.

For the pure dielectric ($\mu = 1$, $k = 0$), small cylinder, the scattering is isotropic since

$$\sigma(\phi) = \frac{\pi(k_0 R)^3 R(\epsilon - 1)^2}{8} \quad (2.29)$$

is a constant independent of the angular position.

A normalized cross section can be defined as the cross section divided by the geometrical cross section. That is,

$$\sigma_n = \frac{\sigma}{2R} \quad (2.30)$$

This parameter is useful in comparing the relative effectiveness of cylinders with different radii. Similar to the remarks for σ given above, we have σ_n greater, equal to, or less than unity, depending on whether the cylinder scatters energy from an area greater than, equal to, or less than its physical size.

Numerical Results

The far field scattering patterns were computed from (2.17) for a typical ferrite. In Appendix C the values of the components of the permeability tensor are found for this material. Figures 2.1 and 2.2 show several patterns and the effects of varying the internal magnetic field and the radius. The frequency is 10 Gc/sec for the curves shown. Each curve has been normalized to have a peak value of unity. The asymmetry and dependence of the patterns on internal magnetic field is the basis for the scanning property of the post. Several patterns are shown for various values of dielectric constant and saturation magnetization in Figs. 2.3 and 2.4. These variations correspond to a change in the material used. The characteristics revealed in Figs. 2.1-2.4 are summarized in Fig. 2.5 and Fig. 2.6. In Fig. 2.5 the beam angle is plotted as a function of internal magnetic field, radius, dielectric constant and saturation magnetization. In Fig. 2.6 the normalized scattering cross section is plotted as a function of the same variables. Figure 2.6(b) shows the inverse cube dependence of the cross section on the wavelength as predicted by (2.24) for small cylinders.

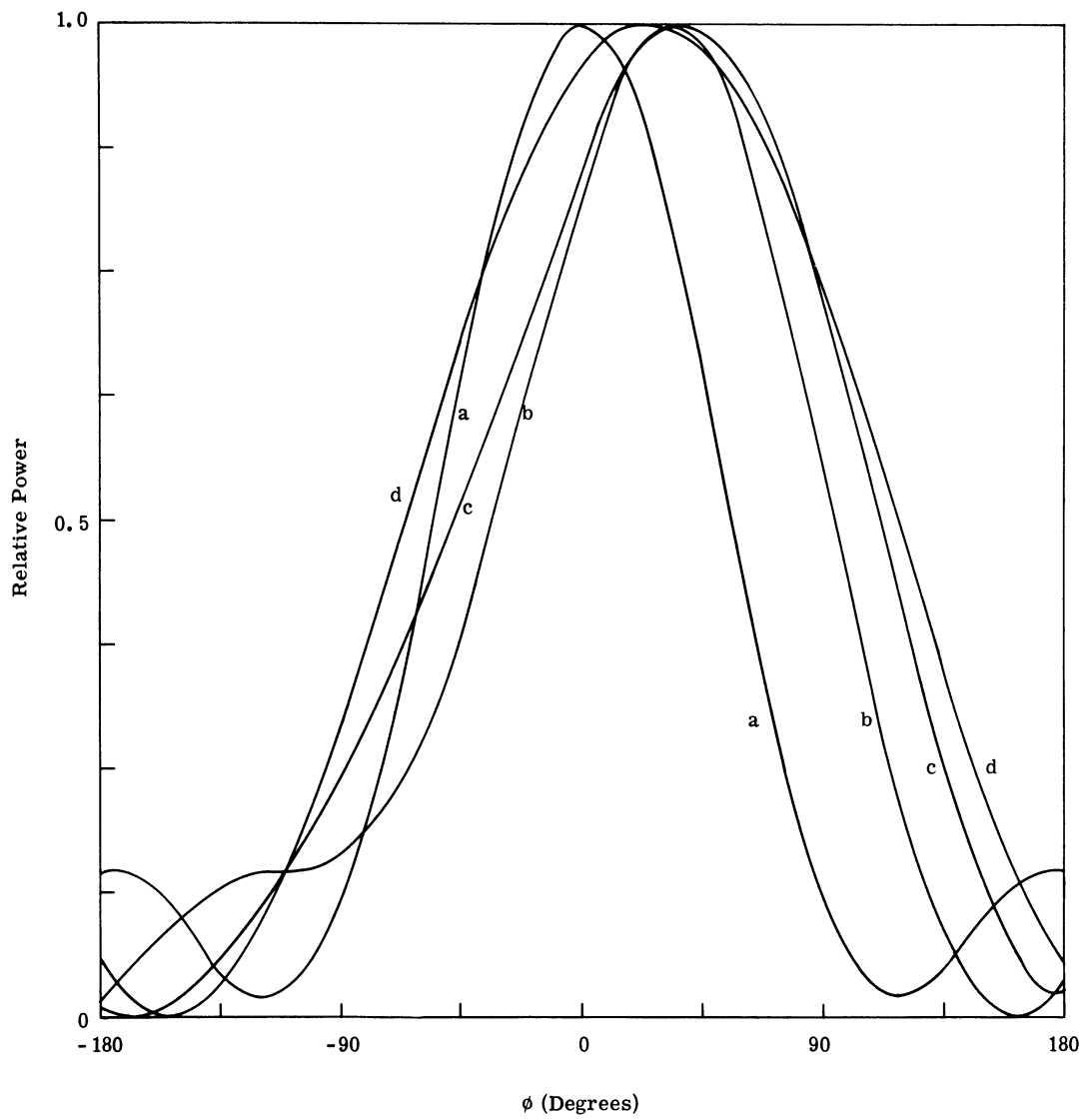


Fig. 2. 1.(a) Far field scattering patterns, showing variations with internal field. $\epsilon = 13$, $k_0 R = .7$. Internal field in oersteds, $a = 0$, $b = 2.5$, $c = 5$, $d = 100$.

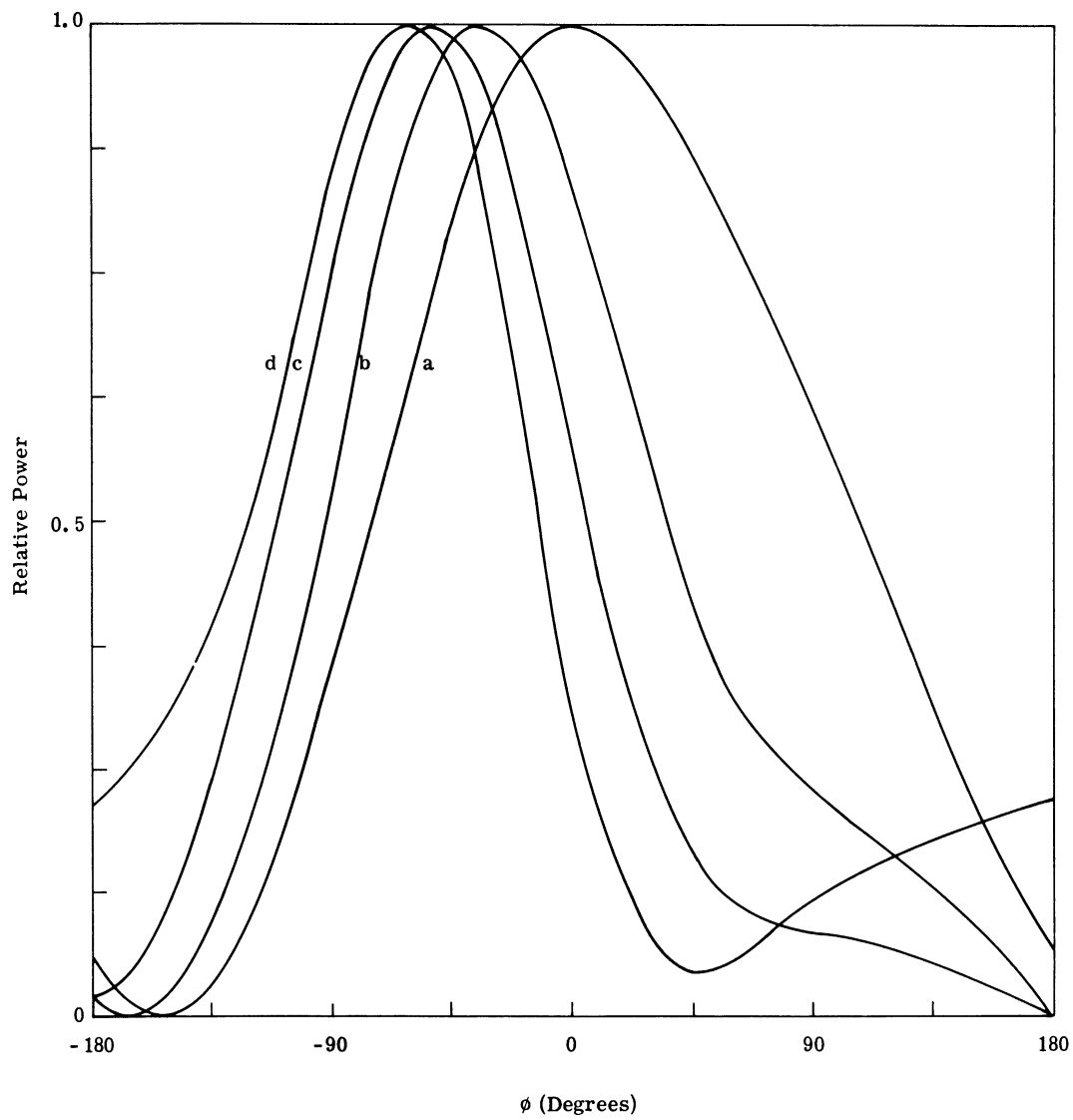


Fig. 2. 1. (b) Far field scattering patterns, showing variations with internal field. $\epsilon = 13$, $k_0 R = .7$. Internal field in oersteds, $a = 500$, $b = 1500$, $c = 2000$, $d = 2400$.

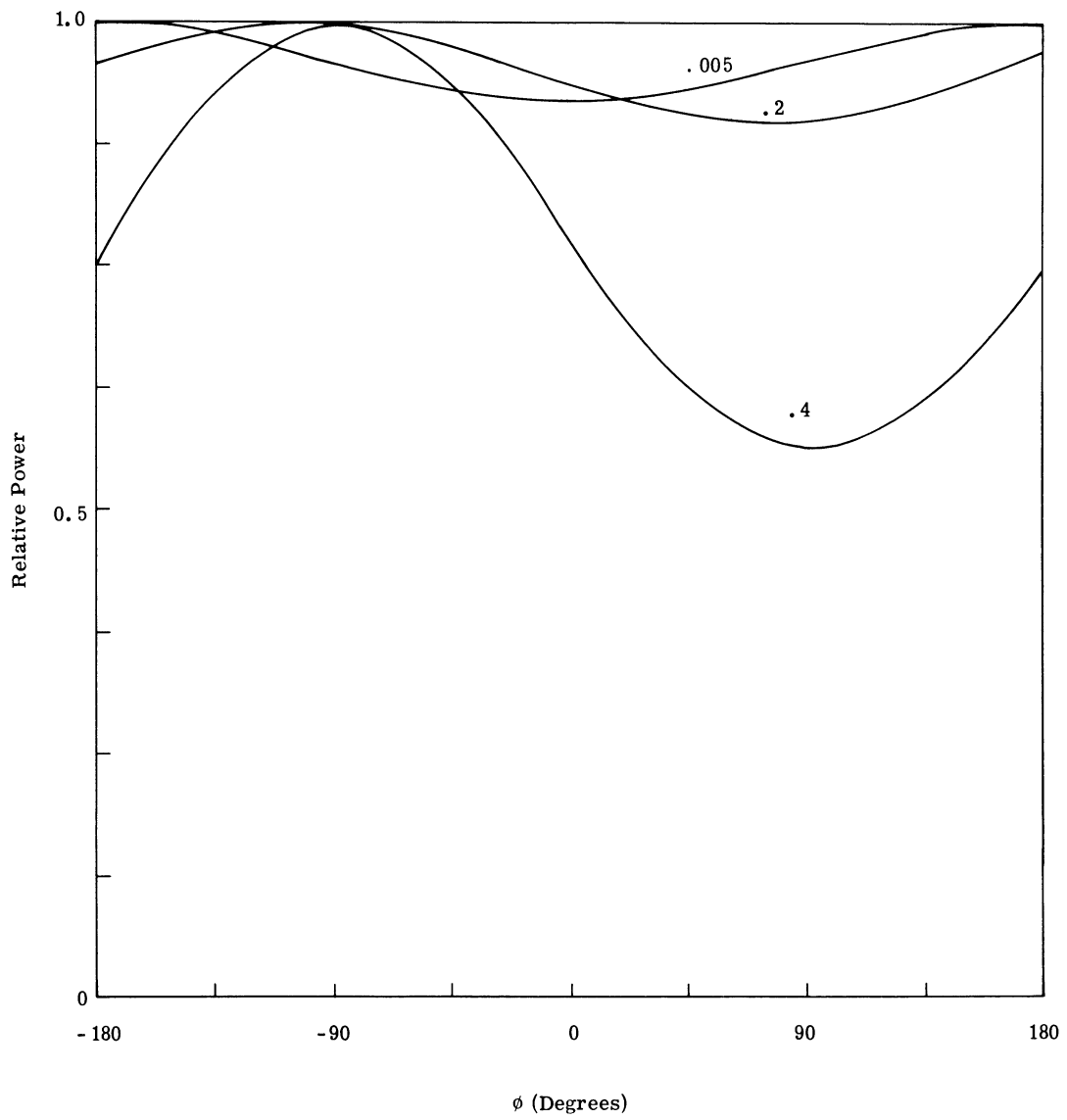


Fig. 2.2. (a) Far field scattering patterns showing variations with k_0R (i. e., variations with radius). Internal field = 200 oersteds, $\epsilon = 13$.

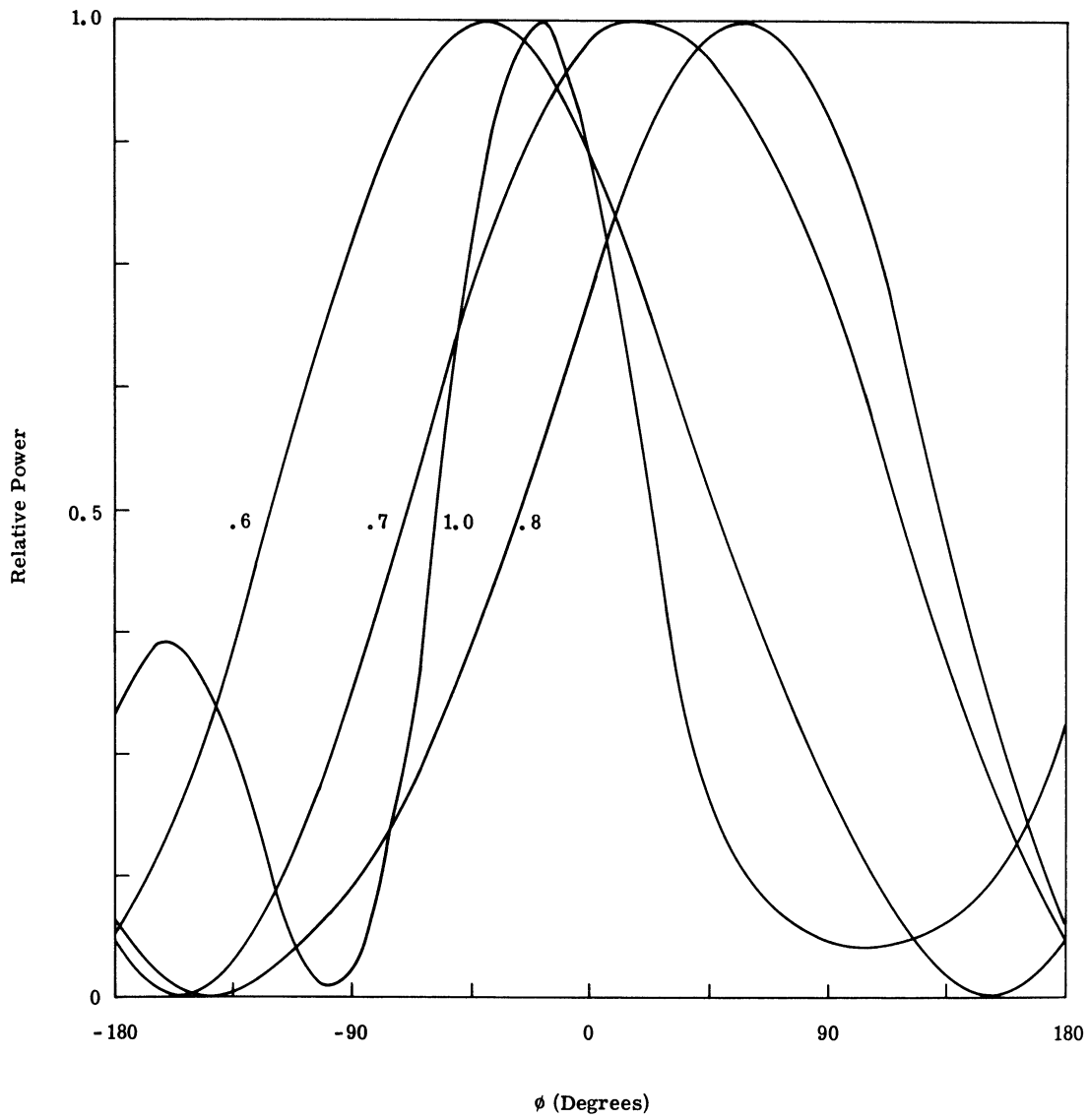


Fig. 2.2. (b) Far field scattering patterns showing variations with k_0R (i. e., variations with radius). Internal field = 200 oersteds, $\epsilon = 13$.

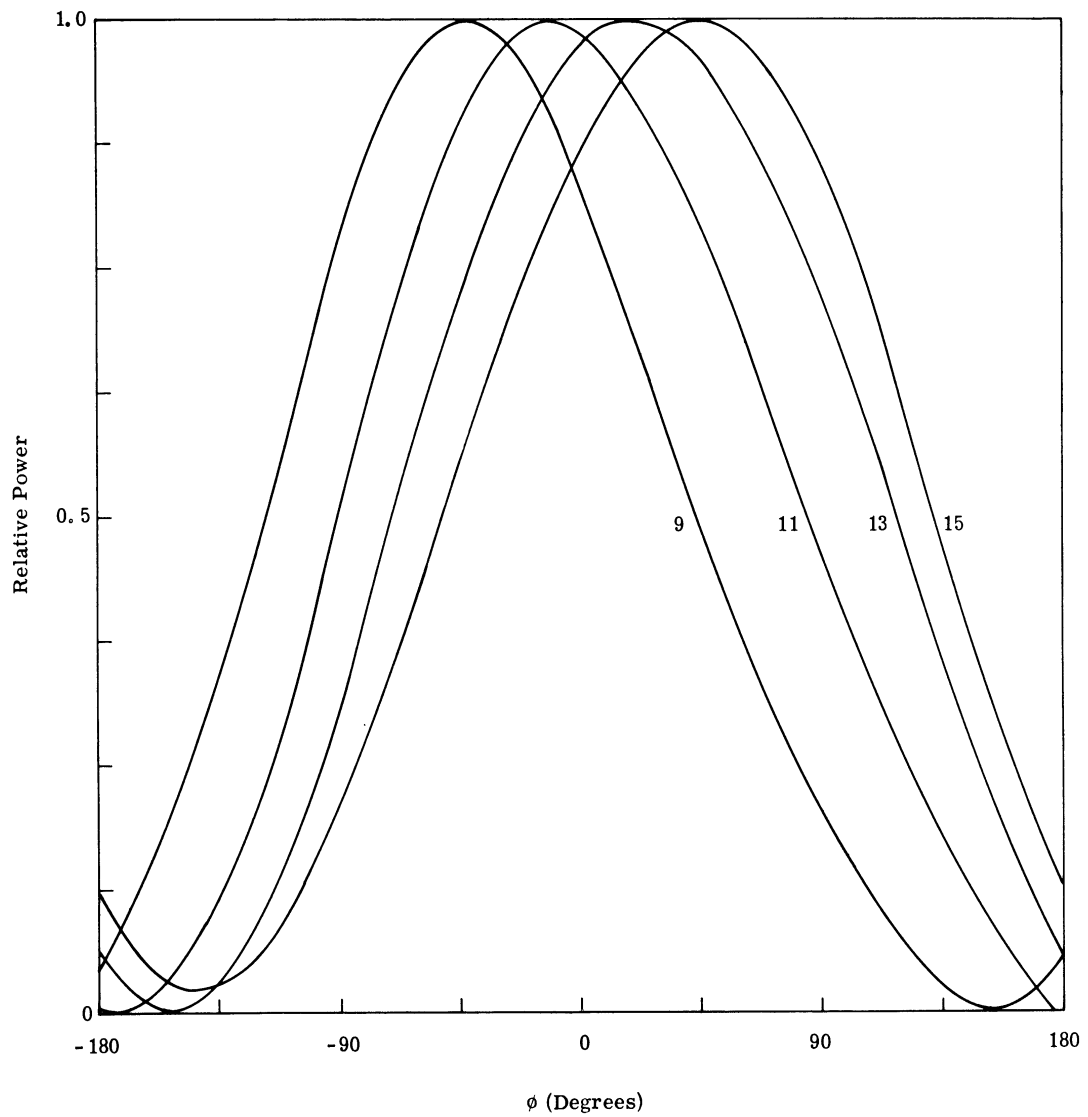


Fig. 2.3. Far field scattering patterns showing variations with dielectric constant. Internal field = 200 oersteds, $k_0R = .7$.

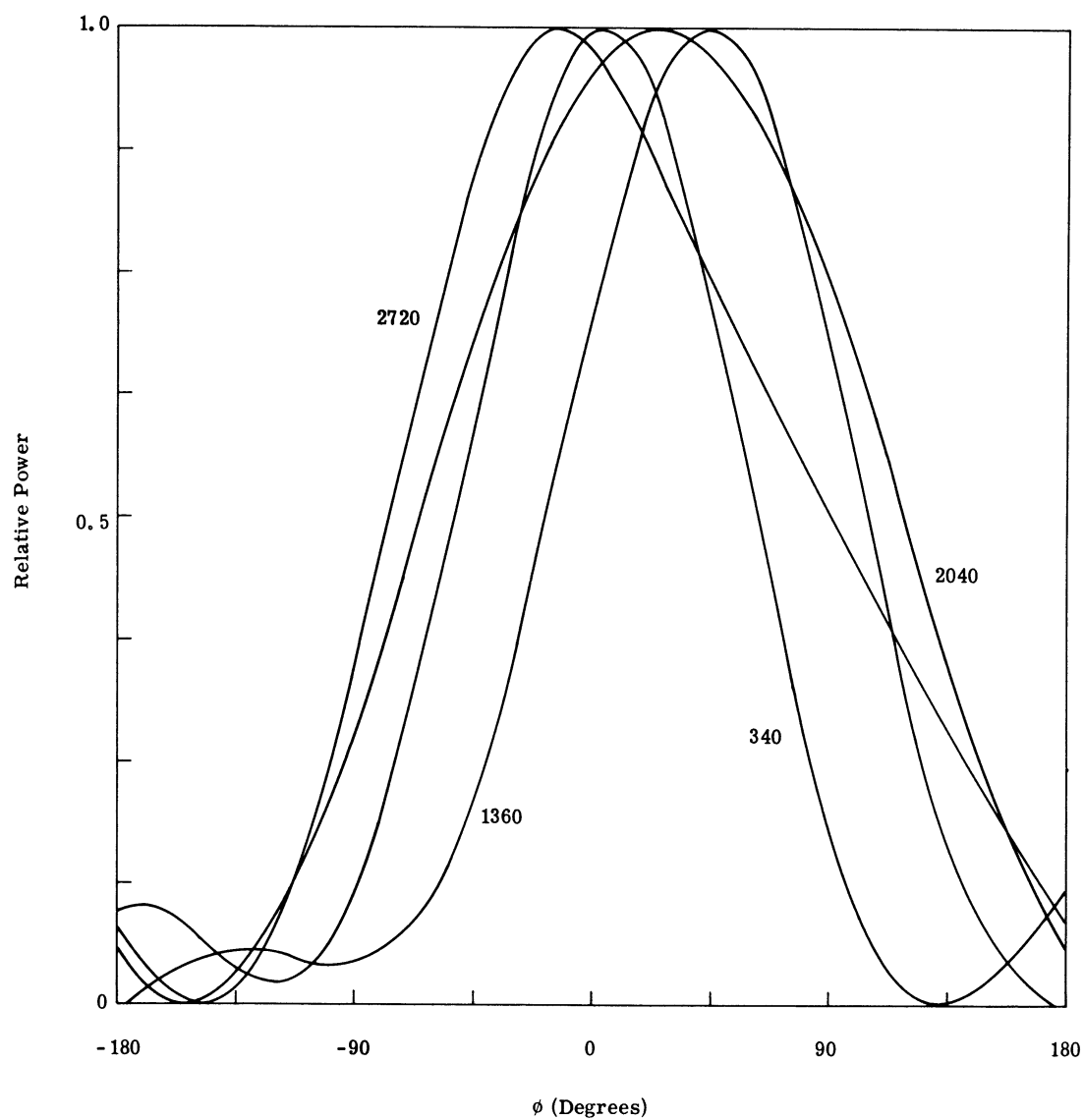
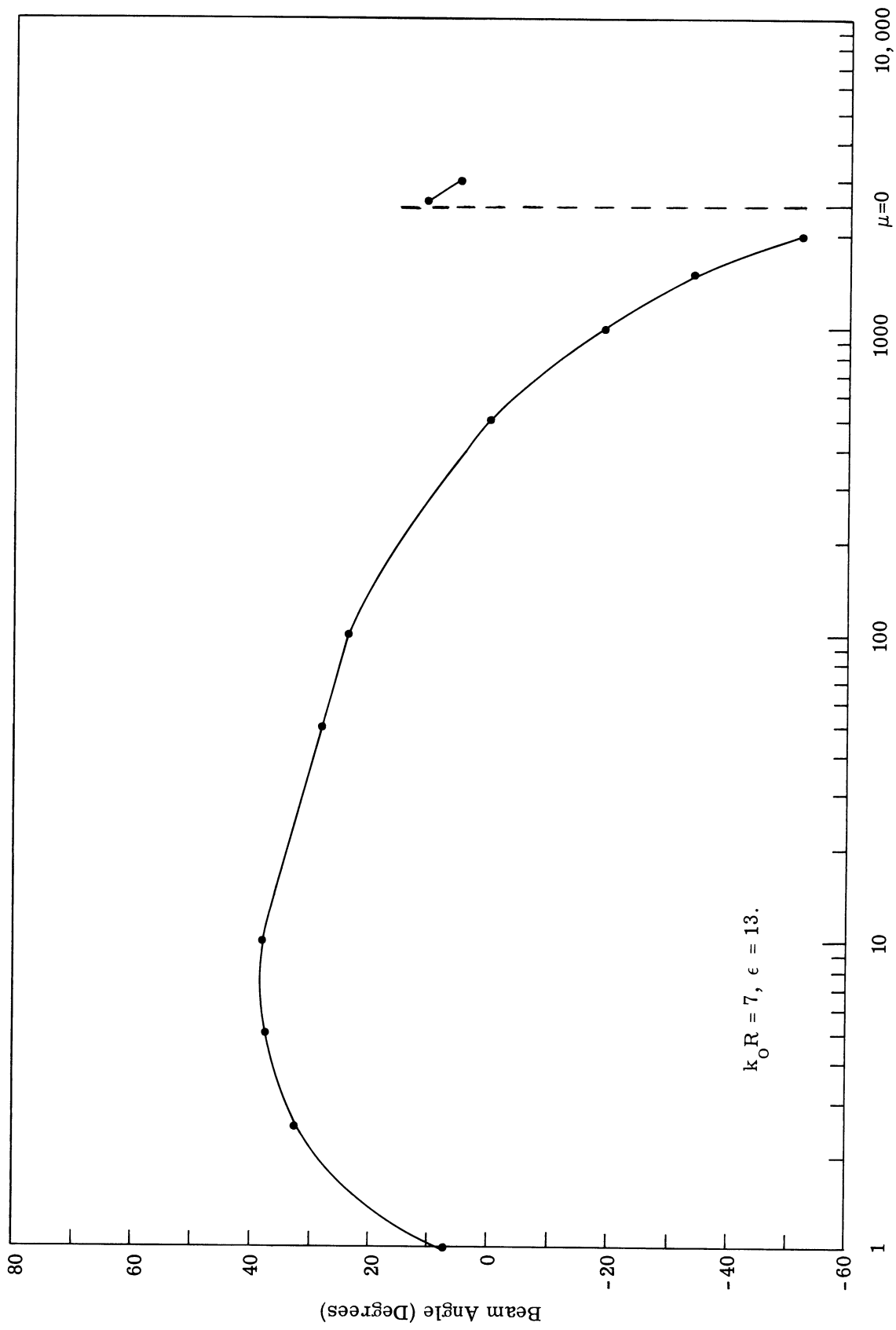


Fig. 2. 4. Far field scattering patterns showing variations with saturation magnetization ($4\pi M_S$). Internal field = 200 oersteds, $k_0R = .7$. $\epsilon = 13$.



Internal Field (Oersteds)

Fig. 2.5. (a) Beam angle vs. internal field. The points show the values obtained from a computer analysis.

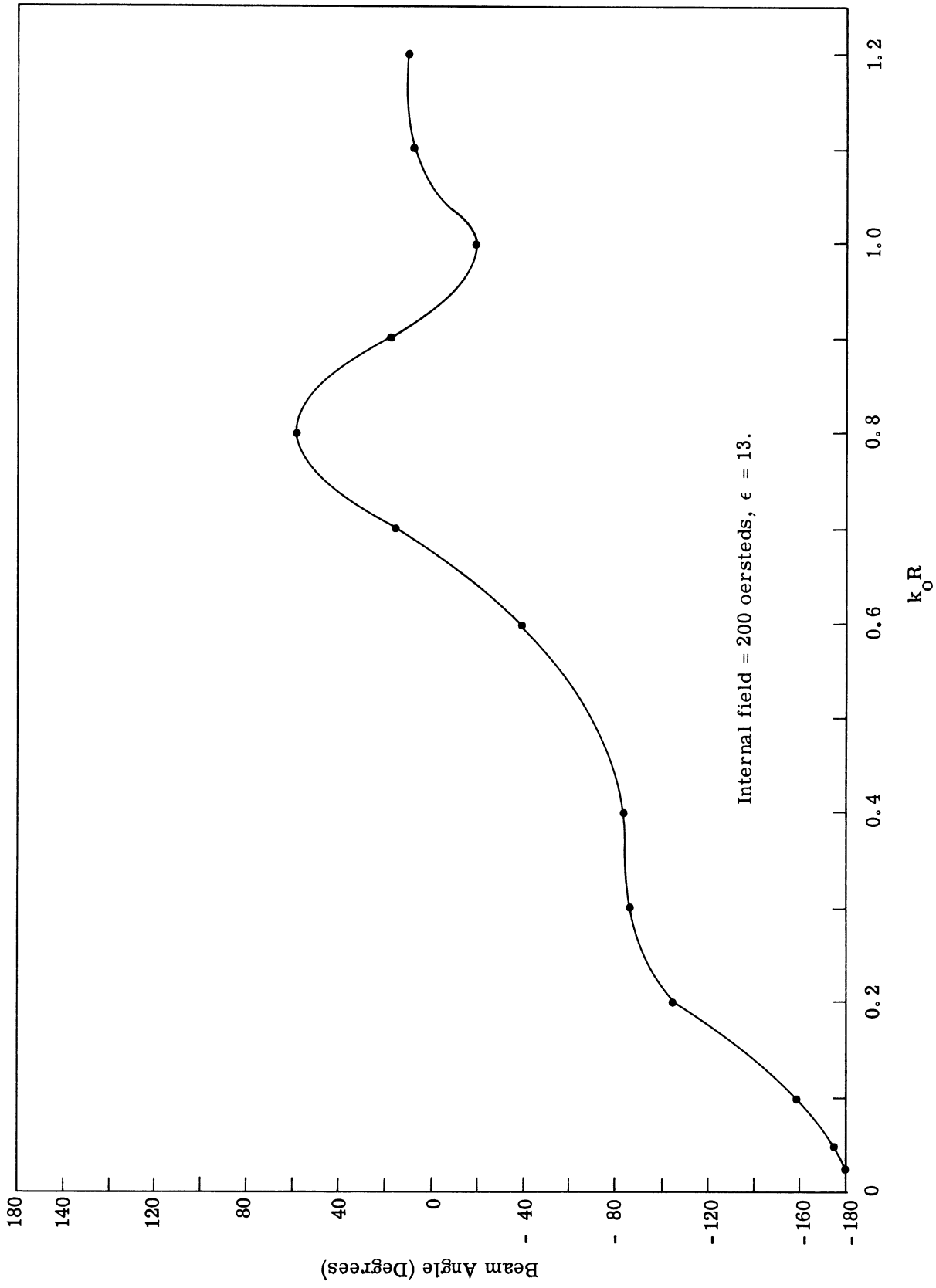


Fig. 2.5.(b) Beam angle vs. $k_0 R$. The points show values obtained from a computer analysis.

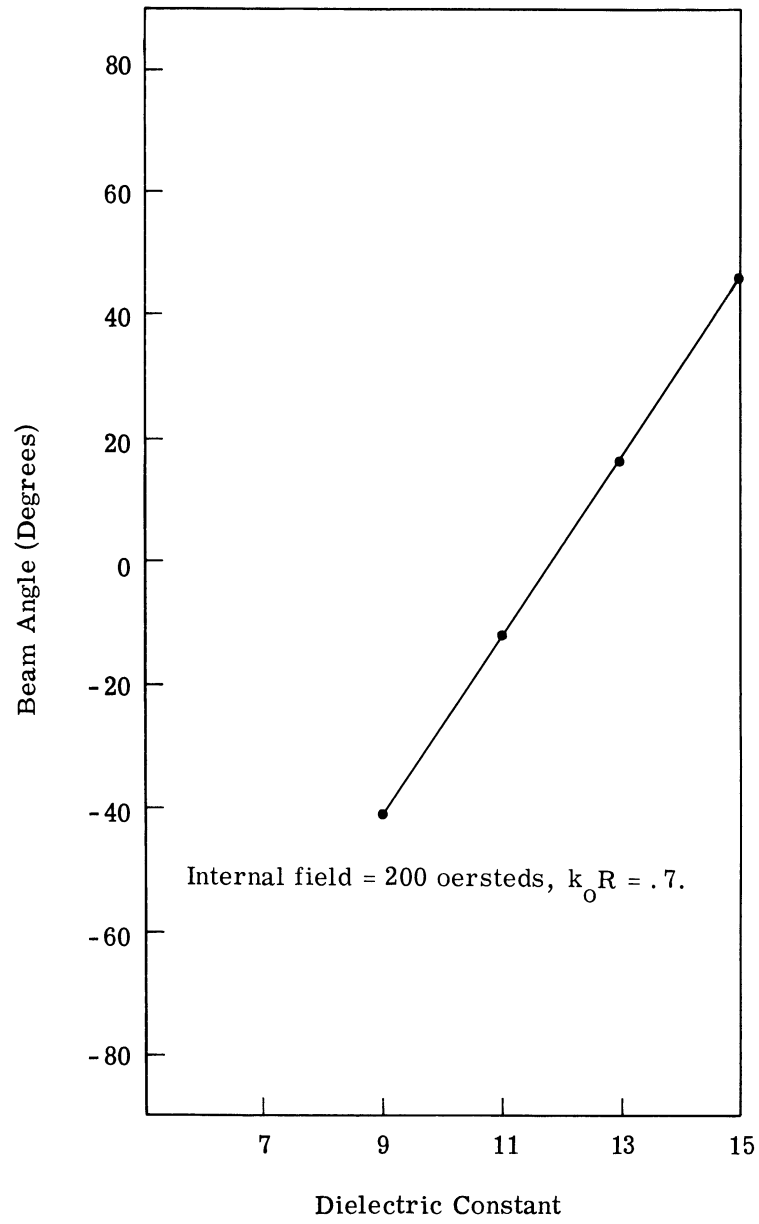


Fig. 2.5.(c) Beam angle vs. dielectric constant. The points show the values obtained from a computer analysis.

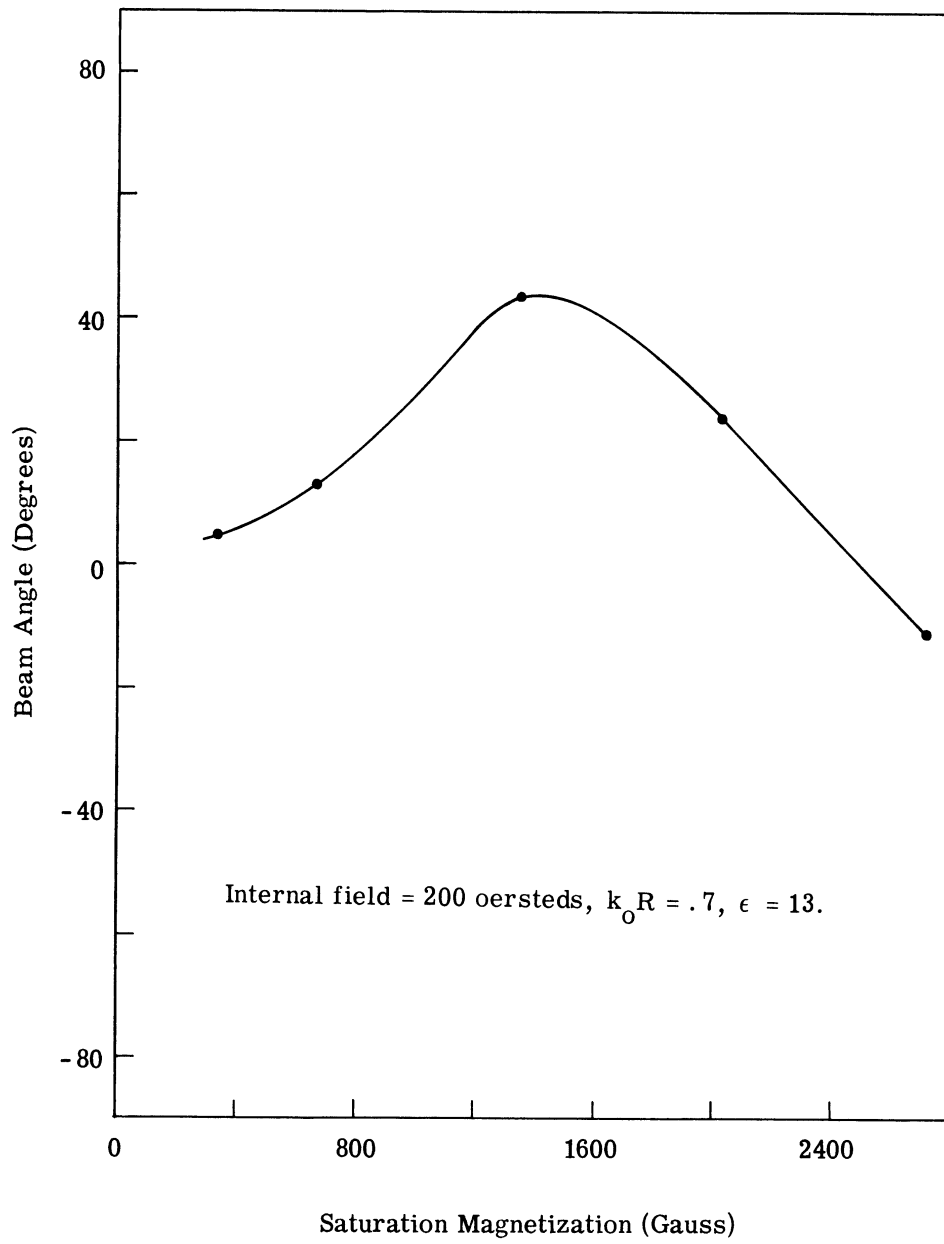


Fig. 2.5.(d) Beam angle vs. saturation magnetization ($4\pi M_S$). The points show the values obtained from a computer analysis.

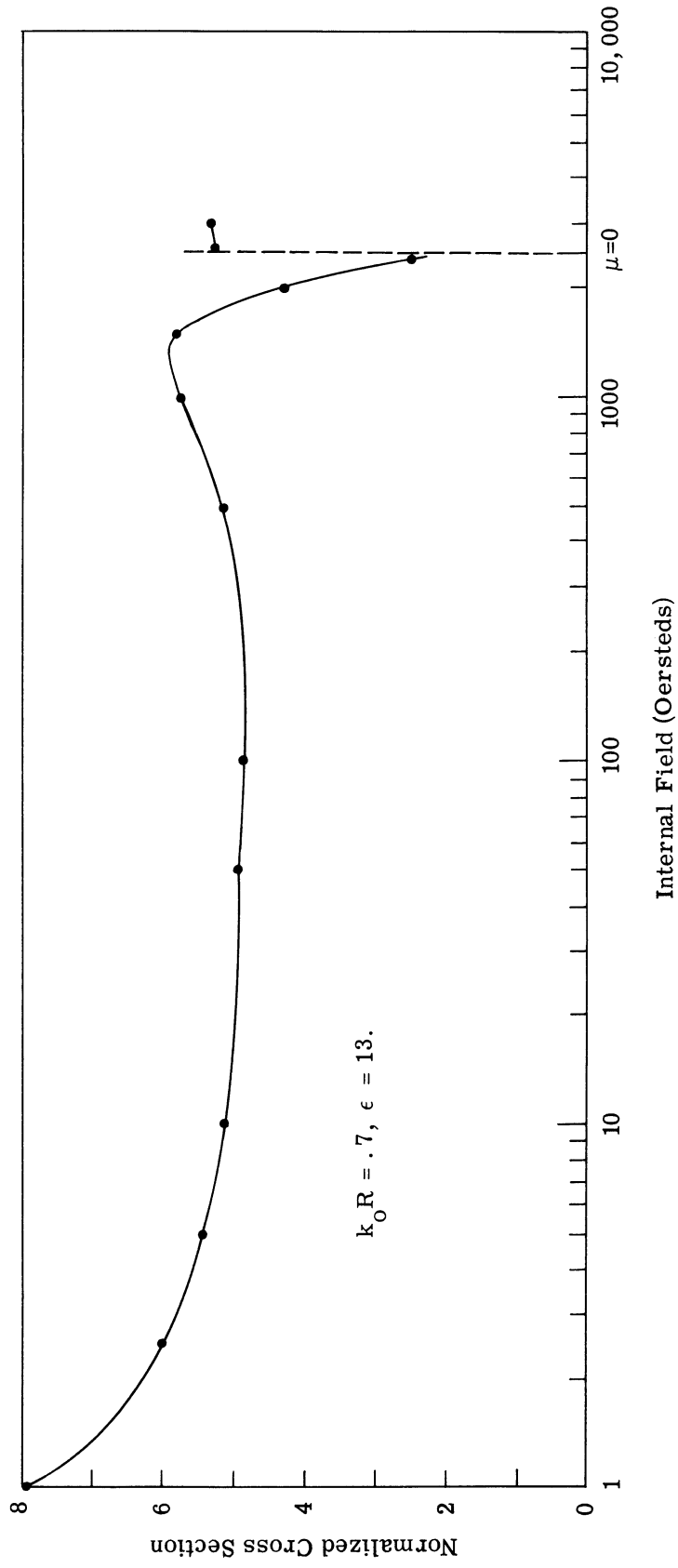


Fig. 2. 6. (a) Normalized scattering cross section vs. internal field. The points show the values obtained from a computer analysis.

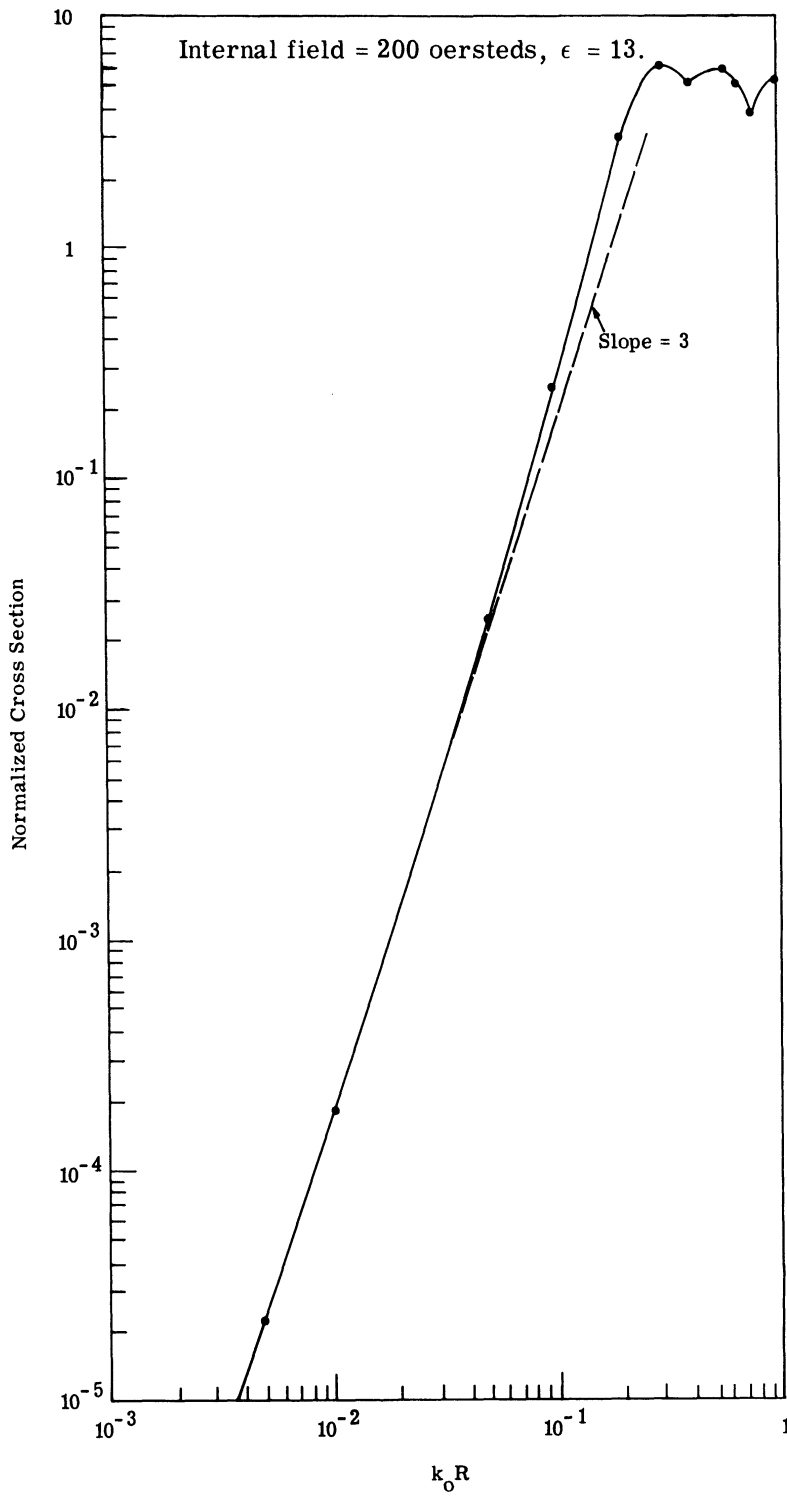


Fig. 2. 6.(b) Normalized scattering cross section vs. $k_0 R$. The points show the values obtained from a computer analysis.

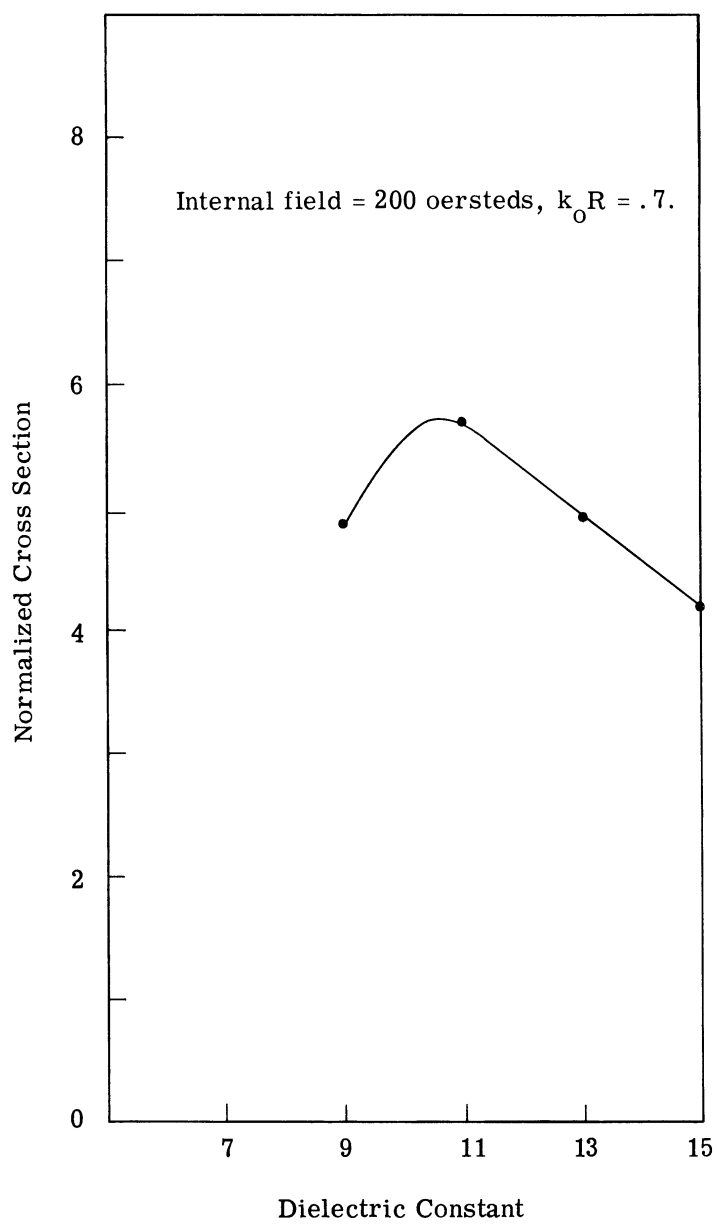


Fig. 2.6.(c) Normalized scattering cross section vs. dielectric constant.
The points show the values obtained from a computer analysis.

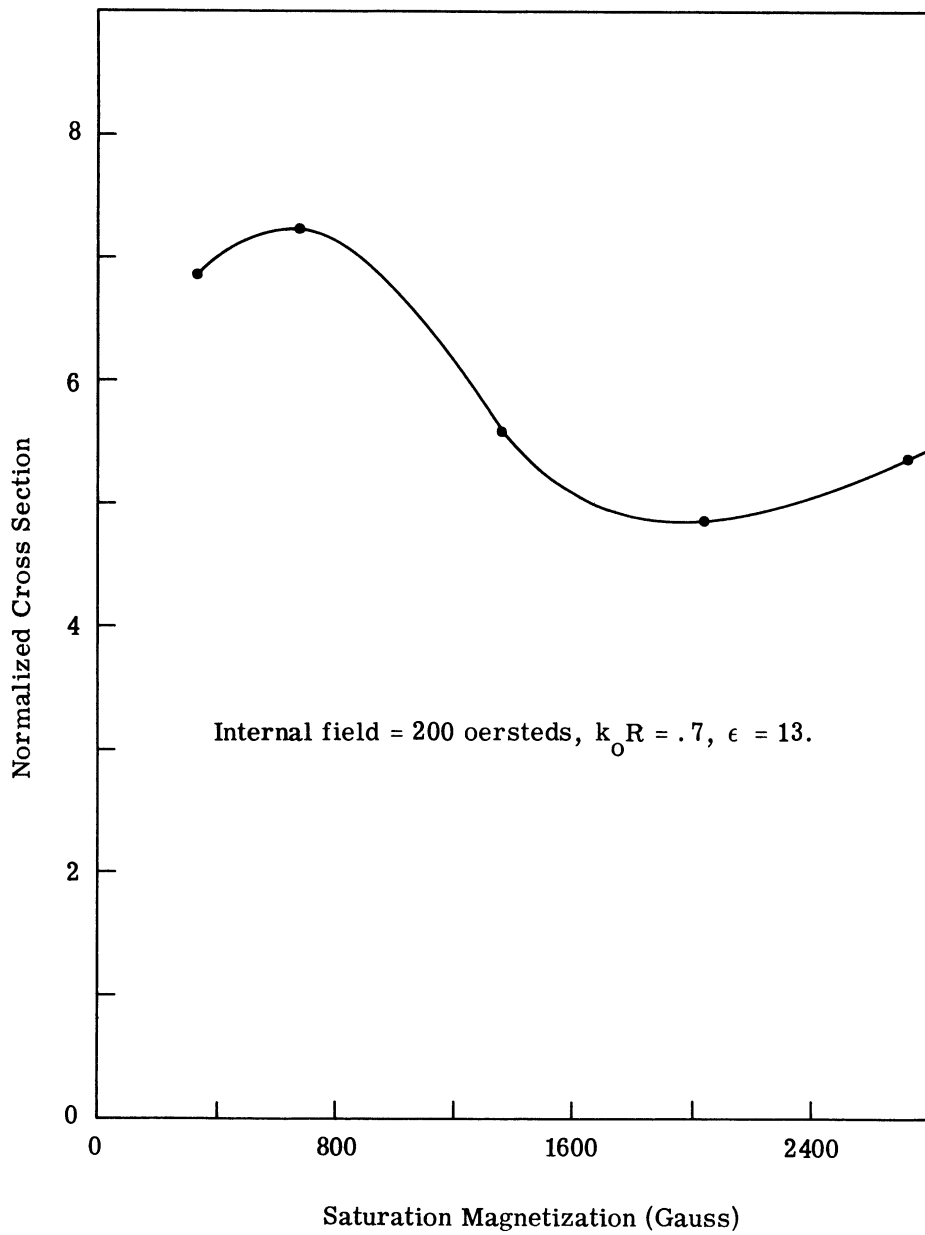


Fig. 2.6.(d) Normalized scattering cross section vs. saturation magnetization ($4\pi M_S$). The points show the values obtained from a computer analysis.

For the parameters used in the preceding curves, the following properties are noted:

1. The beam pattern is in general asymmetric about $\phi = 0$.
2. The energy is scattered mainly in the forward direction.
3. The beam angle is highly dependent on the internal field, the radius, the dielectric constant and the saturation magnetization.
4. The normalized cross section is, in general, greater than unity. This means the cylinder "appears" larger to the incoming wave than its geometrical size.

The major deviations from these characteristics occur when the post is small ($k_0 R \ll 1$). For these cases the pattern is symmetric as predicted by the equation for the differential cross section (2.28). In addition, since the curves in Fig. 2.2 were plotted for $\mu = .95$, $k = .6$, we obtain from (2.28)

$$\sigma(\phi) = \frac{\pi(k_0 R)^3 R}{8} [(\epsilon - 1)^2 + .231 + .465 - .532(\epsilon - 1) \cos \phi - .208 \cos 2\phi].$$

Since $\epsilon = 13$, the dominant term is the first one and the pattern is nearly isotropic as shown in the figure, for $k_0 R = .005$.

The preceding curves and discussion should give some insight into the behavior of the fields scattered from a ferrite cylinder. It should also give the motivation for the application of a ferrite post to electronic scanning. The scattered beam is electronically controllable and the ferrite is electrically large enough to be significant in a practical application. The major problem, obtaining a realizable feeding system for a finite ferrite sample while still maintaining a structure similar to the plane wave—infinite cylinder situation, is solved by placing the ferrite post in the aperture of a rectangular waveguide. This structure is analyzed in the following section.

2.2 Radiation from a Ferrite Cylinder in the Aperture of a Rectangular Waveguide^{*}

Let us now consider the radiation pattern of a ferrite post in the aperture of a rectangular guide with an infinite flange as shown in Fig. 2.7. The TE_{10} mode is incident on the post. This is a very complex geometry made up of a discontinuity caused by the

^{*}This analysis was published by the author earlier in a condensed form. 19

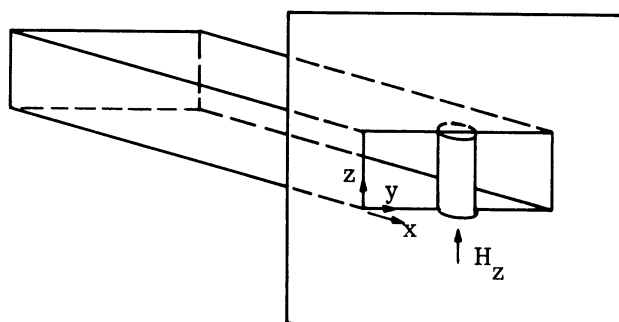


Fig. 2.7. Ferrite post in aperture of waveguide with infinite ground plane.

ferrite obstacle and a discontinuity caused by the open aperture. An exact analysis of the fields radiated from this structure is prohibitive. A simple approximate solution is presented here which neglects the effects of the waveguide side walls on the scattered fields, so that two solutions of the type shown in Section 2.1 can be superimposed to obtain predictions of the beam shifting property. The derivation of the solution and the validity of the method are discussed in the next section.

2.2.1 Formal Solution. A slight modification in the analysis presented in the preceding section can be made to account for the difference in the excitation field. Instead of a plane wave, the TE_{10} waveguide mode is now incident on the post. Since the fields have no z -dependence in this mode, since the waves reflected from the aperture in the absence of an obstacle have very little z -dependence,^{*} and since the post is cylindrical, we will assume no z -variations in any of the resulting fields. This is probably a very good assumption inside the waveguide and in a region close to the ($z = b/2$) plane in free space. Elsewhere in the free space region the approximation is invalid. Thus, the solution given here will be used to provide only the radiation pattern in the ($z = b/2$) plane. In particular, the direction of radiation, or beam angle, is desired. The analysis to be given applies more precisely to either of the cases illustrated in Fig. 2.8. In the first part of the figure, an

* See Appendix B for a discussion of the waves reflected by the open waveguide.

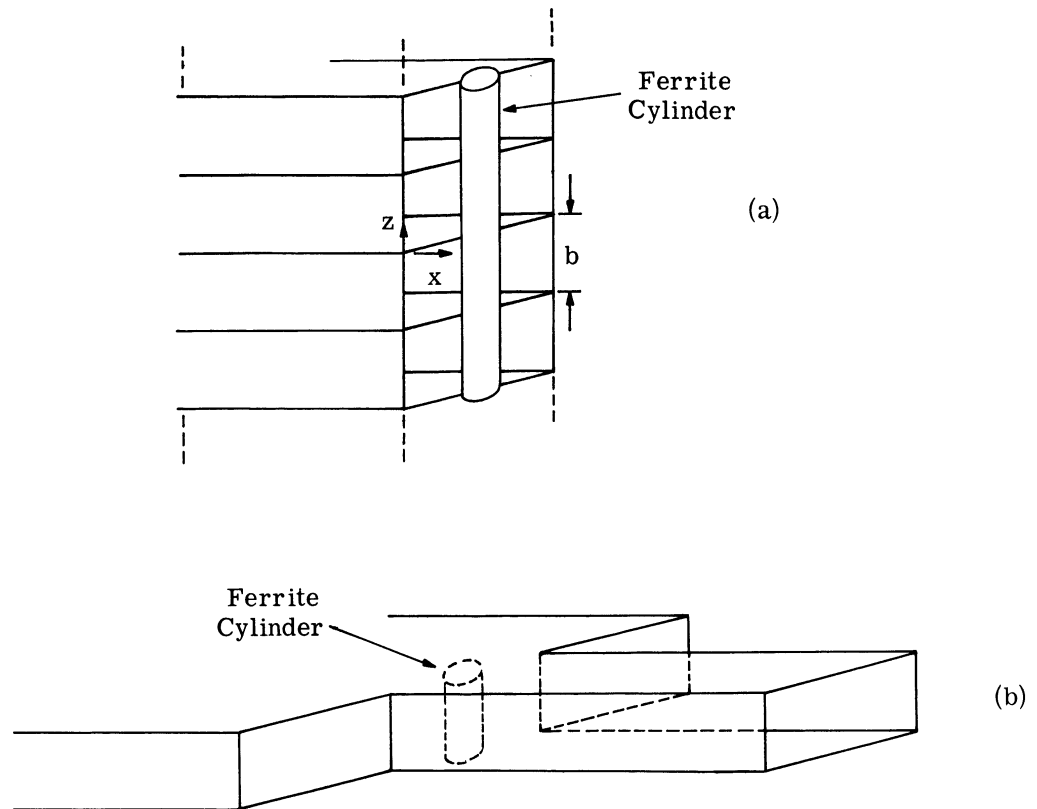


Fig. 2.8. Structures to which the analysis in the text applies.

infinite number of waveguides, all fed by identical signals, are arranged so that the radiated fields have no z -dependence. In Fig. 2.8(b), the rectangular waveguide radiates into a parallel plate structure, so that again no z -dependent fields are present. Obviously, from a consideration of Fig. 2.8(a), the z -variations in the radiated fields can be neglected in the region close to the ($z = b/2$) plane even when several radiators are removed from the ends so that the number of waveguides is not infinite. If, as in the present case, this argument is extended until all but one of the radiators are removed, only a comparison between experiment and theory can provide a justification for the procedure. As this is the case in verifying any theory, no further argument is presented at this point.

Incident Fields

The electric field for the incident wave is,

$$E_z^{\text{inc}} = \cos \frac{\pi y}{a} e^{-j\beta_1 x + j\omega t} \quad (2.31)$$

where

$$\beta_1 = \sqrt{k_0^2 - (\pi/a)^2}$$

By taking (2.31) for the incident wave, we have neglected the wave reflected by the open aperture. This reflected wave is small in the case of an aperture without a ferrite obstacle, i. e., the aperture has a low VSWR by itself. This is a minor approximation compared to others made in the analysis of this section. Now (2.31) can be rewritten as the sum of two plane waves diverging at an angle α . Omitting the $e^{j\omega t}$ term,

$$E_z^{\text{inc}} = \frac{1}{2} \left[e^{-jk_0(y \sin \alpha + x \cos \alpha)} + e^{-jk_0(-y \sin \alpha + x \cos \alpha)} \right] \quad (2.32)$$

where

$$\alpha = \sin^{-1} \lambda/\lambda_c$$

$$\lambda_c = 2a, \text{ the cutoff wavelength in the waveguide}$$

$$\lambda = \text{the free space wavelength.}$$

Or, in cylindrical coordinates

$$E_z^{\text{inc}} = \frac{1}{2} \left[e^{-jk_0 r \cos(\phi - \alpha)} + e^{-jk_0 r \cos(\phi + \alpha)} \right] \quad (2.33)$$

Expanding into a series of Bessel functions gives

$$E_z^{\text{inc}} = \sum_{n=-\infty}^{\infty} \cos(n\alpha) J_n(k_0 r) e^{-jn(\phi + \pi/2)} \quad (2.34a)$$

Using (2.9a) and (2.9b) gives the magnetic field components.

$$H_r^{\text{inc}} = \frac{1}{\omega\mu_0} \sum_{n=-\infty}^{\infty} n \cos(n\alpha) \frac{J_n(k_0 r)}{r} e^{-jn(\phi + \pi/2)} \quad (2.34b)$$

$$H_\phi^{\text{inc}} = \frac{-j}{\omega\mu_0} \sum_{n=-\infty}^{\infty} k_0 \cos(n\alpha) J_n'(k_0 r) e^{-jn(\phi + \pi/2)} \quad (2.34c)$$

Internal Fields

The wave equation (2.8) is still valid if we assume no z-dependences exist, so that the fields inside the ferrite can be written,

$$E_z^{\text{int}} = \sum_{n=-\infty}^{\infty} a_n \cos(n\alpha) J_n(k_2 r) e^{-jn(\phi + \pi/2)} \quad (2.35a)$$

$$H_r^{\text{int}} = \frac{1}{\omega\mu_0(\mu^2 - k^2)} \sum_{n=-\infty}^{\infty} a_n \cos(n\alpha) [k_2 k J_n'(k_2 r) + \frac{n\mu}{r} J_n(k_2 r)] e^{-jn(\phi + \pi/2)} \quad (2.35b)$$

$$H_\phi^{\text{int}} = \frac{-j}{\omega\mu_0(\mu^2 - k^2)} \sum_{n=-\infty}^{\infty} a_n \cos(n\alpha) [\mu k_2 J_n'(k_2 r) + \frac{nk}{r} J_n(k_2 r)] e^{-jn(\phi + \pi/2)} \quad (2.35c)$$

The $\cos(n\alpha)$ term was introduced for convenience and could have been absorbed in the coefficients (a_n).

Scattered Fields

The scattered field can be written as

$$E_z^{\text{scat}} = \sum_{n=-\infty}^{\infty} a_n^s \cos(n\alpha) H_n^{(2)}(k_0 r) e^{-jn(\phi + \pi/2)} \quad (2.36a)$$

$$H_r^{\text{scat}} = \frac{1}{\omega\mu_0} \sum_{n=-\infty}^{\infty} a_n^s n \cos(n\alpha) \frac{H_n^{(2)}(k_0 r)}{r} e^{-jn(\phi + \pi/2)} \quad (2.36b)$$

$$H_\phi^{\text{scat}} = \frac{-j}{\omega\mu_0} \sum_{n=-\infty}^{\infty} a_n^s k_0 \cos(n\alpha) H_n^{(2)}(k_0 r) e^{-jn(\phi + \pi/2)} \quad (2.36c)$$

Boundary Conditions

The boundary conditions, continuity of E_z and H_ϕ at the ferrite boundary, are

$$E_z^{\text{scat}} + E_z^{\text{inc}} = E_z^{\text{int}} \quad \text{at } r = R \quad (2.37a)$$

$$H_\phi^{\text{scat}} + H_\phi^{\text{inc}} = H_\phi^{\text{int}} \quad \text{at } r = R \quad (2.37b)$$

and in addition, the tangential component of the electric field must be zero on the waveguide walls. Since E_z^{inc} is already zero at the walls, then E_z^{scat} must be identically zero on these

metal boundaries. That is,

$$E_z^{\text{scat}} = 0 \quad \text{at} \quad y = \pm a/2. \quad (2.38)$$

In general, additional fields must be added to the scattered fields (2.36) to satisfy this condition. These are sometimes referred to as the image fields and are quite difficult to calculate for the geometry considered. However, referring to the beam patterns in Fig. 2.1 for the infinite cylinder with plane wave incidence, we notice several cases where most of the energy is scattered into the region $x > 0$ ($-90^\circ < \phi < 90^\circ$). For these cases E_z^{scat} is zero (or almost zero) everywhere in the region $x < 0$. A similar result may be expected in the present case. When most of the energy is scattered in the forward direction, E_z^{scat} is zero everywhere in the waveguide, the boundary condition (2.38) is satisfied and the image fields are zero and can be neglected. Since we are mainly interested in explaining the behavior of the structure when it actually does radiate efficiently into free space, the limitation of our results to cases where the image fields can be neglected is not too great.

Applying the conditions (2.37) at the ferrite boundary gives the unknown coefficients. These are identical with those given in (2.16).

$$a_n = \frac{\frac{H_{n+1}^{(2)}(k_o R)}{H_n^{(2)}(k_o R)} - \frac{J_{n+1}(k_o R)}{J_n(k_o R)}}{\sqrt{\frac{\epsilon}{\mu_{\text{eff}}}} \left[\frac{n}{k_2 R} \left(1 + \frac{k}{\mu} \right) - \frac{J_{n+1}(k_2 R)}{J_n(k_2 R)} \right] - \frac{n}{k_o R} + \frac{H_{n+1}^{(2)}(k_o R)}{H_n^{(2)}(k_o R)}} \frac{J_n(k_o R)}{J_n(k_2 R)} \quad (2.39a)$$

$$a_n^s = \frac{-\sqrt{\frac{\epsilon}{\mu_{\text{eff}}}} \left[\frac{n}{k_2 R} \left(1 + \frac{k}{\mu} \right) - \frac{J_{n+1}(k_2 R)}{J_n(k_2 R)} \right] - \frac{n}{k_o R} + \frac{J_{n+1}(k_o R)}{J_n(k_o R)}}{\sqrt{\frac{\epsilon}{\mu_{\text{eff}}}} \left[\frac{n}{k_2 R} \left(1 + \frac{k}{\mu} \right) - \frac{J_{n+1}(k_2 R)}{J_n(k_2 R)} \right] - \frac{n}{k_o R} + \frac{H_{n+1}^{(2)}(k_o R)}{H_n^{(2)}(k_o R)}} \frac{J_n(k_o R)}{H_n^{(2)}(k_o R)} \quad (2.39b)$$

As before, (2.17), in the far-field we can write

$$E_z^{\text{scat}} = \sqrt{\frac{2}{\pi k_o r}} e^{-jk_o r + j\pi/4} \sum_{n=-\infty}^{\infty} a_n^s \cos n\alpha e^{-jn\phi} \quad (2.40)$$

Small Ferrite Radius

For the case of $k_o R \ll 1$ and $k_2 R \ll 1$, the coefficients can be simplified as in Section 2.1. They are, using only positive values of n .

$$a_o^S = -j \frac{\pi(k_o R)^2 (\epsilon - 1)}{4} \quad (2.41a)$$

$$a_{\pm n}^S = j \frac{\pi(k_o R)^{2n}}{n!(n-1)!2^{2n}} \frac{\left[\frac{1}{\mu_{\text{eff}}} \left(1 \pm \frac{k}{\mu}\right) - 1 \right]}{\left[\frac{1}{\mu_{\text{eff}}} \left(1 \pm \frac{k}{\mu}\right) + 1 \right]} \quad (2.41b)$$

The power density in the scattered field is

$$N = \frac{1}{2} \sqrt{\frac{\epsilon_o}{\mu_o}} \left| E_z^{\text{scat}} \right|^2 \quad (2.42)$$

Using (2.40) then gives

$$N = \frac{1}{2} \sqrt{\frac{\epsilon_o}{\mu_o}} \frac{2}{\pi k_o r} \sum_{n=-\infty}^{\infty} \sum_{\ell=-\infty}^{\infty} a_n^S a_{\ell}^{S*} \cos(n\alpha) \cos(\ell\alpha) e^{-jn\phi} e^{j\ell\phi} \quad (2.43)$$

where * denotes the complex conjugate.

Using only the terms through the indices ± 1 , since a_n^S is proportional to $(k_o R)^{2n}$, we obtain

$$\begin{aligned} N &= \sqrt{\frac{\epsilon_o}{\mu_o}} \frac{1}{\pi k_o r} \left\{ \left| a_o^S \right|^2 + \left| a_1^S \right|^2 \cos^2 \alpha + \left| a_{-1}^S \right|^2 \cos^2 \alpha \right. \\ &\quad + a_o^S a_1^{S*} \cos \alpha e^{j\phi} + a_o^S a_{-1}^{S*} \cos \alpha e^{-j\phi} + a_1^S a_o^{S*} \cos \alpha e^{-j\phi} \\ &\quad \left. + a_1^S a_{-1}^{S*} \cos^2 \alpha e^{-j2\phi} + a_{-1}^S a_o^{S*} \cos \alpha e^{j\phi} + a_{-1}^S a_1^{S*} \cos^2 \alpha e^{j2\phi} \right\} \\ &= \frac{\sqrt{\epsilon_o/\mu_o}}{\pi k_o r} \left\{ \left| a_o^S \right|^2 + \left| a_1^S \right|^2 \cos^2 \alpha + \left| a_{-1}^S \right|^2 \cos^2 \alpha \right. \\ &\quad + 2\text{Re}(a_o^S a_1^{S*} e^{j\phi}) \cos \alpha + 2\text{Re}(a_o^S a_{-1}^{S*} e^{-j\phi}) \cos \alpha \\ &\quad \left. + 2\text{Re}(a_1^S a_{-1}^{S*} e^{-j2\phi}) \cos^2 \alpha \right\} \end{aligned}$$

where, $\text{Re}(\)$ indicates the real part.

Now, using (2.41) for the coefficients gives

$$\begin{aligned}
N = & \frac{\sqrt{\epsilon_o/\mu_o}}{\pi k_o R} \frac{\pi^2 (k_o R)^4}{16} \left\{ (\epsilon-1)^2 + \left[\left(\frac{\mu-k-1}{\mu-k+1} \right)^2 + \left(\frac{\mu+k-1}{\mu+k+1} \right)^2 \right] \cos^2 \alpha \right. \\
& + 2(\epsilon-1) \cos \alpha \left(\frac{\mu-k-1}{\mu-k+1} + \frac{\mu+k-1}{\mu+k+1} \right) \cos \phi \\
& \left. + 2 \left(\frac{\mu-k-1}{\mu-k+1} \right) \left(\frac{\mu+k-1}{\mu+k+1} \right) \cos^2 \alpha \cos 2\phi \right\} \quad (2.44)
\end{aligned}$$

For the small post, the beam pattern is symmetric. Because of this, the small post cannot be used for beam shifting. Of course, the small post produces so much backscatter that the theory neglecting the side walls is not valid. It is not expected that the side walls would produce any asymmetries so that beam shifting with the small post is unlikely. In Section 2.1 the normalized cross section for small posts was shown to be less than unity. Thus the small post actually has little effect on the total radiated field.

2.2.2 Numerical Results. Several patterns computed from (2.40) are shown in Fig. 2.9. The values of μ and k were obtained as discussed in Appendix C. The frequency is 10 Gc/sec. This figure shows the effect of varying the external field. Figure 2.9(a) uses values of the components of the permeability tensor calculated for the unsaturated case. Figure 2.9(b) uses the components obtained from the usual formulas applied when the material is magnetically saturated. Figure 2.10 shows the effects of a change in the product $k_o R$ corresponding to a change in radius or frequency.

Two plots of the beam angle vs. the external field are shown in Fig. 2.11 for a frequency of 10 Gc/sec. Both theoretical and experimental curves are shown. In the experimental data the double points mean that a secondary peak exists. In Fig. 2.11(a), agreement between theory and experiment is good at fields below 400 oersteds. Just above 400 oersteds, the theory predicts larger scan angles than are observed. In this region the side walls of the waveguide (neglected in the theory) are affecting the pattern. This was observed by the large measured reflections between 400 and 1800 oersteds. It is also seen from the theoretical far field patterns in Fig. 2.9. For example, for 500 oersteds much of the energy in the beam is directed back into the waveguide ($-180^\circ < \phi < -90^\circ$, $90^\circ < \phi < 180^\circ$), so that our assumptions no longer hold. At higher fields, Fig. 2.9(b) shows that even though the peak in the pattern comes near to zero degrees, the beam has broadened so that much of

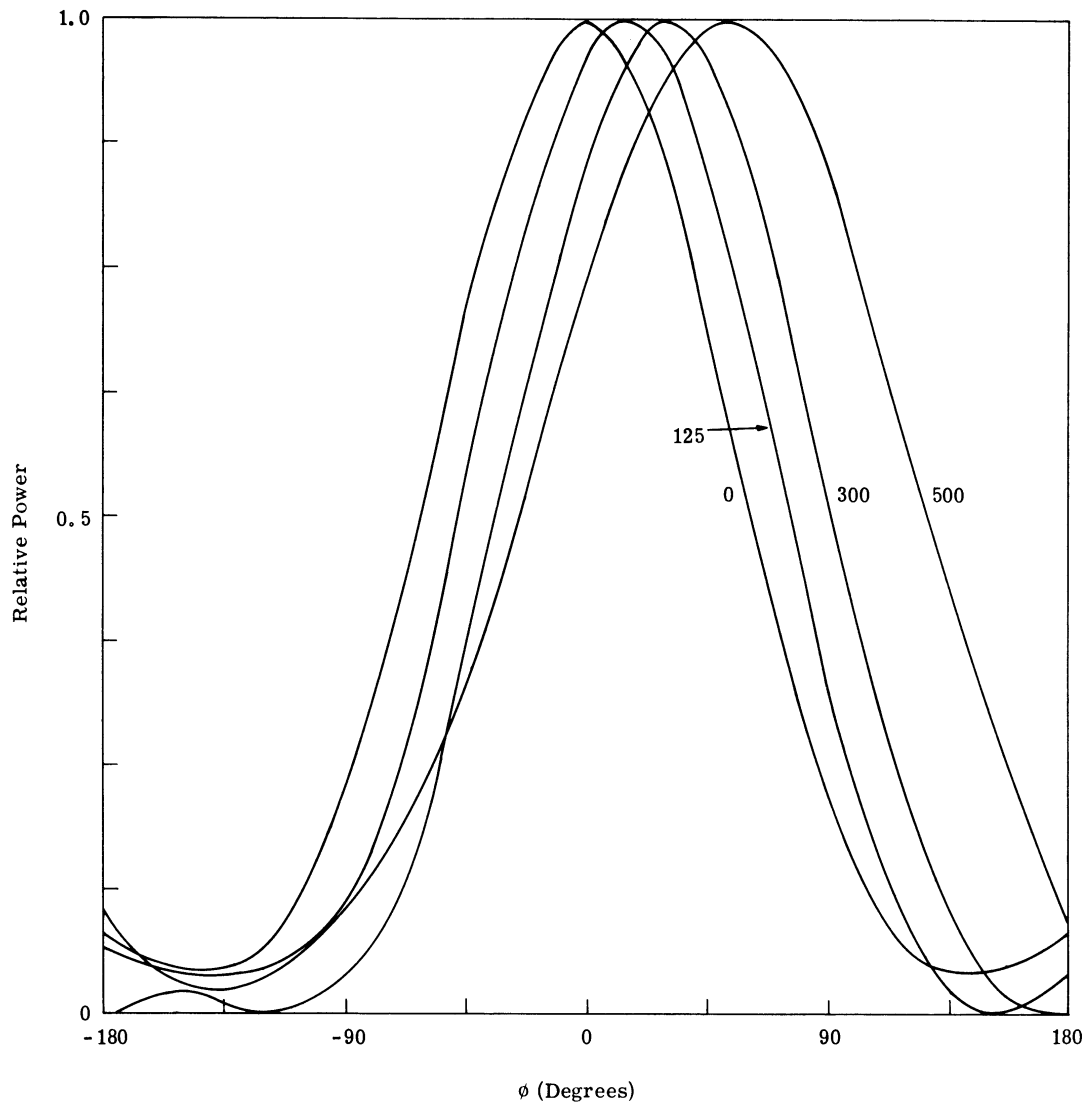


Fig. 2.9. (a) Far field scattering patterns showing variations with external field (oersteds). $\epsilon = 13$, $k_0 R = .786$.

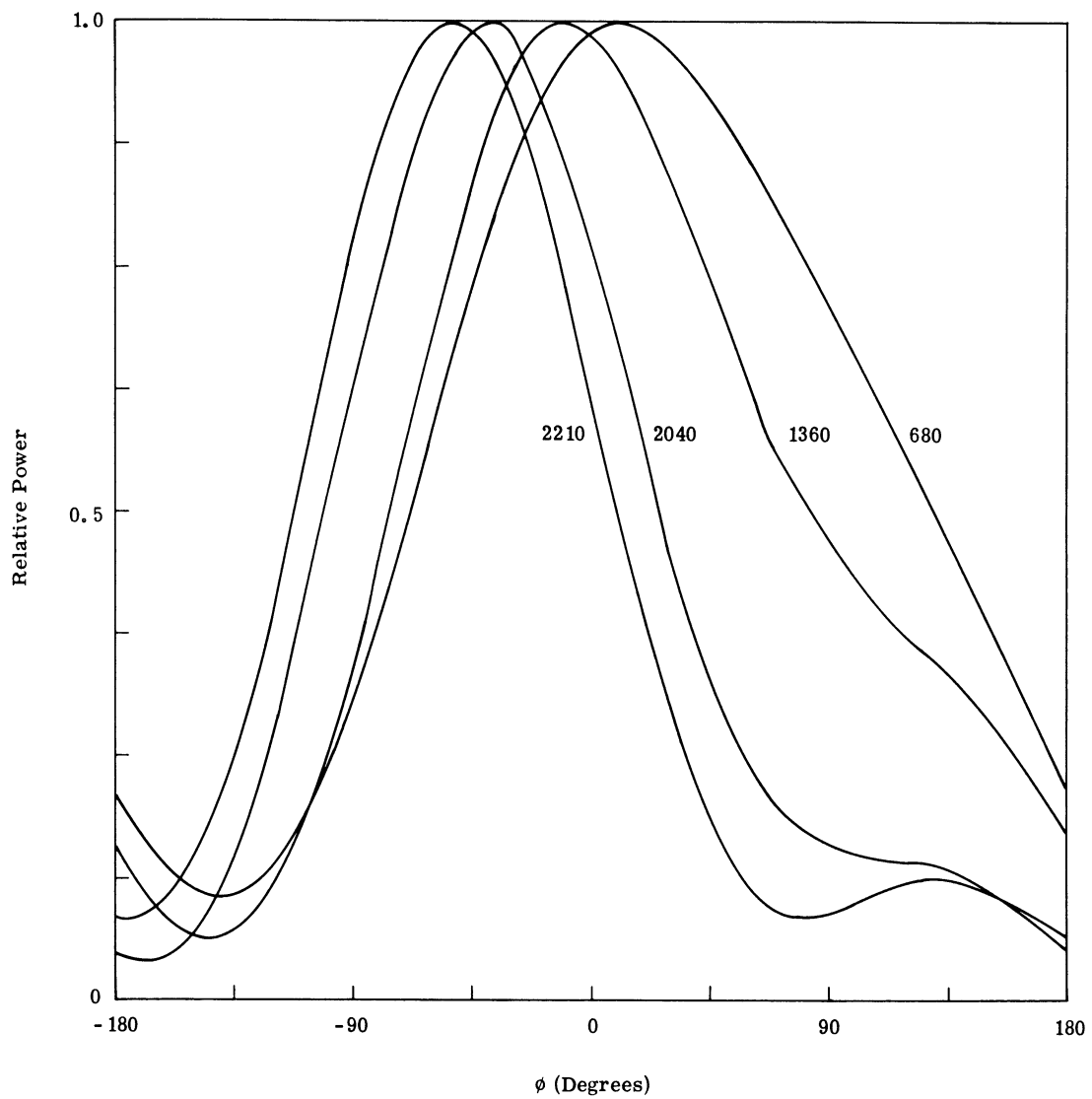


Fig. 2.9. (b) Far field scattering patterns showing variations with external field (oersteds). $\epsilon = 13$, $k_0 R = .786$.

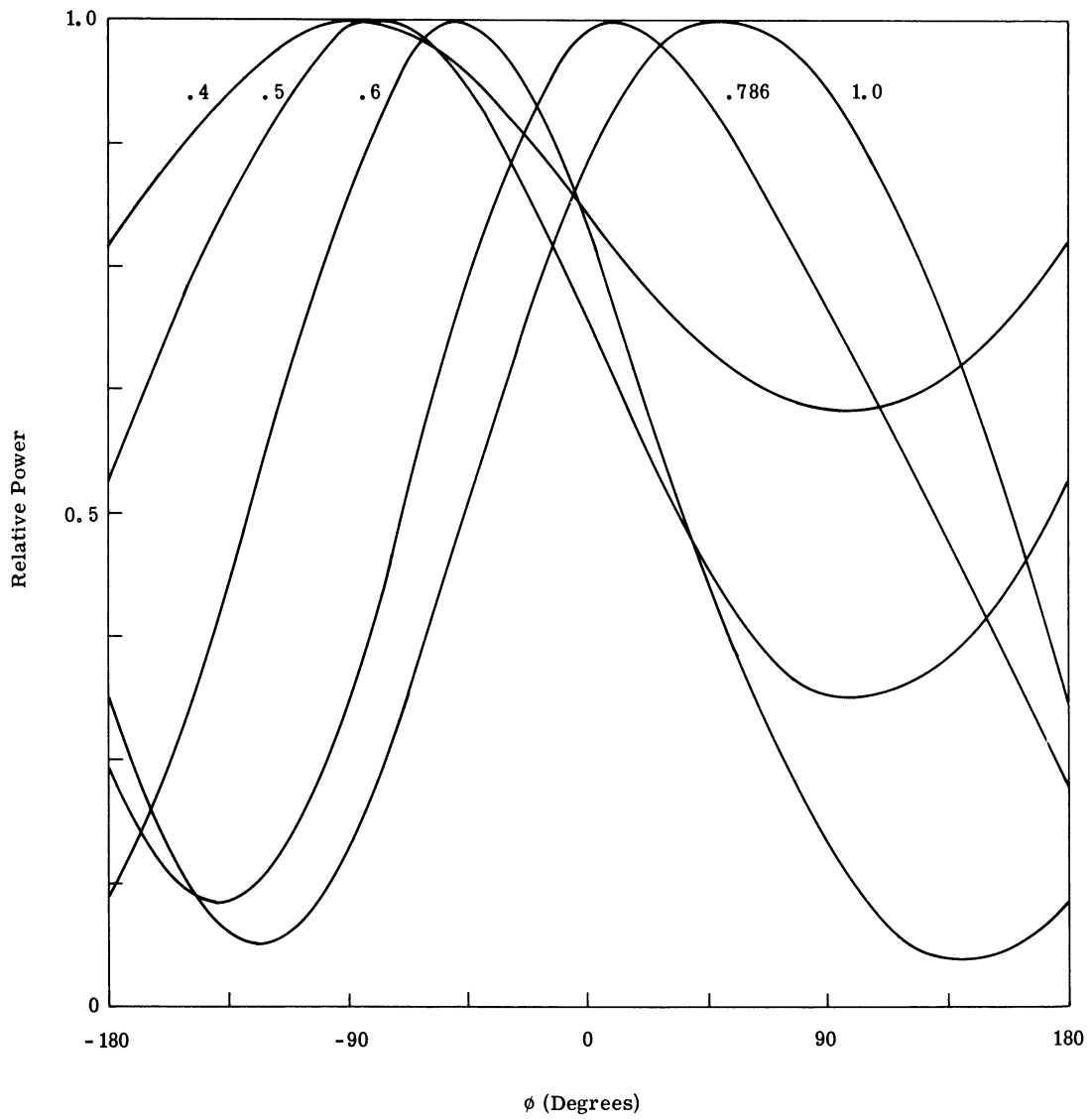


Fig. 2.10. Far field scattering patterns showing variations with k_0R (i. e., variations with radius). External field = 680 oersteds, $\epsilon = 13$.

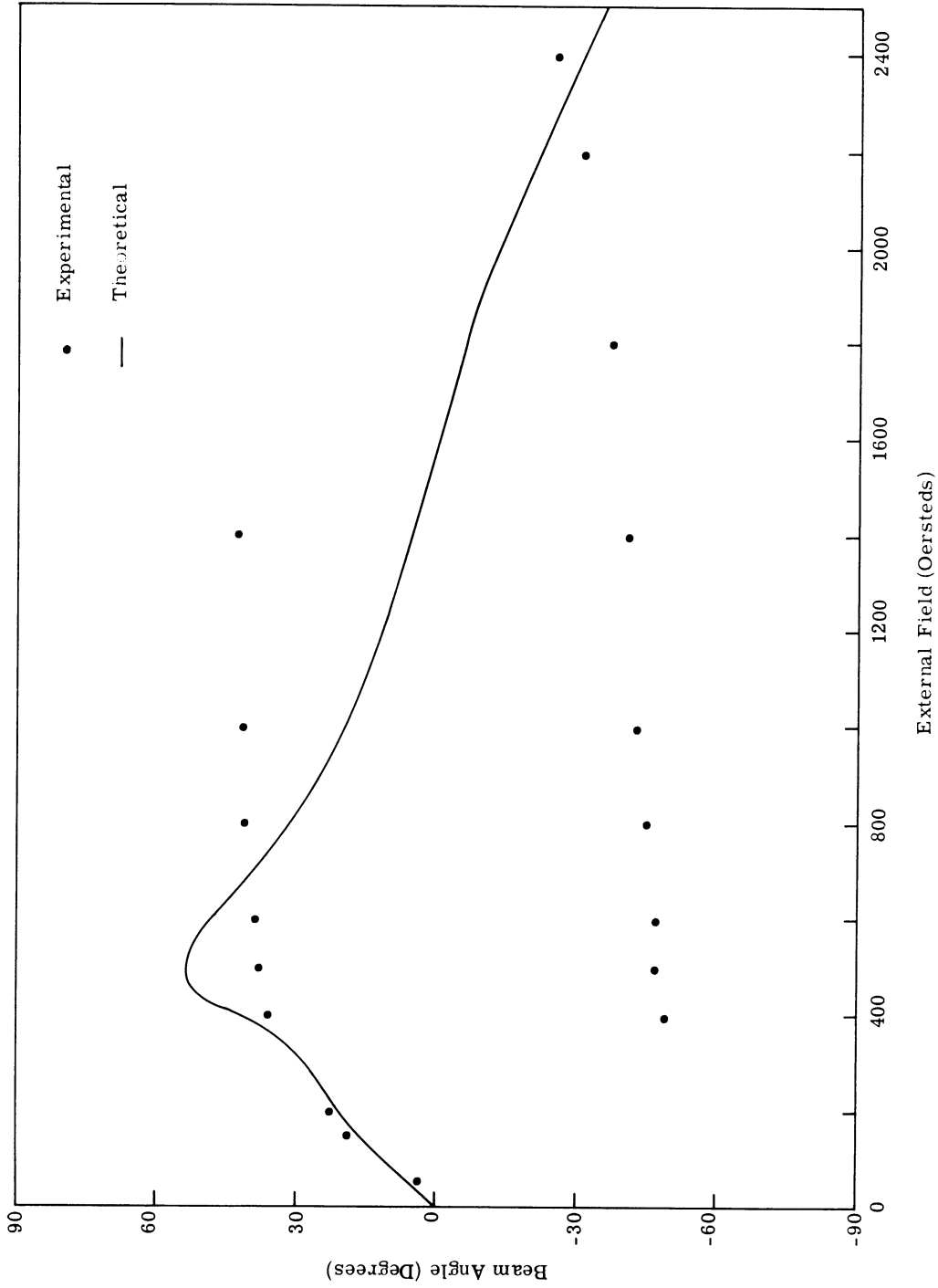


Fig. 2. 11. (a) Experimental and theoretical curves of beam angle vs. external field. Diameter = .295", $\epsilon = 13$, $k_0 R = .786$, $\alpha = 40.92^\circ$.

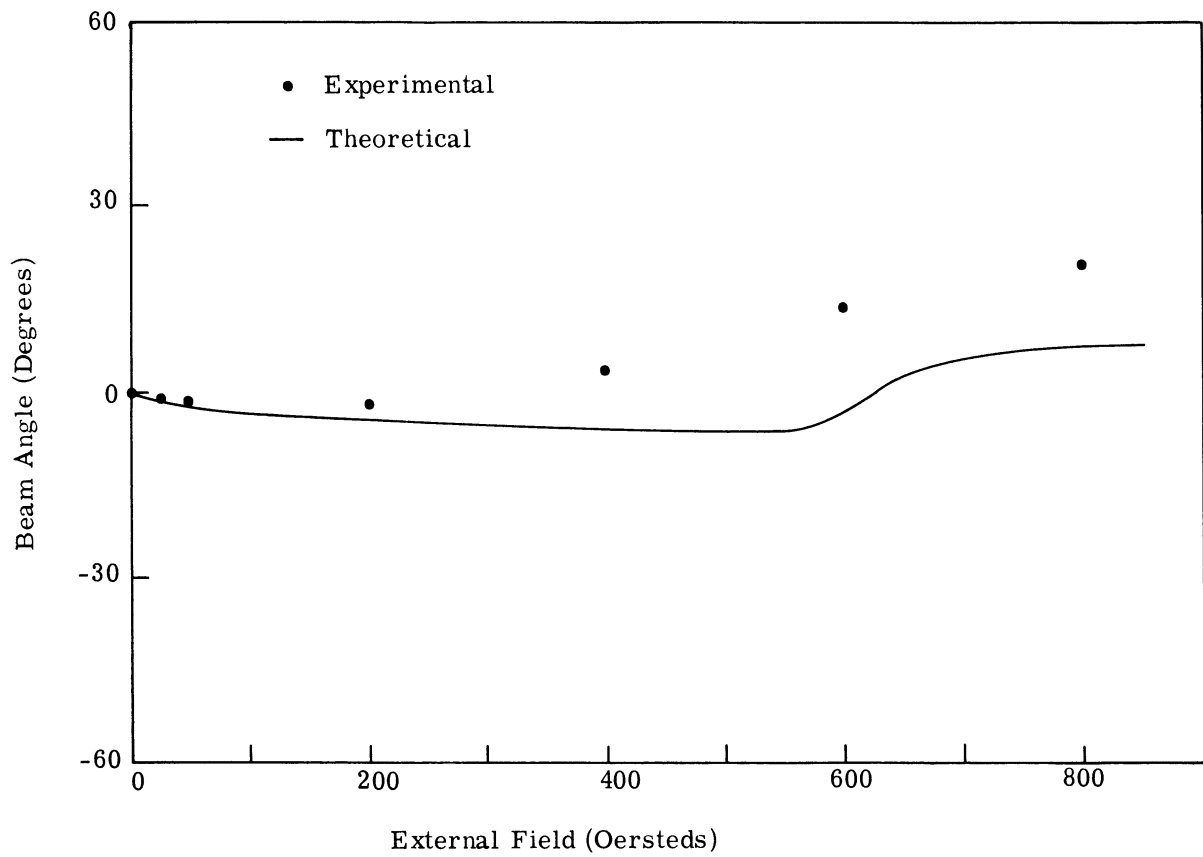


Fig. 2. 11. (b) Experimental and theoretical curves of beam angle vs. external field. Diameter = .295", $\epsilon = 13$, $k_0 R = 1.0$, $\alpha = 40.92^\circ$.

the energy is reflected back into the waveguide and again the simple model is insufficient to predict the observed result. This is confirmed by impedance measurements described in Chapter V, Sections 5.2 and 5.3. In Fig. 2.11(b) the correlation over the range of fields tested was better. It is concluded that the theory is valid when it predicts scattering in the forward direction with very little backscattering. Further analysis and discussion of the experimental data is given in Chapter V.

These last figures confirm the intuitive notion that the beam shift can be explained by the asymmetric scattering from an infinite cylinder. In addition, the theory and experiment agree in the region where the device is useful as a scanning antenna.

A mathematical basis now exists for the observed asymmetry in the far fields. The origin of this property can be investigated by calculating the fields inside the ferrite using (2.35) and (2.39). The results are shown in Fig. 2.12 for a particular set of parameters. The field displacement within the material is vividly shown. The contours of constant electric field intensity and phase are given. The two peaks in the electric field are approximately 180° out of phase and the line connecting them is at a 14° angle. This corresponds to the far field beam pattern, also shown in the figure, with a peak at 14° . On the basis of these data it is advanced that energy is directed by the mechanism of field displacement.

2.2.3 Application to Circulators. A three port junction type circulator was described in Chapter I. Its operation can be explained in terms of the asymmetrical scattering of radiation from a ferrite cylinder. For example, Fig. 2.9(a) shows a set of parameters that would provide a scattering angle of about 60° . An external field of 500 oersteds would redirect the field to the required port where the metallic boundary would then further guide the wave.

It is not to be assumed that this is the only mode possible or the only explanation. As shown experimentally by Davies,²⁰ several modes of operation exist which produce circulation. Little is known about the various modes although Bosma's article¹⁴ does examine some of them for the UHF stripline circulator. The optimum mode of operation has not yet been established.

On the basis of the patterns calculated from the infinite cylinder model, we

FREQ. = 10 GC
 DIA. = .297 "
 FIELD = 125 GAUSS
 MAT'L., MgMn FERRITE
 ——— MAGNITUDE
 - - - - PHASE

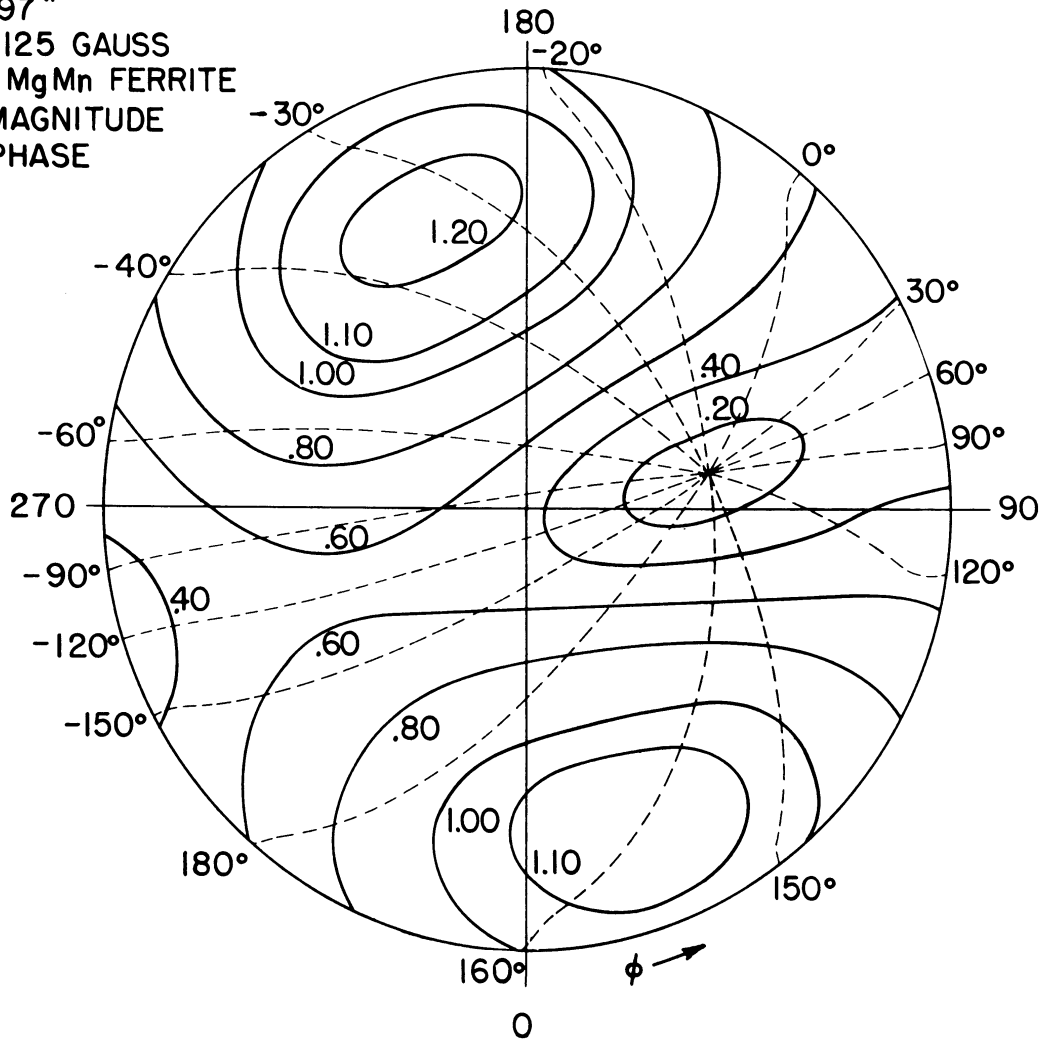


Fig. 2. 12. (a) Internal field distribution. Contours of constant electric field intensity.

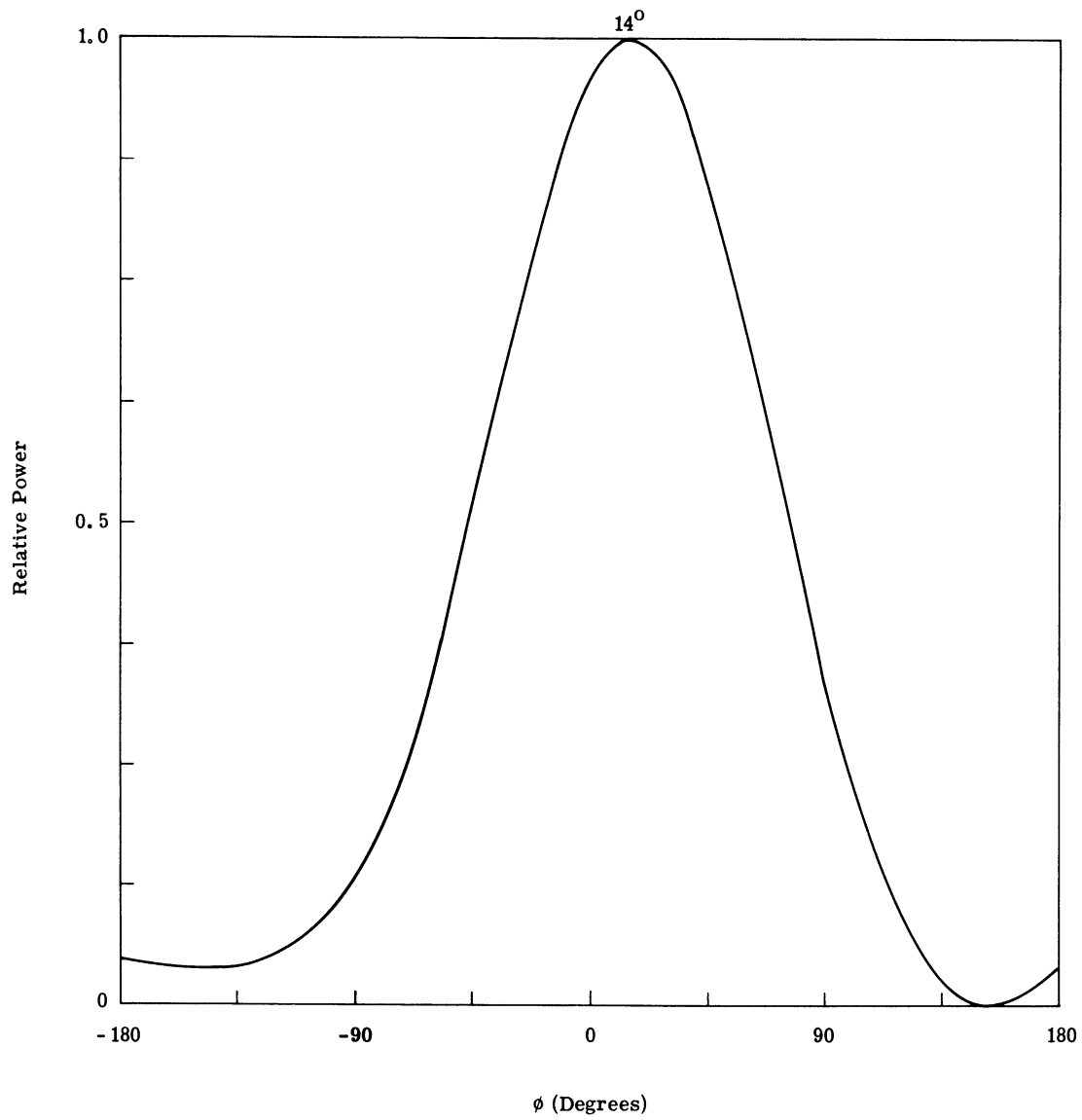


Fig. 2.12. (b) Far field distribution. Far field pattern corresponding to the internal field plot in Fig. 2.12(a).

postulate that one or more of the modes of circulation are caused by asymmetrical scattering (i. e. , field displacement). This model is useful because it gives an intuitively satisfying explanation of the circulator mechanism. Field displacement similar to that in Fig. 2. 12(a) can then be visualized for the 60° far field scattering angle required for circulator action. This is in agreement with the general result found by Bosma¹⁴ in his discussion of the strip-line y-junction circulator. He presented an approximate analysis that also showed the field displacement within the ferrite causing the circulation.

2.3 Conclusions

Initially, this chapter presented an analysis of plane wave scattering from a ferrite cylinder. Theoretical beam patterns showed the asymmetrical scattering controlled by the static magnetic field that motivated the application to electronic scanning. Two additional properties should be stressed that were necessary for the practical realization of the antenna. These were the single peaked characteristic patterns and the relatively large cross sections predicted by the theory. If the patterns were isotropic, there could be no beam shifting; while if there were more than one peak, extraneous lobes would appear in the antenna pattern. If the cross sections were low, then it would be difficult to couple energy from the incident wave into the ferrite. Thus, for a normalized cross section less than one the ferrite would have little effect on the beam pattern. Although from the presentation in the introduction the reader might have been convinced that the scanning application in the waveguide aperture could obviously be realized, this result was actually not obvious without the additional fortunate circumstance of these last two properties.

The physical realization of the antenna was presented as a finite ferrite post in the aperture of a rectangular waveguide. The relationship between this structure and the infinite cylinder problem was investigated with the result that a modification was made to account for the change in incident field. The theory, intending to predict and explain the antenna radiation properties in a single plane, can only be viewed as an approximation to the actual problem. The intuitively satisfying qualitative agreement and the reasonably satisfying quantitative agreement with the experiments make the analysis valuable. A similar field displacement within the ferrite will very likely be found even if a more exact analysis is performed.

CHAPTER III

REFLECTION COEFFICIENT OF A FERRITE OBSTACLE IN A WAVEGUIDE APERTURE

In addition to the radiation properties, the input impedance of the ferrite scanning antenna is also required. The reflection coefficient R_1 (essentially just another form of the impedance, Z) will be calculated in this chapter. The reflection coefficient and the impedance are related by the equation

$$Z = \frac{1 + R_1}{1 - R_1}$$

The major difficulties arising in the calculation of R_1 for the present configuration are the following:

1. The ferrite post is characterized by a tensor permeability. The permeability, given in (2.2), makes this an anisotropic problem. While a scalar solution could be obtained in the purely dielectric case,²¹ a vector solution with its attendant complexities is required here.
2. There are really two discontinuities present, the ferrite cylinder and the open aperture. In general, the "dual discontinuity" type problem has not received much attention in the literature. The ferrite obstacle interacts not only with the field incident from the source but also with the higher order modes created by the aperture discontinuity. In the method of solution used, the effects of the two discontinuities are separated as much as possible. It is assumed that the solution to the aperture discontinuity problem by itself is already known. Appendix B gives this solution.

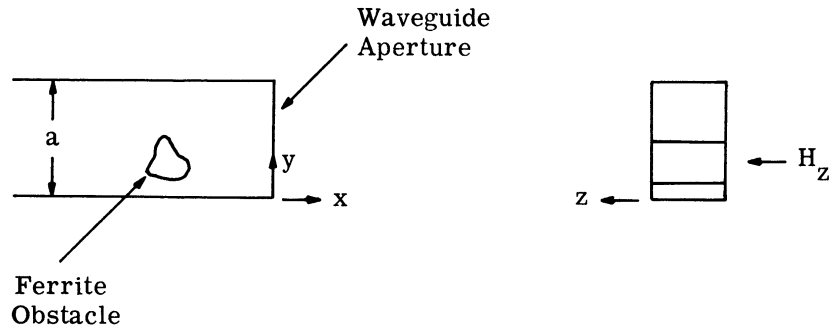


Fig. 3. 1. Cylindrical ferrite obstacle in a rectangular waveguide. The waveguide is terminated by the open aperture.

In addition to the reflection coefficient of the antenna, this chapter generalizes the method of solution presented to include other "dual discontinuity" problems. The degenerate case of a ferrite post in a matched waveguide is directly obtained from the results of the analysis and is also discussed.

3.1 The Variational Technique

For the derivation in this chapter the obstacle is assumed to lie wholly within the waveguide as shown in Fig. 3. 1. The material may be anywhere within the waveguide, however. The case where the obstacle lies partially outside the waveguide is treated in Appendix E. The obstacle is cylindrical (though not necessarily circularly cylindrical). The TE_{10} waveguide mode is incident on the discontinuity. It is assumed that there is no z -dependence in any of the fields inside the waveguide due to the symmetry of the geometrical configuration and the incident wave.

A brief study of the geometry involved reveals the complexity of the problem. Solving the differential equation and applying the boundary conditions seemed less advisable than attempting to formulate the problem in terms of its integral equation and then applying approximating techniques to evaluate the reflection coefficient. The variational method was chosen as the most suitable technique for doing this. This method was applied to a number of waveguide problems by Schwinger.²¹ In particular, he solved the problem of the dielectric cylinder in a matched waveguide. The technique is extended here to the case of an anisotropic cylinder in a loaded waveguide. In this procedure an integral expression is found for R_1 which depends on the fields within the ferrite obstacle and is stationary with respect to small changes of these fields about their true value. The trial fields used can be obtained

in several ways. An approximate solution can be used to derive the fields; an intelligent guess can be made of the fields; or the fields can be expanded in a complete set of functions characteristic of the obstacle and the property of stationarity applied. For example, for a cylinder, the trials fields can be written in a Fourier-Bessel expansion with unknown coefficients. The coefficients are then eliminated from the equation using the stationary property of the variational expression. This last procedure makes best use of the variational method, but for many problems cannot be fruitfully carried out because of the complexity of the results. In the problem presented here it is possible to carry out this procedure without too much difficulty.

The steps taken in the derivation of the variational expression for the reflection coefficient are:

1. Derive the wave equation.
2. Write an integral equation for the fields.
3. Derive the Green's function.
4. Find an exact expression for the reflection coefficient in terms of the fields.
5. Use the results of 2 and 4 to derive a variational expression for the reflection coefficient.

3.1.1 Wave Equation. For a region containing an anisotropic body, Maxwell's equations are:

$$\nabla \times \bar{\mathbf{E}} = - \frac{\partial \bar{\mathbf{B}}}{\partial t} \quad (3.1a)$$

$$\nabla \times \bar{\mathbf{H}} = \frac{\partial \bar{\mathbf{D}}}{\partial t} \quad (3.1b)$$

$$\nabla \cdot \bar{\mathbf{D}} = 0 \quad (3.1c)$$

$$\nabla \cdot \bar{\mathbf{B}} = 0 \quad (3.1d)$$

If the constitutive equations $\bar{\mathbf{B}} = \vec{\mu} \bar{\mathbf{H}}$, $\bar{\mathbf{D}} = \epsilon \bar{\mathbf{E}}$ are used and if $e^{j\omega t}$ time dependence is assumed, the first two of these equations become:

$$\nabla \times \bar{\mathbf{E}} = -j\omega \mu_0 \vec{\mu} \bar{\mathbf{H}} \quad (3.2)$$

$$\nabla \times \bar{\mathbf{H}} = j\omega \epsilon_0 \epsilon \bar{\mathbf{E}} \quad (3.3)$$

The wave equations, derived from these last two equations are then

$$\nabla \times \nabla \times \bar{\mathbf{E}} - k_0^2 \bar{\mathbf{E}} = k_0^2 \chi_e \bar{\mathbf{E}} - j\omega\mu_0 \nabla \times \vec{\chi}_m \bar{\mathbf{H}} \quad (3.4)$$

and

$$\nabla \times \nabla \times \bar{\mathbf{H}} - k_0^2 \bar{\mathbf{H}} = k_0^2 \chi_m \bar{\mathbf{H}} + j\omega\epsilon_0 \nabla \times \chi_e \bar{\mathbf{E}} \quad (3.5)$$

where

$$\vec{\mu} = (1 + \vec{\chi}_m) \quad (3.6a)$$

$$\epsilon = (1 + \chi_e) \quad (3.6b)$$

$$\vec{\chi}_m = \begin{bmatrix} \chi_m & -jk & 0 \\ jk & \chi_m & 0 \\ 0 & 0 & \chi_z \end{bmatrix} \quad (3.6c)$$

The reflection coefficient can be derived from either (3.4) or (3.5). We use (3.4) here. [The derivation using (3.5) is given in Chapter IV.]

Since $\nabla \cdot \bar{\mathbf{E}} = 0$, the substitution $\nabla \times \nabla \times \bar{\mathbf{E}} = -\nabla^2 \bar{\mathbf{E}} + \nabla \nabla \cdot \bar{\mathbf{E}}$ yields for each rectangular component of $\bar{\mathbf{E}}$,

$$\nabla^2 \bar{\mathbf{E}} + k_0^2 \bar{\mathbf{E}} = -(k_0^2 \chi_e \bar{\mathbf{E}} - j\omega\mu_0 \nabla \times \vec{\chi}_m \bar{\mathbf{H}}) \quad (3.7)$$

Now, let

$$\bar{\mathbf{J}} = k_0^2 \chi_e \bar{\mathbf{E}} - j\omega\mu_0 \nabla \times \vec{\chi}_m \bar{\mathbf{H}} \quad (3.8)$$

i. e., consider $\bar{\mathbf{J}}$ as a fictitious source. Then

$$\nabla^2 \bar{\mathbf{E}} + k_0^2 \bar{\mathbf{E}} = -\bar{\mathbf{J}} \quad (3.9)$$

3.1.2 Integral Equation. Now, introduce the dyadic Green's function as a solution to

$$\nabla^2 \bar{\mathbf{G}} + k_0^2 \bar{\mathbf{G}} = -\frac{1}{b} \bar{\mathbf{I}} \delta(x - x_0) \delta(y - y_0) \quad (3.10)$$

where δ is the Dirac delta function, and $\bar{\mathbf{I}}$ a unit dyadic.

Also, let $\vec{\bar{G}}$ have the same boundary conditions as the electric field $\vec{\bar{E}}$.

$$\begin{aligned} \vec{\bar{n}} \times \vec{\bar{G}} &= 0 \quad \text{on the waveguide walls, (see Appendix A for} \\ &\quad \text{a summary of dyadic operations) and} \\ \vec{\bar{G}} &\text{ is continuous at the waveguide aperture.} \\ \vec{\bar{n}} &\text{ is the unit vector normal to the waveguide} \\ &\quad \text{walls.} \end{aligned}$$

The components of the Green's function can be viewed here as the electric fields due to a line source of unit strength located at the point (x_o, y_o) in the absence of the ferrite obstacle. For the present case, let (x_o, y_o) be inside the waveguide. (Appendix E provides the extension to the case where the obstacle extends outside the waveguide.)

The solution to (3.9) can then be written,

$$\vec{\bar{E}} = \int \vec{\bar{G}}(\mathbf{r}|\mathbf{r}_o) \cdot \vec{\bar{J}}(\mathbf{r}_o) dv_o + \vec{\bar{E}}_o \quad (3.11)$$

where $\vec{\bar{E}}_o$ is the field present in the waveguide when the ferrite obstacle is absent. $\vec{\bar{E}}_o$ includes the incident electric field and the field reflected from the aperture and is a solution of the homogeneous wave equation. The letter \mathbf{r} represents the point (x, y) while \mathbf{r}_o represents (x_o, y_o) . The volume of integration encloses the obstacle as illustrated in Fig. 3.2. The volume of integration must enclose the obstacle. It may be bounded by any surface such as the waveguide side walls and reference planes at each end of the waveguide, or a surface just outside and enclosing the ferrite obstacle. The resulting integrations are identical since there are no sources in the region outside the ferrite.

That (3.11) is a solution to (3.9) can be proven by substituting (3.11) for $\vec{\bar{E}}$ into (3.9).

$$\begin{aligned} \nabla^2 \vec{\bar{E}} + k_o^2 \vec{\bar{E}} &= \int (\nabla^2 + k_o^2) \vec{\bar{G}}(\mathbf{r}|\mathbf{r}_o) \cdot \vec{\bar{J}}(\mathbf{r}_o) dv_o + (\nabla^2 + k_o^2) \vec{\bar{E}}_o \\ &= - \int \frac{1}{b} \delta(x - x_o) \delta(y - y_o) \vec{\bar{I}} \cdot \vec{\bar{J}}(\mathbf{r}_o) dv_o + 0 \\ &= -\vec{\bar{J}}(\mathbf{r}) \end{aligned}$$

3.1.3 Green's Function. If the TE_{10} mode is the incident field, only a z-com-

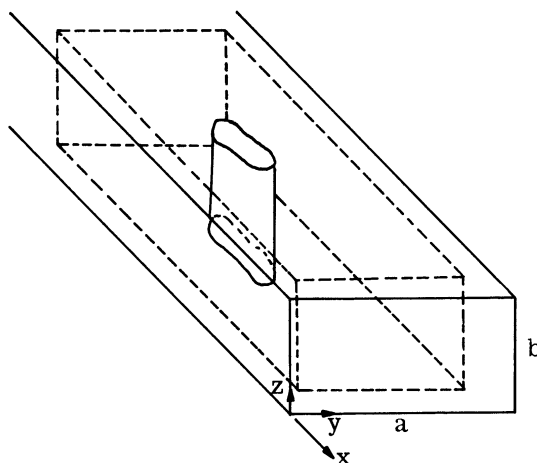


Fig. 3.2. Volume of integration for (3.11). The volume enclosed within the dotted lines is the required region of integration.

ponent of the electric field appears in the waveguide. Due to the symmetry of the problem, only TE_{n0} modes are assumed to be excited by the obstacle and aperture. Thus, \bar{J} has only a z-component, and the only component of \bar{G} required is the $a_z a_z$ term.

The solution for the required component of the Green's function in (3.10) for the case of the perfectly matched waveguide is given by:²²

$$G_{zz} = \sum_{n=1}^{\infty} \frac{\sin \frac{n\pi y}{a} \sin \frac{n\pi y_0}{a} e^{-\gamma_n |x-x_0|}}{\gamma_n ab}$$

where:

$$\gamma_n^2 = (n\pi/a)^2 - k_0^2.$$

In the present case, a term must be added to this to account for the reflections at the aperture ($x=0$). Since G_{zz} is an electric field, the total Green's function in the region $x < 0$ can be written down immediately as

$$G_{zz} = \sum_{n=1}^{\infty} \frac{\sin \frac{n\pi y}{a} \sin \frac{n\pi y_0}{a} e^{-\gamma_n |x-x_0|}}{\gamma_n ab} + \sum_{n=1}^{\infty} \sum_{m=1}^{\infty} \frac{R_{nm}}{\gamma_n ab} \sin \frac{n\pi y_0}{a} e^{\gamma_n x_0} \sin \frac{m\pi y}{a} e^{\gamma_m x} \quad (3.12)$$

R_{nn} is the reflection coefficient when the TE_{no} mode is incident on the aperture, and will be called the self-reflection coefficient.

R_{nm} ($n \neq m$) is the coupling coefficient to the TE_{mo} mode when the TE_{no} mode is incident. Both R_{nn} and R_{nm} are assumed to be known. (See Appendix B for their calculation.)

The interpretation of (3.12) is that the line source at (x_o, y_o) , oriented in the z -direction, gives rise to an infinite number of TE_{no} modes. Each of these modes, upon reflection at the aperture, excites an infinite number of TE_{mo} modes. In deriving the Green's function, the ferrite post has not yet been introduced into the waveguide.

Reciprocity is given by²²

$$\vec{G}(r|r_o) = \vec{G}(r_o|r) \quad (3.13)$$

where \sim means transpose.

In the present case, G_{zz} must satisfy

$$G_{zz}(r|r_o) = G_{zz}(r_o|r)$$

Using this relation in (3.12) gives:

$$\frac{R_{mn}}{\gamma_m} = \frac{R_{nm}}{\gamma_n} \quad (3.14)$$

This is a useful relationship relating the coupling coefficients.

3.1.4 Reflection Coefficient. \vec{E}_o , the field in the waveguide when the ferrite obstacle is absent, can be written

$$\vec{E}_o = \left[\sin \frac{\pi y}{a} e^{-\gamma_1 x} + \sum_{n=1}^{\infty} R_{1n} \sin \frac{n\pi y}{a} e^{\gamma_n x} \right] \vec{a}_z \quad (3.15)$$

The electric field \vec{E} , the field in the waveguide with the obstacle present, can be written

$$\vec{E} = \left[\sin \frac{\pi y}{a} e^{-\gamma_1 x} + \sum_{n=1}^{\infty} R_n \sin \frac{n\pi y}{a} e^{\gamma_n x} \right] \vec{a}_z \quad (3.16)$$

The first term is the incident electric field. The R_{1n} terms are assumed known (see Appendix B). R_1 is the reflection coefficient of the combined ferrite and aperture with the TE_{10} mode incident and is the desired quantity. R_1 is referred to the plane $x = 0$, although the ferrite obstacle may be anywhere in the waveguide.

Now, assume only the TE_{10} mode propagates in the waveguide (all other modes being beyond cutoff), and evaluate (3.11) for the electric field as $x \rightarrow -\infty$. The result is

$$R_1 = R_{11} + \frac{1}{ab\gamma_1} \int \bar{E}_o(r_o) \cdot \bar{J}(r_o) dv_o \quad (3.17)$$

This is the desired quantity. The reflection coefficient of a ferrite obstacle and aperture is given by the reflection coefficient of the aperture alone plus an integral of the field present when the ferrite is absent and the field present with the ferrite. In Appendix E it is shown that this equation is valid even if the ferrite obstacle extends partly outside the aperture into the free space region.

Consideration of the manner in which (3.17) was derived shows that it is valid for a ferrite obstacle with any additional discontinuity at $x = 0$ that excites only TE_{n0} modes. The simplest case, of course, occurs when the waveguide is terminated at $x = 0$ with a matched load so that all the coefficients (R_{nn} , R_{nm}) are zero.

3.1.5 Variational Formulation for the Reflection Coefficient. An exact expression for R_1 is given by (3.17). In order to solve for it, however, the fields inside the ferrite obstacle would be required. In principle these could be found from the integral equation (3.11), but this is a difficult problem. Thus, an expression for R_1 is sought which is stationary with respect to small changes in the true value of the fields.

Let \bar{E}_2 , \bar{H}_2 be the fields present when the direction of the dc magnetic field is reversed. For this case the permeability tensor is given by

$$\bar{\chi}_{m_2} = \begin{bmatrix} \chi_m & jk & 0 \\ -jk & \chi_m & 0 \\ 0 & 0 & \chi_z \end{bmatrix} \quad (3.18)$$

i. e. , $\bar{\chi}_{m_2} = \bar{\chi}_m$.

The wave equation for these fields is

$$\nabla^2 \bar{\mathbf{E}}_2 + k_o^2 \bar{\mathbf{E}}_2 = -\bar{\mathbf{J}}_2 \quad (3.19)$$

where

$$\bar{\mathbf{J}}_2 = k_o^2 \chi_e \bar{\mathbf{E}}_2 - j\omega\mu_o \nabla \times \bar{\chi}_{m_2} \bar{\mathbf{H}}_2 \quad (3.20)$$

The steps taken to obtain (3.17) for the reflection coefficient are repeated to obtain

$$\bar{\mathbf{E}}_2 = \int \bar{\mathbf{G}}(\mathbf{r}|\mathbf{r}_o) \cdot \bar{\mathbf{J}}_2(\mathbf{r}_o) dv_o + \bar{\mathbf{E}}_o \quad (3.21)$$

and

$$R_1^{(2)} = R_{11} + \frac{1}{ab\gamma_1} \int \bar{\mathbf{E}}_o(\mathbf{r}_o) \cdot \bar{\mathbf{J}}_2(\mathbf{r}_o) dv_o \quad (3.22)$$

This is the reflection coefficient obtained when the dc magnetic field is reversed. It will now be shown that $R_1^{(2)} = R_1$, i. e., the reflection coefficient is unchanged when the bias field is reversed. (This statement agrees with the more general results given by Harrington and Villeneuve.²³) Multiply (3.11) by $\bar{\mathbf{J}}_2$ and (3.21) by $\bar{\mathbf{J}}$ and integrate over the volume dv .

This gives

$$\int \bar{\mathbf{E}}_o(\mathbf{r}) \cdot \bar{\mathbf{J}}_2(\mathbf{r}) dv = \int \bar{\mathbf{E}}(\mathbf{r}) \cdot \bar{\mathbf{J}}_2(\mathbf{r}) dv - \int \int \bar{\mathbf{J}}_2(\mathbf{r}) \cdot \bar{\mathbf{G}}(\mathbf{r}|\mathbf{r}_o) \cdot \bar{\mathbf{J}}(\mathbf{r}_o) dv_o dv \quad (3.23a)$$

$$\int \bar{\mathbf{E}}_o(\mathbf{r}) \cdot \bar{\mathbf{J}}(\mathbf{r}) dv = \int \bar{\mathbf{E}}_2(\mathbf{r}) \cdot \bar{\mathbf{J}}(\mathbf{r}) dv - \int \int \bar{\mathbf{J}}(\mathbf{r}) \cdot \bar{\mathbf{G}}(\mathbf{r}|\mathbf{r}_o) \cdot \bar{\mathbf{J}}_2(\mathbf{r}_o) dv_o dv \quad (3.23b)$$

Interchanging the variables of integration, and using reciprocity (3.13) shows that,

$$\begin{aligned} & \int \int \bar{\mathbf{J}}_2(\mathbf{r}) \cdot \bar{\mathbf{G}}(\mathbf{r}|\mathbf{r}_o) \cdot \bar{\mathbf{J}}(\mathbf{r}_o) dv_o dv \\ &= \int \int \bar{\mathbf{J}}_2(\mathbf{r}_o) \cdot \tilde{\bar{\mathbf{G}}}(\mathbf{r}|\mathbf{r}_o) \cdot \bar{\mathbf{J}}(\mathbf{r}) dv_o dv \\ &= \int \int \bar{\mathbf{J}}(\mathbf{r}) \cdot \bar{\mathbf{G}}(\mathbf{r}|\mathbf{r}_o) \cdot \bar{\mathbf{J}}_2(\mathbf{r}_o) dv_o dv \end{aligned} \quad (3.24)$$

Thus, the double integral terms in (3.23a) and (3.23b) are equal. Expanding the single integral term in (3.23a) gives

$$\int \bar{\mathbf{E}}(\mathbf{r}) \cdot \bar{\mathbf{J}}_2(\mathbf{r}) dv = \int k_o^2 \chi_e \bar{\mathbf{E}} \cdot \bar{\mathbf{E}}_2 dv - j\omega\mu_o \int \bar{\mathbf{E}} \cdot \nabla \times \bar{\chi}_{m_2} \bar{\mathbf{H}}_2 dv$$

Using the identity $\bar{\mathbf{A}} \cdot \nabla \times \bar{\mathbf{B}} = \bar{\mathbf{B}} \cdot \nabla \times \bar{\mathbf{A}} - \nabla \cdot (\bar{\mathbf{A}} \times \bar{\mathbf{B}})$ on the second term gives

$$\int \bar{\mathbf{E}} \cdot \nabla \times \vec{\chi}_{m_2} \bar{\mathbf{H}}_2 \, dv = \int \vec{\chi}_{m_2} \bar{\mathbf{H}}_2 \cdot \nabla \times \bar{\mathbf{E}} \, dv - \int \nabla \cdot (\bar{\mathbf{E}} \times \vec{\chi}_{m_2} \bar{\mathbf{H}}_2) \, dv$$

The divergence theorem then shows that

$$\int \nabla \cdot (\bar{\mathbf{E}} \times \vec{\chi}_{m_2} \bar{\mathbf{H}}_2) \, dv = \int (\bar{\mathbf{E}} \times \vec{\chi}_{m_2} \bar{\mathbf{H}}_2) \cdot \bar{\mathbf{n}} \, ds$$

where $\bar{\mathbf{n}}$ is the outward normal to the surface ds (see Fig. 3.2). The integral is zero over the surfaces outside the ferrite since $\vec{\chi}_m$ is zero in these regions. The integral is zero over the top and bottom walls where $\bar{\mathbf{n}} = \pm \bar{\mathbf{a}}_z$, since $\pm \bar{\mathbf{a}}_z \cdot \bar{\mathbf{E}} \times \vec{\chi}_{m_2} \bar{\mathbf{H}}_2 = 0$ (recalling that $\bar{\mathbf{E}}$ has only a z -component). Thus,

$$\begin{aligned} \int \bar{\mathbf{E}} \cdot \nabla \times \vec{\chi}_{m_2} \bar{\mathbf{H}}_2 \, dv &= \int \vec{\chi}_{m_2} \bar{\mathbf{H}}_2 \cdot \nabla \times \bar{\mathbf{E}} \, dv \\ &= \int \vec{\chi}_{m_2} \bar{\mathbf{H}}_2 \cdot (-j\omega\mu_0 \vec{\mu} \bar{\mathbf{H}}) \, dv \end{aligned}$$

Now

$$\begin{aligned} \vec{\chi}_{m_2} \bar{\mathbf{H}}_2 \cdot \vec{\mu} \bar{\mathbf{H}} &= \tilde{\tilde{\mathbf{H}}}_2 \tilde{\tilde{\chi}}_{m_2} \cdot \vec{\mu} \bar{\mathbf{H}} = \tilde{\tilde{\mathbf{H}}}_2 \vec{\chi}_m \cdot \vec{\mu} \bar{\mathbf{H}} \\ &= \tilde{\tilde{\mathbf{H}}}_2 \vec{\mu} \cdot \vec{\chi}_m \bar{\mathbf{H}} = \tilde{\tilde{\mu}} \bar{\mathbf{H}}_2 \cdot \vec{\chi}_m \bar{\mathbf{H}} = \vec{\mu}_2 \bar{\mathbf{H}}_2 \cdot \vec{\chi}_m \bar{\mathbf{H}} \end{aligned}$$

Thus

$$\vec{\chi}_{m_2} \bar{\mathbf{H}}_2 \cdot \nabla \times \bar{\mathbf{E}} = \vec{\chi}_m \bar{\mathbf{H}} \cdot \nabla \times \bar{\mathbf{E}}_2$$

So that, using the divergence theorem again gives

$$\int \bar{\mathbf{E}} \cdot \nabla \times \vec{\chi}_{m_2} \bar{\mathbf{H}}_2 \, dv = \int \vec{\chi}_m \bar{\mathbf{H}} \cdot \nabla \times \bar{\mathbf{E}}_2 \, dv = \int \bar{\mathbf{E}}_2 \cdot \nabla \times \vec{\chi}_m \bar{\mathbf{H}} \, dv$$

Then

$$\begin{aligned} \int \bar{\mathbf{E}}(\mathbf{r}) \cdot \bar{\mathbf{J}}_2(\mathbf{r}) \, dv &= \int \bar{\mathbf{E}}_2 \cdot [\mathbf{k}_0^2 \chi_e \bar{\mathbf{E}} - j\omega\mu_0 \nabla \times \vec{\chi}_m \bar{\mathbf{H}}] \, dv \\ &= \int \bar{\mathbf{E}}_2(\mathbf{r}) \cdot \bar{\mathbf{J}}(\mathbf{r}) \, dv \end{aligned} \tag{3.25}$$

Thus proving that

$$\int \bar{\mathbf{E}}_0 \cdot \bar{\mathbf{J}}_2 \, dv = \int \bar{\mathbf{E}}_0 \cdot \bar{\mathbf{J}} \, dv \quad (3.26)$$

and, by (3.22) and (3.17)

$$R_1^{(2)} = R_1 \quad (3.27)$$

To form the variational expression, multiply (3.11) through by \mathbf{J}_2 and integrate over the volume dv .

$$\int \bar{\mathbf{E}}_0 \cdot \bar{\mathbf{J}}_2 \, dv = \int \bar{\mathbf{E}} \cdot \bar{\mathbf{J}}_2 \, dv - \int \int \bar{\mathbf{J}}_2(\mathbf{r}) \cdot \bar{\mathbf{G}}(\mathbf{r}|\mathbf{r}_0) \cdot \bar{\mathbf{J}}(\mathbf{r}_0) \, dv_0 \, dv$$

Next, divide this expression by (3.17) and (3.22) and invert to give

$$R_1 - R_{11} = \frac{\frac{1}{ab\gamma_1} \int \bar{\mathbf{E}}_0 \cdot \bar{\mathbf{J}} \, dv \int \bar{\mathbf{E}}_0 \cdot \bar{\mathbf{J}}_2 \, dv}{\int \bar{\mathbf{E}} \cdot \bar{\mathbf{J}}_2 \, dv - \int \int \bar{\mathbf{J}}_2(\mathbf{r}) \cdot \bar{\mathbf{G}}(\mathbf{r}|\mathbf{r}_0) \cdot \bar{\mathbf{J}}(\mathbf{r}_0) \, dv_0 \, dv} \quad (3.28)$$

This is an expression for $R_1 - R_{11}$ which is stationary with respect to variations in the functional form of $\bar{\mathbf{E}}$ and $\bar{\mathbf{E}}_2$. We can let $\delta\bar{\mathbf{E}}$ and $\delta\bar{\mathbf{E}}_2$ be these variations. Then, if we denote $\bar{\mathbf{E}}_c$ and $\bar{\mathbf{E}}_{c2}$ as the correct values of $\bar{\mathbf{E}}$ and $\bar{\mathbf{E}}_2$, we obtain $\bar{\mathbf{E}} = \bar{\mathbf{E}}_c + \delta\bar{\mathbf{E}}$ and $\bar{\mathbf{E}}_2 = \bar{\mathbf{E}}_{c2} + \delta\bar{\mathbf{E}}_2$. Since $\bar{\mathbf{J}}$ and $\bar{\mathbf{J}}_2$ are functions of $\bar{\mathbf{E}}$ and $\bar{\mathbf{E}}_2$, they have variations (corresponding to changes in $\bar{\mathbf{E}}$ and $\bar{\mathbf{E}}_2$) which we may write as $\delta\bar{\mathbf{J}}$ and $\delta\bar{\mathbf{J}}_2$. The proof of stationarity follows:

In (3.28) let $\bar{\mathbf{E}}$, $\bar{\mathbf{J}}$ be constant and let $\bar{\mathbf{E}}_2 = \bar{\mathbf{E}}_{c2} + \delta\bar{\mathbf{E}}_2$ (or equivalently, $\bar{\mathbf{J}}_2 = \bar{\mathbf{J}}_{c2} + \delta\bar{\mathbf{J}}_2$). Then, we obtain

$$\begin{aligned} \delta(R_1 - R_{11}) & \left[\int \bar{\mathbf{E}} \cdot \bar{\mathbf{J}}_2 \, dv - \int \int \bar{\mathbf{J}}_2(\mathbf{r}) \cdot \bar{\mathbf{G}}(\mathbf{r}|\mathbf{r}_0) \cdot \bar{\mathbf{J}}(\mathbf{r}_0) \, dv_0 \, dv \right] \\ & + (R_1 - R_{11}) \left[\int \bar{\mathbf{E}} \cdot \delta\bar{\mathbf{J}}_2 \, dv - \int \int \delta\bar{\mathbf{J}}_2(\mathbf{r}) \cdot \bar{\mathbf{G}}(\mathbf{r}|\mathbf{r}_0) \cdot \bar{\mathbf{J}}(\mathbf{r}_0) \, dv_0 \, dv \right] \\ & - \frac{1}{ab\gamma_1} \int \bar{\mathbf{E}}_0 \cdot \bar{\mathbf{J}} \, dv \int \bar{\mathbf{E}}_0 \cdot \delta\bar{\mathbf{J}}_2 \, dv = 0 \end{aligned}$$

Using (3.17) gives

$$\begin{aligned} & \delta(R_1 - R_{11}) \left[\int \bar{\mathbf{E}} \cdot \bar{\mathbf{J}}_2 \, dv - \int \int \bar{\mathbf{J}}_2(\mathbf{r}) \cdot \bar{\mathbf{G}}(\mathbf{r}|\mathbf{r}_o) \cdot \bar{\mathbf{J}}(\mathbf{r}_o) \, dv_o \, dv \right] \\ & + (R_1 - R_{11}) \left[\int \delta \bar{\mathbf{J}}_2 \cdot (\bar{\mathbf{E}} - \int \bar{\mathbf{G}}(\mathbf{r}|\mathbf{r}_o) \cdot \bar{\mathbf{J}}(\mathbf{r}_o) \, dv_o - \bar{\mathbf{E}}_o) \, dv \right] = 0 \quad (3.29) \end{aligned}$$

The integrand of the second term is zero by (3.11). The multiplier of $\delta(R_1 - R_{11})$ is just

$$\int \bar{\mathbf{J}}_2(\mathbf{r}) \cdot \left[\bar{\mathbf{E}}(\mathbf{r}) - \int \bar{\mathbf{G}}(\mathbf{r}|\mathbf{r}_o) \cdot \bar{\mathbf{J}}(\mathbf{r}_o) \, dv_o \right] \, dv$$

which, by (3.11) and (3.17) is equal to

$$\int \bar{\mathbf{J}}_2(\mathbf{r}) \cdot \bar{\mathbf{E}}_o \, dv = ab\gamma_1 (R_1 - R_{11})$$

This is zero only if $R_1 = R_{11}$.

Thus $\delta(R_1 - R_{11})$ is zero (except for the case $R_1 = R_{11}$), and $R_1 - R_{11}$ is stationary with respect to changes in $\bar{\mathbf{E}}_2$ (or $\bar{\mathbf{J}}_2$).

Similarly we can let $\bar{\mathbf{E}}$ (or \mathbf{J}) vary in (3.28). Using (3.25) results in

$$\begin{aligned} & \delta(R_1 - R_{11}) \left[\int \bar{\mathbf{E}} \cdot \bar{\mathbf{J}}_2 \, dv - \int \int \bar{\mathbf{J}}_2(\mathbf{r}) \cdot \bar{\mathbf{G}}(\mathbf{r}|\mathbf{r}_o) \cdot \bar{\mathbf{J}}(\mathbf{r}_o) \, dv_o \, dv \right] \\ & + (R_1 - R_{11}) \left[\int \bar{\mathbf{E}}_2 \cdot \delta \bar{\mathbf{J}} \, dv - \int \int \bar{\mathbf{J}}_2(\mathbf{r}) \cdot \bar{\mathbf{G}}(\mathbf{r}|\mathbf{r}_o) \cdot \delta \bar{\mathbf{J}}(\mathbf{r}_o) \, dv_o \, dv \right] \\ & - \frac{1}{ab\gamma_1} \int \bar{\mathbf{E}}_o \cdot \delta \bar{\mathbf{J}} \, dv \int \bar{\mathbf{E}}_o \cdot \bar{\mathbf{J}}_2 \, dv = 0 \end{aligned}$$

By an argument similar to that used in deriving (3.34) and (3.29) we obtain

$$\begin{aligned} & \delta(R_1 - R_{11}) \left[\int \bar{\mathbf{E}} \cdot \bar{\mathbf{J}}_2 \, dv - \int \int \bar{\mathbf{J}}_2(\mathbf{r}) \cdot \bar{\mathbf{G}}(\mathbf{r}|\mathbf{r}_o) \cdot \bar{\mathbf{J}}(\mathbf{r}_o) \, dv_o \, dv \right] \\ & + (R_1 - R_{11}) \left\{ \int \delta \bar{\mathbf{J}} \cdot \left[\bar{\mathbf{E}}_2 - \int \bar{\mathbf{G}}(\mathbf{r}|\mathbf{r}_o) \cdot \bar{\mathbf{J}}_2(\mathbf{r}_o) \, dv_o - \bar{\mathbf{E}}_o \right] \, dv \right\} = 0 \quad (3.30) \end{aligned}$$

The integrand of the second term is zero by (3.21). Thus, $R_1 - R_{11}$ as given by (3.28) is stationary with respect to changes in $\bar{\mathbf{E}}$ (or $\bar{\mathbf{J}}$).

Hauser¹¹ derived a variational equation comparable to (3.28) but with several differences. He obtained an expression for the reflection coefficient of an anisotropic obstacle of arbitrary shape but in a matched waveguide (i. e., with no additional discontinuity such as the aperture). Also in his variational expression, instead of using the fields present when the static magnetic field was reversed, he used the adjoint fields. The most

important practical difference between the two formulations was Hauser's explicit inclusion of the magnetic fields. In (3.28) \bar{E}_0 , \bar{E} , \bar{J} , \bar{J}_2 and \bar{G} each have only a single component. Thus (3.28) can be easily reduced to a scalar equation. On the other hand Hauser's equation contains the magnetic field (which has two components) and the magnetic Green's function (a dyadic with four nonzero components as shown in Chapter IV). Products of these terms are much more difficult to manipulate than the simple dot products in (3.28).

3.2 Evaluation of Reflection Coefficient

The variational expression (3.28) is still a formidable equation from which to obtain numerical results. The usefulness of any expression is dependent on the amount of information that can be obtained from it. If (3.28) could not be simplified it might be of little use. Fortunately, for the special cases to be treated, the equation can be reduced to simpler forms, the variational property can be applied and numerical results obtained.

We will first reduce the volume integrals of (3.28) to line integrals.

From (3.9)

$$\nabla^2 \bar{E} + k_0^2 \bar{E} = -\bar{J}$$

and we know that

$$\nabla^2 \bar{E}_0 + k_0^2 \bar{E}_0 = 0$$

Multiply the first equation by \bar{E}_0 and the second by \bar{E} and subtract

$$\bar{E}_0 \cdot \nabla^2 \bar{E} - \bar{E} \cdot \nabla^2 \bar{E}_0 = -\bar{E}_0 \cdot \bar{J}$$

Since \bar{E}_0 , \bar{E} and \bar{J} have only a z-component, this can be written as the scalar equation

$$E_0 \nabla^2 E - E \nabla^2 E_0 = -E_0 J$$

Then use the identity $u \nabla \cdot \vec{A} = \nabla \cdot u\vec{A} - \nabla u \cdot \vec{A}$ on

$$E_0 \nabla^2 E = E_0 \nabla \cdot (\nabla E)$$

and

$$E \nabla^2 E_0 = E \nabla \cdot (\nabla E_0)$$

to obtain

$$\nabla \cdot (E \nabla E_0 - E_0 \nabla E) = E_0 J$$

Integrate over dv , and use the divergence theorem to obtain the first term in the numerator of (3.28).

$$\int \bar{\mathbf{E}}_0 \cdot \bar{\mathbf{J}} \, dv = \int (\mathbf{E} \nabla \mathbf{E}_0 - \mathbf{E}_0 \nabla \mathbf{E}) \cdot \bar{\mathbf{n}} \, ds \quad (3.31)$$

where $\bar{\mathbf{n}}$ is the outward normal to the surface. The surface of integration is outside the ferrite obstacle (see Fig. 3.3).

Similarly, the second term in the numerator of (3.28) is

$$\int \bar{\mathbf{E}}_0 \cdot \bar{\mathbf{J}}_2 \, dv = \int (\mathbf{E}_2 \nabla \mathbf{E}_0 - \mathbf{E}_0 \nabla \mathbf{E}_2) \cdot \bar{\mathbf{n}} \, ds \quad (3.32)$$

A similar derivation also reduces the denominator of (3.28) to a line integral as follows. Start with (3.9) and (3.10) in their scalar forms.

$$\nabla_0^2 \mathbf{E} + k_0^2 \mathbf{E} = -\mathbf{J}(\mathbf{r}_0)$$

$$\nabla_0^2 G + k_0^2 G = -\frac{1}{b} \delta(\mathbf{x} - \mathbf{x}_0) \delta(\mathbf{y} - \mathbf{y}_0) = -\frac{1}{b} \delta(\mathbf{r} - \mathbf{r}_0)$$

Multiply the first equation by G , the second by $\mathbf{E}(\mathbf{r}_0)$, subtract, and cancel common factors to obtain

$$\nabla_0 \cdot [\mathbf{E} \nabla_0 G - G \nabla_0 \mathbf{E}] = G\mathbf{J} - \frac{1}{b} \mathbf{E}(\mathbf{r}_0) \delta(\mathbf{r} - \mathbf{r}_0)$$

Now, integrate over dv_0 and use the divergence theorem to obtain

$$\int [\mathbf{E}(\mathbf{r}_0) \nabla_0 G - G \nabla_0 \mathbf{E}(\mathbf{r}_0)] \cdot \bar{\mathbf{n}} \, ds_0 = \int G(\mathbf{r} | \mathbf{r}_0) \mathbf{J}(\mathbf{r}_0) \, dv_0 - \mathbf{E}(\mathbf{r}) \quad (3.33)$$

where the closed surface of integration is just outside the ferrite obstacle.

Let v be defined such that

$$v(\mathbf{r}) = \int G(\mathbf{r} | \mathbf{r}_0) \mathbf{J}(\mathbf{r}_0) \, dv_0 - \mathbf{E} = \int (\mathbf{E} \nabla_0 G - G \nabla_0 \mathbf{E}) \cdot \bar{\mathbf{n}} \, ds_0 \quad (3.34)$$

From (3.11), it is then seen that

$$v = -\mathbf{E}_0 \quad (3.35)$$

so that v satisfies

$$\nabla^2 v + k_0^2 v = 0 \quad (3.36)$$

From (3.19) we have

$$\nabla^2 \mathbf{E}_2 + k_0^2 \mathbf{E}_2 = -\mathbf{J}_2$$

Performing manipulations similar to those used in deriving (3.31), we obtain the desired simplification

$$\begin{aligned} \int \bar{\mathbf{E}} \cdot \bar{\mathbf{J}}_2 \, dv - \int \int \bar{\mathbf{J}}_2(\mathbf{r}) \cdot \bar{\mathbf{G}}(\mathbf{r}|\mathbf{r}_0) \cdot \bar{\mathbf{J}}(\mathbf{r}_0) \, dv_0 \, dv \\ = - \int (\mathbf{E}_2 \nabla v - v \nabla \mathbf{E}_2) \cdot \bar{\mathbf{n}} \, ds \end{aligned} \quad (3.37)$$

where \mathbf{E}_2 and v are again taken just outside the ferrite surface.

We now have that

$$R_1 - R_{11} = \frac{\frac{-1}{ab\gamma_1} \left[\int (\mathbf{E} \nabla \mathbf{E}_0 - \mathbf{E}_0 \nabla \mathbf{E}) \cdot \bar{\mathbf{n}} \, ds \right] \left[\int (\mathbf{E}_2 \nabla \mathbf{E}_0 - \mathbf{E}_0 \nabla \mathbf{E}_2) \cdot \bar{\mathbf{n}} \, ds \right]}{\int (\mathbf{E}_2 \nabla v - v \nabla \mathbf{E}_2) \cdot \bar{\mathbf{n}} \, ds} \quad (3.38)$$

where

$$v = \int (\mathbf{E} \nabla_0 \mathbf{G} - \mathbf{G} \nabla_0 \mathbf{E}) \cdot \bar{\mathbf{n}} \, ds_0$$

So far the obstacle considered has been cylindrical, but not necessarily circular. The above equations are most easily integrated when circular cylinders are considered. These are the types of objects of greatest concern in this study. We now consider the circular cylinder with center at $x = -d$, $y = c$ as shown in Fig. 3.3. For this cylinder $\bar{\mathbf{n}} = \bar{\mathbf{a}}_r$ for the curved surface, and $\pm \bar{\mathbf{a}}_z$ for the top and bottom surface. Since \mathbf{E} and \mathbf{E}_0 are independent of z , $\nabla \mathbf{E}_0 \cdot \bar{\mathbf{a}}_z = \nabla \mathbf{E} \cdot \bar{\mathbf{a}}_z = 0$, and there is no contribution from these terms. For $\bar{\mathbf{n}} = \bar{\mathbf{a}}_r$ the integration is over the surface $ds = r d\phi dz$. The dz integration gives only the constant factor b which eventually cancels out of the equation for $R_1 - R_{11}$. The integrals to be evaluated are then

$$\int_0^{2\pi} \left(\mathbf{E} \frac{\partial \mathbf{E}_0}{\partial r} - \mathbf{E}_0 \frac{\partial \mathbf{E}}{\partial r} \right) R \, d\phi \quad (2.39a)$$

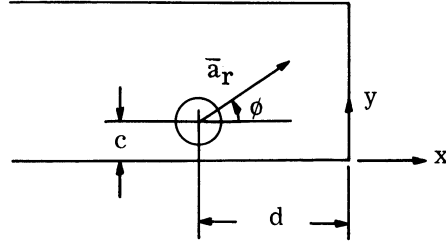


Fig. 3.3. Right cylindrical ferrite obstacle in rectangular waveguide. The waveguide aperture is located at $x = 0$.

$$\int_0^{2\pi} \left(E_2 \frac{\partial E_0}{\partial r} - E_0 \frac{\partial E_2}{\partial r} \right) R d\phi \quad (3.39b)$$

$$\int_0^{2\pi} \left(E_2 \frac{\partial v}{\partial r} - v \frac{\partial E_2}{\partial r} \right) R d\phi \quad (3.39c)$$

$$v = b \int_0^{2\pi} \left[E(r_0) \frac{\partial G(r|r_0)}{\partial r_0} - G(r|r_0) \frac{\partial E(r_0)}{\partial r_0} \right] R d\phi_0 \quad (3.39d)$$

where R is the radius of the cylinder.

The fields to be used in these integrals are those just outside the ferrite. It is more convenient to use the fields inside the obstacle. Using continuity of E , E_0 , and H_ϕ at the ferrite boundary, and the equation

$$j\omega\mu_0 H_\phi = \frac{\partial E}{\partial r}$$

outside the ferrite, we obtain

$$\int_0^{2\pi} \left(E \frac{\partial E_0}{\partial r} - E_0 \frac{\partial E}{\partial r} \right) R d\phi = \int_0^{2\pi} \left(E^{\text{int}} \frac{\partial E_0}{\partial r} - j\omega\mu_0 E_0 H_\phi^{\text{int}} \right) R d\phi \quad (3.40a)$$

$$\int_0^{2\pi} \left(E_2 \frac{\partial E_0}{\partial r} - E_0 \frac{\partial E_2}{\partial r} \right) R d\phi = \int_0^{2\pi} \left(E_2^{\text{int}} \frac{\partial E_0}{\partial r} - j\omega\mu_0 E_0 H_{\phi_2}^{\text{int}} \right) R d\phi \quad (3.40b)$$

$$\int_0^{2\pi} \left(E_2 \frac{\partial v}{\partial r} - v \frac{\partial E_2}{\partial r} \right) R d\phi = \int_0^{2\pi} \left(E_2^{\text{int}} \frac{\partial v}{\partial r} - j\omega\mu_0 v H_{\phi_2}^{\text{int}} \right) R d\phi \quad (3.40c)$$

$$v = b \int_0^{2\pi} \left(E^{\text{int}} \frac{\partial G}{\partial r_0} - j\omega\mu_0 G H_\phi^{\text{int}} \right) R d\phi_0 \quad (3.40d)$$

where the integrals are now taken just inside the ferrite surface. It is important to note here that $\partial E/\partial r$ is not continuous at the surface of the ferrite.

We have now reduced (3.38) to

$$R_1 - R_{11} = \frac{-\frac{1}{a\gamma_1} \left[\int_0^{2\pi} \left(E^{\text{int}} \frac{\partial E_0}{\partial r} - j\omega\mu_0 E_0 H_\phi^{\text{int}} \right) R d\phi \right] \left[\int_0^{2\pi} \left(E_2^{\text{int}} \frac{\partial E_0}{\partial r} - j\omega\mu_0 E_0 H_{\phi_2}^{\text{int}} \right) R d\phi \right]}{b \int_0^{2\pi} \left(E_2^{\text{int}} \frac{\partial v}{\partial r} - j\omega\mu_0 v H_{\phi_2}^{\text{int}} \right) R d\phi}$$

We will next expand the internal fields in a series of functions characteristic of the circular cylinder. These functions will have coefficients undetermined as yet. The coefficients will be eliminated from the evaluation later by using the stationary property. The expansions for the internal fields can be taken as [from (2.12)].

$$E^{\text{int}} = \sum_{n=-\infty}^{\infty} a_n J_n(k_2 r) e^{-jn(\phi + \pi/2)} \quad (3.41a)$$

$$H_\phi^{\text{int}} = \frac{-j}{\omega\mu_0(\mu^2 - k^2)} \sum_{n=-\infty}^{\infty} a_n e^{-jn(\phi + \pi/2)} \left[\mu k_2 J_n'(k_2 r) + \frac{nk}{r} J_n(k_2 r) \right] \quad (3.41b)$$

$$E_2^{\text{int}} = \sum_{n=-\infty}^{\infty} a_n^{(2)} J_n(k_2 r) e^{-jn(\phi + \pi/2)} \quad (3.41c)$$

$$H_{\phi_2}^{\text{int}} = \frac{-j}{\omega\mu_0(\mu^2 - k^2)} \sum_{n=-\infty}^{\infty} a_n^{(2)} e^{-jn(\phi + \pi/2)} \left[\mu k_2 J_n'(k_2 r) - \frac{nk}{r} J_n(k_2 r) \right] \quad (3.41d)$$

The $[a_n, a_n^{(2)}]$ coefficients are not yet known. It is repeated here that \bar{E}_2 and \bar{H}_2 were defined such that

$$E_2^{\text{int}}(k) = E^{\text{int}}(-k) \quad (3.42a)$$

$$H_{\phi_2}^{\text{int}}(k) = H_\phi^{\text{int}}(-k) \quad (3.42b)$$

so that

$$a_n^{(2)}(k) = a_n(-k) \quad (3.43)$$

To perform the integrations in (3.40a through 3.40d), we use the following lemma proved by Schwinger.²¹

Lemma: If $U(x', y') = U(r, \phi)$ is any solution of the two-dimensional source free wave equation, $\nabla^2 U + k_o^2 U = 0$, inside a circle of radius R_o , then for any $r \leq R_o$

$$\frac{1}{2\pi} \int_0^{2\pi} U(r, \phi) e^{jm\phi} d\phi = (j)^m J_m(k_o r) e^{jmD} U(0) \quad (3.44)$$

where e^{jmD} is an operator defined by

$$e^{\pm jmD} = (\cos D \pm j \sin D)^m = \left[\frac{1}{jk_o} \left(\frac{\partial}{\partial x'} \pm j \frac{\partial}{\partial y'} \right) \right]^m$$

and where $e^{jmD} U(0)$ means $e^{jmD} U(x', y')$ evaluated at the center of the circle and where (x', y') are coordinates referred to the center of the circle.

Since (3.44) holds for any $r \leq R_o$, differentiating with respect to r gives the second required equation

$$\frac{1}{2\pi} \int_0^{2\pi} \frac{\partial U(r, \phi)}{\partial r} e^{jm\phi} d\phi = (j)^m k_o J'_m(k_o r) e^{jmD} U(0) \quad (3.45)$$

The lemma can be applied directly to (3.40a, 3.40b, 3.40c), since E_o and v are both solutions of the two-dimensional source free wave equation. Using (3.41a) through (3.41c), in (3.40a, 3.40c) results in

$$\begin{aligned} & \int_0^{2\pi} \left(E_o^{\text{int}} \frac{\partial E_o}{\partial r} - j\omega\mu_o E_o H_\phi^{\text{int}} \right) R d\phi \\ &= \sum_{n=-\infty}^{\infty} a_n 2\pi R \left[e^{-jnD} E_o(0) \right] \left\{ k_o J_n(k_2 R) J'_n(k_o R) \right. \\ & \quad \left. - \frac{1}{\mu^2 - k^2} \left[\mu k_2 J'_n(k_2 R) + \frac{nk}{R} J_n(k_2 R) \right] J_n(k_o R) \right\} \end{aligned} \quad (3.46)$$

$$\equiv \sum_{n=-\infty}^{\infty} a_n B_n e^{-jnD} E_o(0)$$

and

$$\int_0^{2\pi} \left(E_2^{\text{int}} \frac{\partial v}{\partial r} - j\omega\mu_o v H_2^{\text{int}} \right) R d\phi = \sum_{n=-\infty}^{\infty} a_n^{(2)} 2\pi R \left[e^{-jnD} v(0) \right] \left\{ k_o J_n(k_2 R) J_n'(k_o R) - \frac{1}{\mu^2 - k^2} \left[\mu k_2 J_n'(k_2 R) - \frac{nk}{R} J_n(k_2 R) \right] J_n(k_o R) \right\} \equiv \sum_{n=-\infty}^{\infty} a_n^{(2)} B_n^{(2)} e^{-jnD} v(0) \quad (3.47)$$

Similarly for (3.40b), we find

$$\int_0^{2\pi} \left(E_2^{\text{int}} \frac{\partial E_o}{\partial r} - j\omega\mu_o E_o H_{\phi_2}^{\text{int}} \right) R d\phi = \sum_{n=-\infty}^{\infty} a_n^{(2)} B_n^{(2)} e^{-jnD} E_o(0)$$

We note that

$$B_n = B_{-n}^{(2)}$$

The evaluation of v (3.40d) is more complicated since G is not a solution to the free space wave equation but is a solution of

$$\nabla^2 G + k_o^2 G = -\frac{1}{b} \delta(x - x_o) \delta(y - y_o)$$

The Green's function is made up of contributions from a source point inside the waveguide plus contributions from an infinite number of images lying outside the waveguide walls. In fact G could have been derived originally by the method of images, beginning with the two-dimensional free space Green's function²⁴

$$\frac{H_o^{(2)}(k_o |\bar{r} - \bar{r}_o|)}{4j}$$

$H_o^{(2)}$ is the Hankel function and is equal to

$$H_o^{(2)}(z) = J_o(z) - j N_o(z).$$

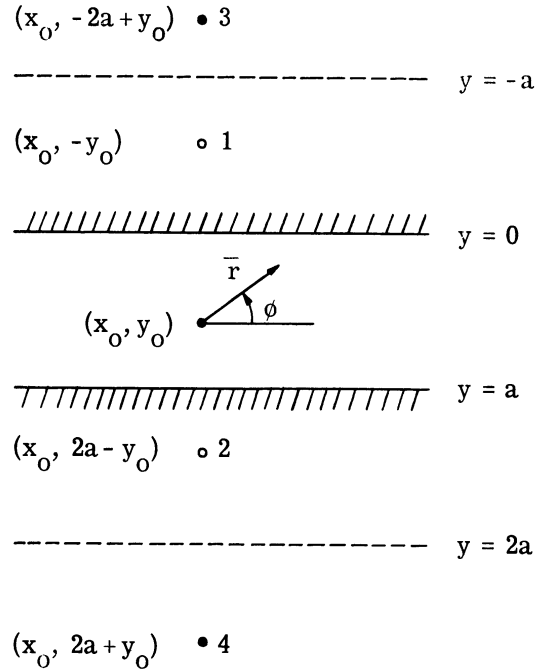


Fig. 3.4. Image points for the rectangular waveguide.

The coordinate system is shown in Fig. 3.4 along with the image points. $H_0^{(2)}/4j$ and $-N_0/4$ satisfy the same equation as G (except for the $1/b$ term) while J_0 satisfies the homogeneous wave equation. Since we want to remove the singularity from G in order to be able to apply the lemma, we only need to remove the term $-N_0/4$. Let

$$-N_0/4 = G_{f. s.}$$

The Green's function can then be written as the free space Green's function ($G_{f. s.}$) plus the image terms (G_i), i. e. ,

$$bG = G_{f. s.} + G_i \quad (3.48)$$

where $G_{f. s.}$ and G_i are solutions of

$$\nabla^2 G_{f. s.} + k_0^2 G_{f. s.} = -\delta(x - x_0) \delta(y - y_0) \quad (3.49a)$$

$$\nabla^2 G_i + k_0^2 G_i = 0 \quad (3.49b)$$

inside the waveguide, since all the image source points lie outside the waveguide.

Then (3.40d) becomes

$$\begin{aligned}
v &= \int_0^{2\pi} \left(\mathbf{E}^{\text{int}} \frac{\partial G_{\text{f. s.}}}{\partial r_0} - j\omega\mu_0 G_{\text{f. s.}} \mathbf{H}_\phi^{\text{int}} \right) R d\phi_0 \\
&+ \int_0^{2\pi} \left(\mathbf{E}^{\text{int}} \frac{\partial G_i}{\partial r_0} - j\omega\mu_0 G_i \mathbf{H}_\phi^{\text{int}} \right) R d\phi_0
\end{aligned} \tag{3.50}$$

where

$$\begin{aligned}
G_{\text{f. s.}} &= \frac{-N_0(k_0 |\bar{r} - \bar{r}_0|)}{4} \\
&= \frac{-1}{4} \sum_{n=-\infty}^{\infty} e^{jn(\phi - \phi_0)} \begin{cases} J_n(k_0 r) N_n(k_0 r_0) & r_0 > r \\ J_n(k_0 r_0) N_n(k_0 r) & r_0 < r \end{cases}
\end{aligned} \tag{3.51}$$

The first integration on the right in (3.50) can be performed directly. The second term can now be integrated using the lemma since G_i satisfies the required conditions. The result is

$$\begin{aligned}
v(r) &= \sum_{\ell=-\infty}^{\infty} a_\ell 2\pi R \left[e^{-j\ell D_0} G_i(r|0) \right] \left\{ k_0 J_\ell(k_2 R) J'_\ell(k_0 R) \right. \\
&- \frac{1}{\mu^2 - k^2} \left[\mu k_2 J'_\ell(k_2 R) + \frac{\ell k}{R} J_\ell(k_2 R) \right] J_\ell(k_0 R) \left. \right\} \\
&- \frac{1}{4} \sum_{\ell=-\infty}^{\infty} a_\ell 2\pi R (j)^{-\ell} J_\ell(k_0 r) e^{-j\ell\phi} \left\{ k_0 J_\ell(k_2 R) N'_\ell(k_0 R) \right. \\
&- \frac{1}{\mu^2 - k^2} \left[\mu k_2 J'_\ell(k_2 R) + \frac{\ell k}{R} J_\ell(k_2 R) \right] N_\ell(k_0 R) \left. \right\} \\
&\equiv \sum_{\ell=-\infty}^{\infty} a_\ell B_\ell e^{-j\ell D_0} G_i(r|0) \\
&+ \sum_{\ell=-\infty}^{\infty} a_\ell C_\ell J_\ell(k_0 r) e^{-j\ell\phi} (j)^{-\ell}
\end{aligned} \tag{3.52}$$

where $e^{-j\ell D_0}$ operates on the (r_0) coordinates.

Now (3.47) can be written

$$\sum_{n=-\infty}^{\infty} \sum_{\ell=-\infty}^{\infty} a_n^{(2)} B_n^{(2)} \left\{ a_\ell B_\ell e^{-jnD} e^{-j\ell D_0} G_i(0|0) + a_\ell (j)^{-\ell} C_\ell e^{-jnD} \left[e^{-j\ell\phi} J_\ell(k_0 r) \right] \right\} \tag{3.53}$$

It can be shown that

$$e^{-jnD} \left[e^{-j\ell\phi} J_\ell(k_o r) \right] = (j)^{-\ell} \delta_{-n\ell}$$

where $\delta_{-n\ell}$ is the Kronecker delta

$$\begin{aligned} \delta_{-n\ell} &= 1, & \ell &= -n \\ &= 0, & \ell &\neq -n \end{aligned}$$

Thus (3.53) becomes

$$\sum_{n=-\infty}^{\infty} \sum_{\ell=-\infty}^{\infty} \left[a_n^{(2)} a_\ell B_n^{(2)} B_\ell e^{-jnD} e^{-j\ell D_o} G_i(0|0) + a_n^{(2)} a_\ell B_n^{(2)} C_\ell (-1)^\ell \delta_{-n\ell} \right] \quad (3.54)$$

We then have

$$R_1 - R_{11} = \frac{-\frac{1}{a\gamma_1} \left[\sum_{n=-\infty}^{\infty} a_n B_n e^{-jnD} E_o(0) \right] \left[\sum_{n=-\infty}^{\infty} a_n^{(2)} B_n^{(2)} e^{-jnD} E_o(0) \right]}{\sum_{n=-\infty}^{\infty} \sum_{\ell=-\infty}^{\infty} \left[a_n^{(2)} a_\ell B_n^{(2)} B_\ell e^{-jnD} e^{-j\ell D_o} G_i(0|0) + a_n^{(2)} B_n^{(2)} a_\ell C_\ell (-1)^\ell \delta_{-n\ell} \right]} \quad (3.55)$$

or

$$R_1 - R_{11} = \frac{-\frac{1}{a\gamma_1} \sum_{n=-\infty}^{\infty} a_n \alpha_n \sum_{n=-\infty}^{\infty} a_n^{(2)} \alpha_n^{(2)}}{\sum_{n=-\infty}^{\infty} \sum_{\ell=-\infty}^{\infty} a_n^{(2)} a_\ell \Gamma_{n\ell}} \quad (3.56)$$

where

$$\alpha_n = B_n e^{-jnD} E_o(0) \quad (3.57a)$$

$$\alpha_n^{(2)} = B_n^{(2)} e^{-jnD} E_o(0) \quad (3.57b)$$

$$\Gamma_{n\ell} = B_n^{(2)} B_\ell e^{-jnD} e^{-j\ell D_o} G_i(0|0) + (-1)^\ell B_n^{(2)} C_\ell \delta_{-n\ell} \quad (3.57c)$$

For any given set of parameters, these last three terms are known constants.

The not so trivial matter of evaluating the operations $e^{-jnD} E_o(0)$ and $e^{-jnD} e^{-j\ell D_o} G_1(0|0)$ is treated in Appendix D.

The reflection coefficient can now be evaluated from (3.56) by any of several means. The terms as yet unknown are the coefficients a_n and $a_n^{(2)}$. Since (3.56) is stationary with respect to these coefficients we could choose as a reasonable approximation for them the values found from the plane wave approximation in Chapter II. This procedure would not take full advantage of the stationary property, however. A better method is to use the stationarity of (3.56) either to find the unknown coefficients or to solve for $R_1 - R_{11}$ directly. The latter procedure will be followed here. The stationarity of (3.56) requires that the derivative of $R_1 - R_{11}$ with respect to any of the coefficients must be zero. For the present case, only the terms $a_o, a_{\pm 1}$ [and $a_o^{(2)}, a_{\pm 1}^{(2)}$] will be used. These few terms were found to give the major contributions to the field expansions for the infinite cylinder problem solved in Chapter II. We can thus use only these terms with a certain amount of confidence. Taking the derivatives yields

$$(R-R_{11}) \sum_{n=-1}^1 a_n^{(2)} \Gamma_{nk} + A \alpha_k \sum_{n=-1}^1 a_n^{(2)} \alpha_n^{(2)} = 0 \quad k = 0, \pm 1 \quad (3.58a)$$

and

$$(R-R_{11}) \sum_{\ell=-1}^1 a_\ell \Gamma_{k\ell} + A \alpha_k^{(2)} \sum_{\ell=-1}^1 a_\ell \alpha_\ell = 0 \quad k = 0, \pm 1 \quad (3.58b)$$

where $A = 1/a\gamma_1$

We have six homogeneous equations in six unknowns. For a solution to exist for the $[a_n, a_n^{(2)}]$ coefficients the determinant must vanish. When the determinant is set to zero, the unknown coefficients are removed and a solution for $R_1 - R_{11}$ remains. Actually, either (3.58a) or (3.58b) alone may be used. That is, take either equation and equate the determinant to zero. The solution for $R_1 - R_{11}$ comes out to be the same no matter which of the above methods is used. The solution is

$$R_1 - R_{11} = \frac{-A \alpha_{-1}^{(2)} \begin{vmatrix} \Gamma_{11} & \Gamma_{01} & \alpha_1 \\ \Gamma_{10} & \Gamma_{00} & \alpha_0 \\ \Gamma_{1-1} & \Gamma_{0-1} & \alpha_{-1} \end{vmatrix} - A \alpha_0^{(2)} \begin{vmatrix} \Gamma_{11} & \alpha_1 & \Gamma_{-11} \\ \Gamma_{10} & \alpha_0 & \Gamma_{-10} \\ \Gamma_{1-1} & \alpha_{-1} & \Gamma_{-1-1} \end{vmatrix} - A \alpha_1^{(2)} \begin{vmatrix} \alpha_1 & \Gamma_{01} & \Gamma_{-11} \\ \alpha_0 & \Gamma_{00} & \Gamma_{-10} \\ \alpha_{-1} & \Gamma_{0-1} & \Gamma_{-1-1} \end{vmatrix}}{\begin{vmatrix} \Gamma_{11} & \Gamma_{01} & \Gamma_{-11} \\ \Gamma_{10} & \Gamma_{00} & \Gamma_{-10} \\ \Gamma_{1-1} & \Gamma_{0-1} & \Gamma_{-1-1} \end{vmatrix}} \quad (3.59)$$

This equation is most easily evaluated using a digital computer. The results for the case when the aperture is replaced by a matched load (i. e. , $R_{nn} = R_{nm} = 0$) are shown in Fig. 3.5. This Smith Chart representation shows how the impedance of the post varies as the static field is changed. The reference plane is at the center of the cylinder. The values of the components of the permeability tensor were obtained as described in Appendix C. The experimental data, also shown on the chart, agree quite well with the theory. There appears to be a constant difference in reflection coefficient angle of a little less than 10° . This corresponds to a shift in the reference plane of about .022" which might easily be attributed to experimental error. Because of the difference between H_{external} and the measured static field H_{app} (as discussed in Appendix C) the Smith Chart presentation is most suitable for comparison between theory and experiment. On the chart only the theoretical static field, H_{ext} , is shown. The agreement between experiment and theory shows that the three terms of the field expansion inside the ferrite used in the stationary expression were sufficient.

The second Smith Chart (Fig. 3.6) shows the impedance of a post just inside the waveguide, tangent to the aperture. For this case the theory and experiment are still similar but are further apart than for the matched case. This is attributed to two main causes: (1) because of the aperture discontinuity the field distribution within the ferrite may require more than just three terms to describe it accurately; (2) the reflection and coupling coefficients are difficult to calculate, and an infinite number of them are required in the evaluation of (3.59).*

* See Appendix D for the type of summation involved.

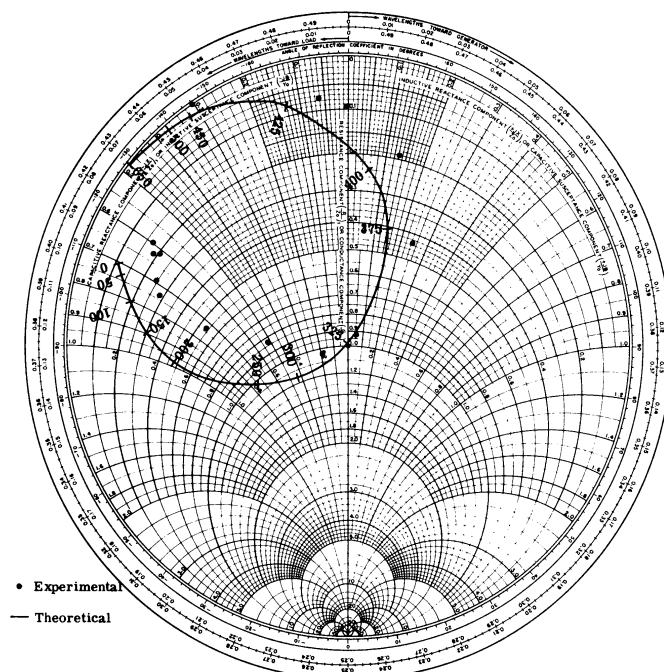


Fig. 3.5. Impedance of a ferrite post in a matched waveguide as the static external field (shown in oersteds) is varied. Frequency = 10 Gc/sec, diameter = .295", TT 390 ferrite, $\epsilon = 13$.

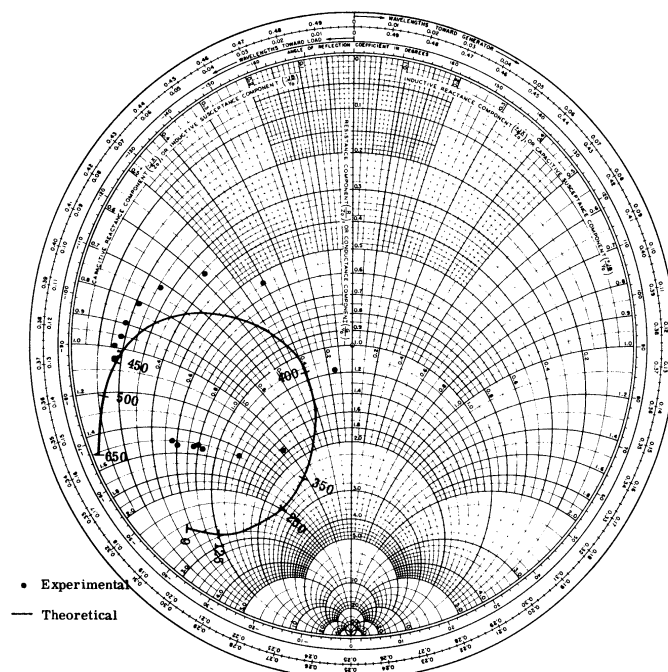


Fig. 3.6. Impedance of a ferrite post just inside the waveguide, tangent to the aperture, as the static external field (shown in oersteds) is varied. Frequency = 10 Gc/sec, diameter = .295", TT 390 ferrite, $\epsilon = 13$, $d = .148$ ".

volved has been assumed. For the data shown in Fig. 3.6, the only coefficients taken into account in the calculation were R_{11} , R_{22} and R_{33} . The addition of several more coefficients would improve the result. In any case, the theoretical curve predicts the behavior of the impedance as the static field is increased and is accurate enough to be used advantageously to design a matching network for the post-aperture structure.

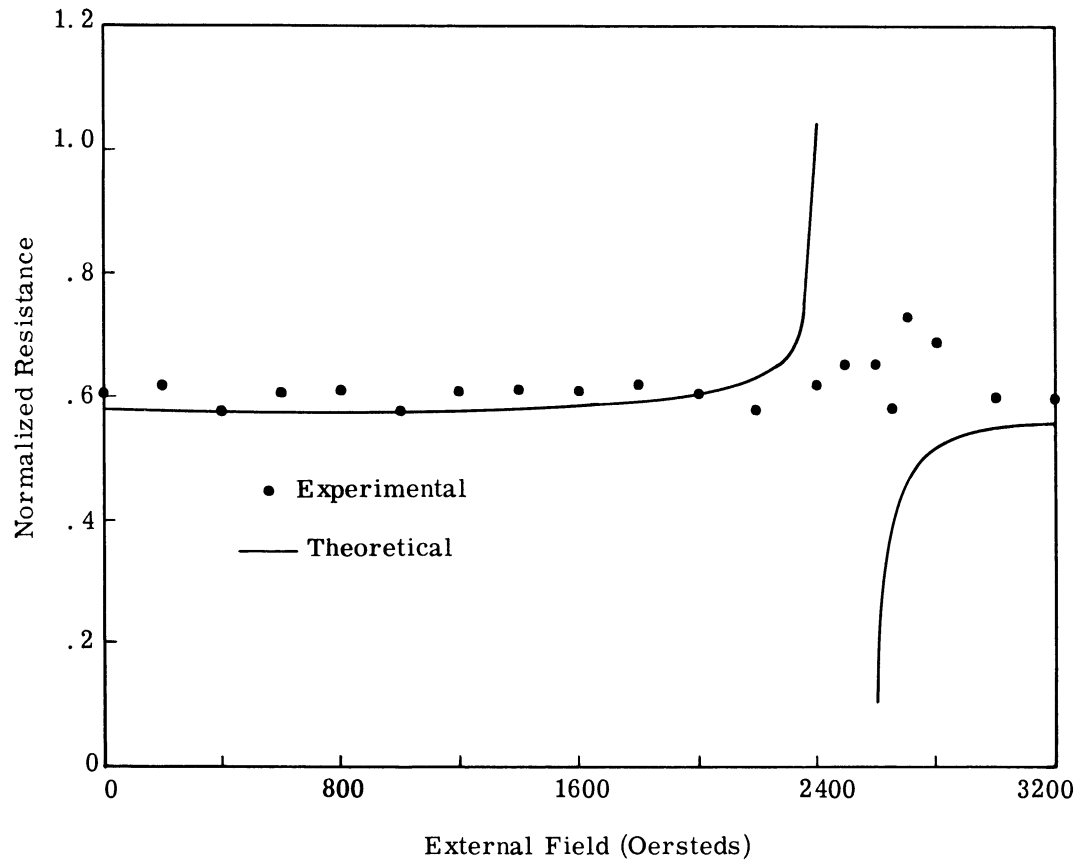
The method of improving the accuracy of the theoretical results follows straightforwardly (but perhaps tediously) from the procedures already performed. More terms in the field expansion can be included in (3.56) and the stationarity property applied again exactly as in deriving (3.59). Also, more of the reflection and coupling coefficients (R_{nn} , R_{nm}) can be found (as derived in Appendix B) and used in the evaluation of the reflection coefficient.

The next set of curves (Fig. 3.7) were plotted for a relatively small post, centered in the waveguide with respect to the side wall and placed one waveguide wavelength away from the open aperture. The experimental and theoretical curves agree very well for this case. The region around 2400 gauss is where ferromagnetic resonance occurs. The high losses existing here were not accounted for in the calculation. The excellent agreement for the small post can be explained in terms of the simple field structure within the cylinder. Because of the small cross-sectional area, it is almost certain that the fields are almost constant over the cylinder and can thus be accurately represented by the first few terms of the Bessel function expansion (3.41).

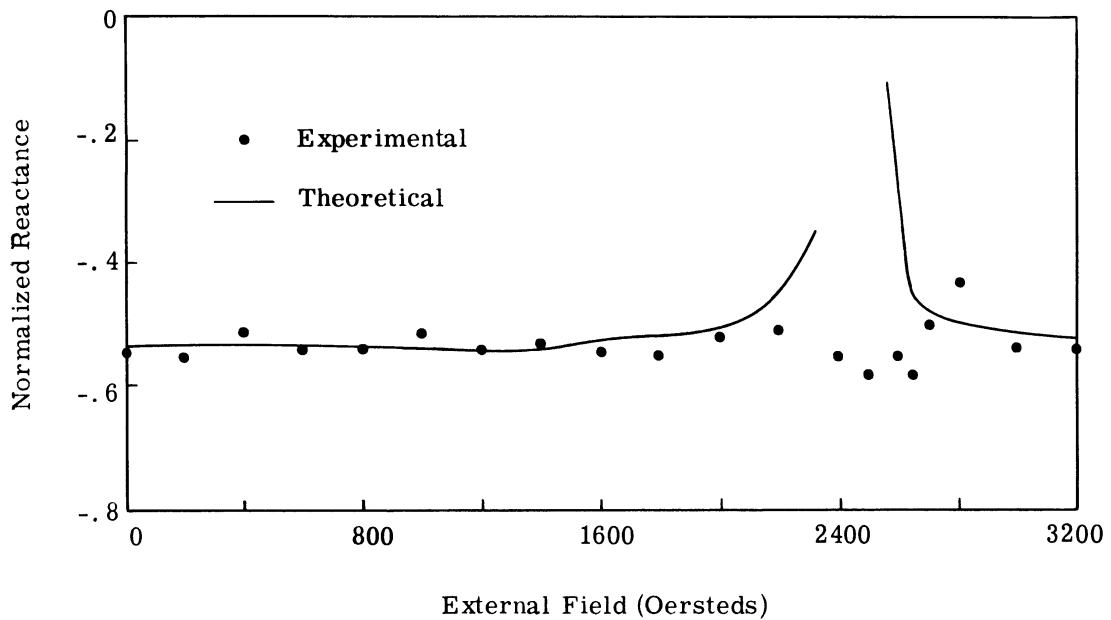
3.3 Reflection Coefficient for Small Posts

The reflection coefficient (3.59) can be evaluated easily for the case of small posts. In particular for the cases where $k_o R \ll 1$, $k_2 R \ll 1$, the Bessel functions can be replaced by the leading term of their series expansions. The post is not necessarily centered in the waveguide. We can neglect Γ_{10} , Γ_{01} , Γ_{11} , Γ_{-1-1} since they turn out to be proportional to $(k_o R)^2$. We can approximate $\Gamma_{n\ell}$ by the dominant terms.

$$\Gamma_{n\ell} \cong (-1)^\ell B_n^{(2)} C_\ell \delta_{-n\ell} = (-1)^\ell B_{-n} C_\ell \delta_{-n\ell}$$



(a)



(b)

Fig. 3.7. Impedance of a small ferrite post near a waveguide aperture. Frequency = 10 Gc/sec, $d = 1.56''$, diameter = $.049''$, TT 390 ferrite, $\epsilon = 13$. (a) Resistance vs. external field. (b) Reactance vs. external field.

Equation 3.59 then simplifies to

$$R_1 - R_{11} = \frac{-A \alpha_{-1}^{(2)} \begin{vmatrix} 0 & 0 & \alpha_1 \\ 0 & \Gamma_{00} & \alpha_0 \\ \Gamma_{1-1} & 0 & \alpha_{-1} \end{vmatrix} - A \alpha_0^{(2)} \begin{vmatrix} 0 & \alpha_1 & \Gamma_{-11} \\ 0 & \alpha_0 & 0 \\ \Gamma_{1-1} & \alpha_{-1} & 0 \end{vmatrix} - A \alpha_1^{(2)} \begin{vmatrix} \alpha_1 & 0 & \Gamma_{-11} \\ \alpha_0 & \Gamma_{00} & 0 \\ \alpha_{-1} & 0 & 0 \end{vmatrix}}{\begin{vmatrix} 0 & 0 & \Gamma_{-11} \\ 0 & \Gamma_{00} & 0 \\ \Gamma_{1-1} & 0 & 0 \end{vmatrix}} \quad (3.60)$$

Then

$$R_1 - R_{11} = \frac{+ A \alpha_{-1}^{(2)} (\alpha_1 \Gamma_{00} \Gamma_{1-1}) + A \alpha_0^{(2)} (\alpha_0 \Gamma_{-11} \Gamma_{1-1}) + A \alpha_1^{(2)} (\alpha_{-1} \Gamma_{00} \Gamma_{-11})}{-\Gamma_{-11} \Gamma_{00} \Gamma_{1-1}} \quad (3.61)$$

or

$$R_1 - R_{11} = -A \left[\frac{\alpha_0^{(2)} \alpha_0}{\Gamma_{00}} + \frac{\alpha_{-1}^{(2)} \alpha_1}{\Gamma_{-11}} + \frac{\alpha_1^{(2)} \alpha_{-1}}{\Gamma_{1-1}} \right] \quad (3.62)$$

now, evaluating the terms in $R_1 - R_{11}$ gives,

$$\frac{\alpha_0^{(2)} \alpha_0}{\Gamma_{00}} = \frac{[B_o E_o(0)]^2}{B_o C_o} = \frac{B_o [E_o(0)]^2}{C_o}$$

$$\frac{\alpha_{-1}^{(2)} \alpha_1}{\Gamma_{-11}} = \frac{[B_1 e^{jD} E_o(0)] [B_1 e^{-jD} E_o(0)]}{-B_1 C_1} = \frac{-B_1 e^{jD} E_o(0) e^{-jD} E_o(0)}{C_1}$$

$$\frac{\alpha_1^{(2)} \alpha_{-1}}{\Gamma_{1-1}} = \frac{[B_{-1} e^{-jD} E_o(0)] [B_{-1} e^{jD} E_o(0)]}{-B_{-1} C_{-1}} = \frac{-B_{-1} e^{jD} E_o(0) e^{-jD} E_o(0)}{C_{-1}}$$

Evaluating these expressions for small $k_o R$, $k_2 R$ gives

$$\frac{\alpha_0^{(2)} \alpha_0}{\Gamma_{00}} \cong \frac{-\pi R^2 k_o^2 (\epsilon - 1) [E_o(0)]^2}{1 + \frac{k_o^2 R^2 \epsilon}{2} \ln \left(\frac{\gamma' k_o R}{2} \right)}$$

$$\frac{\alpha_{-1}^{(2)} \alpha_1}{\Gamma_{-11}} \cong \frac{\pi R^2 k_o^2 \left(1 - \frac{1}{\mu-k}\right) e^{jD} E_o(0) e^{-jD} E_o(0)}{1 + \frac{1}{\mu-k}}$$

$$\frac{\alpha_1^{(2)} \alpha_{-1}}{\Gamma_{1-1}} \cong \frac{\pi R^2 k_o^2 \left(1 - \frac{1}{\mu+k}\right) e^{jD} E_o(0) e^{-jD} E_o(0)}{1 + \frac{1}{\mu+k}}$$

where \ln is the natural logarithm, $\gamma' = 1.781$ and where terms in the denominator proportional to $(k_o R)$ were omitted. Combining the terms, and using (D-1)* for $E_o(0)$ and $e^{\pm jD} E_o(0)$ and taking only the first two terms of these expressions gives finally

$$\begin{aligned} R_1 = R_{11} + \frac{\pi R^2}{j a \beta_1} \left\{ k_o^2 (\epsilon - 1) \left(1 - \frac{k_o^2 R^2 \epsilon}{2} \ln \frac{\gamma' k_o R}{2} \right) \left(e^{j\beta_1 d} + R_{11} e^{-j\beta_1 d} \right)^2 \sin^2 \frac{\pi c}{a} \right. \\ \left. - 2 \left[\frac{\mu^2 - k^2 - 1}{(\mu+1)^2 - k^2} \right] \left[\beta_1^2 \sin^2 \frac{\pi c}{a} \left(e^{j\beta_1 d} - R_{11} e^{-j\beta_1 d} \right)^2 \right. \right. \\ \left. \left. - \frac{\pi^2}{a^2} \cos^2 \frac{\pi c}{a} \left(e^{j\beta_1 d} + R_{11} e^{-j\beta_1 d} \right)^2 \right] \right\} \end{aligned} \quad (3.63)$$

where $j\beta_1 = \gamma_1$.

This equation agrees with Berk and Epstein's result⁹ for the small post not close to the side wall in a matched waveguide, and with Schwinger's solution²¹ for a small dielectric post in a matched waveguide. It is likely that (3.63) applies even for noncircular cylinders of small cross sections (and small sides). In this case the term πR^2 in (3.63) would be replaced by the cross-sectional area. This result was obtained by Schwinger²¹ for the small dielectric post in a matched waveguide.

When (3.63) was used on the ferrite post described in Fig. 3.7, the results were very close to those obtained using the computer program. This is about the largest radius that can still be considered small since $k_o R$ is about 1/8 and $k_2 R$ is a little less than 1/2. In Fig. 3.8 a comparison between (3.63) and experiment is made when the small post is moved sideways and back and forth in the waveguide. Again very good correlation is obtained for the small post.

* This refers to Equation D-1 in Appendix D.

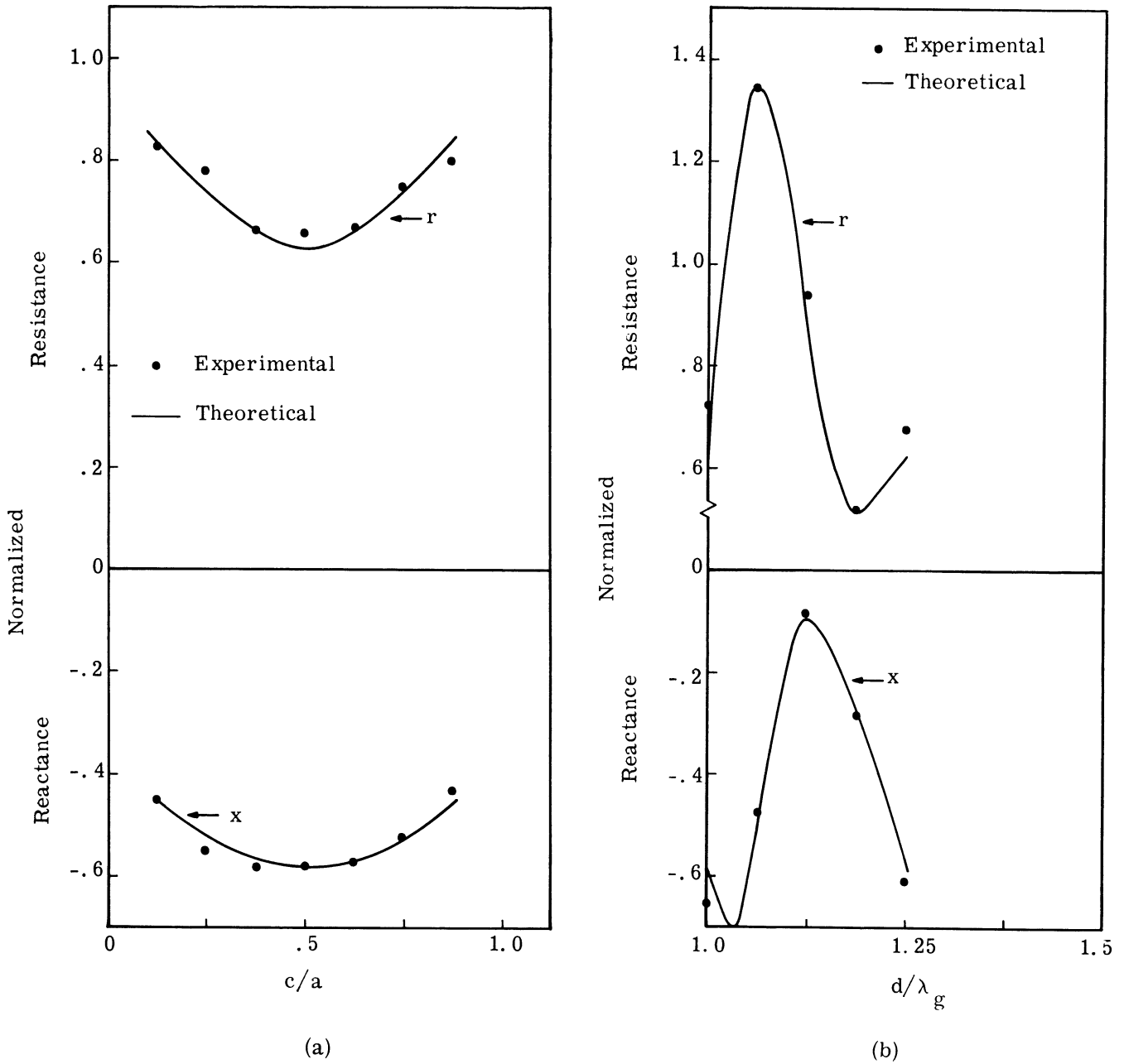


Fig. 3.8. Impedance of a small ferrite post near a waveguide aperture. Frequency = 10 Gc/sec, diameter = .049", TT 390 ferrite, $\epsilon = 13$, external field = 0 oersteds. (a) Impedance vs. post distance from the side wall. (b) Impedance vs. post distance from the aperture.

3.4 Application to Other Dual Discontinuity Problems

The reflection coefficient given by (3.17) was derived for a cylindrical ferrite obstacle combined with the aperture of an open-ended rectangular waveguide. Actually, this equation is valid if any discontinuity which has no z-variation replaces the aperture. For example, instead of the aperture we might have an iris opening into free space, an iris opening into another waveguide, a change in width of the waveguide, a dielectric loading of the waveguide, etc. The Green's function for all these geometries has exactly the same form as (3.12). The only change is in the evaluation of the reflection and coupling coefficients which must be rederived for the different discontinuities. The construction of the stationary expression follows exactly as in Section 3.1.5. Equation 3.28 is then valid for these new structures.

This method opens the way to analysis and derivation of design curves for a number of elements such as matching devices, and filters, which consist of a dual discontinuity. The restrictions on the class of problems solved are:

1. There must be no z-variation in the obstacle.
2. The problem must be entirely solvable when the ferrite obstacle is absent in order to obtain the Green's function.

A particularly simple dual discontinuity problem is the ferrite cylinder backed by an open or short circuit. For this case the reflection coefficients (R_{nn}) are all +1 for the open circuit, and -1 for the short circuit, and the coupling coefficients (R_{nm}) are all zero. For the case of a small circular cylinder ($k_0 R \ll 1$, $k_2 R \ll 1$), the results of the analysis are given by (3.63) with R_{11} taken as +1 for the open and -1 for the short. The results when $e^{j\beta_1 d} = 1$ (i. e., the obstacle is an integral number of wavelengths from the short or open) are given by the following:

1. For the short circuit case

$$\begin{aligned}
 R_1 &= -1 + \frac{\pi R^2}{j a \beta_1} \left\{ -8 \frac{\mu^2 - k^2 - 1}{(\mu+1)^2 - k^2} \beta_1^2 \sin^2 \frac{\pi c}{a} \right\} && \equiv -1 + \delta_{sc} \\
 &&& \equiv -1 + jX_{sc} \quad (3.64)
 \end{aligned}$$

2. For the open circuit case

$$\begin{aligned}
 R_1 &= 1 + \frac{\pi R^2}{j a \beta_1} \left\{ k_o^2 (\epsilon - 1) \left(1 - \frac{k_o^2 R^2 \epsilon}{2} \ln \frac{\gamma' k_o R}{2} \right) 4 \sin^2 \frac{\pi c}{a} \right. \\
 &\quad \left. + 8 \frac{\mu^2 - k^2 - 1}{(\mu + 1)^2 - k^2} \left[\left(\frac{\pi}{a} \right)^2 \cos^2 \left(\frac{\pi c}{a} \right) \right] \right\} \equiv 1 + \delta_{oc} \\
 &\equiv 1 + jX_{oc} \quad (3.65)
 \end{aligned}$$

Using the standard formula for the input impedance

$$Z = \frac{1 + R_1}{1 - R_1}$$

we obtain

$$Z_{oc} = \frac{2 + \delta_{oc}}{-\delta_{oc}} \simeq -\frac{2}{\delta_{oc}} \quad (3.66a)$$

when the output is open circuited, and

$$Z_{sc} = \frac{\delta_{sc}}{2 - \delta_{sc}} \simeq \frac{\delta_{sc}}{2} \quad (3.66b)$$

when the output is short circuited, since δ_{sc} and δ_{oc} are small for the small post.

We can also obtain the equivalent circuit of the post in a matched waveguide from these equations. The T-equivalent circuit is shown in Fig. 3.9. By alternately short circuiting and open circuiting one set of terminals and measuring the input impedance at the other pair we can obtain the values of the impedance elements. It is easy to see that

$$Z_{oc} = Z_{11} \quad (3.67a)$$

$$Z_{sc} = \frac{Z_{11}^2 - Z_{12}^2}{Z_{11}} \quad (3.67b)$$

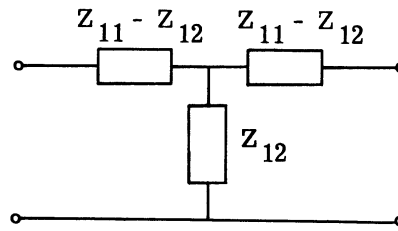


Fig. 3.9. T-equivalent circuit.

Solving for Z_{12} and $Z_{11} - Z_{12}$ using (3.66) and (3.67) gives

$$Z_{12} = - \left(\frac{2}{\delta_{oc}} + \frac{\delta_{sc}}{4} \right) \quad (3.68a)$$

and

$$Z_{11} - Z_{12} = \frac{\delta_{sc}}{4} \quad (3.68b)$$

The following simplifying cases can be analyzed.

Case I, Dielectric Post, $\mu=1$, $k=0$

For this case

$$\frac{\delta_{sc}}{4} = 0$$

Thus

$$Z_{11} - Z_{12} = 0$$

and

$$Z_{12} = \frac{-2}{\delta_{oc}} = \frac{-j\beta_1 a \csc^2 \frac{\pi c}{a}}{2\pi R^2 k_o^2 (\epsilon - 1)} = -jX_c$$

The equivalent circuit is then as shown in Fig. 3.10.

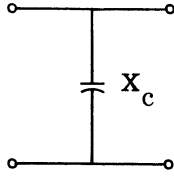


Fig. 3. 10. Equivalent circuit of a small dielectric post in a matched waveguide.

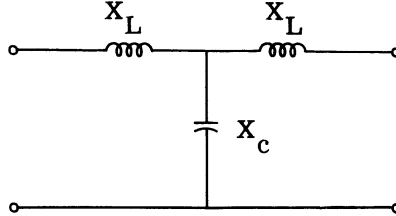


Fig. 3. 11. Equivalent circuit of a small isotropic permeable post with $\mu > 1$ in a matched waveguide.

Case II, Magnetic Post, $\epsilon=1$, $k=0$

$$Z_{12} = \frac{-2}{\delta_{oc}} - \frac{\delta_{sc}}{4} = \frac{-j\beta_1 a \sec^2 \frac{\pi c}{a}}{4\pi R^2 \left(\frac{\mu-1}{\mu+1}\right) \left(\frac{\pi}{a}\right)^2} - j \frac{2\pi R^2}{a} \left(\frac{\mu-1}{\mu+1}\right) \beta_1 \sin^2 \frac{\pi c}{a} = -jX_c$$

$$Z_{11} - Z_{12} = j \frac{2\pi R^2}{a} \left(\frac{\mu-1}{\mu+1}\right) \beta_1 \sin^2 \frac{\pi c}{a} = jX_L$$

For the case $\mu > 1$ the equivalent circuit is shown in Fig. 3. 11.

Equations (3. 64) and (3. 65) can also be used to measure the permeability and permittivity of a dielectric or ferrite. If a small post is placed an integral number of half wavelengths from the short position, the angle of the reflection coefficient is [from (3. 64)]

$$\theta_{sc} = \tan^{-1} \frac{X_{sc}}{-1}$$

This equation involves only the permeability of the material. Since θ_{sc} is a function of the sample distance from the side wall, several readings can be taken to obtain the equations necessary to determine both μ and k .

For the open circuit, the angle of reflection is [from (3. 65)]

$$\theta_{oc} = \tan^{-1} X_{oc}$$

This equation involves only the permittivity if the sample is centered in the waveguide with respect to the side wall.

Measurements of the reflection coefficient angle can be very accurate since the minimum on the slotted line will be very sharp because of the high standing wave ratio.

3.5 Conclusions

In this chapter the main theoretical work of the study was performed. A variational solution was obtained for the reflection coefficient of a ferrite post in a rectangular waveguide terminated in an aperture radiating into free space. The results were generalized to the case of a noncircular cylinder combined with any z-independent discontinuity terminating the waveguide. The results were shown to be particularly accurate for the matched waveguide and for the small post. The results for the large post at the aperture were accurate enough to be useful. Although possibly tedious, more precise numerical data can be obtained by straightforwardly extending the evaluation method described in Section 3.2. More terms in the series expansion for the internal fields can be taken and more of the higher order reflection coefficients and coupling coefficients can be evaluated.

Possibly the most useful contribution of this chapter is the development of a method of solving a number of problems of the "dual discontinuity" type. An immediate solution is obtained from this chapter for obstacles with no z-dependence. For z-dependent obstacles a new analysis is required, but it is probable that the procedures in this chapter can be followed with the same result of partial separation of the effects of each discontinuity.

Several examples of "dual discontinuity" problems are suggested in Section 3.4. The particular problem of this type where one of the obstacles is a short or an open circuit is shown to provide a technique for the measurement of the material properties.

CHAPTER IV

DERIVATION OF THE REFLECTION COEFFICIENT USING THE MAGNETIC GREEN'S FUNCTION

The wave equations for the electric and magnetic fields were derived in Chapter III. They are

$$\nabla \times \nabla \times \bar{\mathbf{E}} - k_0^2 \bar{\mathbf{E}} = k_0^2 \chi_e \bar{\mathbf{E}} - j\omega\mu_0 \nabla \times \vec{\chi}_m \bar{\mathbf{H}} \quad (3.4)$$

and

$$\nabla \times \nabla \times \bar{\mathbf{H}} - k_0^2 \bar{\mathbf{H}} = k_0^2 \vec{\chi}_m \bar{\mathbf{H}} + j\omega\epsilon_0 \nabla \times \chi_e \bar{\mathbf{E}} \quad (3.5)$$

In Chapter III, the reflection coefficient was derived using the electric field wave equation. Since we are dealing primarily with a magnetic material, it occurs that the obvious equation to solve would be that involving the magnetic fields. It turns out, however, because of the symmetry in the incident field and in the discontinuity, only one component of electric field (E_z) exists, while two components of the magnetic field are present (H_x and H_y). The derivation in Chapter III illustrated the several simplifications possible using only E_z . In particular, the tensor Green's function (which is called the electric Green's function) had only one component. Thus, the electric fields were used to derive the reflection coefficient. However, there is some merit in going through the derivation using the magnetic fields. It can be seen that this is especially true when the material is purely magnetic (i. e. , the relative dielectric constant is unity and $\chi_e = 0$), since then the curl term can be omitted from the right hand side of (3.5). In the following sections the derivation will be for a material with $\chi_e \neq 0$, $\vec{\chi}_m \neq 0$. In Chapter III the motivation was discussed for a number of the steps taken. Since the procedure is very similar in the present case the discussions will not be repeated.

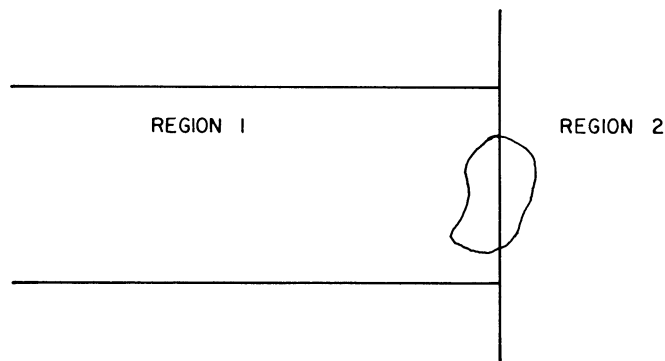
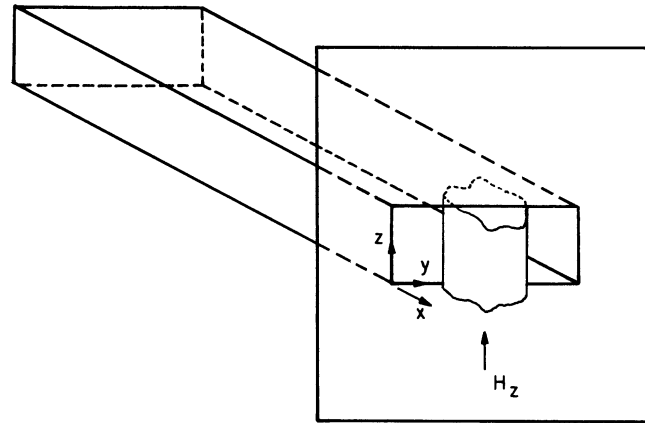


Fig. 4.1. Cylindrical ferrite obstacle in the aperture of a rectangular waveguide.

4.1 The Variational Solution

As in Chapter III, the TE_{10} mode is incident and the assumption of no z -dependent fields is made. Figure 4.1 illustrates the problem which is again reduced essentially to two dimensions. We will consider that the ferrite obstacle may extend beyond the aperture a short distance.

4.1.1 Wave Equation. The wave equation for the magnetic fields (3.5) can be written in terms of a fictitious source distribution

$$\nabla \times \nabla \times \bar{H} - k_0^2 \bar{H} = \bar{J}_m \quad (4.1)$$

where

$$\bar{J}_m = k_0^2 \vec{\chi}_m \bar{H} + j\omega\epsilon_0 \nabla \times \chi_e \bar{E} \quad (4.2)$$

The solution to this equation can be written in terms of an integral of the magnetic Green's function (\vec{G}_m),

$$\vec{H} = \vec{H}_0 + \int \vec{G}_m(\mathbf{r}|\mathbf{r}_0) \cdot \vec{J}_m(\mathbf{r}_0) dv_0 \quad (4.3)$$

where the volume dv_0 includes the entire ferrite obstacle, and where \vec{H}_0 is the total field present when the obstacle is not there. \vec{H}_0 is a solution of

$$\nabla \times \nabla \times \vec{H}_0 - k_0^2 \vec{H}_0 = \nabla^2 \vec{H}_0 + k_0^2 \vec{H}_0 = 0$$

The magnetic Green's function (\vec{G}_m) is a dyadic. It is a solution of the equation

$$\nabla \times \nabla \times \vec{G}_m - k_0^2 \vec{G}_m = \frac{1}{b} \vec{I} \delta(\mathbf{x} - \mathbf{x}_0) \delta(\mathbf{y} - \mathbf{y}_0) \quad (4.4)$$

where \vec{I} is the two-dimensional unit dyadic. The boundary conditions are the same as \vec{H} , that is,

$$\vec{n} \cdot \vec{G}_m = 0 \quad \text{on all metal walls.}$$

Since we will be dealing with a number of dyadic equations in the following development, a summary of the dyadic operations used is given in Appendix A for easy reference.

A proof that (4.3) is a solution to the wave equation can be given as follows.

From (4.1)

$$\nabla \times \nabla \times \vec{H} - k_0^2 \vec{H} = \vec{J}_m$$

Substitution for \vec{H} from (4.3) yields

$$\begin{aligned} & \nabla \times \nabla \times \vec{H}_0 - k_0^2 \vec{H}_0 + \int (\nabla \times \nabla \times - k_0^2) \vec{G}(\mathbf{x}, \mathbf{y}|\mathbf{x}_0, \mathbf{y}_0) \cdot \vec{J}_m(\mathbf{x}_0, \mathbf{y}_0) dv_0 \\ & = 0 + \int \frac{1}{b} \vec{I} \delta(\mathbf{x} - \mathbf{x}_0) \delta(\mathbf{y} - \mathbf{y}_0) \cdot \vec{J}_m(\mathbf{x}_0, \mathbf{y}_0) dv_0 \\ & = + \vec{J}_m(\mathbf{x}, \mathbf{y}) \left. \begin{array}{l} \text{if the point } \mathbf{x}, \mathbf{y} \text{ is in } v_0 \\ \text{if the point } \mathbf{x}, \mathbf{y} \text{ is not in } v_0 \end{array} \right\} \\ & = 0 \end{aligned}$$

Thus, (4.3) is the required solution.

4.1.2 Magnetic Green's Function. The field scattered by the ferrite is just

$$\bar{H}_s = \int \bar{G}_m(r|r_o) \cdot \bar{J}_m(r_o) dv_o \quad (4.5)$$

For the two-dimensional case considered here

$$\bar{J}_m = J_x \bar{a}_x + J_y \bar{a}_y \quad (4.6)$$

and

$$\bar{G}_m = \begin{bmatrix} G_{xx} & G_{xy} \\ G_{yx} & G_{yy} \end{bmatrix} \quad (4.7)$$

In order to identify the components of \bar{G} let $J_y = 0$ and $J_x(r_1) = (1/b)\delta(r_1 - r_o)$.

Then

$$\bar{H}_s = \frac{1}{b} \int \bar{G}_m(r|r_1) \cdot \delta(r_1 - r_o) \bar{a}_x dv_1 = \frac{1}{b} \int (G_{xx} \bar{a}_x + G_{yx} \bar{a}_y) \delta(r_1 - r_o) dv_1$$

$$\bar{H}_s = G_{xx}(r|r_o) \bar{a}_x + G_{yx}(r|r_o) \bar{a}_y$$

$$\bar{H}_s = H_x \bar{a}_x + H_y \bar{a}_y \quad (4.8)$$

G_{xx} can be interpreted as the x-component of magnetic field due to an x-directed delta function source of strength $1/b$ at the point r_o . G_{yx} is the y-component of the magnetic field. These are the fields resulting when the aperture discontinuity exists, but the ferrite obstacle is not present.

Similarly, J_x can be zero and $J_y(r_1) = (1/b)\delta(r_1 - r_o)$. Then

$$\bar{H}_s = G_{xy} \bar{a}_x + G_{yy} \bar{a}_y \quad (4.9)$$

G_{xy} is then the x-component of magnetic field due to a y-directed delta function source at the point r_o . G_{yy} is the y-component of the magnetic field.

These interpretations of the components of the Green's function will be useful in their derivation. The reciprocity theorem for the Green's function will also be helpful. It

states that the Green's dyadic with the variables interchanged is equal to the transpose of the original dyadic, that is,²²

$$\vec{G}_m(r|r_o) = \vec{G}_m(r_o|r) \quad (4.10)$$

Solutions to (4.4) for \vec{G}_m are needed for four cases depending on the positions of the source and field points. If we let Region 1 refer to the waveguide ($x < 0$) and Region 2 to free space ($x > 0$) the four cases are:

1. Both source point (r_o) and field point (r) are inside the waveguide. Call this solution \vec{G}_{11} . The first subscript refers to the field point and the second to the source point.
2. The source point (r_o) is in free space, and the field point (r) is in the waveguide. Call this solution \vec{G}_{12} .
3. The source point (r_o) is in the waveguide and the field point (r) is in free space. Call this solution \vec{G}_{21} .
4. The source point (r_o) and the field point (r) are both in free space. Call this solution \vec{G}_{22} .

\vec{G}_m can thus be written as

$$\begin{aligned} \vec{G}_m &= \vec{G}_{11} u(-x_o) u(-x) + \vec{G}_{12} u(x_o) u(-x) \\ &+ \vec{G}_{21} u(-x_o) u(x) + \vec{G}_{22} u(x_o) u(x) \end{aligned}$$

where the step functions $u(x)$, $u(x_o)$, are included to specify the region in which $\vec{G}_{n\ell}$ is valid. The step functions have a value of unity when their argument is positive and zero when their argument is negative.

Equation 4.4 in component form becomes

$$\nabla \times \nabla \times \vec{G}_{11} - k_o^2 \vec{G}_{11} = \frac{1}{b} \vec{I} \delta(x - x_o) \delta(y - y_o) \quad (4.11a)$$

$$\nabla \times \nabla \times \vec{G}_{12} - k_o^2 \vec{G}_{12} = 0 \quad (4.11b)$$

$$\nabla \times \nabla \times \vec{G}_{21} - k_o^2 \vec{G}_{21} = 0 \quad (4.11c)$$

$$\nabla_x \nabla_x \bar{G}_{22} - k_0^2 \bar{G}_{22} = \frac{1}{b} \bar{I} \delta(x - x_0) \delta(y - y_0) \quad (4.11d)$$

since

$$\delta(x - x_0) \delta(y - y_0) = 0 \quad \text{for } x \neq x_0, y \neq y_0$$

The boundary condition at the metal walls, $\bar{n} \cdot \bar{G} = 0$, must be satisfied for each $\bar{G}_{n\ell}$.

Since the components of \bar{G}_m represent magnetic fields, they must also satisfy certain boundary conditions at the rectangular aperture. These are continuity of H_x and H_y at $x = 0$. This condition yields

$$\bar{G}_{11}(r|r_0)|_{x=0} = \bar{G}_{21}(r|r_0)|_{x=0} \quad (4.12a)$$

$$\bar{G}_{22}(r|r_0)|_{x=0} = \bar{G}_{12}(r|r_0)|_{x=0} \quad (4.12b)$$

It should be noted that if the ferrite obstacle does not extend into Region 2, then only \bar{G}_{11} is needed. Similarly, if the obstacle is entirely in Region 2, then only \bar{G}_{22} is needed. If, however, the ferrite extends into both regions then all four solutions for \bar{G} must be used. This chapter is mainly concerned with obstacles either wholly within Region 1 or extending only a small amount (compared to a wavelength) into Region 2.

Derivation of \bar{G}_{11}

For the two-dimensional case considered, the dyadic \bar{G}_{11} can be written as

$$G_{11} = \begin{bmatrix} G_{11}^{\underline{xx}} & G_{11}^{\underline{xy}} \\ G_{11}^{\underline{yx}} & G_{11}^{\underline{yy}} \end{bmatrix} \quad (4.13)$$

\vec{G}_{11} is a solution of (4. 11a)

$$\nabla \times \nabla \times \vec{G}_{11} - k_o^2 \vec{G}_{11} = \frac{1}{b} \vec{I} \delta(x - x_o) \delta(y - y_o)$$

where $x < 0$ and $x_o < 0$.

\vec{G}_{11} must satisfy the boundary conditions on the waveguide walls

$$\vec{n} \cdot \vec{G}_{11} = 0 \quad \text{at} \quad y = 0, y = a \quad (4. 14a)$$

In terms of the components of \vec{G}_{11} this is:

$$G_{yx} = G_{yy} = 0 \quad \text{at} \quad y = 0, y = a \quad (4. 14b)$$

This, of course, agrees with the interpretation of G_{yx} and G_{yy} as y-components of a magnetic field.

In addition, all four components must be continuous across the aperture with the components of \vec{G}_{21} . (Since \vec{G}_{21} represents the fields in free space due to the source in the waveguide.)

We can break up \vec{G}_{11} arbitrarily into two parts due to the linearity of (4. 11a).

$$\vec{G}_{11} = \vec{G}_{11}^A + \vec{G}_{11}^B \quad (4. 15)$$

Such that \vec{G}_{11}^A and \vec{G}_{11}^B satisfy

$$\nabla \times \nabla \times \vec{G}_{11}^A - k_o^2 \vec{G}_{11}^A = \frac{1}{b} \vec{I} \delta(x - x_o) \delta(y - y_o) \quad (4. 16a)$$

$$\nabla \times \nabla \times \vec{G}_{11}^B - k_o^2 \vec{G}_{11}^B = 0 \quad (4. 16b)$$

and where both \vec{G}_{11}^A and \vec{G}_{11}^B satisfy the boundary condition (4. 14). Both are necessary to satisfy the continuity condition at the aperture.

We will first derive \vec{G}_{11}^A . Writing (4. 16) in component form gives

$$\frac{\partial^2 G_{yx}}{\partial y \partial x} - \frac{\partial^2 G_{xx}}{\partial y^2} - k_o^2 G_{xx} = \frac{1}{b} \delta(x - x_o) \delta(y - y_o) \quad (4. 17a)$$

$$\frac{\partial^2 G_{yy}}{\partial x \partial y} - \frac{\partial^2 G_{xy}}{\partial y^2} - k_o^2 G_{xy} = 0 \quad (4. 17b)$$

$$\frac{\partial^2 G_{xx}}{\partial y \partial x} - \frac{\partial^2 G_{yx}}{\partial x^2} - k_o^2 G_{yx} = 0 \quad (4.17c)$$

$$\frac{\partial^2 G_{xy}}{\partial x \partial y} - \frac{\partial^2 G_{yy}}{\partial x^2} - k_o^2 G_{yy} = \frac{1}{b} \delta(x - x_o) \delta(y - y_o) \quad (4.17d)$$

As can be seen, the equation does not separate into equations each involving only a single component. Instead of attempting to solve this system of coupled differential equations, it is simpler to derive \vec{G}_{11}^A from a potential function \vec{G}_1 , where

$$\vec{G}_{11}^A = \vec{G}_1 + \frac{\nabla \nabla \cdot \vec{G}_1}{k_o^2} \quad (4.18)$$

Substituting this into (4.16a) gives the equation that \vec{G}_1 must satisfy

$$\nabla^2 \vec{G}_1 + k_o^2 \vec{G}_1 = -\frac{1}{b} \vec{I} \delta(x - x_o) \delta(y - y_o) \quad (4.19)$$

In the two-dimensional case considered here, \vec{G}_1 is represented by

$$\vec{G}_1 = \begin{bmatrix} G_{xx} & G_{xy} \\ G_{yx} & G_{yy} \end{bmatrix} \quad (4.20)$$

Separation of (4.19) into components yields

$$\frac{\partial^2 G_{xx}}{\partial x^2} + \frac{\partial^2 G_{xx}}{\partial y^2} + k_o^2 G_{xx} = -\frac{1}{b} \delta(x - x_o) \delta(y - y_o) \quad (4.21a)$$

$$\frac{\partial^2 G_{yy}}{\partial x^2} + \frac{\partial^2 G_{yy}}{\partial y^2} + k_o^2 G_{yy} = -\frac{1}{b} \delta(x - x_o) \delta(y - y_o) \quad (4.21b)$$

$$\frac{\partial^2 G_{xy}}{\partial x^2} + \frac{\partial^2 G_{xy}}{\partial y^2} + k_o^2 G_{xy} = 0 \quad (4.21c)$$

$$\frac{\partial^2 G_{yx}}{\partial x^2} + \frac{\partial^2 G_{yx}}{\partial y^2} + k_o^2 G_{yx} = 0 \quad (4.21d)$$

G_{xy} and G_{yx} are zero.

The boundary conditions $\bar{n} \cdot \vec{G}_{11} = 0$ on the walls requires that

$$\frac{\partial^2 G_{xx}}{\partial x \partial y} = 0 \quad y = 0, a \quad (4.22a)$$

$$G_{yy} + \frac{\partial^2 G_{yy}}{\partial y^2} = 0 \quad y = 0, a \quad (4.22b)$$

To find G_{xx} multiply (4.21a) through by $\cos \frac{n\pi y}{a}$ and integrate from $0 \leq y \leq a$. (Essentially, the Fourier cosine transform is being taken.)

$$\left[k_0^2 - \left(\frac{n\pi}{a} \right)^2 + \frac{\partial}{\partial x^2} \right] \int_0^a G_{xx} \cos \frac{n\pi y}{a} dy = -\frac{1}{b} \cos \frac{n\pi y_0}{a} \delta(x - x_0) \quad (4.23)$$

where integration by parts showed that

$$\int_0^a \frac{\partial^2 G_{xx}}{\partial y^2} \cos \frac{n\pi y}{a} dy = -\left(\frac{n\pi}{a} \right)^2 \int_0^a G_{xx} \cos \frac{n\pi y}{a} dy$$

Let

$$\gamma_n^2 = \left(\frac{n\pi}{a} \right)^2 - k_0^2$$

and

$$G_{n_{xx}}(x) = \int_0^a G_{xx} \cos \frac{n\pi y}{a} dy.$$

Then

$$\left[\frac{\partial^2}{\partial x^2} - \gamma_n^2 \right] G_{n_{xx}}(x) = -\frac{1}{b} \cos \frac{n\pi y_0}{a} \delta(x - x_0) \quad (4.24)$$

For $x \neq x_0$, $\delta(x - x_0) = 0$ is obtained and the solutions are waves propagating away from the source at x_0 .

$$\begin{aligned} G_{n_{xx}} &= b_n e^{\gamma_n x} & \text{for } x < x_0 \\ &= c_n e^{-\gamma_n x} & \text{for } x > x_0 \end{aligned}$$

At $x = x_0$, $G_{n_{xx}}$ is continuous. Thus

$$b_n e^{\gamma_n x_0} = c_n e^{-\gamma_n x_0}$$

Now integrate (4.24) from $x_0 - \Delta$ to $x_0 + \Delta$.

$$\lim_{\Delta \rightarrow 0} \int_{x_0 - \Delta}^{x_0 + \Delta} \left(\frac{\partial^2}{\partial x^2} - \gamma_n^2 \right) G_{n_{xx}}(x) = -\frac{1}{b} \cos \frac{n\pi y_0}{a}; \left. \frac{\partial G_{n_{xx}}(x)}{\partial x} \right|_{x_0^-}^{x_0^+} = -\frac{1}{b} \cos \frac{n\pi y_0}{a} \quad (4.25)$$

$$\gamma_n c_n e^{-\gamma_n x_0} + \gamma_n b_n e^{\gamma_n x_0} = \frac{1}{b} \cos \frac{n\pi y_0}{a}$$

Then

$$b_n = \frac{1}{2\gamma_n b} \cos \frac{n\pi y_0}{a} e^{-\gamma_n x_0}$$

Thus

$$G_{n_{xx}}(x) = \frac{1}{2\gamma_n b} \cos \frac{n\pi y_0}{a} \begin{cases} e^{-\gamma_n x_0} e^{\gamma_n x} & x < x_0 \\ e^{\gamma_n x_0} e^{-\gamma_n x} & x > x_0 \end{cases}$$

$$= \frac{1}{2\gamma_n b} \cos \frac{n\pi y_0}{a} e^{-\gamma_n |x - x_0|} \quad (4.26)$$

Now, the inverse Fourier cosine transform is taken to obtain

$$G_{xx}(x, y | x_0, y_0) = \sum_{n=0}^{\infty} \frac{\epsilon_n}{ab\gamma_n} \cos \frac{n\pi y}{a} \cos \frac{n\pi y_0}{a} e^{-\gamma_n |x - x_0|} \quad (4.27)$$

where

$$\begin{aligned} \epsilon_n &= 1/2, & n &= 0 \\ &= 1, & n &\neq 0 \end{aligned}$$

The equation for G_{yy} can be treated in a similar manner, but this time using the Fourier sine transform. The results are:

$$G_{yy}(x, y | x_0, y_0) = \sum_{n=1}^{\infty} \frac{1}{ab\gamma_n} \sin \frac{n\pi y}{a} \sin \frac{n\pi y_0}{a} e^{-\gamma_n |x - x_0|} \quad (4.28)$$

We can verify the boundary conditions. It is easy to see from (4.27) and (4.28) that (4.22) is satisfied.

\bar{G}_{11}^A is now obtained from (4.18). The result is

$$G_{xx}^A = \frac{1}{k_0^2 ab} \sum_{n=1}^{\infty} \frac{\left(\frac{n\pi}{a}\right)^2}{\gamma_n} \cos \frac{n\pi y}{a} \cos \frac{n\pi y_0}{a} e^{-\gamma_n |x - x_0|} - \frac{1}{k_0^2 ab} \sum_{n=1}^{\infty} \cos \frac{n\pi y}{a} \cos \frac{n\pi y_0}{a} \frac{\partial}{\partial x} \left[\frac{(x - x_0)}{|x - x_0|} \right] \quad (4.29a)$$

$$G_{xy}^A = + \frac{1}{k_0^2 ab} \frac{(x_0 - x)}{|x_0 - x|} \sum_{n=1}^{\infty} \frac{n\pi}{a} \cos \frac{n\pi y}{a} \sin \frac{n\pi y_0}{a} e^{-\gamma_n |x - x_0|} \quad (4.29b)$$

$$G_{yx}^A = - \frac{1}{k_0^2 ab} \frac{(x_0 - x)}{|x_0 - x|} \sum_{n=1}^{\infty} \frac{n\pi}{a} \sin \frac{n\pi y}{a} \cos \frac{n\pi y_0}{a} e^{-\gamma_n |x - x_0|} \quad (4.29c)$$

$$G_{yy}^A = - \frac{1}{k_0^2 ab} \sum_{n=1}^{\infty} \gamma_n \sin \frac{n\pi y}{a} \sin \frac{n\pi y_0}{a} e^{-\gamma_n |x - x_0|} \quad (4.29d)$$

These components represent the fields radiated outward from the source. G_{xx}^A and G_{xy}^A are the magnetic fields due to an x-directed delta function source while G_{yx}^A and G_{yy}^A are the fields due to a y-directed source as discussed earlier. Using Maxwell's curl equations the electric fields due to these sources can be derived. That is, use

$$\nabla \times \bar{H} = j\omega\epsilon_0 \bar{E}$$

For $\bar{J}_m(r_1) = \frac{1}{b} \delta(r_1 - r_0) \bar{a}_x$,

$$E_z = \sum_{n=1}^{\infty} E_n = \frac{1}{j\omega\epsilon_0 ab} \sum_{n=1}^{\infty} \frac{n\pi}{a} \sin \frac{n\pi y}{a} \cos \frac{n\pi y_0}{a} e^{-\gamma_n |x - x_0|} \quad (4.30a)$$

For $\bar{J}_m(r_1) = \frac{1}{b} \delta(r_1 - r_0) \bar{a}_y$,

$$E_z = \sum_{n=1}^{\infty} E_n = \frac{1}{j\omega\epsilon_0 ab} \frac{(x_0 - x)}{|x_0 - x|} \sum_{n=1}^{\infty} \sin \frac{n\pi y}{a} \sin \frac{n\pi y_0}{a} e^{-\gamma_n |x - x_0|} \quad (4.30b)$$

The problem is now probably a little clearer. Due to the delta function sources there are an infinite number of modes (all TE_{n0} modes here) incident on the waveguide aperture. It should be remembered that we are now dealing with a source inside an open-ended waveguide and that the ferrite obstacle is not present. To complete the solution the reflected modes must be included. Each incident mode reflects (or couples) to an infinite set of modes. Using the standard definition for the reflection coefficients, the electric field can be written:

For $\bar{J}_m(r_1) = \frac{1}{b} \delta(r_1 - r_0) \bar{a}_x$,

$$E_z = \sum_{n=1}^{\infty} E_n = \frac{1}{j\omega\epsilon_0 ab} \sum_{n=1}^{\infty} \frac{n\pi}{\gamma_n} \sin \frac{n\pi y}{a} \cos \frac{n\pi y_0}{a} e^{-\gamma_n |x - x_0|} + \frac{1}{j\omega\epsilon_0 ab} \sum_{n=1}^{\infty} \sum_{m=1}^{\infty} R_{nm} \frac{n\pi}{\gamma_n} \cos \frac{n\pi y_0}{a} e^{\gamma_n x_0} \sin \frac{m\pi y}{a} e^{\gamma_m x} \quad (4.31a)$$

For $\bar{J}_m(r_1) = \frac{1}{b} \delta(r_1 - r_0) \bar{a}_y$,

$$E_z = \sum_{n=1}^{\infty} E_n = \frac{1}{j\omega\epsilon_0 ab} \sum_{n=1}^{\infty} \frac{(x_0 - x)}{|x_0 - x|} \sin \frac{n\pi y}{a} \sin \frac{n\pi y_0}{a} e^{-\gamma_n |x - x_0|} - \frac{1}{j\omega\epsilon_0 ab} \sum_{n=1}^{\infty} \sum_{m=1}^{\infty} R_{nm} \sin \frac{n\pi y_0}{a} e^{\gamma_n x_0} \sin \frac{m\pi y}{a} e^{\gamma_m x} \quad (4.31b)$$

Only TE_{n0} modes have been retained in the reflected wave. For completeness TE_{nm} waves should also be included but the coefficients of these waves are small and will be neglected here. Inclusion of these modes would turn the double summation into a triple summation making the analysis cumbersome.

Using Maxwell's curl equations with a magnetic current source, we can now write \bar{G}_{11}^B . That is, use

$$\nabla \times \bar{E} = -j\omega\mu_0 \bar{H} + \frac{\bar{J}_m}{j\omega\epsilon_0}$$

where

$$G_{\begin{smallmatrix} 11 \\ \text{xx} \end{smallmatrix}} = H_x, \quad G_{\begin{smallmatrix} 11 \\ \text{yx} \end{smallmatrix}} = H_y \quad \text{if } \bar{E} \text{ from (4.31a) is used, and}$$

$$G_{\begin{smallmatrix} 11 \\ \text{yx} \end{smallmatrix}} = H_x, \quad G_{\begin{smallmatrix} 11 \\ \text{yy} \end{smallmatrix}} = H_y \quad \text{if } \bar{E} \text{ from (4.31b) is used.}$$

\bar{G}_{11}^B is thus the field due to the reflection from the open aperture.

The following important result for \bar{G}_{11} is thus obtained.

$$\begin{aligned} G_{\begin{smallmatrix} 11 \\ \text{xx} \end{smallmatrix}}(r|r_0) = & \left[\frac{1}{k_0^2 ab} \sum_{n=1}^{\infty} \frac{\left(\frac{n\pi}{a}\right)^2}{\gamma_n} \cos \frac{n\pi y}{a} \cos \frac{n\pi y_0}{a} e^{-\gamma_n |x-x_0|} \right. \\ & + \frac{1}{k_0^2 ab} \sum_{n=1}^{\infty} \sum_{m=1}^{\infty} R_{nm} \frac{\frac{n\pi}{a} \frac{m\pi}{a}}{\gamma_n} \cos \frac{m\pi y}{a} e^{\gamma_m x} \cos \frac{n\pi y_0}{a} e^{\gamma_n x_0} \\ & \left. - \frac{\delta(x-x_0) \delta(y-y_0)}{b k_0^2} \right] u(-x) u(-x_0) \end{aligned} \quad (4.32a)$$

$$\begin{aligned} G_{\begin{smallmatrix} 11 \\ \text{xx} \end{smallmatrix}}(r|r_0) = & \left[\frac{1}{k_0^2 ab} \sum_{n=1}^{\infty} \frac{(x_0-x)}{|x_0-x|} \frac{n\pi}{a} \cos \frac{n\pi y}{a} \sin \frac{n\pi y_0}{a} e^{-\gamma_n |x-x_0|} \right. \\ & \left. - \frac{1}{k_0^2 ab} \sum_{n=1}^{\infty} \sum_{m=1}^{\infty} R_{nm} \frac{m\pi}{a} \cos \frac{m\pi y}{a} e^{\gamma_m x} \sin \frac{n\pi y_0}{a} e^{\gamma_n x_0} \right] u(-x) u(-x_0) \end{aligned} \quad (4.32b)$$

$$\begin{aligned} G_{\begin{smallmatrix} 11 \\ \text{yx} \end{smallmatrix}}(r|r_0) = & - \left[\frac{1}{k_0^2 ab} \sum_{n=1}^{\infty} \frac{(x_0-x)}{|x_0-x|} \frac{n\pi}{a} \sin \frac{n\pi y}{a} \cos \frac{n\pi y_0}{a} e^{-\gamma_n |x-x_0|} \right. \\ & \left. + \frac{1}{k_0^2 ab} \sum_{n=1}^{\infty} \sum_{m=1}^{\infty} R_{nm} \frac{n\pi}{a} \gamma_m \sin \frac{m\pi y}{a} e^{\gamma_m x} \cos \frac{n\pi y_0}{a} e^{\gamma_n x_0} \right] u(-x) u(-x_0) \end{aligned} \quad (4.32c)$$

$$\begin{aligned} G_{\begin{smallmatrix} 11 \\ \text{yy} \end{smallmatrix}}(r|r_0) = & - \left[\frac{1}{k_0^2 ab} \sum_{n=1}^{\infty} \gamma_n \sin \frac{n\pi y}{a} \sin \frac{n\pi y_0}{a} e^{-\gamma_n |x-x_0|} \right. \\ & \left. - \frac{1}{k_0^2 ab} \sum_{n=1}^{\infty} \sum_{m=1}^{\infty} R_{nm} \gamma_m \sin \frac{m\pi y}{a} e^{\gamma_m x} \sin \frac{n\pi y_0}{a} e^{\gamma_n x_0} \right] u(-x) u(-x_0) \end{aligned} \quad (4.32d)$$

The quantities $u(-x)$ and $u(-x_0)$ are step functions having unit value for $x < 0$, $x_0 < 0$ and are zero for $x > 0$, $x_0 > 0$. They are used to indicate that \bar{G}_{11} is only valid when both source

and field point are in the waveguide. The reflection coefficients R_{nn} and the coupling coefficients R_{nm} still need to be evaluated. Methods of doing this are derived in Appendix B.

When the reciprocity theorem $\bar{G}_m(r|r_o) = \tilde{\bar{G}}_m(r_o|r)$ is used, the interesting result

$$\frac{R_{mn}}{\gamma_m} = \frac{R_{nm}}{\gamma_n} \quad (4.34)$$

is obtained, relating the coupling coefficients. This checks with (3.14) derived from the electric Green's function.

Derivation of \bar{G}_{12} and \bar{G}_{21}

The Green's function \bar{G}_{12} and \bar{G}_{21} can be written in general as

$$\bar{G}_{12} = \begin{bmatrix} G_{12}^{\underline{xx}} & G_{12}^{\underline{xy}} \\ G_{12}^{\underline{yx}} & G_{12}^{\underline{yy}} \end{bmatrix} \quad (4.35a)$$

$$\bar{G}_{21} = \begin{bmatrix} G_{21}^{\underline{xx}} & G_{21}^{\underline{xy}} \\ G_{21}^{\underline{yx}} & G_{21}^{\underline{yy}} \end{bmatrix} \quad (4.35b)$$

From the reciprocity relationship (4.10) we can write

$$\bar{G}_{12}(r|r_o) = \tilde{\bar{G}}_{21}(r_o|r)$$

In component form this becomes

$$G_{12}^{\underline{xx}}(r|r_o) = G_{21}^{\underline{xx}}(r_o|r) \quad (4.36a)$$

$$G_{12}^{\underline{yx}}(r|r_o) = G_{21}^{\underline{xy}}(r_o|r) \quad (4.36b)$$

$$G_{12}^{\underline{xy}}(r|r_o) = G_{21}^{\underline{yx}}(r_o|r) \quad (4.36c)$$

$$G_{12}^{\underline{yy}}(r|r_o) = G_{21}^{\underline{yy}}(r_o|r) \quad (4.36d)$$

We will solve for \vec{G}_{21} and then obtain \vec{G}_{12} using these equations.

\vec{G}_{12} and \vec{G}_{21} are solutions of the homogeneous wave equation since $x \neq x_0$ is true for them both.

$$\nabla \times \nabla \times \vec{G}_{12} - k_0^2 \vec{G}_{12} = 0 \quad (4.11b)$$

$$\nabla \times \nabla \times \vec{G}_{21} - k_0^2 \vec{G}_{21} = 0 \quad (4.11c)$$

\vec{G}_{21} represents magnetic fields in free space due to a source inside the waveguide. As before, in (4.5), we can alternately let \vec{J}_m be an x-directed delta function of strength $\frac{1}{b}$ and a y-directed delta function and then identify the components of \vec{G}_{21} with H_x and H_y . We have for the x-directed source

$$\vec{J}_m(r_1) = \frac{1}{b} \delta(r_1 - r_0) \vec{a}_x$$

$$G_{21}^{\text{xx}} = H_x$$

$$G_{21}^{\text{yx}} = H_y$$

The electric field in the aperture, due to this source, is given by (4.31a) with $x = 0$. In Appendix B, a method of deriving the radiated fields from the aperture distribution of electric field is given. From (B-5b) and (B-7) we obtain

$$H_x^n = \frac{1}{2\pi(j\omega\mu_0)} \int_0^a \int_0^b E_n(\xi, \eta) \frac{\partial^2}{\partial x \partial y} \frac{e^{-jk_0 r}}{r} d\xi d\eta \quad (4.37a)$$

$$H_y^n = \frac{1}{2\pi(j\omega\mu_0)} \int_0^a \int_0^b E_n(\xi, \eta) \left(\frac{\partial^2}{\partial y^2} + k_0^2 \right) \frac{e^{-jk_0 r}}{r} d\xi d\eta \quad (4.37b)$$

where

$$r = \sqrt{x^2 + (y-\eta)^2 + (z-\xi)^2}$$

These equations give the magnetic field in free space when the aperture distribution of electric field is $E_n(\xi, \eta)$. The dummy variables of integration ξ and η correspond to the z and y

directions, respectively. We then have that

$$\left. \begin{aligned} G_{\text{xx}}^{21} &= \sum_{n=1}^{\infty} H_x^n \\ G_{\text{yx}}^{21} &= \sum_{n=1}^{\infty} H_y^n \end{aligned} \right\} \text{using (4.31a) for } E_n(x=0) \quad (4.38a)$$

Similarly, we have for the y-directed source

$$\bar{J}_m(r_1) = \frac{1}{b} \delta(r_1 - r_o) \bar{a}_y$$

$$G_{\text{xy}}^{21} = H_x$$

$$G_{\text{yy}}^{21} = H_y$$

So that

$$\left. \begin{aligned} G_{\text{xy}}^{21} &= \sum_{n=1}^{\infty} H_x^n \\ G_{\text{yy}}^{21} &= \sum_{n=1}^{\infty} H_y^n \end{aligned} \right\} \text{using (4.31b) for } E_n(x=0) \quad (4.38b)$$

Finally, \bar{G}_{12} can be obtained from (4.36) and (4.38). The result is

$$G_{\text{xx}}^{12} = \frac{-1}{2\pi k_o^2 ab} \sum_{n=1}^{\infty} \frac{n\pi}{\gamma_n} \cos \frac{n\pi y}{a} e^{\gamma_n x} \int_0^a \int_0^b \left(\sin \frac{n\pi\eta}{a} + \sum_{m=1}^{\infty} R_{nm} \sin \frac{m\pi\eta}{a} \right) \frac{\partial^2}{\partial x_o \partial y_o} \frac{e^{-jk_o r_o}}{r_o} d\xi d\eta \quad (4.39a)$$

$$G_{\text{xy}}^{12} = \frac{-1}{2\pi k_o^2 ab} \sum_{n=1}^{\infty} \frac{n\pi}{\gamma_n} \cos \frac{n\pi y}{a} e^{\gamma_n x} \int_0^a \int_0^b \left(\sin \frac{n\pi\eta}{a} + \sum_{m=1}^{\infty} R_{nm} \sin \frac{m\pi\eta}{a} \right) \left(\frac{\partial^2}{\partial y_o^2} + k_o^2 \right) \frac{e^{-jk_o r_o}}{r_o} d\xi d\eta \quad (4.39b)$$

$$G_{\text{yx}}^{12} = \frac{1}{2\pi k_o^2 ab} \sum_{n=1}^{\infty} \sin \frac{n\pi y}{a} e^{\gamma_n x} \int_0^a \int_0^b \left(\sin \frac{n\pi\eta}{a} + \sum_{m=1}^{\infty} R_{nm} \sin \frac{m\pi\eta}{a} \right) \frac{\partial^2}{\partial x_o \partial y_o} \frac{e^{-jk_o r_o}}{r_o} d\xi d\eta \quad (4.39c)$$

$$G_{\text{yy}}^{12} = \frac{1}{2\pi k_o^2 ab} \sum_{n=1}^{\infty} \sin \frac{n\pi y}{a} e^{\gamma_n x} \int_0^a \int_0^b \left(\sin \frac{n\pi\eta}{a} + \sum_{m=1}^{\infty} R_{nm} \sin \frac{m\pi\eta}{a} \right) \left(\frac{\partial^2}{\partial y_o^2} + k_o^2 \right) \frac{e^{-jk_o r_o}}{r_o} d\xi d\eta \quad (4.39d)$$

4.1.3 The Reflection Coefficient.

We will now find an integral expression for the reflection coefficient.

The incident electric field is again taken to be in the TE_{10} mode. From (3.15) we have the electric field in the waveguide when the ferrite obstacle is absent.

$$\bar{E}_o = \left[\sin \frac{\pi y}{a} e^{-\gamma_1 x} + \sum_{n=1}^{\infty} R_{1n} \sin \frac{n\pi y}{a} e^{\gamma_n x} \right] \bar{a}_z \quad (4.40a)$$

Use of Maxwell's equation

$$\nabla \times \bar{E} = -j\omega\mu_o \bar{H}$$

then gives the magnetic fields inside the waveguide in the absence of the ferrite.

$$\begin{aligned} \bar{H}_o = \frac{1}{j\omega\mu_o} \left\{ \left[-\frac{\pi}{a} \cos \frac{\pi y}{a} e^{-\gamma_1 x} - \sum_{n=1}^{\infty} \frac{n\pi}{a} R_{1n} \cos \frac{n\pi y}{a} e^{\gamma_n x} \right] \bar{a}_x \right. \\ \left. + \left[-\gamma_1 \sin \frac{\pi y}{a} e^{-\gamma_1 x} + \sum_{n=1}^{\infty} \gamma_n R_{1n} \sin \frac{n\pi y}{a} e^{\gamma_n x} \right] \bar{a}_y \right\} \end{aligned} \quad (4.40b)$$

The magnetic fields in free space when the post is absent can be obtained from (4.37) and (4.40a).

$$H_{ox} = \frac{1}{2\pi(j\omega\mu_o)} \int_0^a \int_0^b \left[\sin \frac{\pi\eta}{a} + \sum_{n=1}^{\infty} R_{1n} \sin \frac{n\pi\eta}{a} \right] \frac{\partial^2}{\partial x \partial y} \frac{e^{-jk_o r}}{r} d\xi d\eta \quad (4.41a)$$

$$H_{oy} = \frac{1}{2\pi(j\omega\mu_o)} \int_0^a \int_0^b \left[\sin \frac{\pi\eta}{a} + \sum_{n=1}^{\infty} R_{1n} \sin \frac{n\pi\eta}{a} \right] \left[\frac{\partial^2}{\partial y^2} + k_o^2 \right] \frac{e^{-jk_o r}}{r} d\xi d\eta \quad (4.41b)$$

Again, as in Chapter III, the electric field in the waveguide with the ferrite obstacle present can be written

$$\bar{E} = \left[\sin \frac{\pi y}{a} e^{-\gamma_1 x} + \sum_{n=1}^{\infty} R_n \sin \frac{n\pi y}{a} e^{\gamma_n x} \right] \bar{a}_z \quad (4.42a)$$

The magnetic fields inside the waveguide but outside the region occupied by the ferrite are then

$$\begin{aligned} \bar{\mathbf{H}} = \frac{1}{j\omega\mu_0} \left\{ \left[-\frac{\pi}{a} \cos \frac{\pi y}{a} e^{-\gamma_1 x} - \sum_{n=1}^{\infty} \frac{n\pi}{a} R_n \cos \frac{n\pi y}{a} e^{\gamma_n x} \right] \bar{\mathbf{a}}_x \right. \\ \left. + \left[-\gamma_1 \sin \frac{\pi y}{a} e^{-\gamma_1 x} + \sum_{n=1}^{\infty} \gamma_n R_n \sin \frac{n\pi y}{a} e^{\gamma_n x} \right] \bar{\mathbf{a}}_y \right\} \end{aligned} \quad (4.42b)$$

The quantity R_1 is the reflection coefficient of the combined ferrite and aperture and is the desired quantity. R_1 is referred to the plane $x = 0$, although the ferrite obstacle may be anywhere in the waveguide or extending slightly outside the aperture.

The integral equation for the fields (4.3) is

$$\bar{\mathbf{H}} = \bar{\mathbf{H}}_0 + \int \bar{\mathbf{G}}_m(\mathbf{r} | \mathbf{r}_0) \cdot \bar{\mathbf{J}}_m(\mathbf{r}_0) dv_0 \quad (4.3)$$

In particular, the fields in the waveguide are given by

$$\begin{aligned} \bar{\mathbf{H}} = \bar{\mathbf{H}}_0 + \int \left[\bar{\mathbf{G}}_{11}(\mathbf{r} | \mathbf{r}_0) \cdot \bar{\mathbf{J}}_m(\mathbf{r}_0) u(-x_0) u(-x) \right. \\ \left. + \bar{\mathbf{G}}_{12}(\mathbf{r} | \mathbf{r}_0) \cdot \bar{\mathbf{J}}_m(\mathbf{r}_0) u(x_0) u(-x) \right] dv_0 \end{aligned}$$

For H_x we have

$$\begin{aligned} H_x = H_{0x} + \int \left[G_{\frac{11}{xx}} J_x(\mathbf{r}_0) + G_{\frac{11}{xy}} J_y(\mathbf{r}_0) \right] u(-x_0) u(-x) dv_0 \\ + \int \left[G_{\frac{12}{xx}} J_x(\mathbf{r}_0) + G_{\frac{12}{xy}} J_y(\mathbf{r}_0) \right] u(x_0) u(-x) dv_0 \end{aligned} \quad (4.43)$$

Now in (4.43) take the limit as $x \rightarrow -\infty$, using (4.32) and (4.39) for the Green's functions and (4.40), (4.41), and (4.42) for the magnetic fields. The result is

$$R_1 = R_{11} - \frac{\omega^2 \mu_0^2}{k_0^2 a b \gamma_1} \int \bar{\mathbf{H}}_0(\mathbf{r}_0) \cdot \bar{\mathbf{J}}_m(\mathbf{r}_0) dv_0 \quad (4.44)$$

This is the reflection coefficient for the case where the incident field is

$$\bar{\mathbf{E}} = \sin \frac{\pi y}{a} e^{\gamma_1 x} \bar{\mathbf{a}}_z$$

The expression for the reflection coefficient derived from the magnetic Green's function can be shown to be equal to that derived from the electric Green's function (3.17).

4.1.4 Variational Expression. As in Chapter III, the variational expression for the reflection coefficient can be derived by introducing the field $\bar{\mathbf{E}}_2$, $\bar{\mathbf{H}}_2$, where these are the fields if the dc magnetic bias is reversed on the ferrite. The integral equation which $\bar{\mathbf{H}}_2$ satisfies is

$$\bar{\mathbf{H}}_2 = \bar{\mathbf{H}}_0 + \int \bar{\mathbf{G}}_m(\mathbf{r}, \mathbf{r}_0) \cdot \bar{\mathbf{J}}_m^{(2)}(\mathbf{r}_0) dv_0 \quad (4.45)$$

where

$$\begin{aligned} \bar{\mathbf{J}}_m^{(2)} &= k_0^2 \bar{\chi}_{m_2} \bar{\mathbf{H}}_2 + j\omega\epsilon_0 \nabla \times \chi_e \bar{\mathbf{E}}_2 \text{ and} \\ \bar{\chi}_{m_2} &= \bar{\chi}_m \end{aligned}$$

The reflection coefficient when the field is reversed is

$$R_1^{(2)} = R_{11} - \frac{\omega^2 \mu_0^2}{abk_0^2 \gamma_1} \int \bar{\mathbf{H}}_0(\mathbf{r}_0) \cdot \bar{\mathbf{J}}_m^{(2)}(\mathbf{r}_0) dv_0 \quad (4.46)$$

This is equal to R_1 as proven in Chapter III (3.27).

The variational expression is obtained by multiplying (4.3) by $\bar{\mathbf{J}}_m^{(2)}(\mathbf{r})$, integrating over the volume dv , and then dividing both sides by $(R_1 - R_{11}) \int \bar{\mathbf{J}}_m^{(2)} \cdot \bar{\mathbf{H}}_0 dv$. The result is

$$R_1 - R_{11} = \frac{-\frac{\omega \mu_0^2}{abk_0^2 \gamma_1} \int \bar{\mathbf{J}}_m \cdot \bar{\mathbf{H}}_0 dv \int \bar{\mathbf{J}}_m^{(2)} \cdot \bar{\mathbf{H}}_0 dv}{\int \bar{\mathbf{J}}_m^{(2)} \cdot \bar{\mathbf{H}} dv - \int \int \bar{\mathbf{J}}_m^{(2)}(\mathbf{r}) \cdot \bar{\mathbf{G}}_m(\mathbf{r}, \mathbf{r}_0) \cdot \bar{\mathbf{J}}(\mathbf{r}_0) dv_0 dv} \quad (4.47)$$

This is the desired stationary expression for $R_1 - R_{11}$.

4.2 Conclusions

Comparing (4.47) with the expression (3.28) where the electric Green's function was used, we see that the equations appear quite similar. This similarity is deceptive for the magnetic equation (4.47) is much more complex and difficult to solve. This is because \bar{J}_m , $\bar{J}_m^{(2)}$, \bar{H} , \bar{H}_2 and \bar{H}_0 have two components each and \vec{G}_m has four nonzero components. On the other hand, the electric field formulation (3.28) involves \bar{J} , \bar{J}_2 , \bar{E} , \bar{E}_2 , \bar{E}_0 and \vec{G} which have only one component each. The magnetic expression is a vector formulation while the electric expression can be immediately written as a scalar one.

Although in the example presented the formulation in terms of the electric fields and the electric Green's function was simpler than that obtained using the corresponding magnetic quantities, in problems where the geometry is such that \bar{E} has more than one component the magnetic formulation may be more useful. This would be particularly true if the obstacle had a relative permittivity of unity.

CHAPTER V

EXPERIMENTAL WORK AND CONCLUSIONS

The basic aim of the experimental work was to observe and measure the asymmetrical field patterns and the reflections produced when an electromagnetic wave is incident on a magnetized ferrite cylinder. A ferrite post placed in or near the aperture of a rectangular waveguide was the structure used for most of the tests. This configuration was found to have the characteristics of an electronic scanning antenna. A number of experiments were performed on this structure to substantiate the theory presented in the preceding sections and to investigate the scanning property. In addition, the experiments provided motivation for much of the analysis and led to the design of practical working models. As in most experimental work, new ideas emerged during the tests for the development and use of the properties investigated. Several of the more novel and interesting ideas were tried and the results will be reported.

Because of the complexity involved in radiation measurements and in order to give more meaning to the test results, the test apparatus will be described before the observed data are presented.

5.1 Test Apparatus

The equipment used to record the beam patterns is shown in Fig. 5.1. A block diagram of the test circuit is shown in Fig. 5.2. The ferrite in the waveguide aperture is shown between the electromagnet pole faces. For clarity, the magnet gap is large in the picture but during tests the pole faces are brought near to the ferrite to produce as uniform a field as possible. Also, during actual tests, the effects of reflections from the measuring equipment are eliminated by placing a sheet of absorbing material around the aperture as shown in Fig. 5.3 or by using a metal ground plane. A Hall effect probe is used to measure the applied magnetic field.

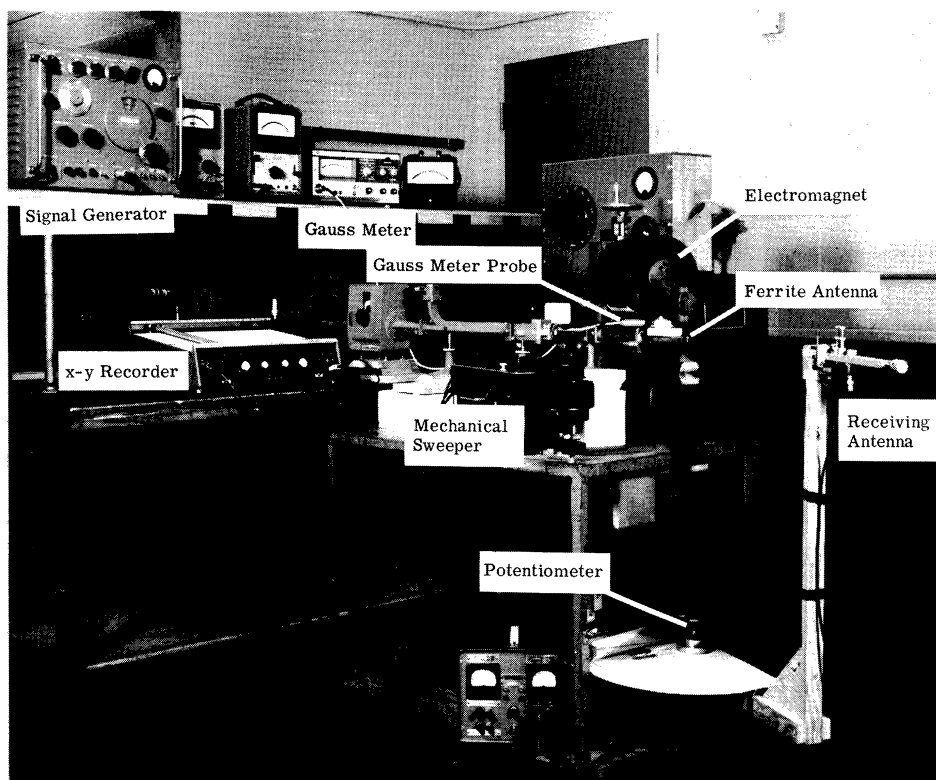


Fig. 5. 1. Equipment for recording beam patterns.

The distance between the transmitting and receiving antennas is 17 inches. This is more than 11 wavelengths at 8.2 Gc/sec, the largest wavelength used in any of the experiments. The receiving antenna, an open-ended rectangular waveguide, is mounted on a frame which rotates in the horizontal plane at a constant distance from the transmitter. The frame is driven automatically by a General Radio Sweep Drive. The beam angle is measured and recorded using a biased potentiometer attached to the moving frame. The Moseley x-y Recorder plots the beam pattern. The range of beam angles covered is between $+90^{\circ}$ and -90° . A directional coupler and sliding short are used to measure the magnitude of the reflection coefficient.

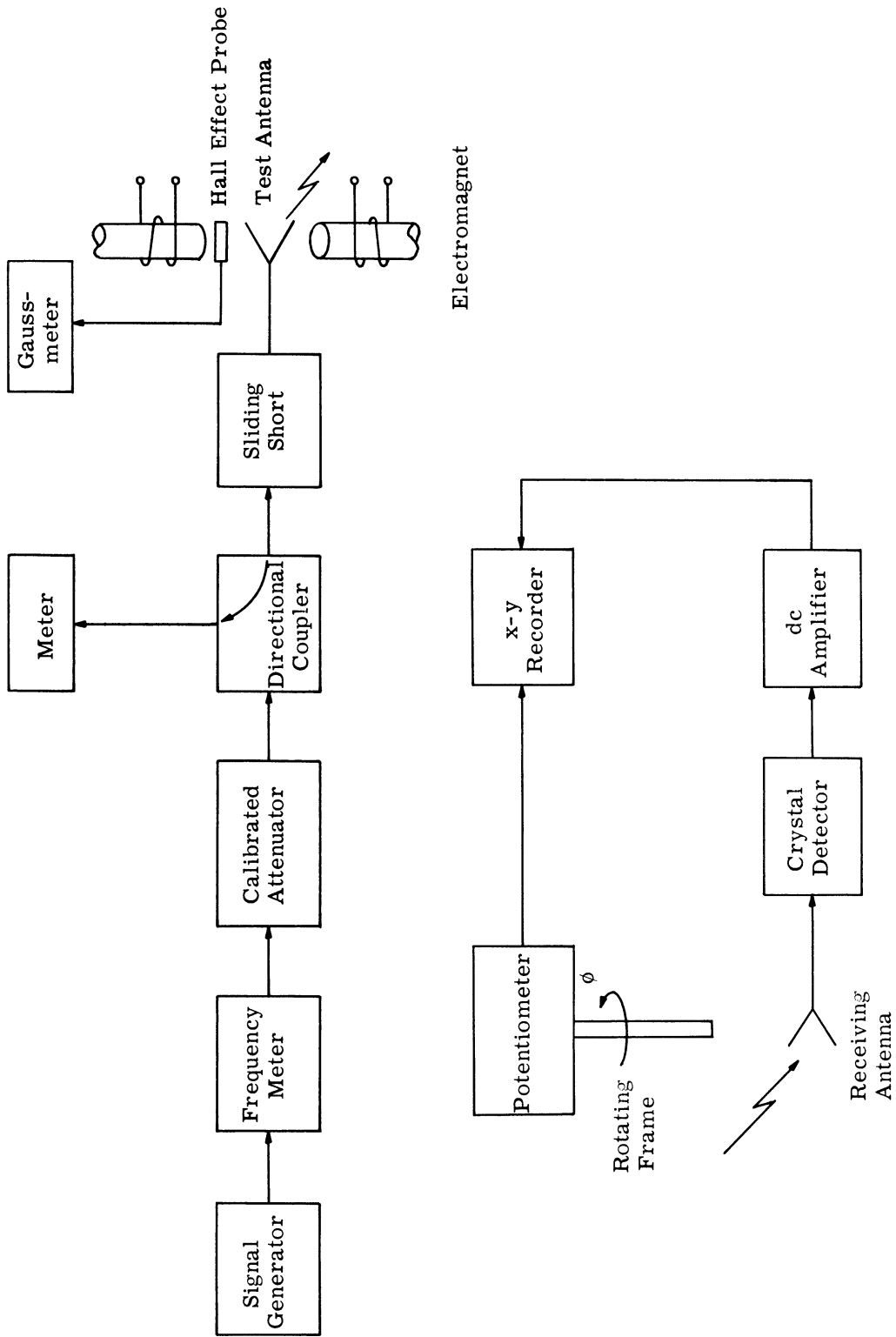


Fig. 5.2. Block diagram of the test circuit pictured in Fig. 5.1.

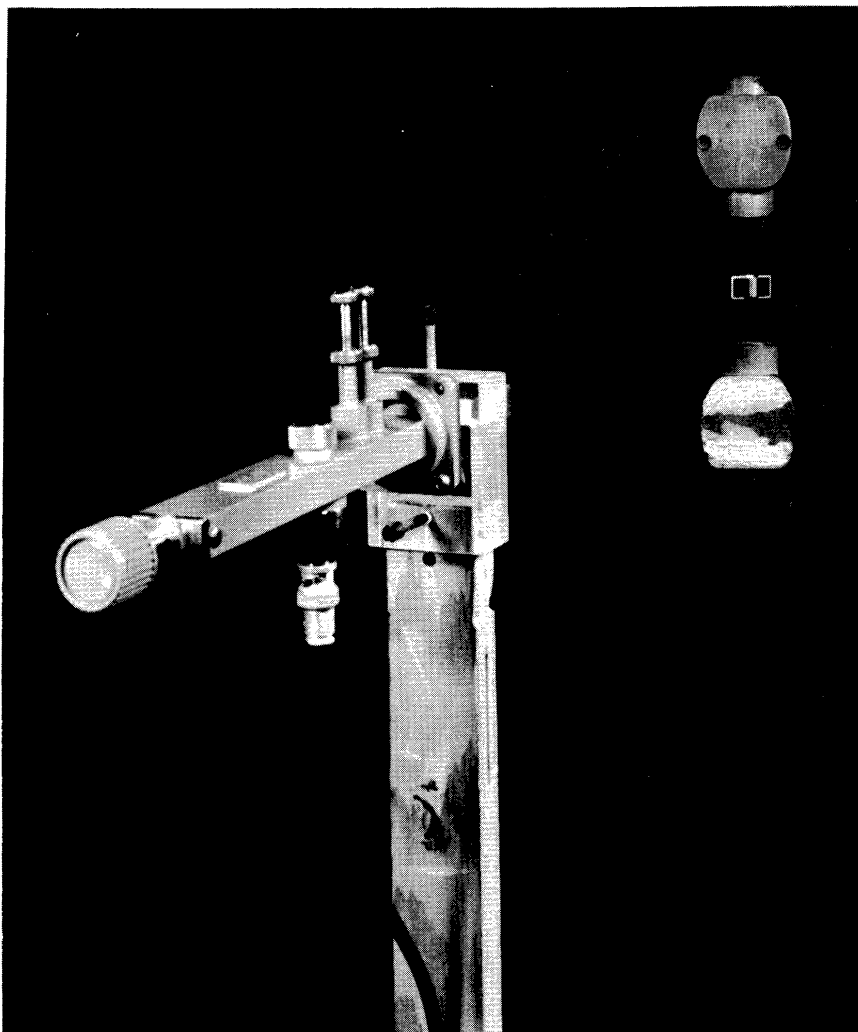


Fig. 5.3. Test set-up showing absorbing material around the aperture.

5.2 Radiation Patterns

Beam patterns for the antenna in Fig. 5.3, traced from the x-y recorder plots, are shown in Fig. 5.4 displaying the beam directing property of the device. The labeling of the angular coordinate should be noted as being reversed from the plots in Chapter II for the theoretical results. As the applied field is increased the beam is shifted away from $\phi = 0^\circ$ toward positive values of ϕ . At about 300 oersteds the main lobe begins to diminish and a new lobe appears at a negative ϕ value. Only the beam pattern is shown. The amplitudes have been normalized. The change in VSWR as the applied field is increased is shown in Fig. 5.5. Above about 300 oersteds the efficiency is reduced greatly because of the large reflections. For very high fields the VSWR is improved, but in this region the ferrite ab-

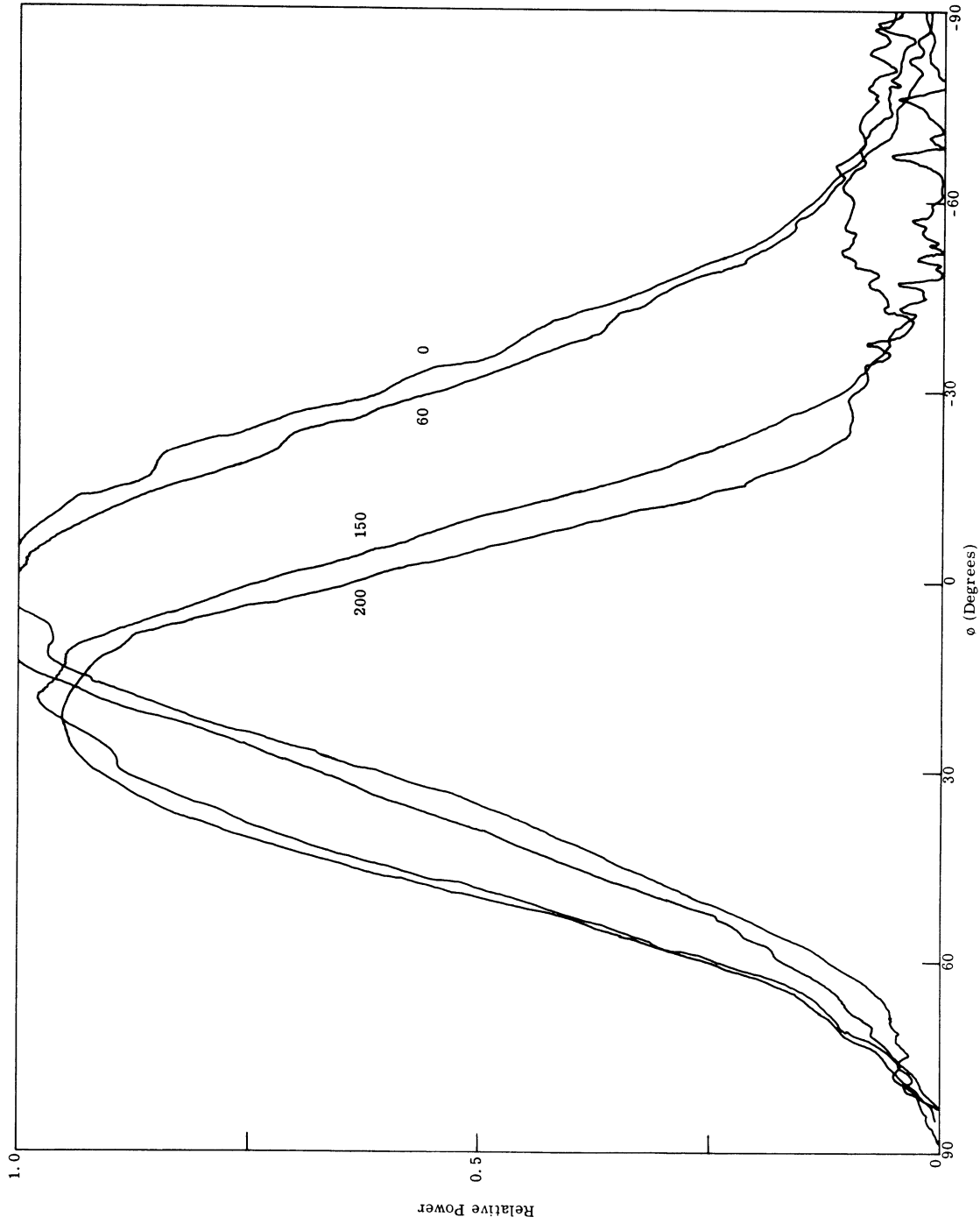


Fig. 5. 4. (a) Experimental beam patterns measured when the applied field (shown in oersteds on the figure) is varied. Frequency = 10 Gc/sec, diameter = .295", TT 390 ferrite.

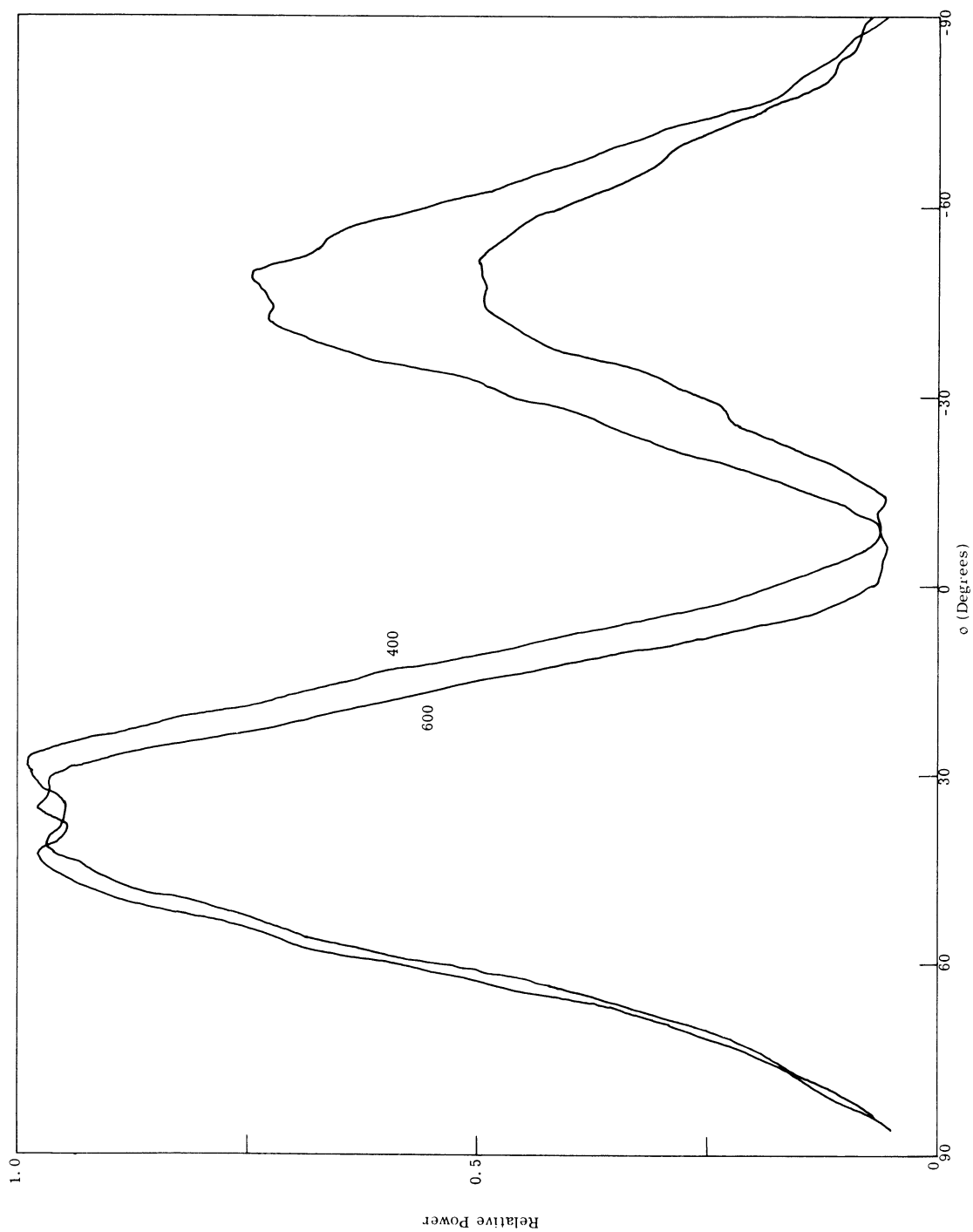


Fig. 5. 4. (b) Experimental beam patterns measured when the applied field (shown in oersteds on the figure) is varied. Frequency = 10 Gc/sec, diameter = .295", TT 390 ferrite.

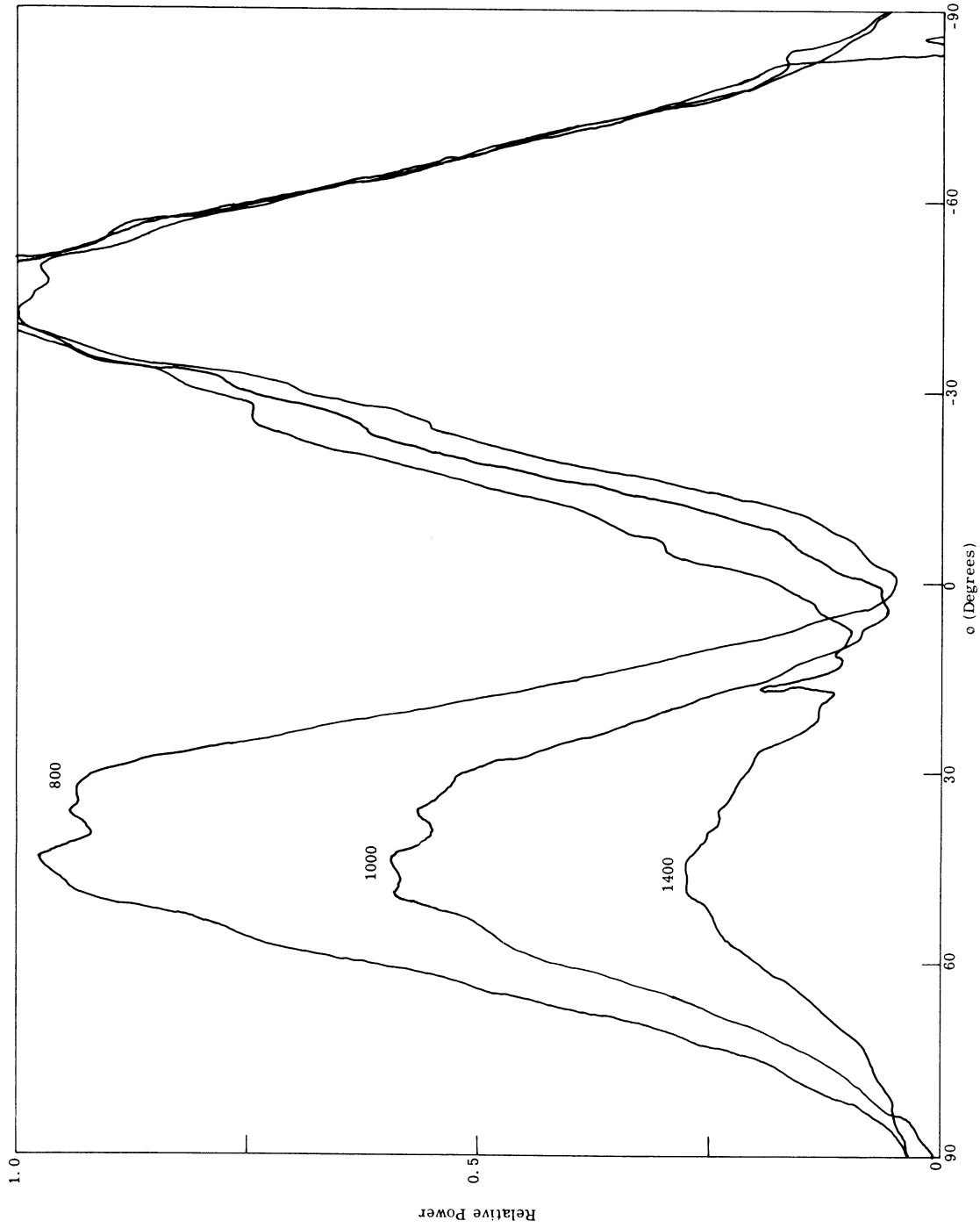


Fig. 5. 4. (c) Experimental beam patterns measured when the applied field (shown in oersted on the figure) is varied. Frequency = 10 Gc/sec, diameter = .295", TT 390 ferrite.

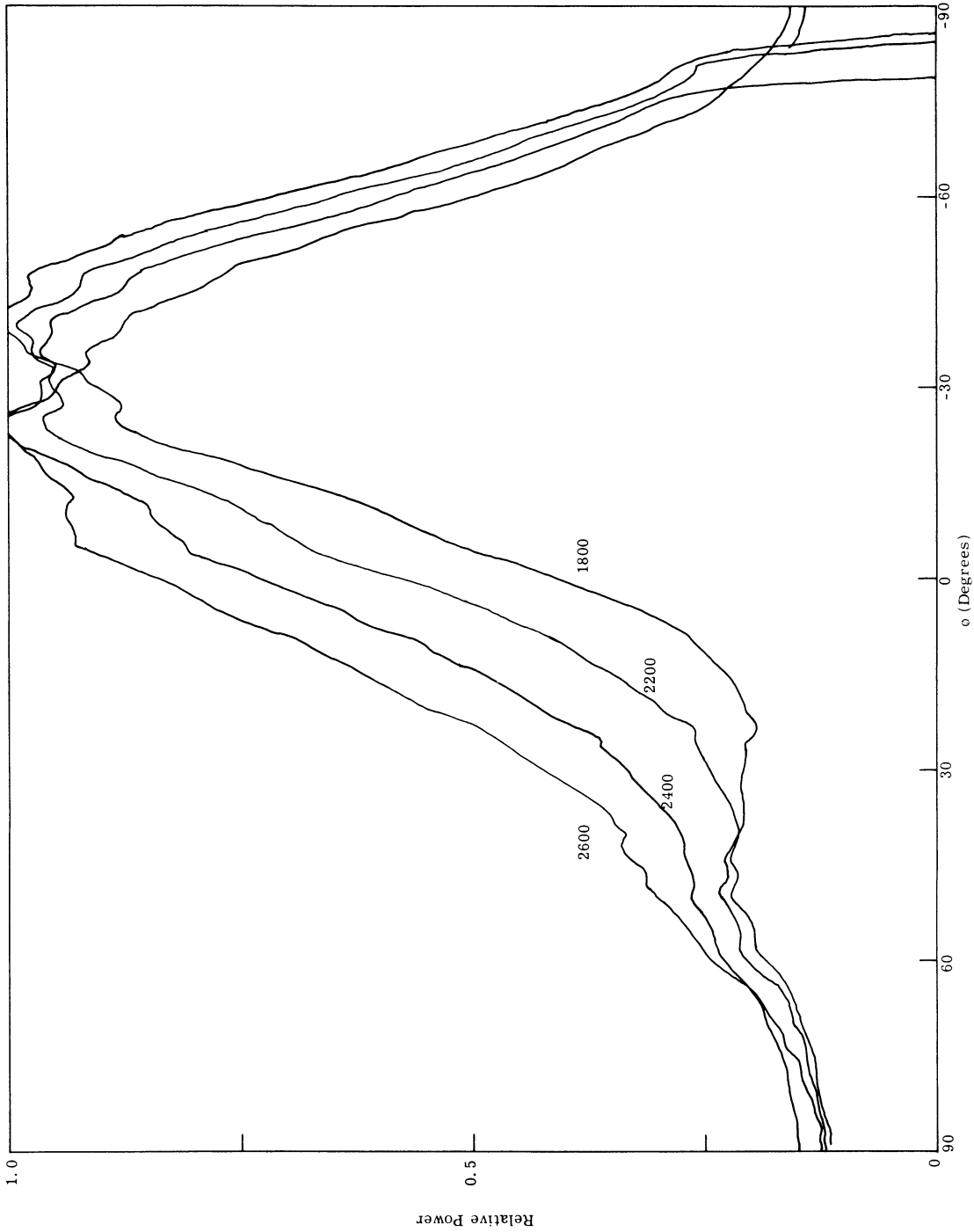


Fig. 5. 4. (d) Experimental beam patterns measured when the applied field (shown in oersted on the figure) is varied. Frequency = 10 Gc/sec, diameter = .295", TT 390 ferrite.

sorption losses are great because the ferrite is near ferromagnetic resonance. The peak absorption was measured to occur at 2850 oersteds.

A comparison between the observed beam shifting and the theoretical result was given in Chapter II. In particular, the theory predicted the beam position correctly for the low values of applied fields. In this region the device has a low VSWR so that little interaction exists between the scattered waves and the waveguide walls. Thus, the low field case satisfies the restrictions on the theory. Above 300 oersteds however, the high measured VSWR reveals the increasing interaction between the scattered wave and the waveguide walls. The theory does not apply in this region so that predictions of the beam angle cannot be made. This accounts for the separation in the theoretical and experimental curves in Fig. 2.11(a).

As predicted by the theory in Chapter II, reversing the applied bias field results in imaging the beam pattern about $\phi = 0^\circ$. Figure 5.6 illustrates this effect. This property increases the range of scan angles by a factor of two.

The preceding curves show that the device operates as a beam shifting or scanning antenna at low applied fields. The beam angle can be varied over a total range of about 60° before undesired lobes appear and the VSWR becomes large. The relatively low field requirement is fortunate for two reasons.

1. Creation of large magnetic fields requires a large electromagnet. (The electromagnet shown in the photograph, Fig. 5.1, is used for test purposes only and a much smaller magnet can produce the needed fields as will be shown in Section 5.4.)
2. For fast electronic scanning, the applied magnetic field must be varied at a very high rate. An analysis of the simplified equivalent circuit of the electromagnet coil (Fig. 5.7) indicates the large amounts of power required. The impedance of the coil is

$$Z = R_{eq.} + jX_{eq.} = \frac{R_s R_p^2 + \omega^2 L^2 (R_p + R_s)}{(\omega L)^2 + R_p^2} + j \frac{\omega L R_p^2}{(\omega L)^2 + R_p^2} \quad (5.1)$$

The series resistance (R_s) is very small and the parallel resistance (R_p) is very high for most coils. As the frequency is in-

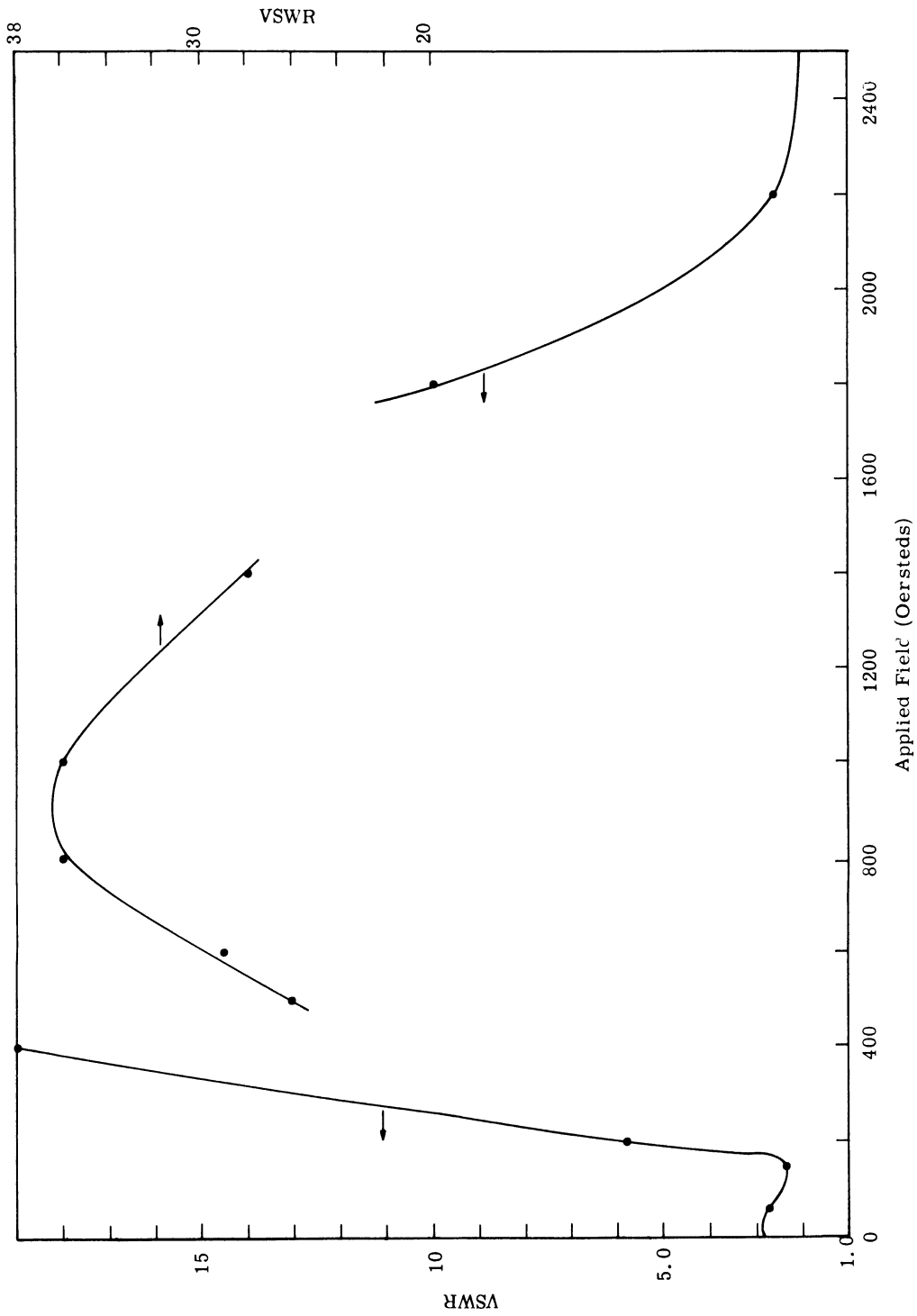


Fig. 5.5. VSWR vs. applied field. Frequency = 10 Gc/sec, diameter = .295", TT 390 ferrite.

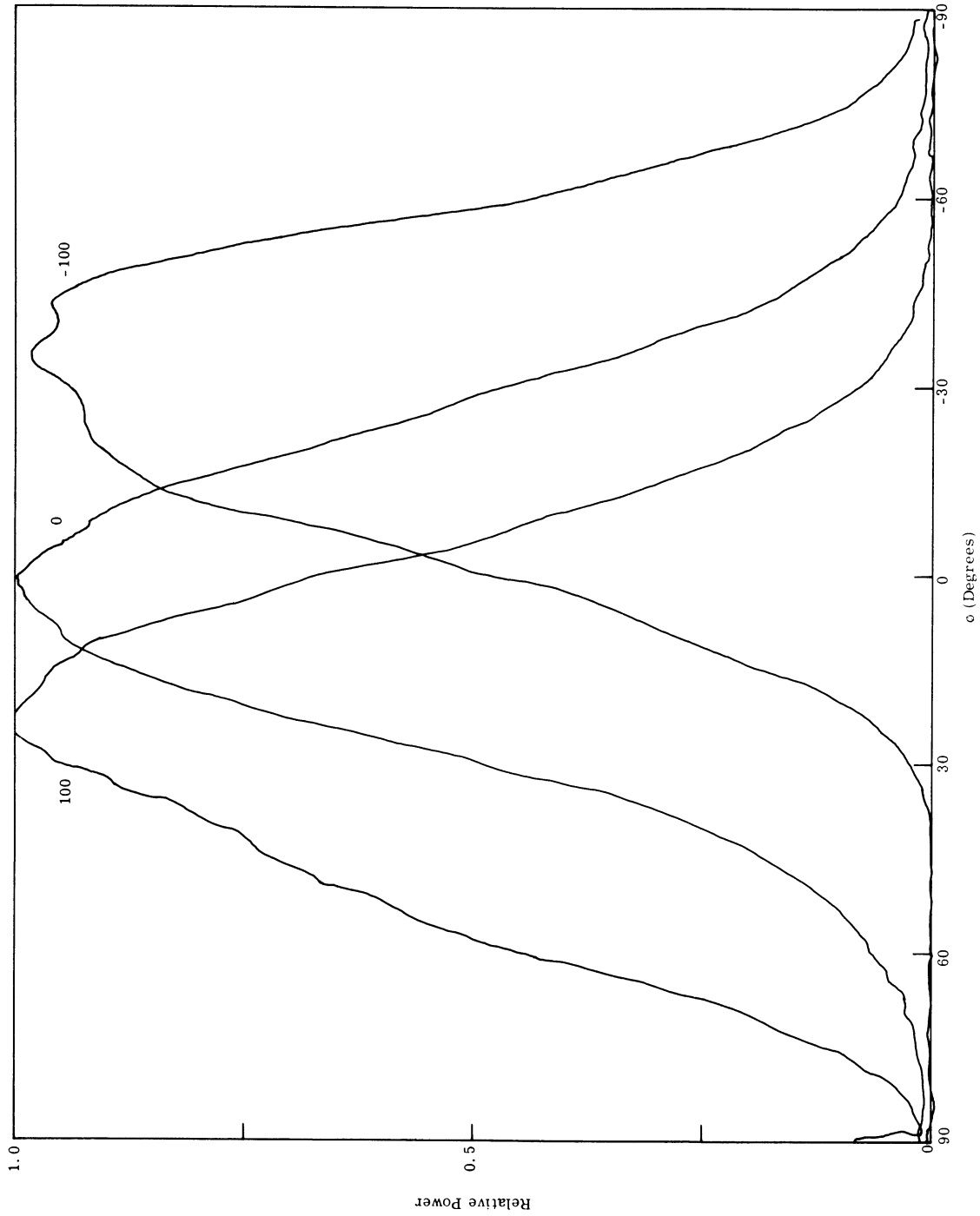


Fig. 5. 6. Effect of reversing the applied field (shown in oersteds on the figure). Frequency = 10 Gc/sec, diameter = .295", TT 390 ferrite.

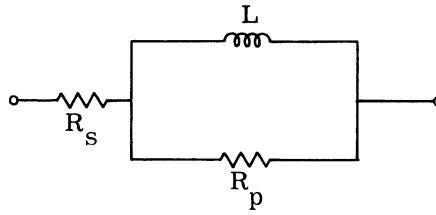


Fig. 5.7. Equivalent circuit of the windings of an electromagnet.

creased from 0 cps, the equivalent resistance increases so that large amounts of power are needed to create the required high fields. Even when capacitance is added to the circuit to tune out the inductive reactance, the R_i^2 losses are still high. The advantage in requiring only small fields (and thus small coil currents) is apparent.

Figure 5.8 shows the beam shifting obtained when cylinders with different diameters are used. The beam angle curves terminate at the value of applied field where a new lobe appears in the pattern.

5.3 Reflection Characteristics

The impedance of the scanning antenna is shown in Fig. 5.9. The measured applied field values are labeled on the curve. The impedance match to the waveguide is fairly good between 0 and 175 oersteds. As proven theoretically in Chapter III, the impedance will be the same for both positive and negative values of applied field. The range of low reflection then corresponds to a total shift in the beam of $60^\circ (\pm 30^\circ)$ as shown in Fig. 5.4(a).

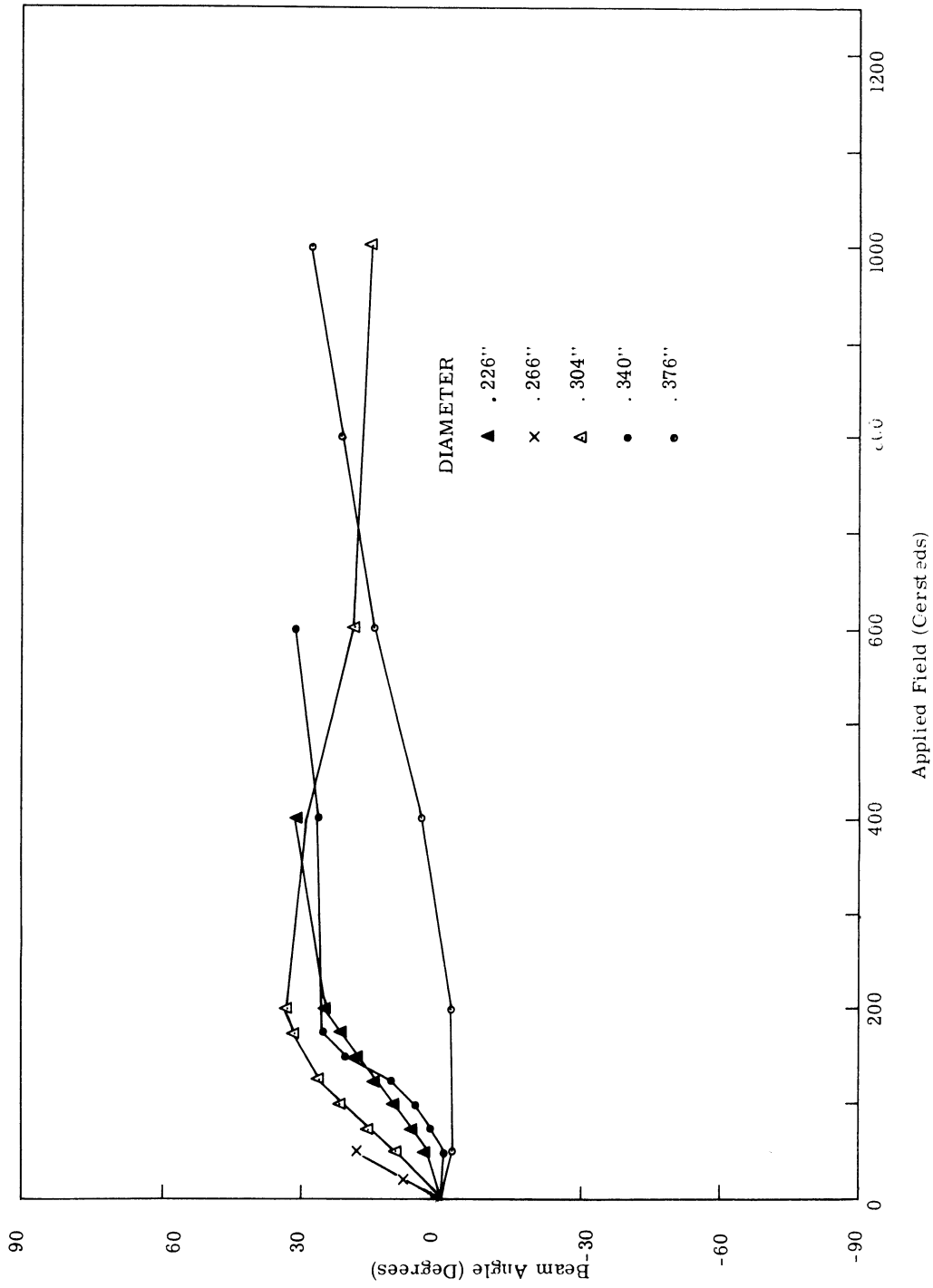


Fig. 5. 8. Changes in radiation characteristics for various diameters of the ferrite post. Frequency = 10 Gc/sec, TT 390 ferrite.
 (a) Beam angle vs. applied field.

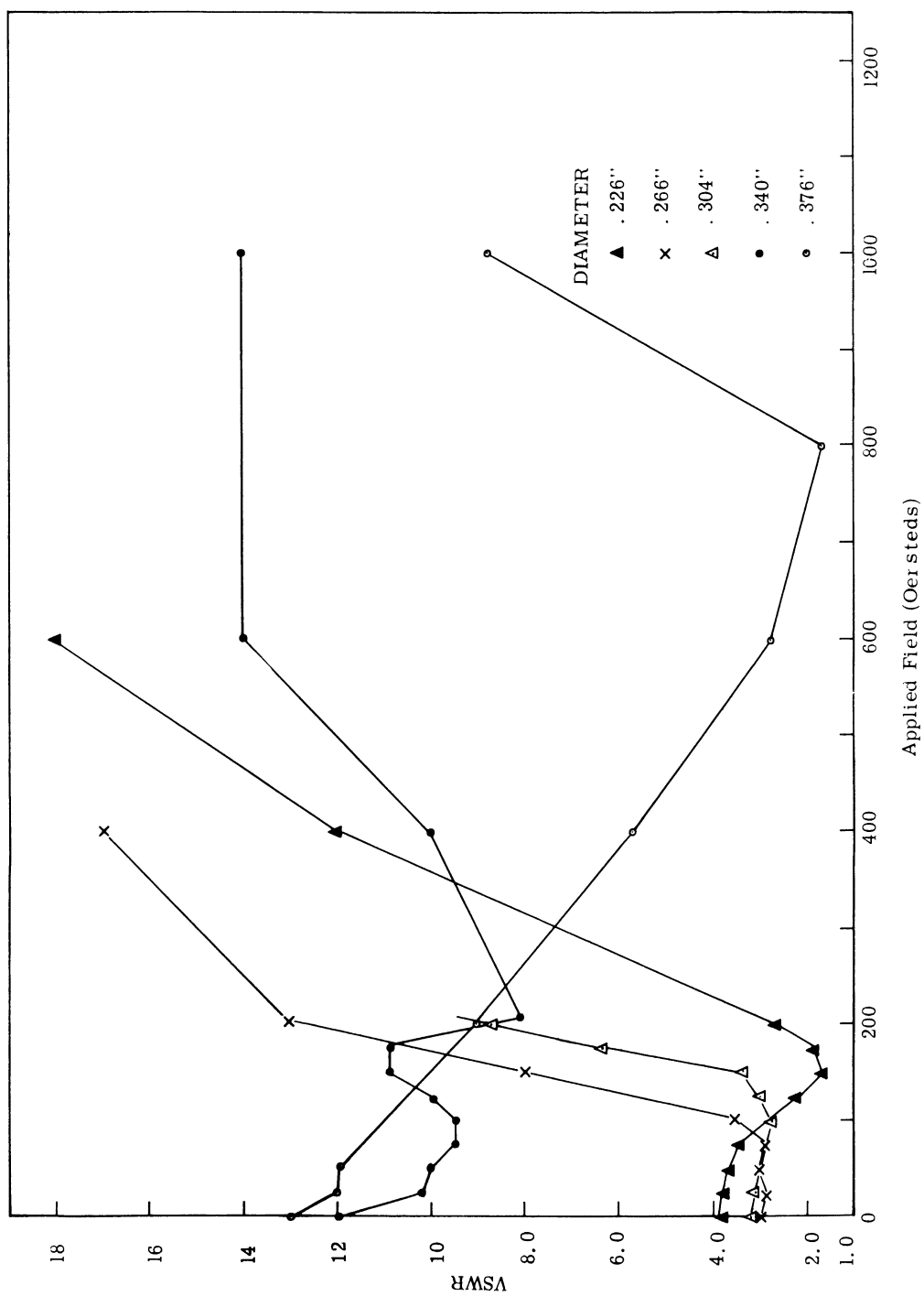


Fig. 5. 8. Changes in radiation characteristics for various diameters of the ferrite post. Frequency = 10 Gc/sec, TT 390 ferrite.
(b) VSWR vs. applied field.

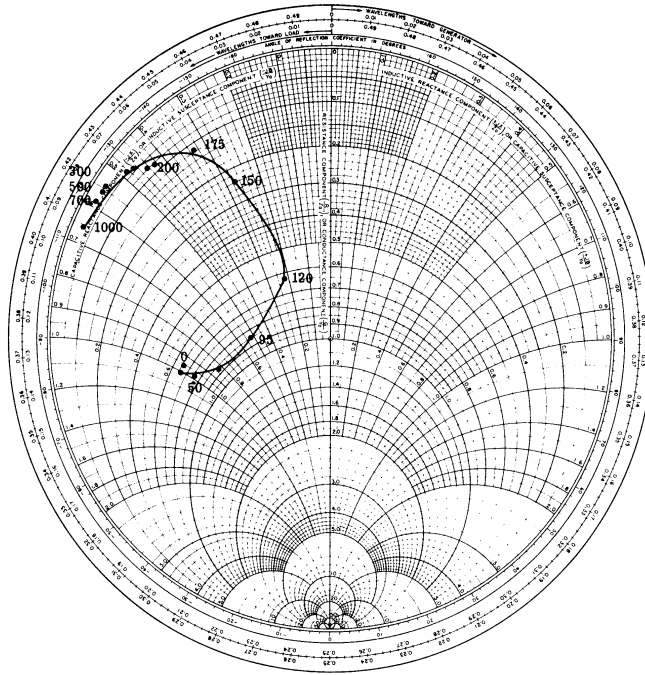


Fig. 5.9. Measured impedance of the ferrite scanning antenna as a function of the applied field. Frequency = 10 Gc/sec, diameter = 295", TT 390 ferrite.

5.4 Practical Models

For many applications, such as in satellite or other airborne equipment, small size and weight are required. To obtain a practical device, a small electromagnet was constructed to provide the bias field. Figure 5.10 pictures the magnet, the waveguide, and the ferrite cylinder. Figure 5.11 shows the assembled antenna. The simplicity of the construction can be noted from these illustrations. A slight modification (shown in Fig. 5.12) was made to shield the magnet pole faces from the radiating field. Both antennas shown exhibit radiation characteristics very close to those noted when the large electromagnet was used. Figure 5.13 shows the beam pattern tracings of the x-y recorder plots obtained for the antenna in Fig. 5.12 for several frequencies. In addition, the patterns for the unloaded waveguide are given. The VSWR is given in Fig. 5.14. Normalized power is given in Fig. 5.13, but the value of the peak relative to the peak when the ferrite is removed is given in Fig. 5.15. From a comparison of the beam patterns of the empty waveguide and the ferrite antenna in Fig. 5.13 and a comparison of the relative peak values of their patterns in Fig. 5.15, it is

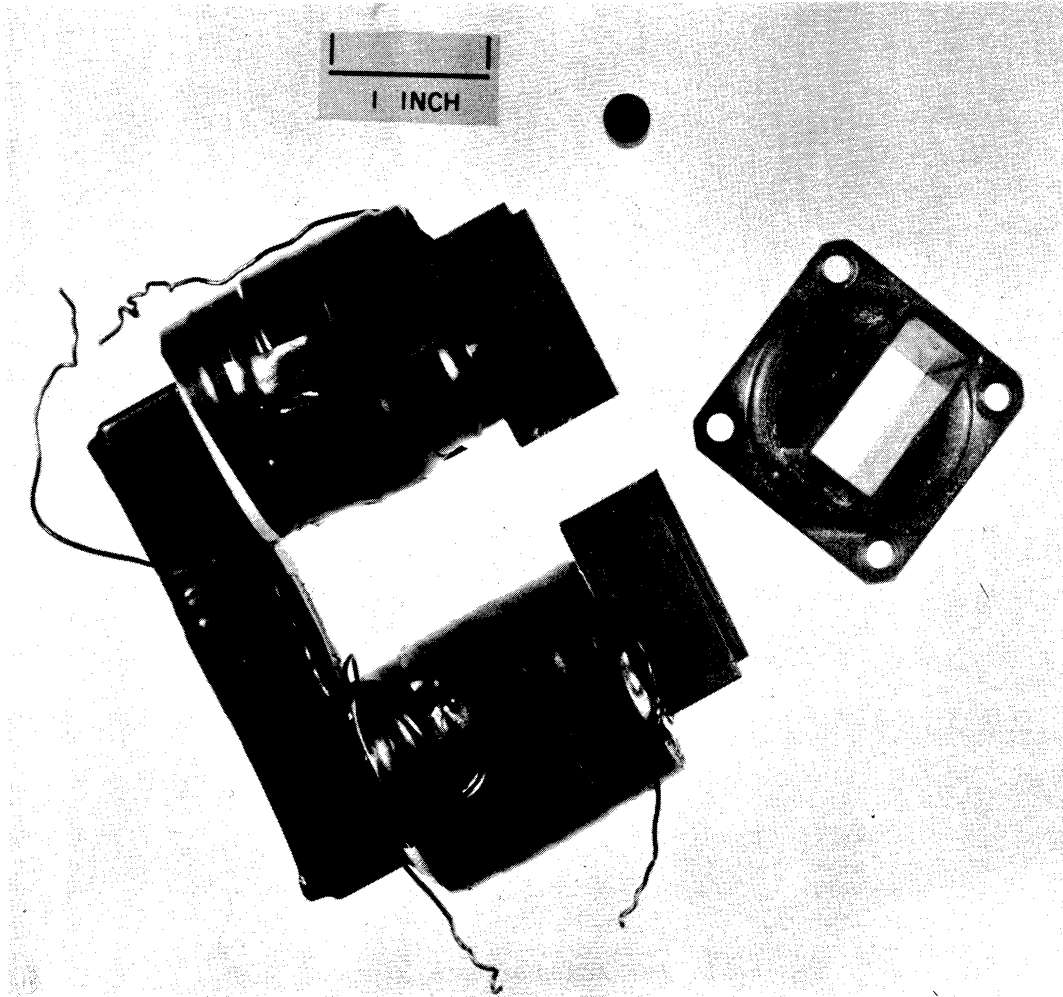


Fig. 5.10. Components of a practical scanning antenna.

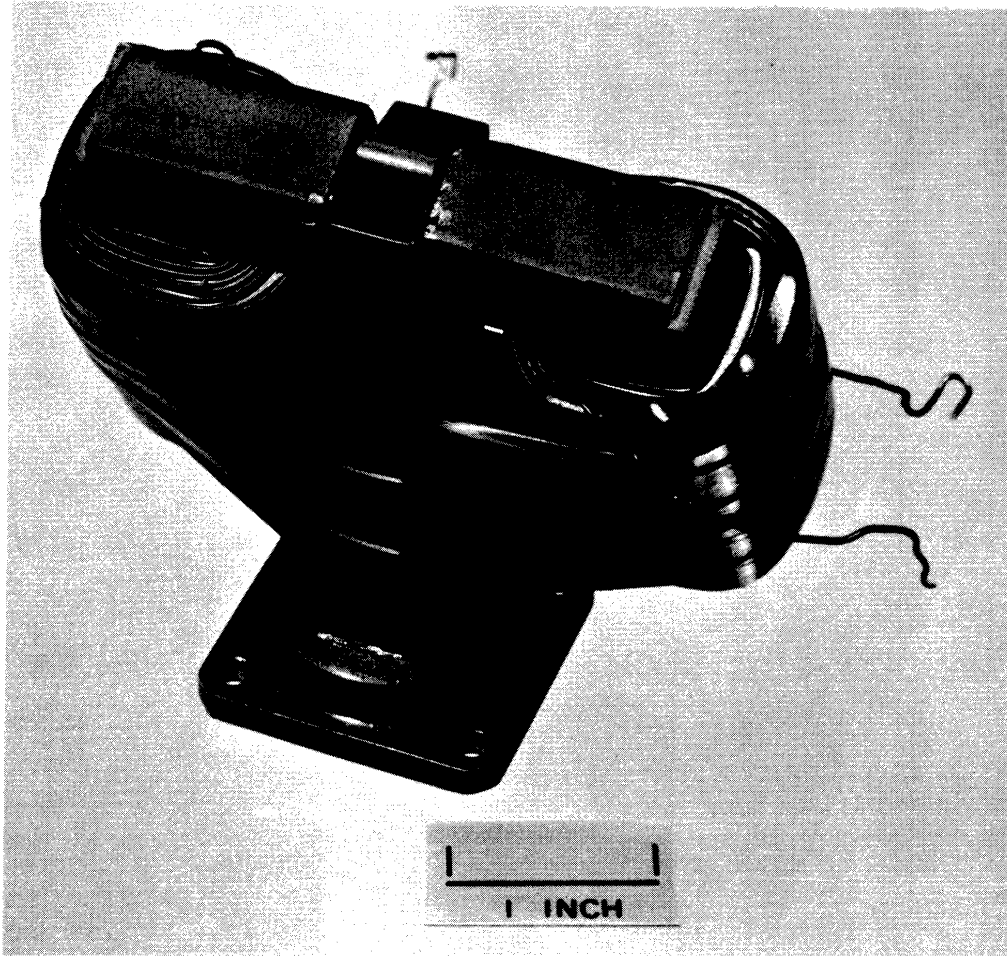


Fig. 5. 11. Assembled scanning antenna.

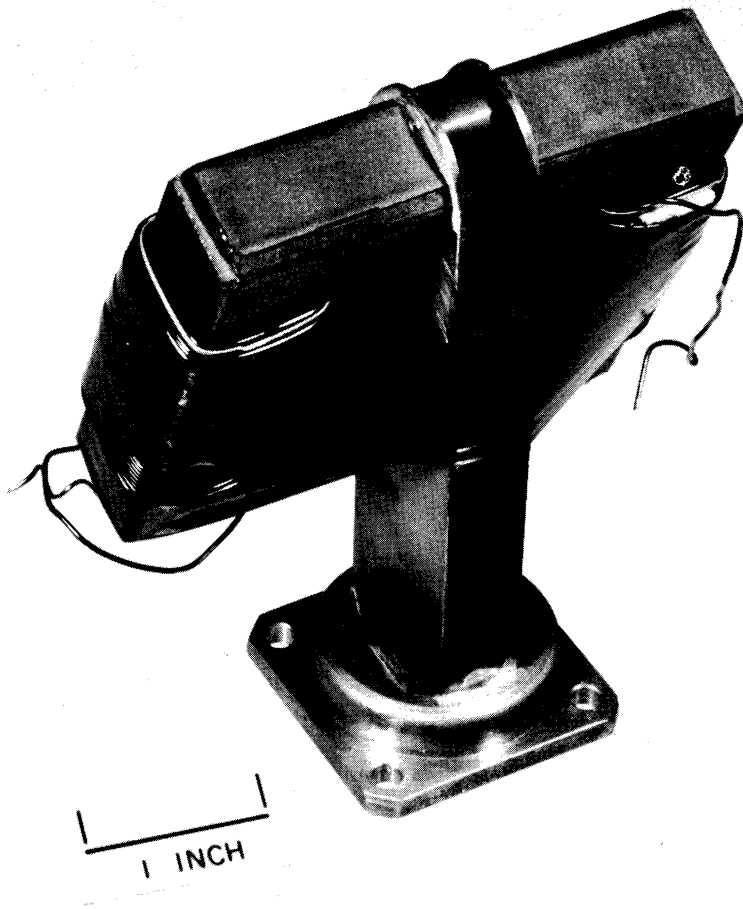


Fig. 5.12. Modified practical scanning antenna.

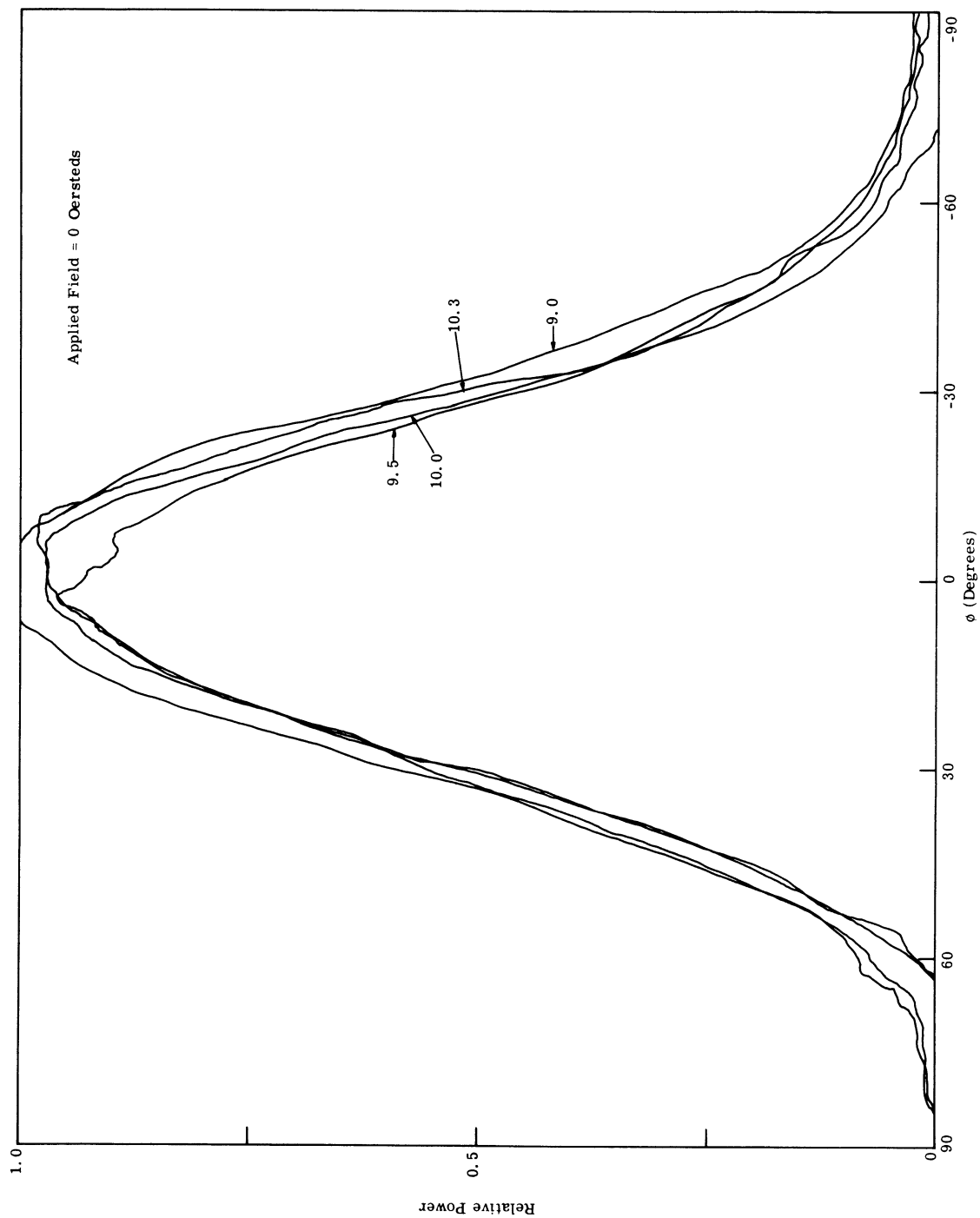


Fig. 5. 13. (a) Beam patterns of the antenna in Fig. 5. 12. Empty waveguide at 9.0, 9.5, 10.0, and 10.3 Gc/sec.

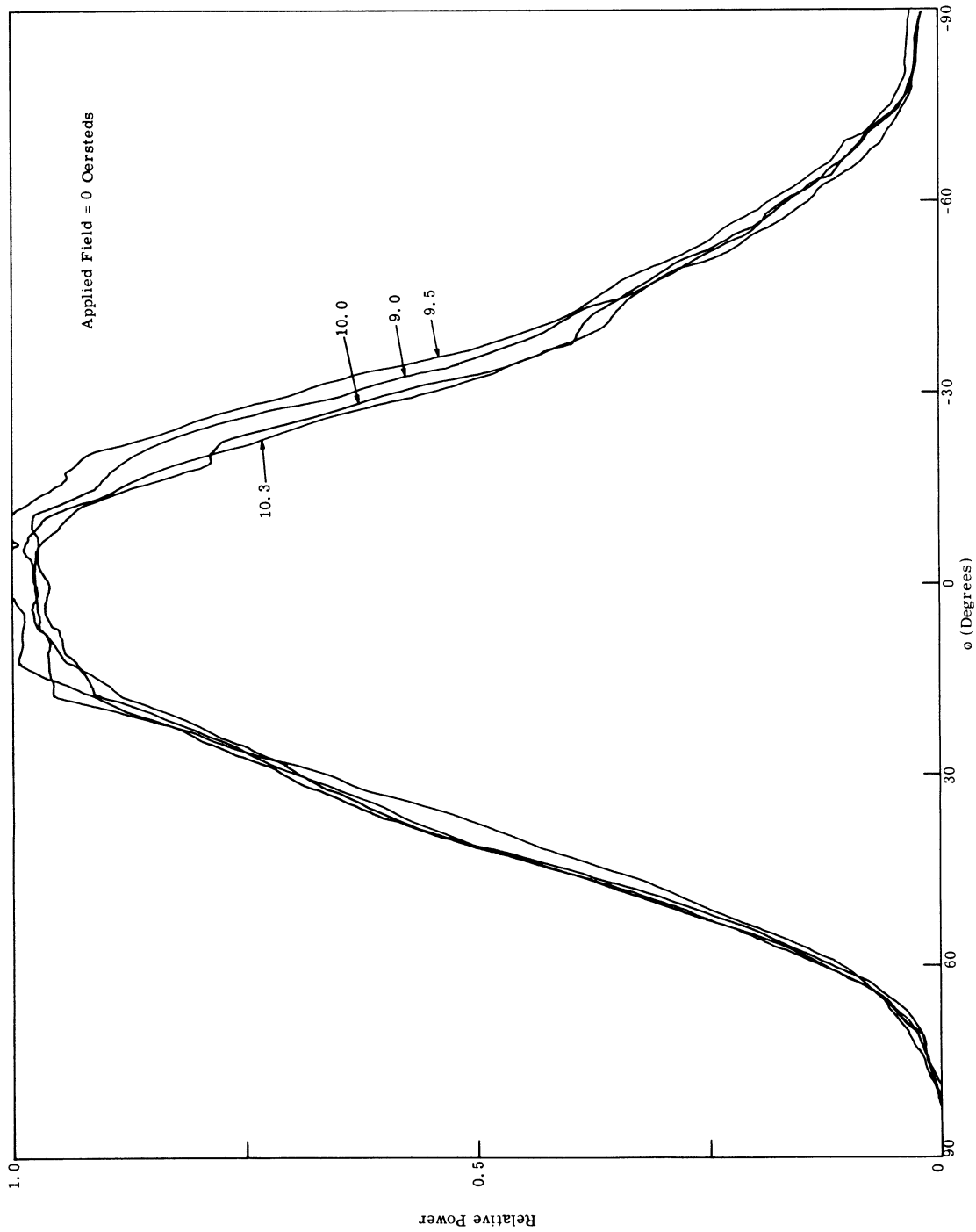


Fig. 5.13. (b) Beam patterns of the antenna in Fig. 5.12. The patterns are shown for the frequencies 9.0, 9.5, 10.0, and 10.3 Gc/sec, diameter = .295", TT 390 ferrite.

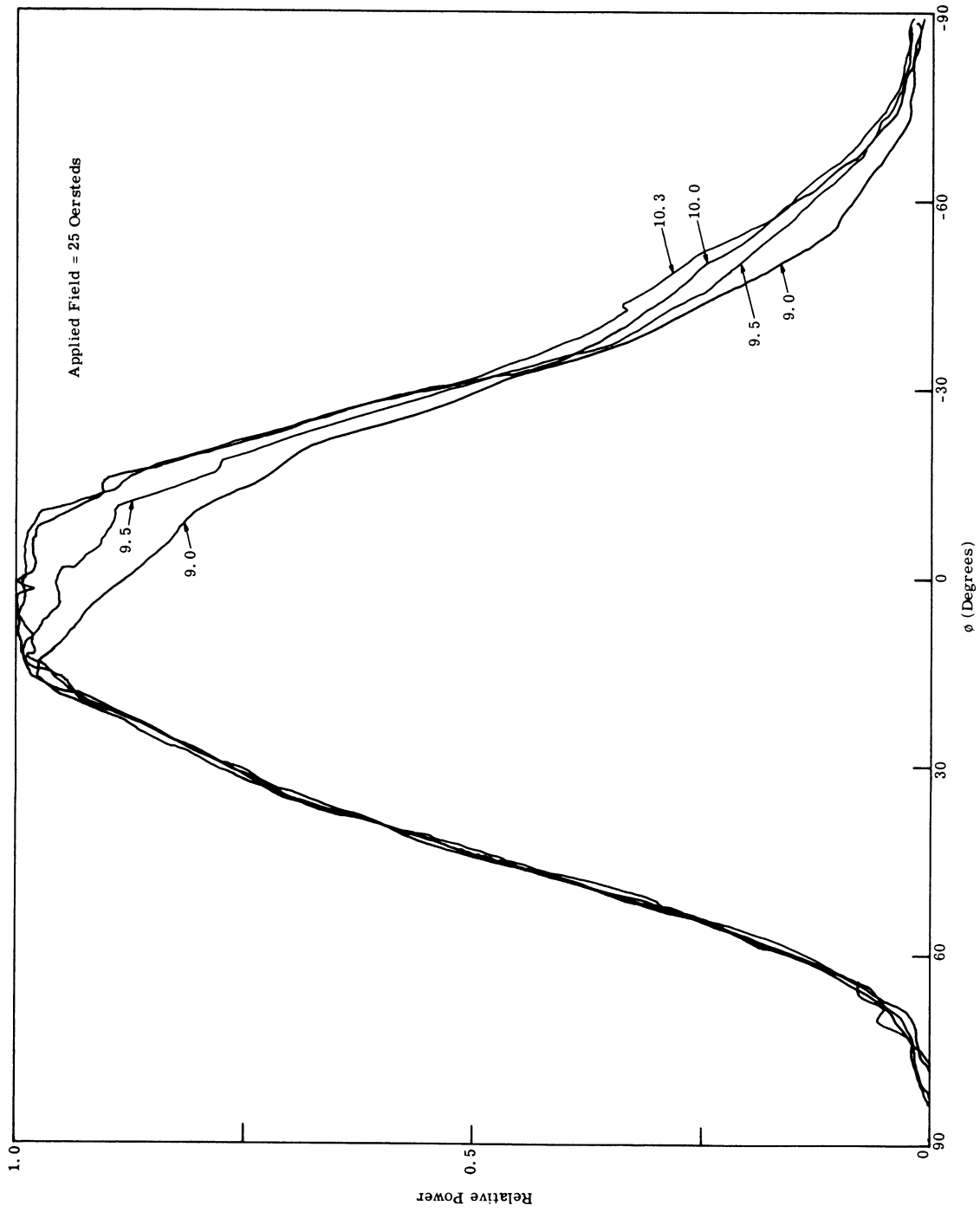


Fig. 5.13. (c) Beam patterns of the antenna in Fig. 5.12. The patterns are shown for the frequencies 9.0, 9.5, 10.0, and 10.3 Gc/sec, diameter = .295", TT 390 ferrite.

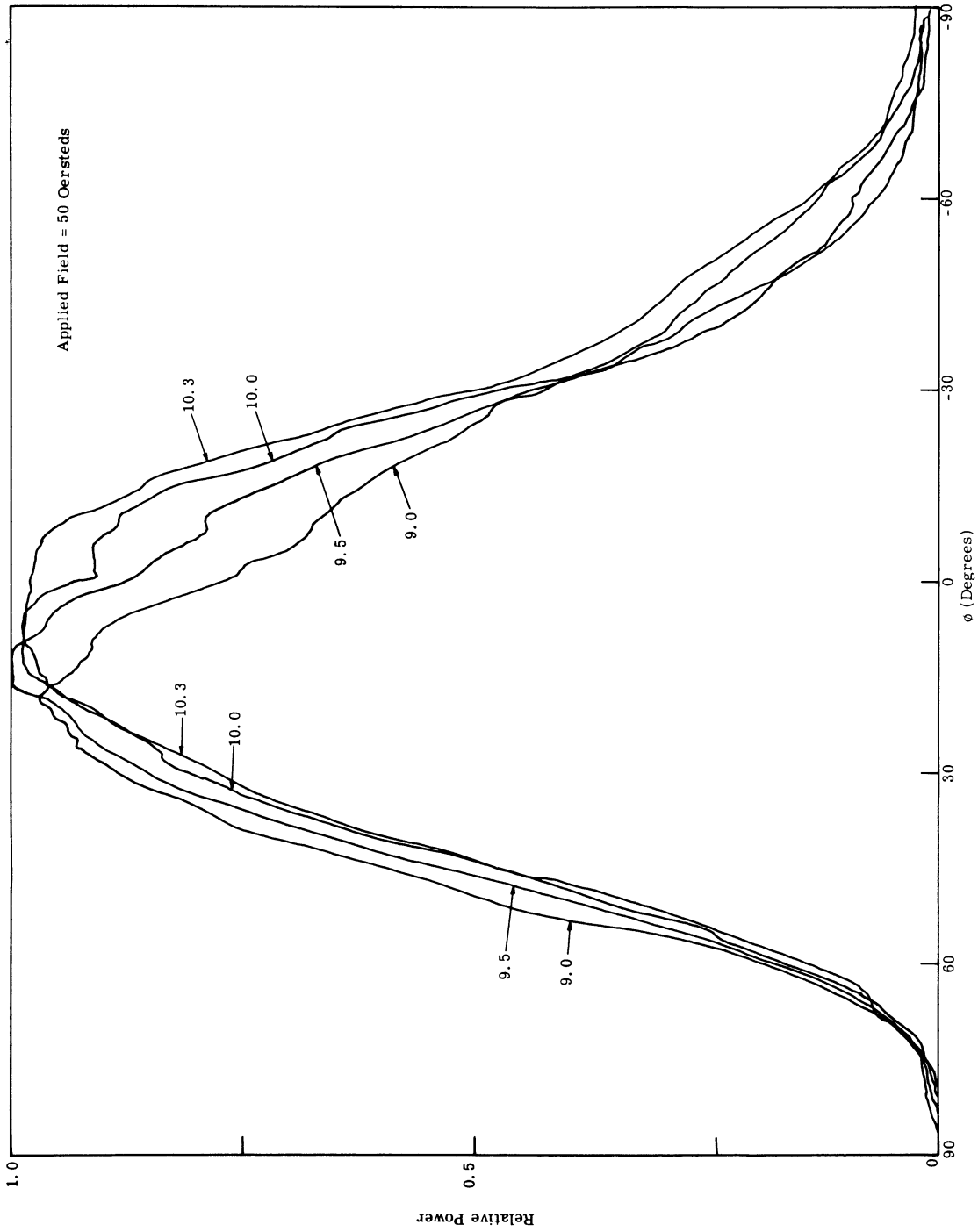


Fig. 5.13. (d) Beam patterns of the antenna in Fig. 5.12. The patterns are shown for the frequencies 9.0, 9.5, 10.0, and 10.3 Gc/sec, diameter = .295", TT 390 ferrite.

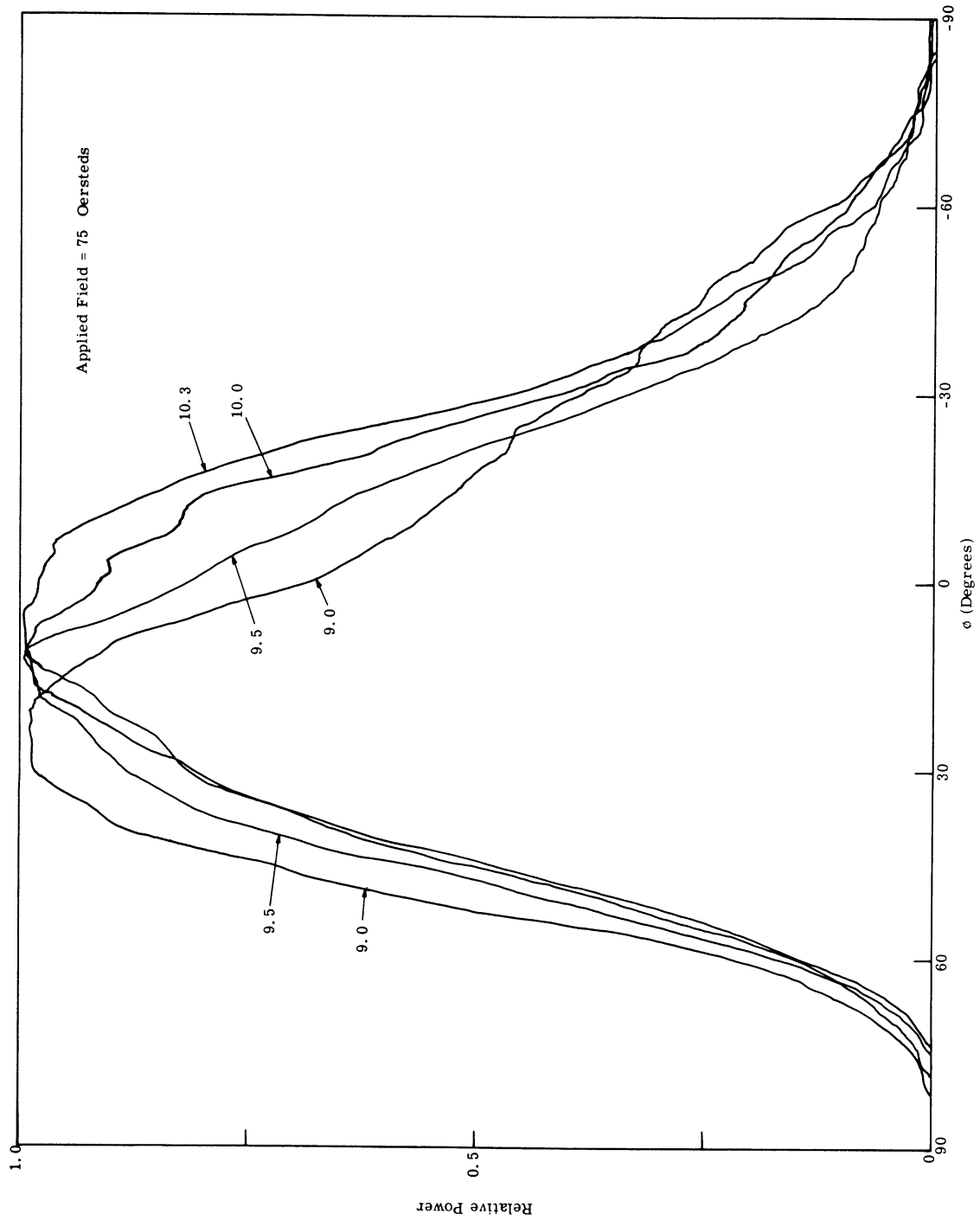


Fig. 5.13. (e) Beam patterns of the antenna in Fig. 5.12. The patterns are shown for the frequencies 9.0, 9.5, 10.0, and 10.3 Gc/sec, diameter = .295", TT 390 ferrite.

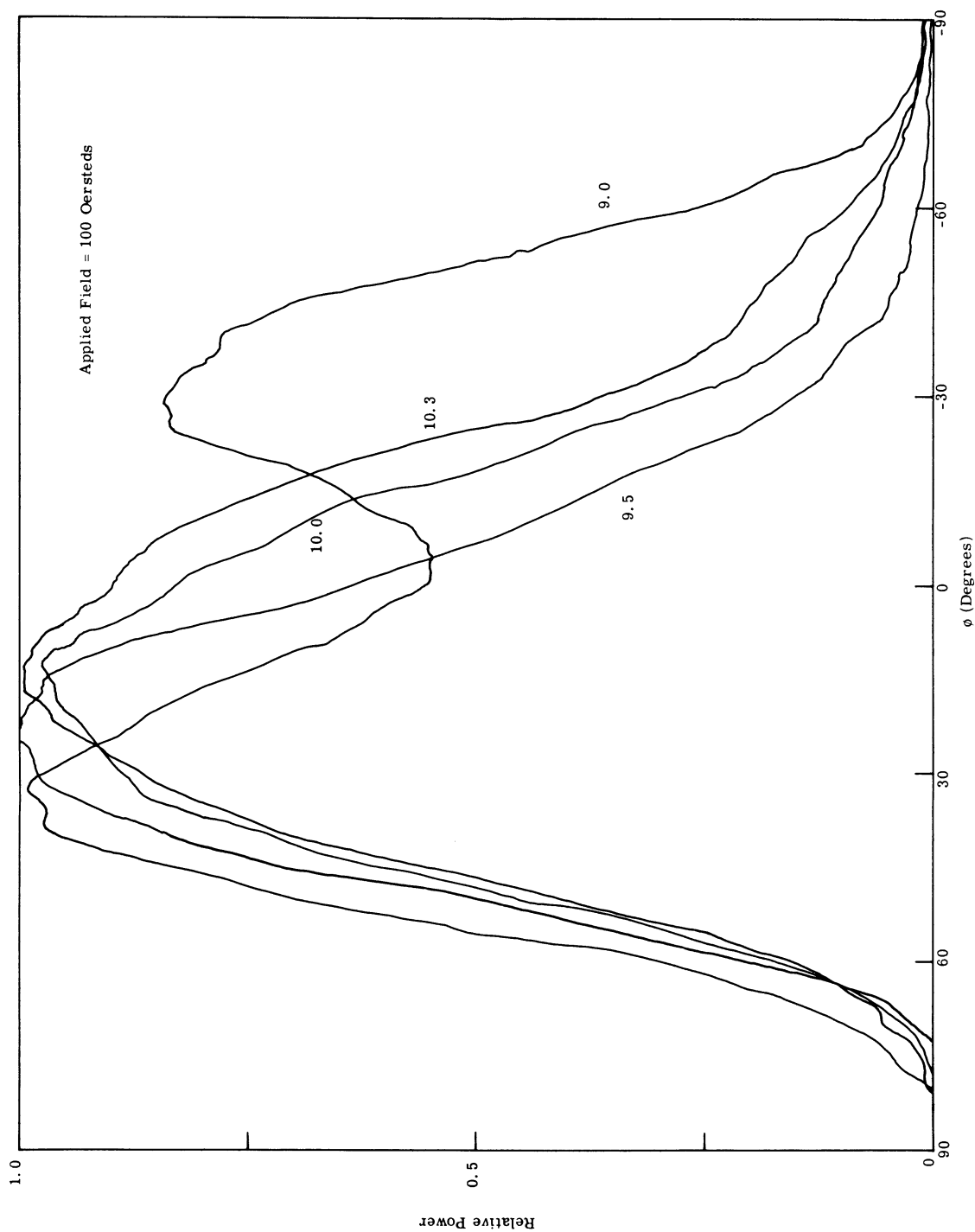


Fig. 5.13. (f) Beam patterns of the antenna in Fig. 5.12. The patterns are shown for the frequencies 9.0, 9.5, 10.0, and 10.3 Gc/sec, diameter = .295", TT 390 ferrite.

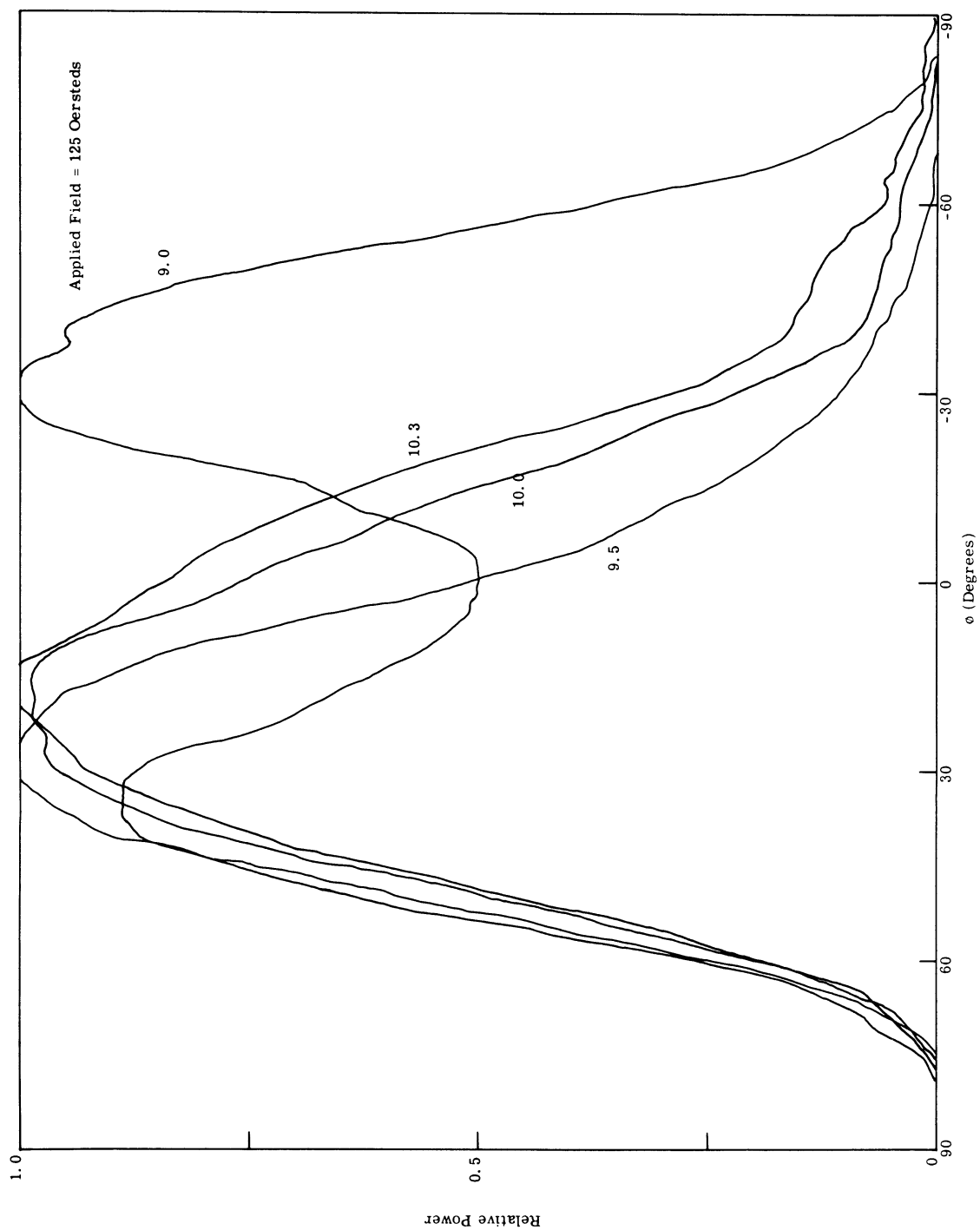


Fig. 5.13. (g) Beam patterns of the antenna in Fig. 5.12. The patterns are shown for the frequencies 9.0, 9.5, 10.0, and 10.3 Gc/sec, diameter = .295", TT 390 ferrite.

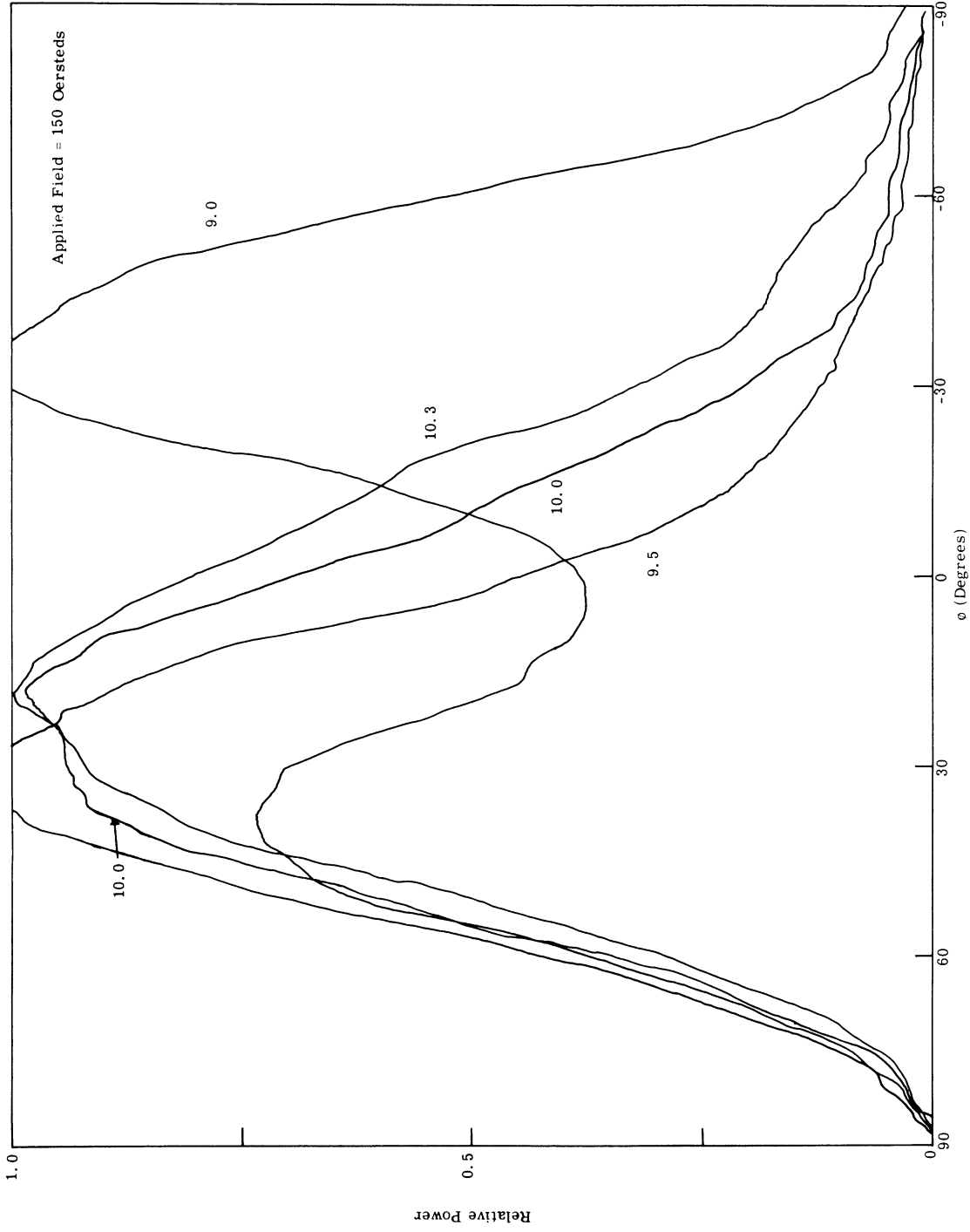


Fig. 5.13. (h) Beam patterns of the antenna in Fig. 5.12. The patterns are shown for the frequencies 9.0, 9.5, 10.0, and 10.3 Gc/sec, diameter = .295", TT 390 ferrite.

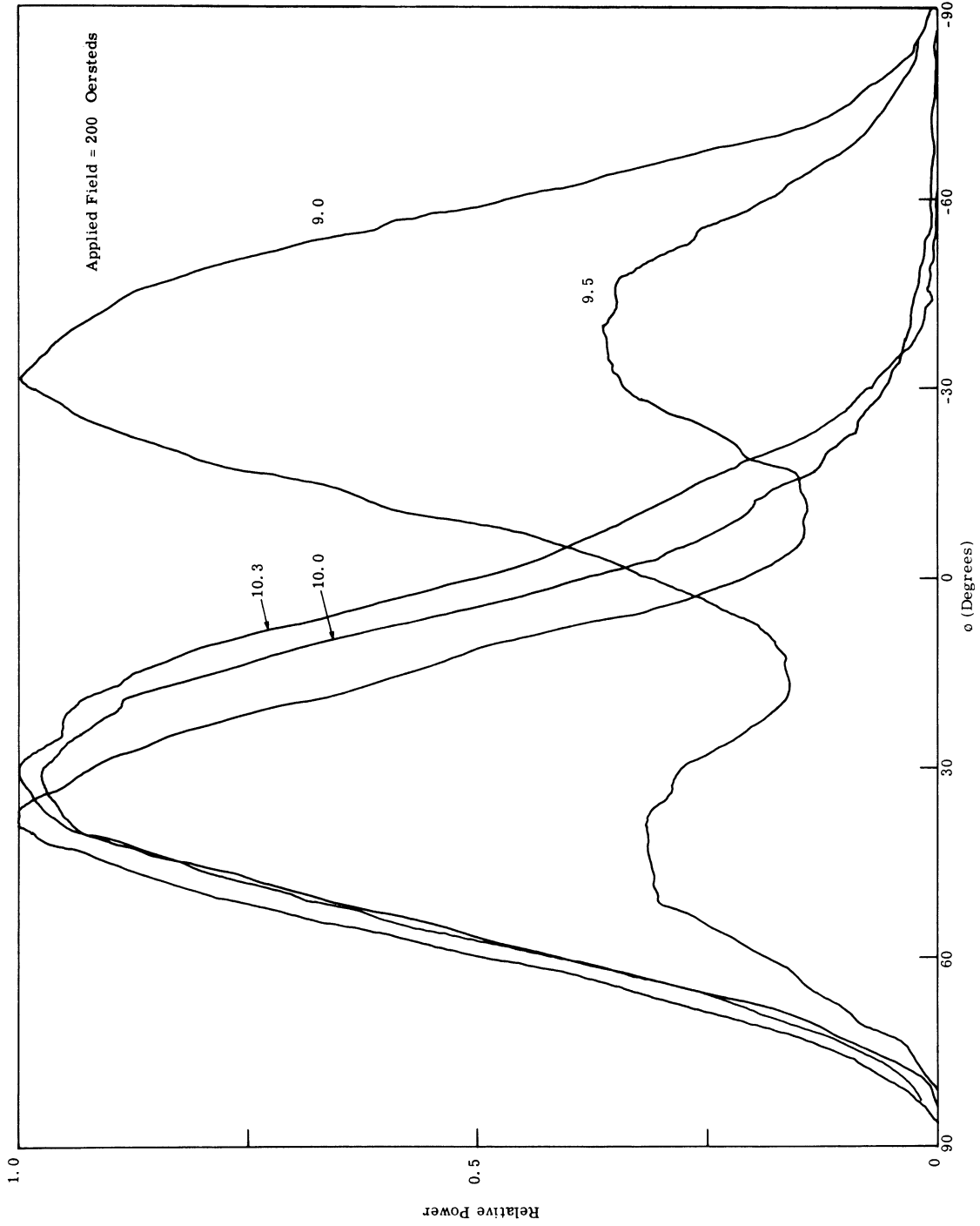


Fig. 5.13.(i) Beam patterns of the antenna in Fig. 5.12. The patterns are shown for the frequencies 9.0, 9.5, 10.0, and 10.3 Gc/sec, diameter = .295", TT 390 ferrite.

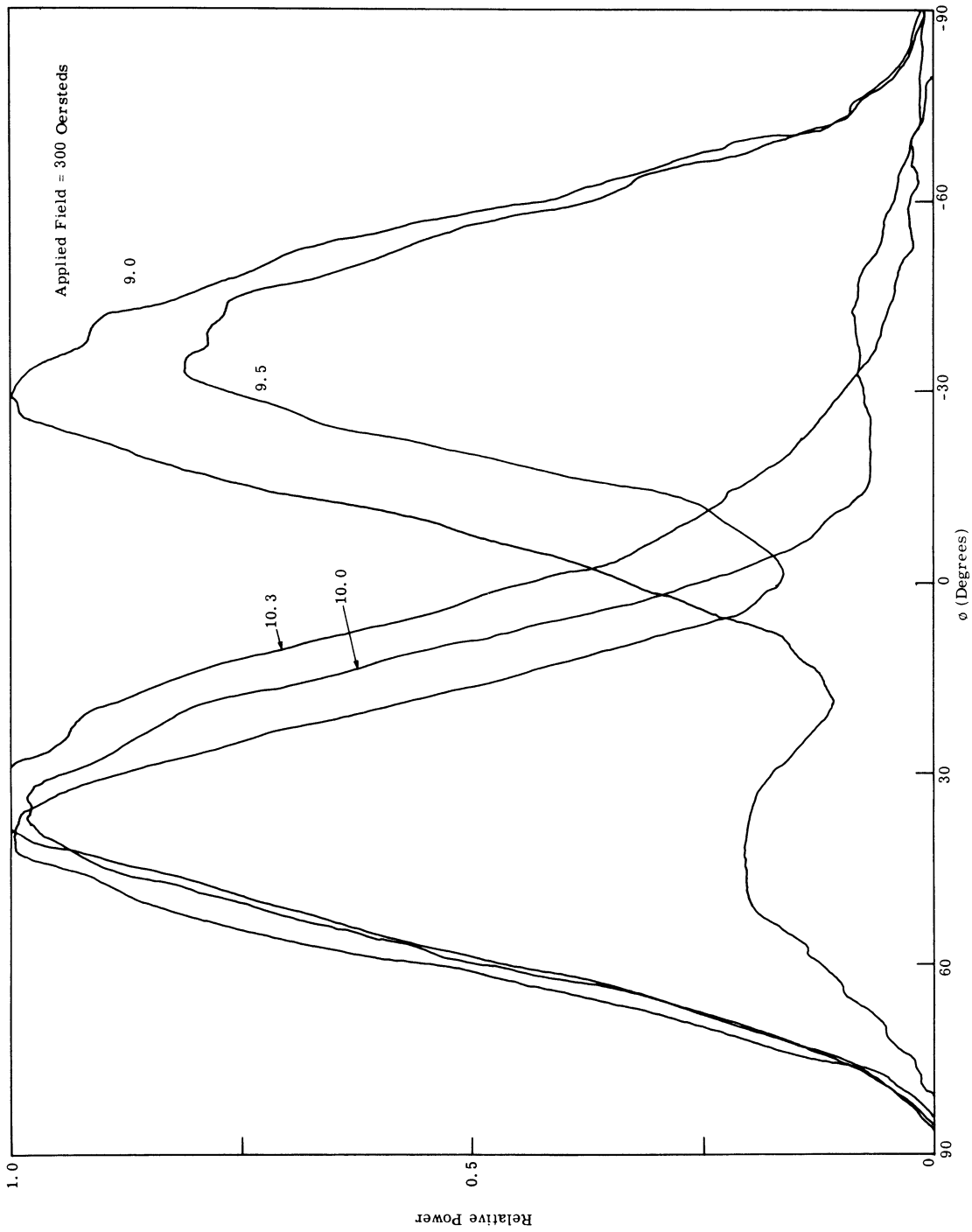


Fig. 5.13. (j) Beam patterns of the antenna in Fig. 5.12. The patterns are shown for the frequencies 9.0, 9.5, 10.0, and 10.3 Gc/sec, diameter = .295", TT 390 ferrite.

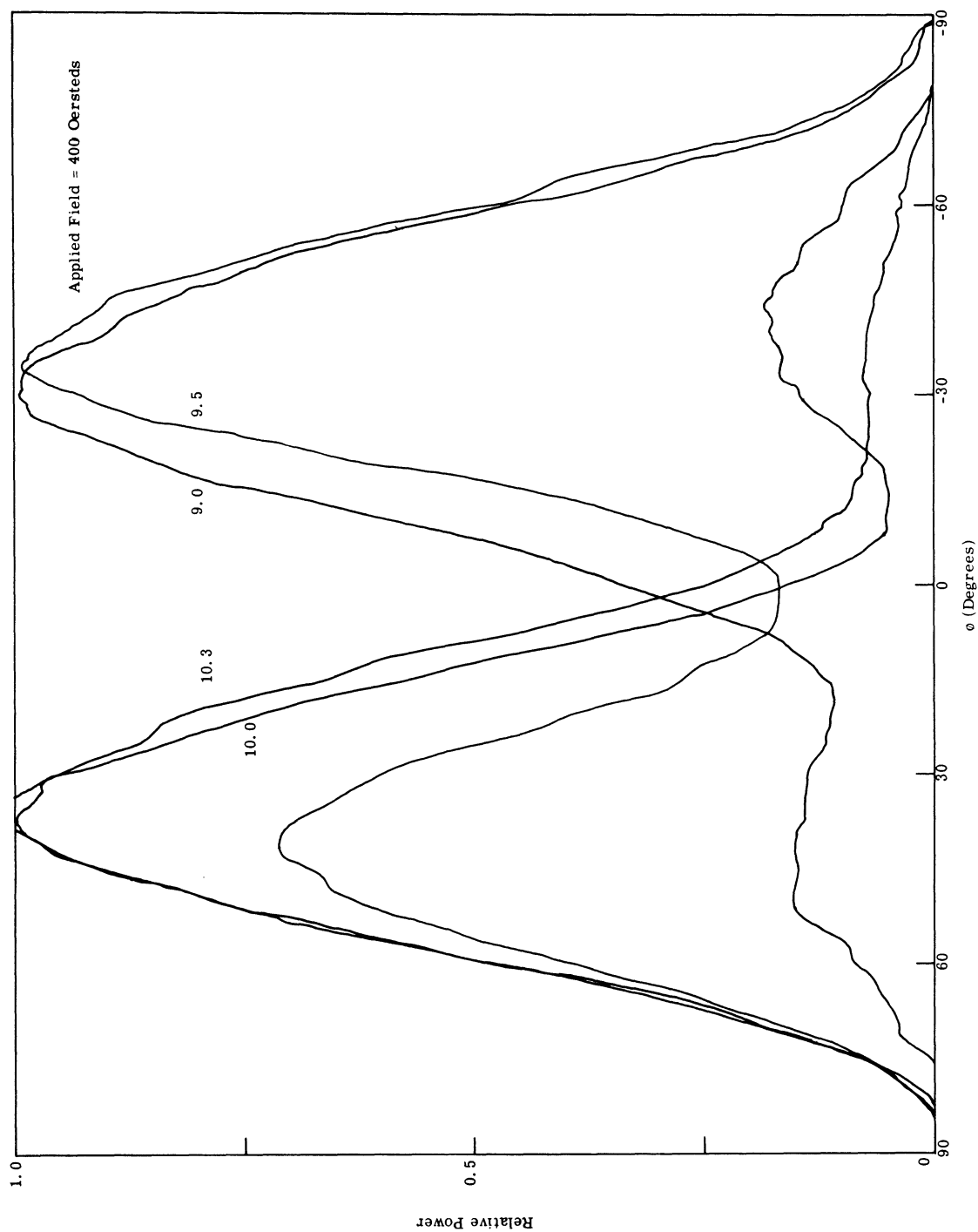


Fig. 5.13.(k) Beam patterns of the antenna in Fig. 5.12. The patterns are shown for the frequencies 9.0, 9.5, 10.0, and 10.3 Gc/sec, diameter = .295", TT 390 ferrite.

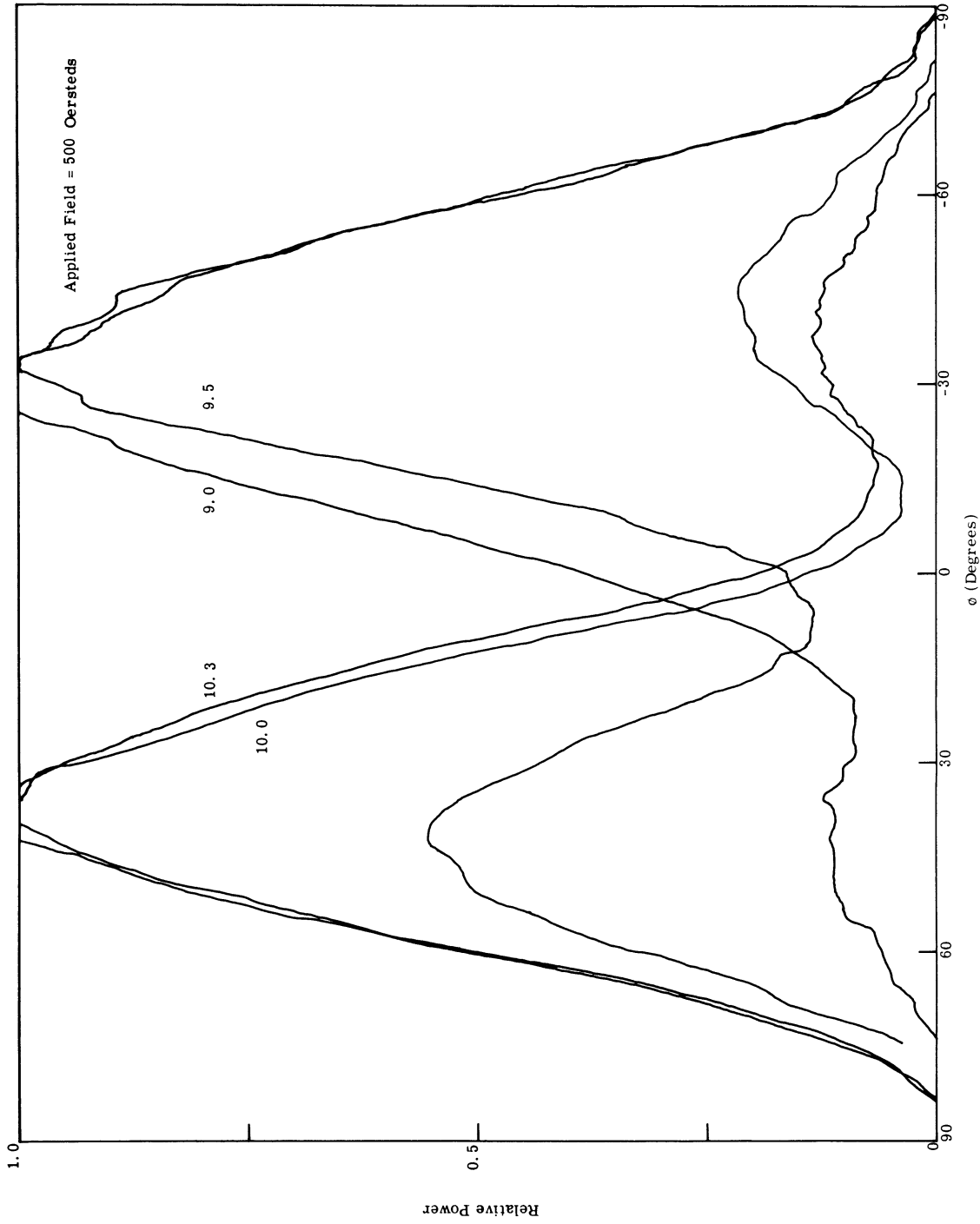


Fig. 5.13. (1) Beam patterns of the antenna in Fig. 5.12. The patterns are shown for the frequencies 9.0, 9.5, 10.0, and 10.3 Gc/sec, diameter = .295", TT 390 ferrite.

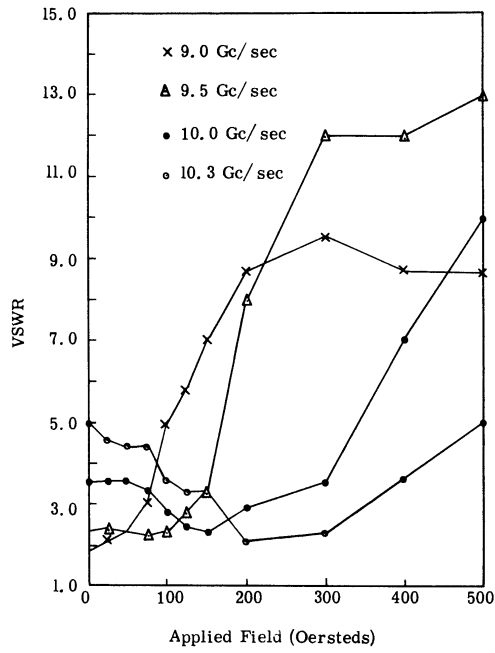


Fig. 5.14. VSWR vs. applied field for the antenna in Fig. 5.12. Diameter = .295", TT 390 ferrite.

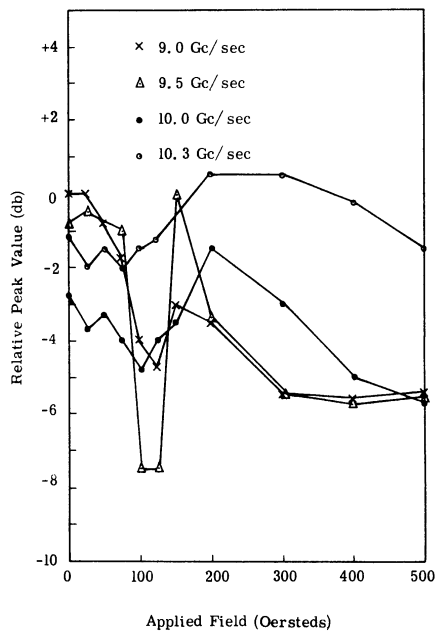


Fig. 5.15. Peak magnitude of the beam relative to the peak magnitude obtained when the ferrite is removed. Diameter = .295", TT 390 ferrite.

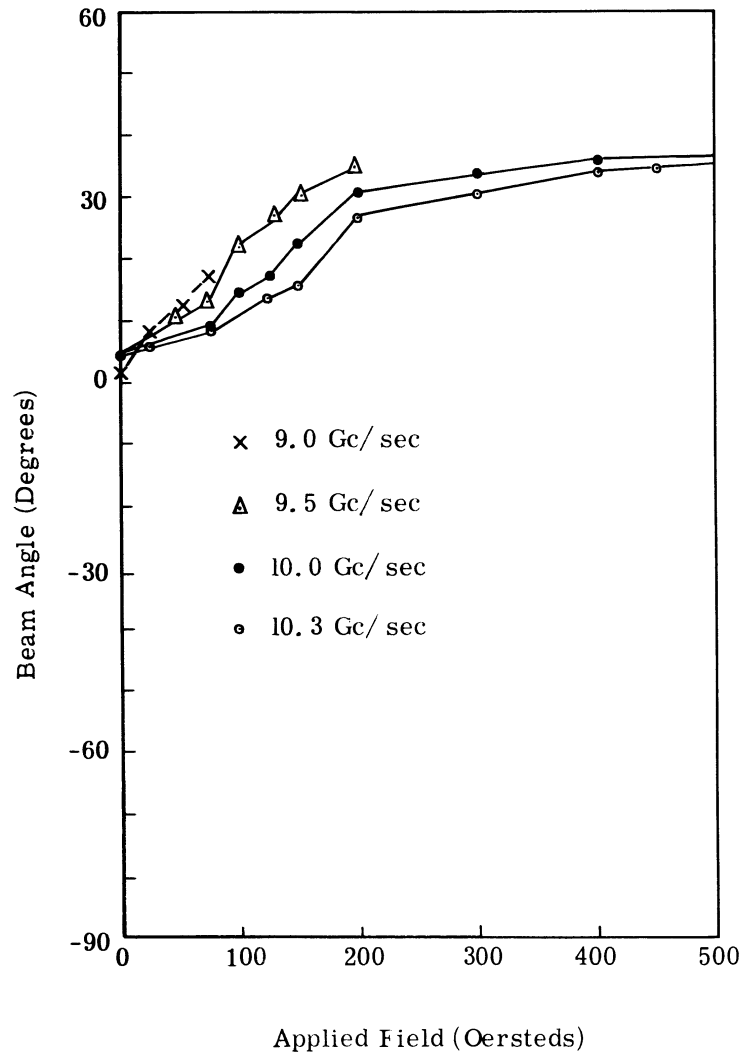


Fig. 5. 16. Measured beam angle vs. applied field for the antenna in Fig. 5. 12. Diameter = .295", TT 390 ferrite.

seen that the efficiency of the scanning antenna is comparable to that of the empty radiating slot. The beam angle as a function of applied field is given in Fig. 5. 16, summarizing some of the results.

The small electromagnet permitted the scanning property to be observed. An ac signal was applied to the electromagnet and the transmitted signal was measured at various angular positions. Scanning rates up to 200 cps could be observed. Higher rates were not obtained because of the increased electromagnet drive power required at higher frequencies as implied by (5. 1). Faster scanning rates can be obtained by the following methods.

1. Use more power to drive the electromagnet.
2. Optimize the magnet design.

3. Resonate the inductance by insertion of a capacitor in series with the coil.

A limitation on scanning rate imposed by the ferrite itself arises from the finite time required to magnetize the material. These times may be on the order of 3×10^{-10} seconds.²⁵ This corresponds to a maximum scanning frequency around 3000 Mc. It appears that although scanning rates approaching this speed may be unattainable, rates in the Mc region are possible with the device.

Instead of varying the beam position continuously, the device can also be used to switch the beam angle between just two positions. For example, by reversing the polarity of the applied field the beam moves from an angle $+\phi$ to $-\phi$. Operation in this manner is very similar to the use of a three port circulator as a switch. Switching times on the order of 10^{-6} seconds have been reported for the circulator.²⁶ Similar times can be expected for switching the antenna.

In general, the beam patterns for a sweeping beam vary from those of the static beams. This is true regardless of the particular scanning antenna used. Limitations on the scanning rate were discussed by Ponomarev.²⁷ His analysis shows that if the beam sweeping rate is not large, the static and dynamic patterns almost coincide. The two conditions limiting the maximum scanning rate are:

1. The scanning frequency must be much smaller than the carrier frequency.
2. The largest dimension over which radiating currents exist must be much smaller than the wavelength of the scanning frequency.

Using these criteria for the ferrite scanning antenna operating at X-band, scanning frequencies of a few Mc are not unreasonable.

5.5 Additional Experiments

Several novel applications and experiments were suggested by the scanning antenna tests. Some of these were tried with the results given below in this section. These throw further light on the operating characteristics of the ferrite antenna and are valuable

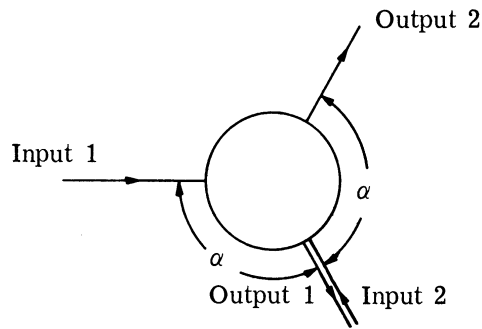


Fig. 5.17. Example of the "redirecting" of energy by a magnetized cylinder.

for this purpose. In addition, while some of the applications might remain only as interesting laboratory phenomena, others might become practical and useful.

Repeater

The operation of the device has been described as a redirecting of energy by the post. Because of the rotational symmetry of the cylinder, any input, regardless of the direction of incidence, will be redirected by the same angle and in the same direction relative to its original direction. An example is shown in Fig. 5.17. It can be seen from the example that the transmitting and receiving patterns for the scanning antenna cannot be the same but must be the images of each other reflected about the angle $\phi = 0^\circ$. This property was verified experimentally and suggested a use for the device as part of an active microwave repeater station. The circuit envisioned is shown in Fig. 5.18. A signal is received at an angle $+\phi$, passed through a circulator, amplified, returned through the circulator to the antenna and then retransmitted at an angle $-\phi$. Since the angle of incidence equals the angle of transmission, the operation can be compared to the reflection from an infinite plane (but with gain). This circuit was tested in the laboratory with an incident angle of 25° . Absorbers were placed between the transmitting and receiving antennas to simulate the condition that no direct coupling exists. Reflections from the repeating antenna were calibrated out by operating with the amplifier off (giving only reflected power at the receiver) and then with it on. The difference in the two received signals gave the amount of signal actually amplified and repeated. A 15 db difference was obtained in the experiment. This same type of operation could be performed more efficiently with the ferrite antenna feeding directly into a parametric amplifier. For this situation the circulator in Fig. 5.17 would be eliminated. Actually,

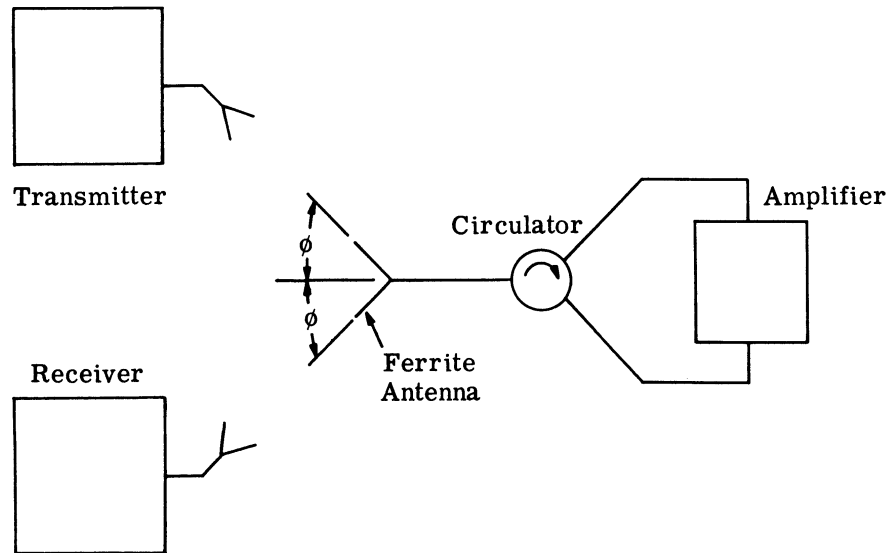


Fig. 5. 18. Microwave repeater circuit.

in this application the antenna itself performs the circulator function, normally found in complete parametric amplifier packages, of separation of the incident and amplified waves.

Modulator

Consider that the receiver and transmitter positions in Fig. 5. 19 are fixed relative to each other and the scanning antenna is biased to some fixed dc field. Now, if an ac signal is applied to the electromagnet, the amplitude of the transmitted wave will vary at the receiver in accordance with this signal. The set of unnormalized radiation patterns shown in Fig. 5. 20 illustrate the situation. In reality, the beam is being moved back and forth across the receiving antenna. For an example, if the receiver is located at $\phi = -30^\circ$ and the dc bias is set at 130 oersteds, an ac signal changing the total field by ± 45 oersteds will amplitude modulate the carrier by more than 20%. Using zero dc bias and an audio oscillator for the modulation signal, a 10 Gc/sec carrier was modulated and detected from zero to 2000 cps. The angle between transmitter and receiver was 30° for this experiment illustrating the modulation capability. High modulation frequencies have the same limitation as high scanning rates, so that the discussion in Section 5. 4 applies here as well.

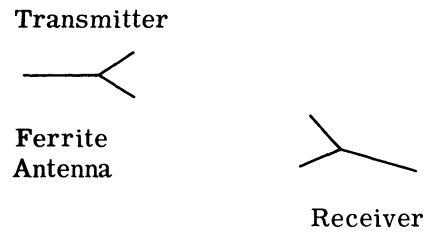


Fig. 5. 19. Modulation circuit.

Frequency Scanning

An examination of Figs. 5. 13 and 5. 16 reveals that beam shifting takes place when the dc applied field is fixed (at some value other than zero) and the frequency is changed. For example, (referring to Fig. 5. 16), if the applied field is set at 200 oersteds, the beam can be shifted 15° by varying the frequency from 9. 5 to 10. 3 Gc/sec. Thus, both electronic scanning and amplitude modulation of the RF wave (by beam shifting as in the paragraph above) can be obtained by varying the carrier frequency. Experiments performed using a sweep oscillator verified this property. The carrier frequency was varied at a rate of 100 cps. In this method the scanning (or modulation) rate is chiefly limited by the rate at which the frequency can be swept.

Electronic SPST Switch

The antenna VSWR varies with applied field and while for some values of field the cylinder is well matched, for others the reflections are very high. This characteristic is even more pronounced when the ferrite post is placed in a matched waveguide instead of in the aperture as shown theoretically in Fig. 3. 5. A reflection type SPST electronic switch (Fig. 5. 21) was constructed using this property. The results are shown in Fig. 5. 22. The theoretical curve (Fig. 3. 5) accurately predicts these results.

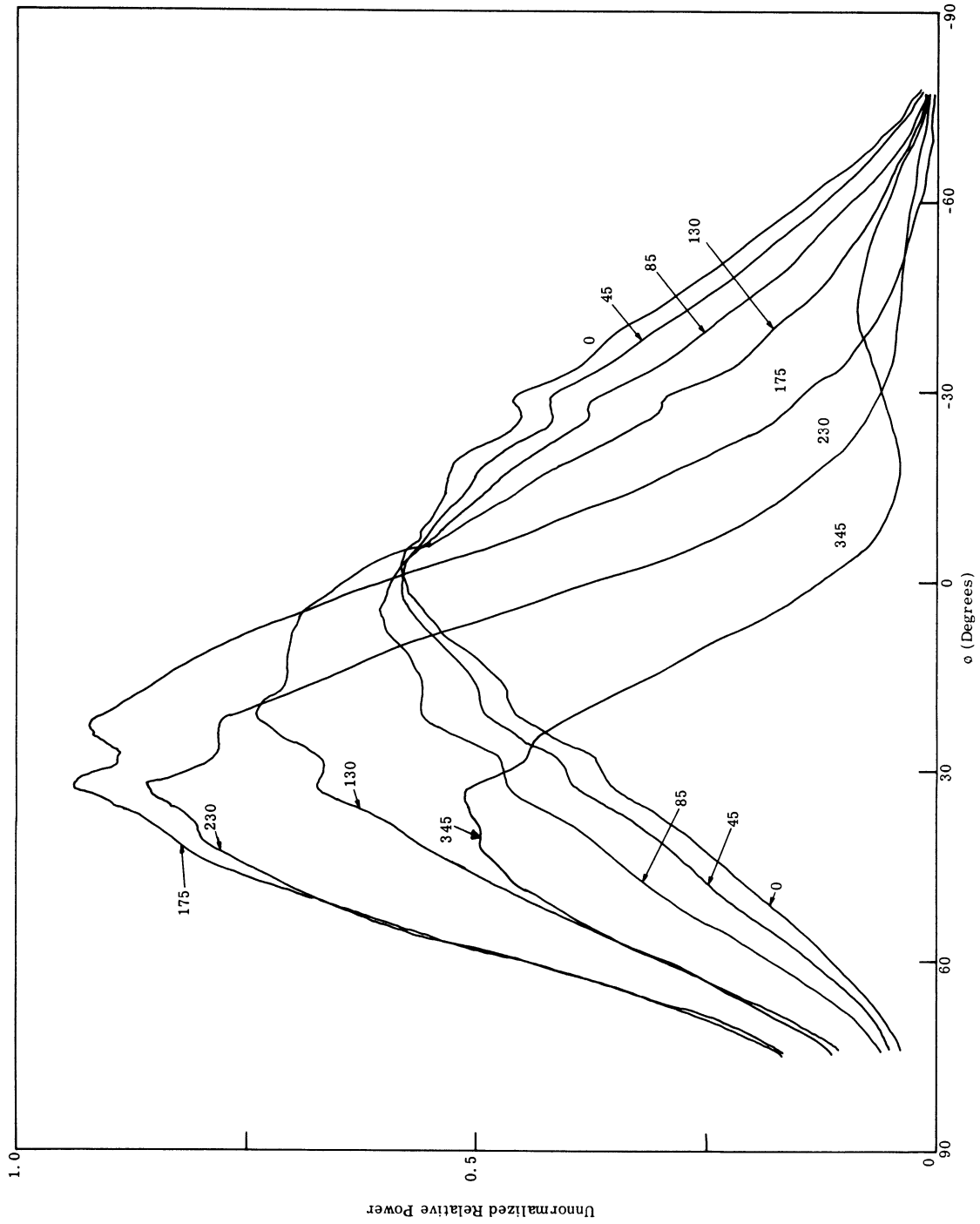


Fig. 5.20. Experimental beam patterns. The patterns shown here are not normalized. Frequency = 10 Gc/sec, diameter = .295", TT 390 ferrite.

5.6 Special Applications

In addition to the experiments discussed in Section 5.5, several other applications for the ferrite antenna were suggested by its special properties. These were not tested, but are presented in this section as possibilities for future study.

Multichannel Systems

Circulators are often used as duplexers (circuit elements which make possible the simultaneous transmission of two messages in opposite directions over the same line). Figure 5.23(a) illustrates this duplexing property. The ferrite scanning antenna also performs this function when operating as in Fig. 5.23(b). Circulators can also be used as diplexers²⁸ (circuit elements which permit the simultaneous transmission of two messages at different carrier frequencies in the same direction over the same line). Figure 5.24(a) illustrates the diplexing property for the circulator. Diplexing occurs when the direction of circulation is opposite for the two frequencies f_1 and f_2 at one value of bias field. Diplexing can also be performed by the ferrite antenna as seen from Fig. 5.13(j) and illustrated in Fig. 5.24(b). The diplexing is not too efficient for the parameters used in the figure since the matching is poor. A design might be found to improve the diplexing quality however.

A device which combines both duplexing and diplexing is called a quadruplexer (a device permitting the simultaneous sending of two messages in either direction over a single line). The circulator can be used as a quadruplexer²⁹ as illustrated in Fig. 5.25(a). Likewise, the scanning antenna is shown in Fig. 5.25(b) as a quadruplexer. Such a device could be used as illustrated in Fig. 5.26. Two information channels with different carriers are operating simultaneously to communicate to stations at two different locations. Each station receives at one frequency and transmits at the other.

Actually, as noted in Sections 5.4 and 5.5, a fixed bias field can be found where the beam pattern corresponding to each frequency is slightly displaced from the pattern due to the neighboring frequency. In essence, the antenna acts as a microwave prism, spreading out the microwave spectrum in space (Fig. 5.27). In this respect the antenna is a multiplexer, allowing simultaneous transmission of more than two messages in the same direction over the same line. If messages are both sent and received (duplexing) and more than two messages

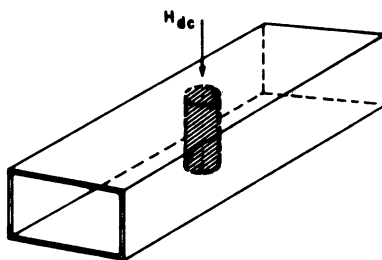


Fig. 5.21. Waveguide reflection type switch.

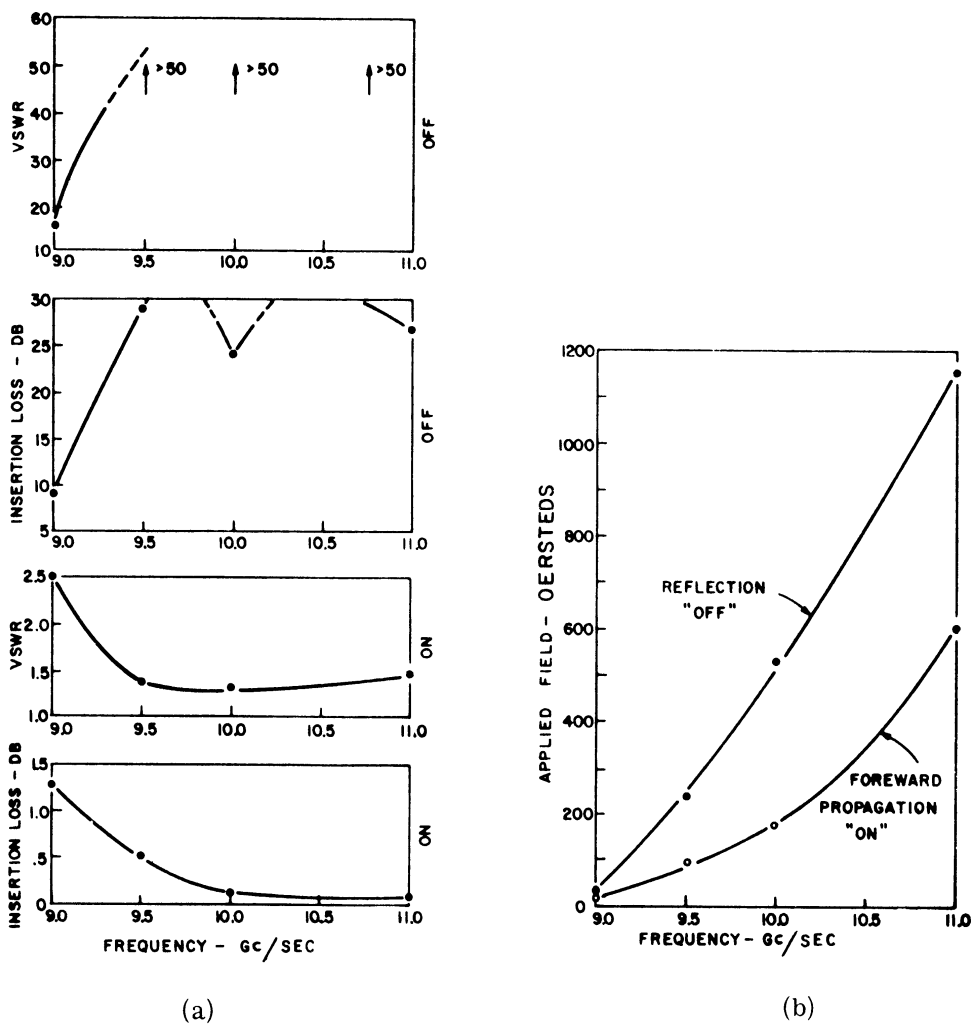


Fig. 5.22. Experimental waveguide switch characteristics. Diameter = .295", TT 390 ferrite. (a) Insertion loss and VSWR vs. frequency. (b) Required applied field for "on" and "off" operation vs. frequency.

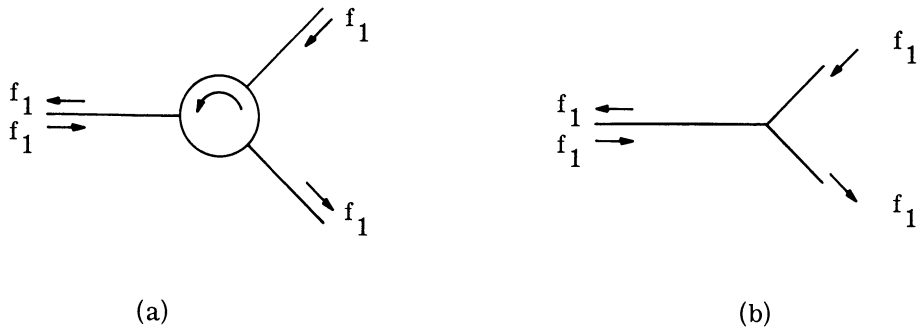


Fig. 5.23. Duplexers. (a) Circulator performing as a duplexer.
(b) Ferrite scanning antenna performing as a duplexer.

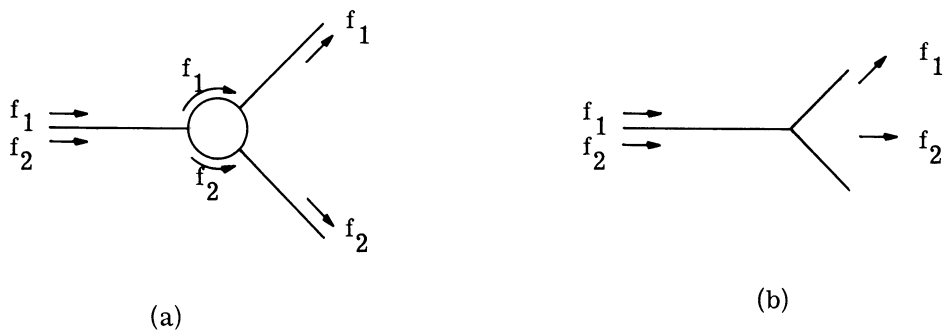


Fig. 5.24. Duplexers. (a) Circulator performing as a duplexer.
(b) Ferrite scanning antenna performing as a duplexer.

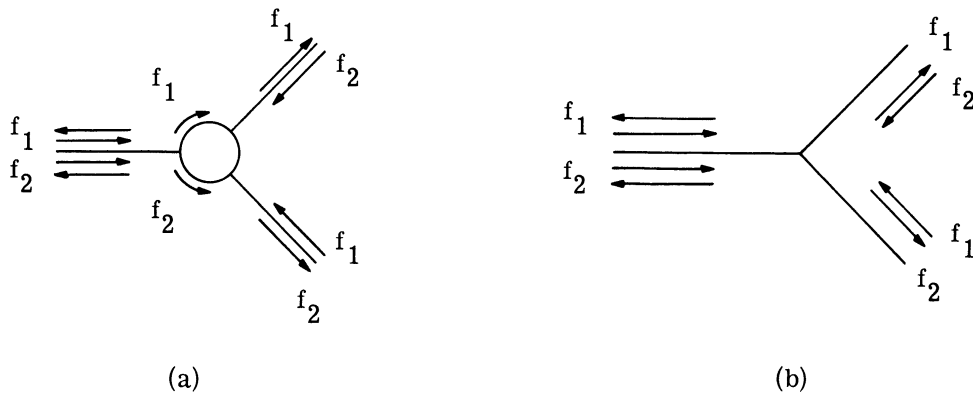


Fig. 5.25. Quadruplexers. (a) Circulator performing as a quadruplexer.
(b) Ferrite scanning antenna performing as a quadruplexer.

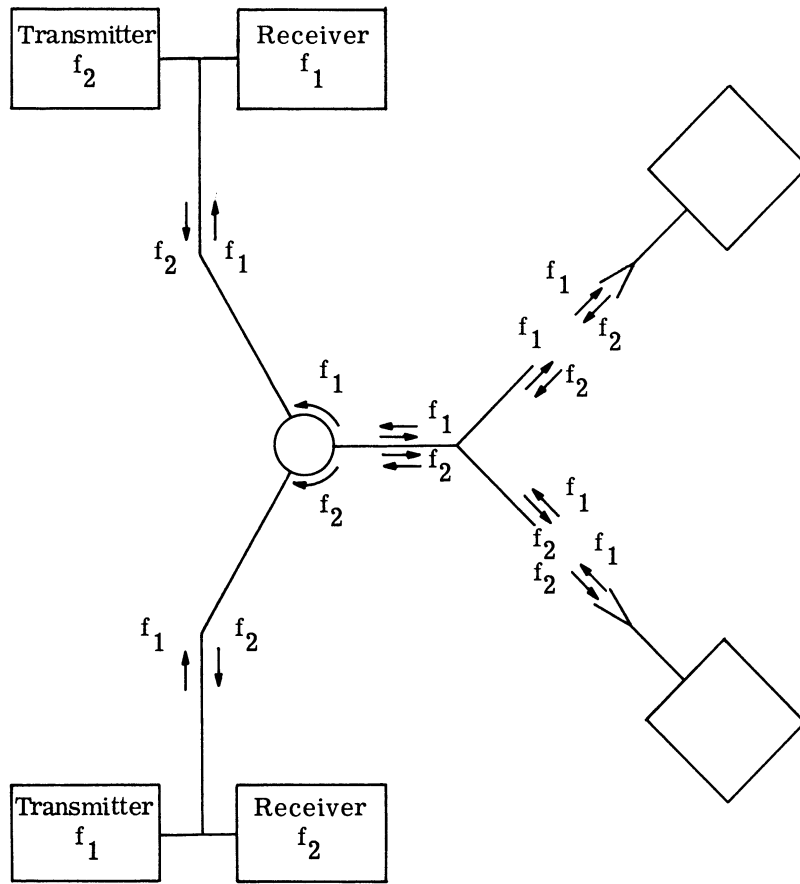


Fig. 5.26. Quadruplex system.

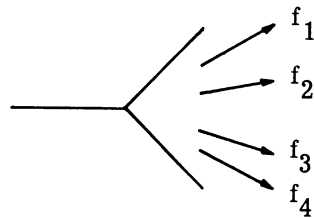


Fig. 5.27. Spreading of the microwave spectrum in space.

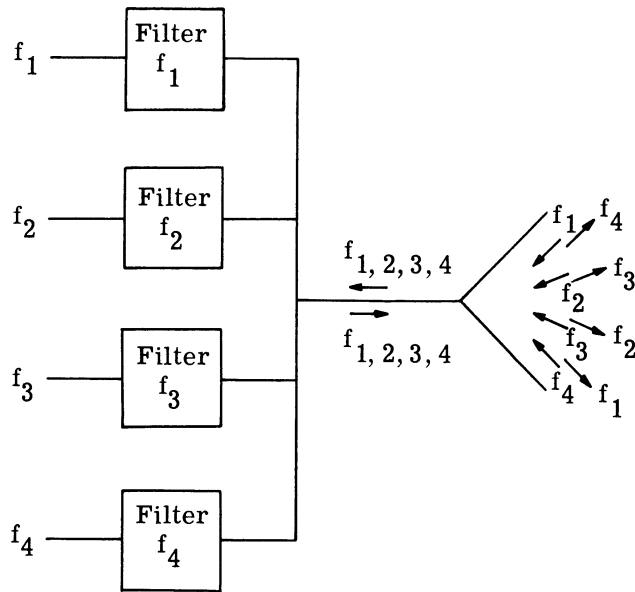


Fig. 5.28. Multiquadruplex system.

are present, the device may then be called a multiquadruplexer. This operation may be visualized by referring to Fig. 5.28. The problem of separating the several signals is solved using filters and duplexers.

Arrays

If a narrow beam is desired instead of the wide beam exhibited by the single scanning element, an array of ferrite antennas can be constructed. When properly phased such an array should be capable of steering a narrow beam. Experiments will have to be performed to verify the narrow beam scanning performance. It is possible that an array of this type would be smaller than an array of the phase shift type for a given angle of maximum beam shift. This is certainly true for the degenerate case of just a single element where the ferrite antenna can shift the beam by an angle of around 60° while a single, phase controlled antenna can produce no beam shifting.

The ferrite antenna array could be used as a self-phasing antenna of the type described in Ref. 30. Figure 5.29 illustrates a single element of the array using standard antennas. Between the receiving and retransmitting antennas there is a network that takes the conjugate of the incident wave. The operation can be described as follows:

The signal at the source is

$$A_0 e^{j\phi}$$

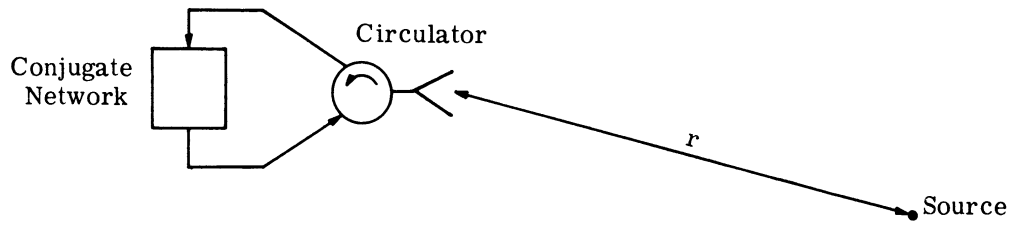


Fig. 5.29. Single element of a self-phasing antenna array.

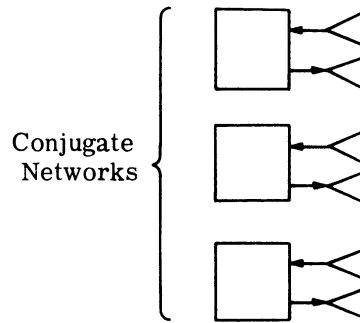


Fig. 5.30. A self-phasing antenna array using the ferrite scanning antenna.

The received signal is then (for $e^{j\omega t}$ time dependence)

$$A_0 A_1 e^{-j(k_0 r - \phi)}$$

where A_1 accounts for the amplitude attenuation over the path r .

Performing the conjugating operation gives

$$A_0 A_1 e^{j(k_0 r - \phi)}$$

Retransmitting this wave then gives back at the source (1)

$$A_0 A_1^2 e^{-j\phi}$$

It is seen that the phase of the wave received at the source is independent of the distance between the source and the conjugating circuit. Thus an array of identical antennas and circuits like this one produces a group of waves all in phase back at the source, and is called a self-phasing array. Such an array can be used to retain contact with a moving source such

as a satellite. One disadvantage of this system is that although the waves returning to the source are all in phase, their individual amplitudes do not remain maximum for the various source positions. Undesirable side lobes can thus occur and the amplitude of the wave returned to the source may be low. An array of ferrite antennas could overcome this disadvantage by pointing the receiving and retransmitting beams at the source as well as phasing the individual beams properly. A ferrite array is shown schematically in Fig. 5.30.

5.7 Conclusions

In this section, the conclusions are summarized for the entire study. The application of anisotropic ferrite materials to microwave devices opened an intriguing avenue for exploration. Many ideas found along the way have borne fruit in the form of useful devices. Most of the devices were first designed experimentally; their corresponding theories have usually resisted attempts at discovery and have yielded only to the most intense and inventive mathematics. In this study, a theoretical and experimental investigation of a ferrite device representative of the group of devices based on the circular cylinder has been carried out. The ferrite scanning antenna has been studied in detail while related devices and topics have been considered where appropriate.

Following is a summary of the main contributions and conclusions of this study.

1. A new, single element, electronic scanning antenna has been developed. The practicality of the device has been shown experimentally. The properties and advantages of this antenna have been shown to be the following:
 - (a) A scanning angle of about 60° can be obtained with reasonable efficiency and reflection characteristics.
 - (b) The size and weight of the antenna are small so that it is suitable for airborne equipment.
 - (c) Relatively low fields are required to produce the beam shift, thus keeping the power supply requirements low.

2. A theoretical analysis of the radiation patterns has been made. This analysis, although approximate in nature, has predicted the observed beam shifting and has shown that the scanning can be explained in terms of the field displacement within the material.
3. A mathematical analysis based on the variational technique has been made of the reflection coefficient of the antenna. The analysis includes the case where the ferrite cylinder is in the aperture or anywhere within the rectangular waveguide. The evaluation has been carried out in detail for the case of a circular cylinder. Simplified formulas have been derived for the special case of cylinders with small radii.
4. The analysis in (3) has been generalized to include any z-independent discontinuity in place of the aperture. That is, the methods introduced have been shown to be applicable to a number of problems of the "dual discontinuity" type. Applications of the method have been performed for the case of a small ferrite post with a short or open circuit for the second discontinuity. The results of this problem have been applied to outline a technique for measurement of the ferrite permeability and permittivity.
5. The analysis in (2) has been applied to symmetrical junction type circulators to provide an intuitively satisfying explanation of their mechanism of operation. Field displacement within the material was shown to cause the circulation.
6. Several applications for the scanning antenna have been presented, including its use as part of a microwave repeater station, as a modulator, and in an array. The ferrite post in a matched waveguide has been shown experimentally and

theoretically to operate as an electronically controlled single-pole, single-throw, switch.

Extension of the work presented here on the scanning antenna can be profitably undertaken in the following areas:

1. Matching of the antenna can be studied. The theory in Chapter III and the experiments in Chapter V can be used to develop matching techniques. In particular, the results of the present study show that the antenna reactance is always capacitive so that inductive loading can be used to improve the reflection coefficient. Methods of matching similar to those already developed for waveguide y-junction circulators might also be found useful.
2. Investigating the properties of an array of ferrite scanning antennas would be very interesting. The possibility of reducing array size for a given desired range of scanning angles was pointed out in Chapter V. In addition, the array might be found to be useful as a self-phasing antenna. Theoretical and experimental studies in this area would involve the general case of determining the performance characteristics of an array of individually steerable elements.

Use of the method developed in this report to solve "dual discontinuity" problems other than the specific ones mentioned in the text opens a broad region in which to extend the results of this study.

APPENDIX A

DYADIC ALGEBRA

Several formulas involving dyadic algebra have been used in the text. They are listed here for easy reference.

Let \vec{A} be a dyadic quantity given by

$$\vec{A} = \begin{bmatrix} A_{xx} & A_{xy} & A_{xz} \\ A_{yx} & A_{yy} & A_{yz} \\ A_{zx} & A_{zy} & A_{zz} \end{bmatrix}$$

Let \vec{B} be a vector given by

$$\vec{B} = B_x \vec{a}_x + B_y \vec{a}_y + B_z \vec{a}_z$$

Then

$$\begin{aligned} \vec{B} \cdot \vec{A} &= (B_x A_{xx} + B_y A_{yx} + B_z A_{zx}) \vec{a}_x \\ &+ (B_x A_{xy} + B_y A_{yy} + B_z A_{zy}) \vec{a}_y \\ &+ (B_x A_{xz} + B_y A_{yz} + B_z A_{zz}) \vec{a}_z \end{aligned}$$

We also have

$$\vec{B} \cdot \vec{A} = \vec{\tilde{A}} \cdot \vec{B}$$

where $\vec{\tilde{A}}$ means transpose \vec{A} .

The dyadic \vec{A} can be written in terms of three suitably defined vectors as follows:²²

$$\vec{A} = \vec{A}_1 \vec{a}_x + \vec{A}_2 \vec{a}_y + \vec{A}_3 \vec{a}_z$$

where

$$\bar{A}_1 = A_{xx}\bar{a}_x + A_{yx}\bar{a}_y + A_{zx}\bar{a}_z$$

$$\bar{A}_2 = A_{xy}\bar{a}_x + A_{yy}\bar{a}_y + A_{zy}\bar{a}_z$$

$$\bar{A}_3 = A_{xz}\bar{a}_x + A_{yz}\bar{a}_y + A_{zz}\bar{a}_z$$

The cross product of a vector and a dyadic is then given by the dyadic:

$$\bar{B} \times \bar{A} = (\bar{B} \times \bar{A}_1)\bar{a}_x + (\bar{B} \times \bar{A}_2)\bar{a}_y + (\bar{B} \times \bar{A}_3)\bar{a}_z$$

In the text a number of operations were performed on a dyadic with only four non-zero components such as

$$\bar{C} = \begin{bmatrix} C_{xx} & C_{xy} & 0 \\ C_{yx} & C_{yy} & 0 \\ 0 & 0 & 0 \end{bmatrix}$$

For this dyadic we can obtain the following formulas

$$\nabla \times \bar{C} = \begin{bmatrix} 0 & 0 & 0 \\ 0 & 0 & 0 \\ \frac{\partial C_{yx}}{\partial x} - \frac{\partial C_{xx}}{\partial y} & \frac{\partial C_{yy}}{\partial x} - \frac{\partial C_{xy}}{\partial y} & 0 \end{bmatrix}$$

$$\nabla \times \nabla \times \bar{C} = \begin{bmatrix} \frac{\partial^2 C_{yx}}{\partial y \partial x} - \frac{\partial^2 C_{xx}}{\partial y^2} & \frac{\partial^2 C_{yy}}{\partial x \partial y} - \frac{\partial^2 C_{xy}}{\partial y^2} & 0 \\ \frac{\partial^2 C_{xx}}{\partial y \partial x} - \frac{\partial^2 C_{yx}}{\partial x^2} & \frac{\partial^2 C_{xy}}{\partial x \partial y} - \frac{\partial^2 C_{yy}}{\partial x^2} & 0 \\ 0 & 0 & 0 \end{bmatrix}$$

$$\nabla^2 \bar{C} = \begin{bmatrix} \nabla^2 C_{xx} & \nabla^2 C_{xy} & 0 \\ \nabla^2 C_{yx} & \nabla^2 C_{yy} & 0 \\ 0 & 0 & 0 \end{bmatrix}$$

$$\nabla \cdot \vec{C} = \left(\frac{\partial C_{xx}}{\partial x} + \frac{\partial C_{yx}}{\partial y} \right) \bar{a}_x + \left(\frac{\partial C_{xy}}{\partial x} + \frac{\partial C_{yy}}{\partial y} \right) \bar{a}_y$$

Since the divergence of a dyadic is a vector we need the formula for the gradient of a vector

$$\nabla D = \begin{bmatrix} \frac{\partial D_x}{\partial x} & \frac{\partial D_y}{\partial x} & 0 \\ \frac{\partial D_x}{\partial y} & \frac{\partial D_y}{\partial y} & 0 \\ 0 & 0 & 0 \end{bmatrix}$$

where $D_z = 0$.

Then we can obtain

$$\nabla \nabla \cdot \vec{C} = \begin{bmatrix} \frac{\partial^2 C_{xx}}{\partial x^2} + \frac{\partial^2 C_{yx}}{\partial x \partial y} & \frac{\partial^2 C_{xy}}{\partial x^2} + \frac{\partial^2 C_{yy}}{\partial x \partial y} & 0 \\ \frac{\partial^2 C_{xx}}{\partial x \partial y} + \frac{\partial^2 C_{yx}}{\partial y^2} & \frac{\partial^2 C_{xy}}{\partial y \partial x} + \frac{\partial^2 C_{yy}}{\partial y^2} & 0 \\ 0 & 0 & 0 \end{bmatrix}$$

APPENDIX B

THE REFLECTIONS FROM AN OPEN-ENDED RECTANGULAR WAVEGUIDE

An open-ended rectangular waveguide with an infinite flange (Fig. B.1) is considered. If the TE_{10} mode is incident on the aperture the z-component of electric field can be written as:

$$E = \sin \frac{\pi y}{a} e^{-j\beta_{10}x} + \sum_{k=1}^{\infty} \sum_{\ell=0}^{\infty} R_{k\ell}^{10} \sin \frac{k\pi y}{a} \cos \frac{\ell\pi z}{b} e^{\gamma_{k\ell}x} \quad (B-1)$$

The superscript on $R_{k\ell}$ indicates that the TE_{10} mode is incident. Only TE_{n0} mode incidence will be considered. Evaluation of the $R_{k\ell}$ coefficients would completely determine the field in the waveguide. The problem of obtaining the reflection coefficient R_{10}^{10} was solved by Lewin⁸ using the variational technique. His analysis showed that if the trial functions were assumed to have no z-dependence then all the z-dependent terms in (B-1) integrated to zero, i. e., they could be ignored in the derivation. Thus, for simplicity in the derivations to follow, the z-dependence of the waveguide fields will be eliminated. For the case of the TE_{n0} mode incident on the aperture, the electric field is then

$$E^{(n)} = \sin \frac{n\pi y}{a} e^{-\gamma_n x} + \sum_{m=1}^{\infty} R_{nm} \sin \frac{m\pi y}{a} e^{\gamma_m x} \quad (B-2)$$

The R_{nn} terms represent the amount of reflection of the nth mode when the nth mode is incident. The R_{nm} terms ($n \neq m$) represent the coupling from the nth incident mode to the mth reflected mode. R_{nn} will be referred to as the self-reflection coefficient while R_{nm} ($n \neq m$) will be called the coupling coefficient. Extensions of Lewin's derivation will be made in the following ways:

1. In addition to the calculation of the TE_{10} self-reflection

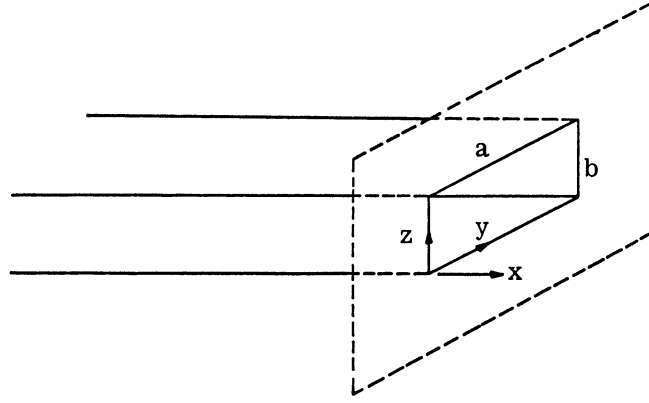


Fig. B. 1. An open-ended rectangular waveguide with an infinite flange.

coefficient, a variational expression will be derived for the coupling coefficients.

2. Expressions for the self-reflection coefficient and the coupling coefficients will be derived for any TE_{no} mode incident field.

B. 1 Derivation of the Self-Reflection Coefficients R_{nn}

y-component Π_y^* . The fields are given by

$$\bar{E} = -j\omega\mu_0 \nabla \times \bar{\Pi}^* \quad (B-3)$$

$$\bar{H} = \nabla \nabla \cdot \bar{\Pi}^* + k^2 \bar{\Pi}^* \quad (B-4)$$

$$E_z = -j\omega\mu_0 \frac{\partial \Pi_y^*}{\partial x}$$

$$E_x = j\omega\mu_0 \frac{\partial \Pi_y^*}{\partial z} \quad (B-5a)$$

$$E_y = 0$$

$$H_x = \frac{\partial^2 \Pi_y^*}{\partial x \partial y}$$

$$H_y = \frac{\partial^2 \Pi_y^*}{\partial y^2} + k_0^2 \Pi_y^* \quad (B-5b)$$

$$H_z = \frac{\partial^2 \Pi_y^*}{\partial y \partial x}$$

For Region 1 (the waveguide), take Π_y^* for the nth mode as

$$-j\omega\mu_0\Pi_1^{(n)} = -\frac{1}{\gamma_n}\sin\frac{n\pi y}{a}e^{-\gamma_n x} + \sum_{m=1}^{\infty}\frac{R_{nm}}{\gamma_m}\sin\frac{m\pi y}{a}e^{\gamma_m x} \quad (\text{B-6})$$

While in Region 2 (free space), we take for Π_y^* a form similar to Lewin's.

$$\Pi_2^{(n)} = \frac{1}{j\omega\mu_0 2\pi} \int_0^a \int_0^b E^{(n)}(\xi, \eta) \frac{e^{-jk_0 r}}{r} d\xi d\eta \quad (\text{B-7})$$

where $r = [x^2 + (y - \eta)^2 + (z - \xi)^2]^{\frac{1}{2}}$.

$E^{(n)}$ is the field at the aperture when the TE_{no} mode is incident. It is given by (B-2) with $x = 0$. The boundary conditions are continuity of E_z and H_y at the aperture ($x = 0$).

Continuity of E_z at $x = 0$ gives:

$$E^{(n)}(y, z) = \left[\sin\frac{n\pi y}{a} + \sum_{m=1}^{\infty} R_{nm} \sin\frac{m\pi y}{a} \right] = \left[\sin\frac{n\pi y}{a} (1 + R_{nn}) + \sum_{m=1}^{\infty'} R_{nm} \sin\frac{m\pi y}{a} \right] \quad (\text{B-8})$$

where the prime signifies omission of the $m = n$ term in the series.

Equation B-8 is a Fourier series for $E^{(n)}(y, z)$. The coefficients are given by

$$(1 + R_{nn}) = \frac{2}{ab} \int_0^a \int_0^b E^{(n)}(\xi, \eta) \sin\frac{n\pi\eta}{a} d\xi d\eta \quad (\text{B-9})$$

$$R_{nm} = \frac{2}{ab} \int_0^a \int_0^b E^{(n)}(\xi, \eta) \sin\frac{m\pi\eta}{a} d\xi d\eta \quad (\text{B-10})$$

Continuity of H_y at $x = 0$ gives

$$- \int_0^a \int_0^b E^{(n)}(\xi, \eta) \left(\frac{\partial^2}{\partial y^2} + k_0^2 \right) \left(\frac{e^{-jk_0 r}}{2\pi r} \right) d\xi d\eta = \gamma_n \sin\frac{n\pi y}{a} (1 - R_{nn}) - \sum_{m=1}^{\infty'} R_{nm} \gamma_m \sin\frac{m\pi y}{a} \quad (\text{B-11})$$

where here, since $x = 0$,

$$r = [(z - \xi)^2 + (y - \eta)^2]^{\frac{1}{2}}$$

First, a stationary form for the self-reflection coefficients will be found.

Substituting R_{nm} from (B-10) into (B-11) gives

$$\begin{aligned} - \int_0^a \int_0^b E^{(n)}(\xi, \eta) \left(\frac{\partial^2}{\partial y^2} + k_o^2 \right) \left(\frac{e^{-jk_o r}}{2\pi r} \right) d\xi d\eta = (1 - R_{nn}) \gamma_n \sin \frac{n\pi y}{a} \\ - \sum_{m=1}^{\infty'} \frac{2}{ab} \gamma_m \sin \frac{m\pi y}{a} \int_0^a \int_0^b E^{(n)}(\xi, \eta) \sin \frac{m\pi \eta}{a} d\xi d\eta \end{aligned} \quad (B-12)$$

This is an integral equation for the aperture field $E^{(n)}(\xi, \eta)$.

A stationary form for the self-reflection coefficient results if we multiply (B-12) on both sides by $E^{(n)}(y, z)$ and integrate over the aperture. Divide (B-9) into the result twice to obtain:

$$\frac{1-R_{nn}}{1+R_{nn}} = \left(-\frac{ab}{2\gamma_n} \right) \frac{\int_0^a \int_0^b \int_0^a \int_0^b E^{(n)}(y, z) E^{(n)}(\xi, \eta) G_n(y, z | \xi, \eta) dz dy d\xi d\eta}{D_n^2} \quad (B-13)$$

where

$$\begin{aligned} G_n &= \left(\frac{\partial}{\partial y^2} + k_o^2 \right) \frac{e^{-jk_o r}}{2\pi r} - \sum_{m=1}^{\infty'} \frac{2\gamma_m}{ab} \sin \frac{m\pi y}{a} \sin \frac{m\pi \eta}{a} \\ D_n &= \int_0^a \int_0^b E^{(n)}(\xi, \eta) \sin \frac{n\pi \eta}{a} d\xi d\eta \end{aligned}$$

The proof of stationarity is given at the end of this section.

Values of R_{nn} are found by substituting trial values of $E^{(n)}$ into (B-13). A good trial function for any incident mode is just the field distribution of the incident field itself, i. e., let

$$E^{(n)} = \sin \frac{n\pi y}{a} \quad (B-14)$$

then, (B-13) becomes

$$\frac{1-R_{nn}}{1+R_{nn}} = -\frac{2}{ab\gamma_n} \int_0^a \int_0^b \int_0^a \int_0^b \sin \frac{n\pi y}{a} \sin \frac{n\pi \eta}{a} \left[\frac{\partial^2}{\partial y^2} + k_0^2 \right] \frac{e^{-jk_0 r}}{2\pi r} d\xi d\eta dz dy \quad (\text{B-15})$$

This is exactly the result that would have been obtained had z-dependent reflected modes been considered also. The z-dependent terms would have appeared as a factor in G_n and would have integrated to zero when the trial function (B-14) was used.

Integration of (B-15) gives the self-reflection coefficients for TE_{n0} modes. Two of the integrations can be performed by using the transformation

$$\begin{aligned} y - \eta &= \lambda & x - \xi &= \sigma \\ y + \eta &= a + \mu & x + \xi &= b + v \end{aligned}$$

Then

$$\frac{1-R_{nn}}{1+R_{nn}} = \frac{2\gamma_n}{\pi ab} \int_0^{a-\lambda} \int_0^{b-\sigma} \left[(a-\lambda) \cos \frac{n\pi\lambda}{a} + \frac{a}{n\pi} \frac{k_0^2 + \left(\frac{n\pi}{a}\right)^2}{k_0^2 - \left(\frac{n\pi}{a}\right)^2} \sin \frac{n\pi\lambda}{a} \right] \cdot (b-\sigma) \frac{e^{-jk_0(\lambda^2 + \sigma^2)^{1/2}}}{(\lambda^2 + \sigma^2)^{1/2}} d\lambda d\sigma \quad (\text{B-16})$$

Proof of Stationarity

Vary $E^{(n)}$ in (B-13), that is let $E^{(n)} = E_c^{(n)} + \delta E^{(n)}$ where $E_c^{(n)}$ is the correct value for $E^{(n)}$. Then we obtain

$$\begin{aligned} \frac{1-R_{nn}}{1+R_{nn}} & \left[D_n \int_0^a \int_0^b \delta E^{(n)}(y, z) \sin \frac{n\pi y}{a} dz dy + D_n \int_0^a \int_0^b \delta E^{(n)}(\xi, \eta) \sin \frac{n\pi \eta}{a} d\xi d\eta \right] + D_n^2 \delta \left(\frac{1-R_{nn}}{1+R_{nn}} \right) \\ & = -\frac{ab}{2\gamma_n} \left[\int_0^a \int_0^b \int_0^a \int_0^b \delta E^{(n)}(y, z) E^{(n)}(\xi, \eta) G_n(y, z | \xi, \eta) dz dy d\xi d\eta \right. \\ & \quad \left. + \int_0^a \int_0^b \int_0^a \int_0^b E^{(n)}(y, z) \delta E^{(n)}(\xi, \eta) G_n(y, z | \xi, \eta) dz dy d\xi d\eta \right] \end{aligned}$$

From (B-9), we can use the relationship

$$D_n = 1 + R_{nn}$$

If we now use the symmetry of G_n in y, η and z, ξ in the above integral equation, we get

$$2 \int_0^a \int_0^b \delta E^{(n)}(y, z) \left[(1-R_{nn}) \sin \frac{n\pi y}{a} + \frac{ab}{2\gamma_n} \int_0^a \int_0^b E^{(n)}(\xi, \eta) G_n d\xi d\eta \right] = -D_n^2 \delta \left(\frac{1-R_{nn}}{1+R_{nn}} \right)$$

The integrand on the left is zero by (B-12). Thus

$$D_n^2 \delta \left(\frac{1-R_{nn}}{1+R_{nn}} \right) = 0$$

Since D_n is zero only for $R_{nn} = -1$, we have in general that

$$\delta \left(\frac{1-R_{nn}}{1+R_{nn}} \right) = 0$$

and (B-13) is stationary with respect to small variations in $E^{(n)}$.

B.2 Derivation of the Coupling Coefficients R_{nm}

Next, a variational expression for the coupling terms, R_{nm} , will be developed since a direct method of evaluating these terms is desirable.

Write (B-12) as:

$$(1-R_{nn}) \gamma_n \sin \frac{n\pi y}{a} = - \int_0^a \int_0^b E^{(n)}(\xi, \eta) G_n(y, z | \xi, \eta) d\xi d\eta \quad (B-17)$$

Multiplying this through by $E^{(m)}(y, z)$, integrating over the aperture and then using (B-10) to introduce R_{mn} gives

$$- \int_0^a \int_0^b \int_0^a \int_0^b E^{(m)}(y, z) E^{(n)}(\xi, \eta) G_n d\xi d\eta dz dy = (1-R_{nn}) \gamma_n (-j\omega\mu_0) \frac{ab}{2} R_{mn} \quad (B-18)$$

Now, divide both sides by $R_{nm} R_{mn}$ as given by (B-10). The result is

$$\frac{-\gamma_n (1-R_{nn})}{R_{nm}} = \frac{\iiint E^{(m)}(y, z) E^{(n)}(\xi, \eta) G_n d\xi d\eta dz dy}{\frac{2}{ab} \int_0^a \int_0^b E^{(n)}(\xi, \eta) \sin \frac{m\pi\eta}{a} d\xi d\eta \int_0^a \int_0^b E^{(m)}(z, y) \sin \frac{n\pi y}{a} dz dy} \quad (B-19)$$

This is not a stationary expression for the term on the left in the present form. To obtain a stationary expression from this equation, let:

$$G_n = G + \frac{2\gamma_n}{ab} \sin \frac{n\pi y}{a} \sin \frac{n\pi \eta}{a}$$

where

$$G = \left(\frac{\partial^2}{\partial y^2} + k_o^2 \right) \frac{e^{-jk_o r}}{2\pi r} - \sum_{m=1}^{\infty} \frac{2\gamma_m}{ab} \sin \frac{m\pi y}{a} \sin \frac{m\pi \eta}{a}$$

Then (B-19) becomes

$$\begin{aligned} \frac{-\gamma_n(1-R_{nn})}{R_{nm}} &= \frac{\iiint E^{(m)}(y,z) E^{(n)}(\xi,\eta) G \, d\xi \, d\eta \, dz \, dy}{\frac{2}{ab} \iint E^{(n)}(\xi,\eta) \sin \frac{m\pi \eta}{a} \, d\xi \, d\eta \iint E^{(m)}(y,z) \sin \frac{n\pi y}{a} \, dz \, dy} \\ &+ \frac{\iiint E^{(m)}(y,z) E^{(n)}(\xi,\eta) \frac{2\gamma_n}{ab} \sin \frac{n\pi y}{a} \sin \frac{n\pi \eta}{a} \, d\xi \, d\eta \, dz \, dy}{\frac{2}{ab} \iint E^{(n)}(\xi,\eta) \sin \frac{m\pi \eta}{a} \, d\xi \, d\eta \iint E^{(m)}(y,z) \sin \frac{n\pi y}{a} \, dz \, dy} \end{aligned} \quad (B-20)$$

The second term on the right can be integrated using (B-8) for $E^{(m)}$ and $E^{(n)}$ to give

$$\frac{\gamma_n(1+R_{nn})}{R_{nm}}$$

Combining terms in (B-20) then gives

$$\frac{-2\gamma_n}{R_{nm}} = \frac{\int_0^a \int_0^b \int_0^a \int_0^b E^{(m)}(y,z) E^{(n)}(\xi,\eta) G(y,z|\xi,\eta) \, d\xi \, d\eta \, dz \, dy}{\frac{2}{ab} \int_0^a \int_0^b E^{(n)}(\xi,\eta) \sin \frac{m\pi \eta}{a} \, d\xi \, d\eta \int_0^a \int_0^b E^{(m)}(y,z) \sin \frac{n\pi y}{a} \, dz \, dy} \quad (B-21)$$

This is a stationary expression for the coupling coefficients. The proof of stationarity is given at the end of the appendix. Appropriate trial functions are:

$$\begin{aligned} E^{(m)} &= A_m \sin \frac{m\pi y}{a} + A_n \sin \frac{n\pi y}{a} \\ E^{(n)} &= B_n \sin \frac{n\pi \eta}{a} + B_m \sin \frac{m\pi \eta}{a} \end{aligned} \quad (B-22)$$

The coupling coefficient can be evaluated using these trial functions in (B-21)

and using a procedure like that discussed in obtaining (3.59).

Proof of Stationarity of R_{nm}

Vary $E^{(n)}(\xi, \eta)$ in (B-21).

$$\begin{aligned} & \frac{-4\gamma_n}{R_{nm} ab} \iint \delta E^{(n)}(\xi, \eta) \sin \frac{m\pi\eta}{a} d\xi d\eta \iint E^{(m)}(y, z) \sin \frac{n\pi y}{a} dz dy \\ & - \iint \delta E^{(n)}(\xi, \eta) \left[\iint E^{(m)}(y, z) G(y, z|\xi, \eta) dz dy \right] d\xi d\eta \\ & - \left[\frac{4\gamma_n}{ab} \iint E^{(n)}(\xi, \eta) \sin \frac{m\pi\eta}{a} d\xi d\eta \iint E^{(m)}(y, z) \sin \frac{n\pi y}{a} dz dy \right] \delta \left(\frac{1}{R_{nm}} \right) = 0 \end{aligned}$$

The multiplier of the $\delta E^{(n)}$ term is [using (B-10) and the reciprocity relation $\gamma_m R_{nm} = \gamma_n R_{mn}$]

$$-2\gamma_m \sin \frac{m\pi\eta}{a} - \iint E^{(m)}(y, z) G(y, z|\xi, \eta) dz dy$$

This reduces to

$$(1 - R_{mm}) \gamma_m \sin \frac{m\pi\eta}{a} + \iint E^{(m)} G_m dz dy$$

which is identically zero by (B-17). Thus (B-21) is stationary with respect to small arbitrary variations in $E^{(n)}$.

A similar result is obtained by varying $E^{(m)}$. Thus (B-21) is the required stationary form for R_{nm} .

APPENDIX C

THE COMPONENTS OF THE FERRITE PERMEABILITY TENSOR

In this appendix the values of the components of the tensor permeability are found. They are needed to obtain numerical results for the theoretical equations derived in Chapters II and III.

The relative permeability of a ferrite medium magnetized in the z-direction is described by a tensor of the form^{2, 25}

$$\vec{\mu} = \begin{bmatrix} \mu & -jk & 0 \\ jk & 0 & 0 \\ 0 & 0 & \mu_z \end{bmatrix} \quad (C-1)$$

If the medium is saturated, the values of the tensor components for the lossless case are given by

$$\mu = 1 + \frac{\omega_m \omega_o / \omega^2}{(\omega_o / \omega)^2 - 1} \quad (C-2a)$$

$$k = - \frac{\omega_m / \omega}{(\omega_o / \omega)^2 - 1} \quad (C-2b)$$

where:

$$\omega_m = -\gamma_e M_s$$

$$M_s = \text{saturation magnetization}$$

$$\omega_o = -\gamma_e H_{\text{int}}$$

$$H_{\text{int}} = \text{internal dc magnetic field}$$

$$\gamma_e = \text{gyromagnetic ratio, (taken here as } -2.94 \text{ Mc/oersted)}$$

$\mu_z \cong 1$, at microwave frequencies.

These equations are valid when the material is magnetically saturated and when the losses are neglected. The losses are generally small at microwave frequencies except near ferromagnetic resonance. We are not concerned with the resonance behavior in this study. The region where the applied fields are small (and the materials are not saturated) is of prime interest, however. This is the region where the antenna described in Chapter V operates.

For the unsaturated medium, the off-diagonal component of the permeability is:^{31,32}

$$k = \frac{-\gamma_e M}{\omega} \quad (C-3)$$

where M is the unsaturated magnetization. While M_s is given for most ferrite materials by the manufacturer, curves of M as a function of the internal magnetic field are noticeably lacking. The magnetization curve for a typical MgMn ferrite is shown in Fig. C. 1.* It is seen that saturation occurs at an internal field of about 200 oersteds. This curve, along with (C-2) and (C-3), was used to evaluate k and the result is shown in Fig. C. 2. The diagonal component, μ , was obtained from measured values reported by LeCraw and Spencer³¹ for the unsaturated region for a MgMn ferrite and are only approximate. The ferrite is diamagnetic ($\mu < 1$) at microwave frequencies for zero internal field as seen from Fig. C. 2 where the results are plotted. For the saturated region (C-2) was used to obtain μ .

In the graph, μ and k are given as functions of the internal field. Since the external field is more convenient to measure than the internal field, a plot of the tensor components as functions of the external field is desired. Usually the circuit is visualized as a ferrite placed in a static field uniform through all space. For this case, the external field differs from the internal field because of shape dependent demagnetizing effects which can be approximately accounted for. The two fields are related by the equation

$$H_{int} = H_{ext} - N_z M \quad (C-4)$$

* The measurements for this curve were performed at the National Bureau of Standards. The plot appears in Ref. 33. The material is General Ceramics R1, a material similar to the one used for the experiments in this report (TT390).

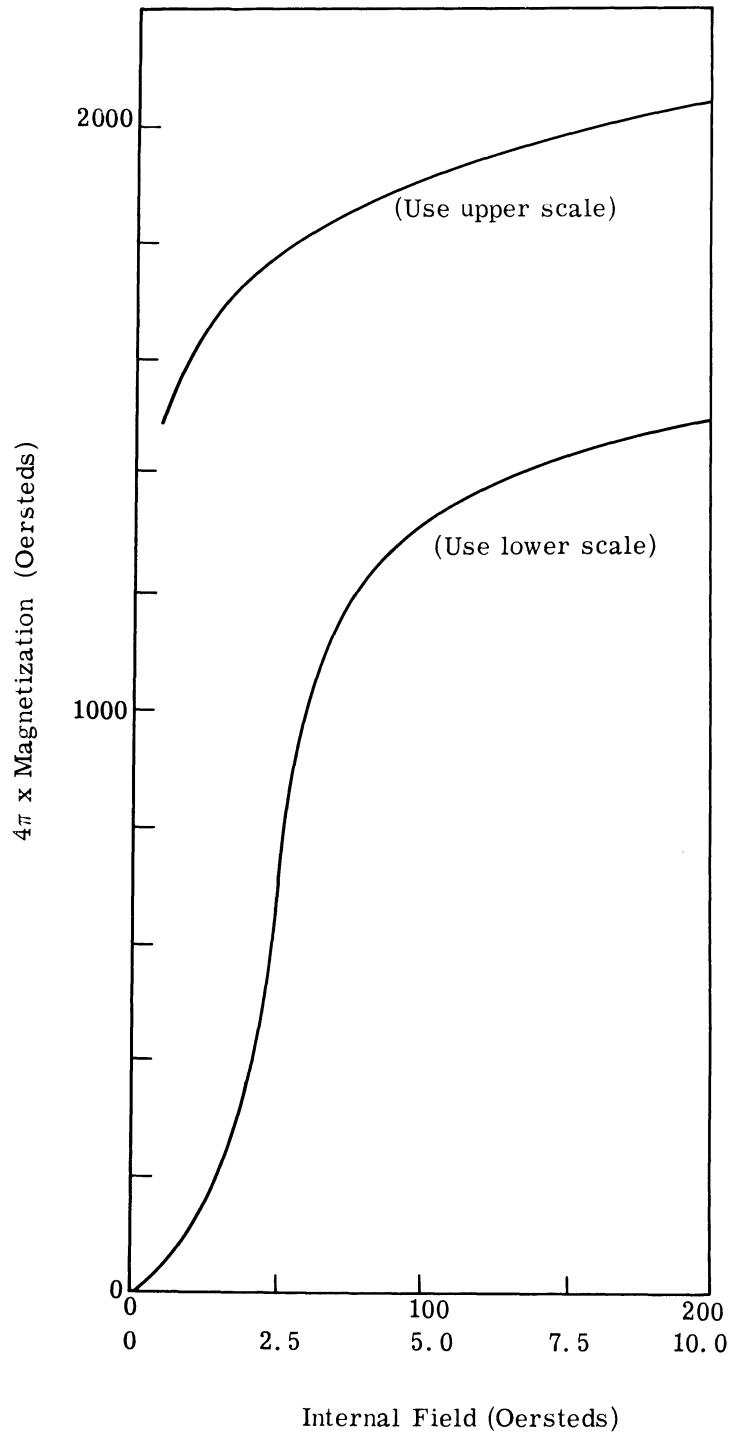


Fig. C. 1. Magnetization curve.

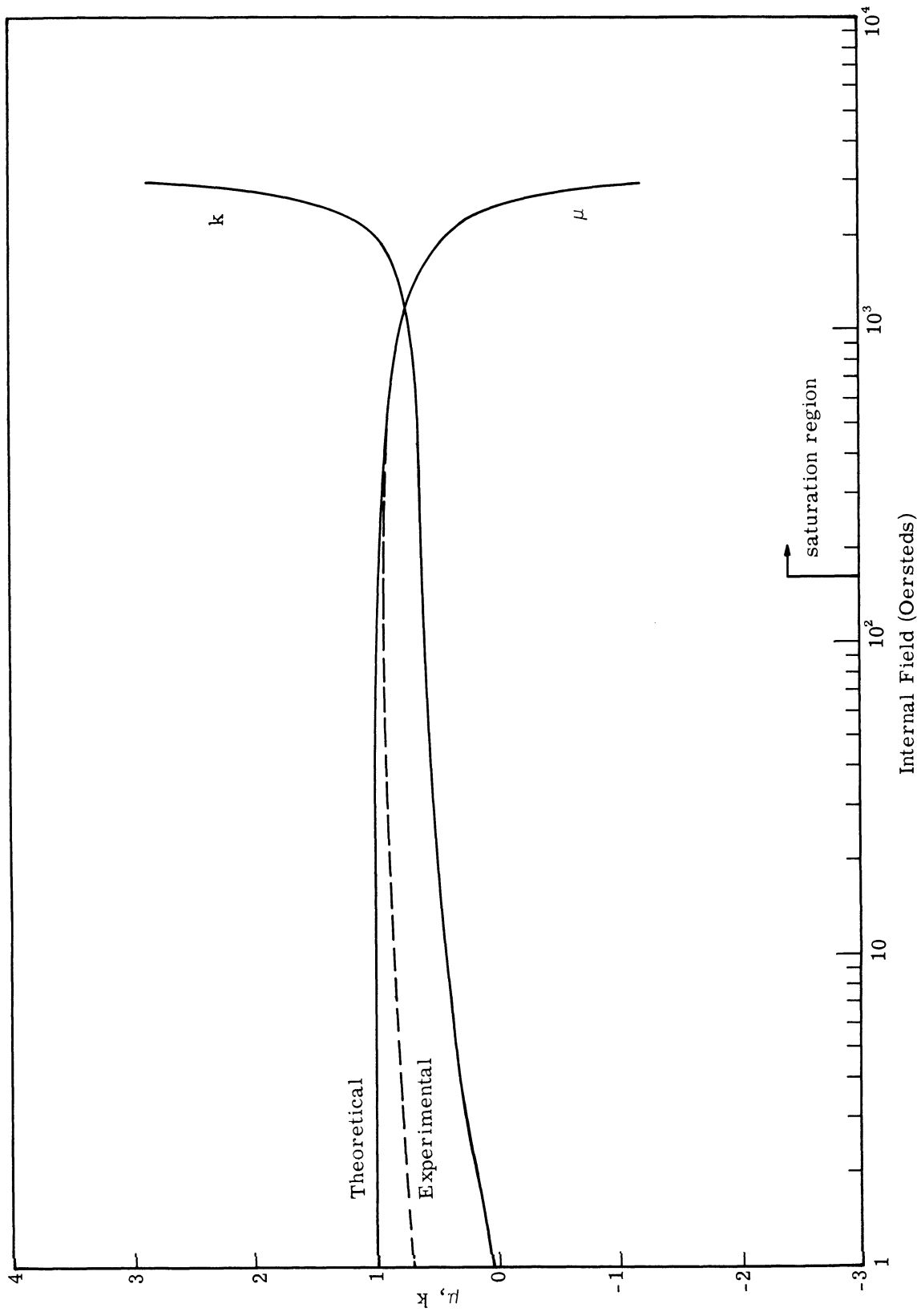


Fig. C. 2. Permeability as a function of the internal static field. Frequency = 10 Gc/sec.

where H_{ext} is the external field and N_z is the demagnetization factor.

For the cylinder, N_z depends on the length to diameter ratio. Values of N_z are plotted in Ref. 32 for various ratios. Using these values and the magnetization values from Fig. C. 1 in (C-4) gives the relationship between the internal and external fields. Two such results are given in Fig. C. 3. Finally, combining Figs. C. 2 and C. 3 gives the values of the tensor components as functions of the external field. Figure C. 4 gives the result for the cylinder used in many of the experiments.

Unfortunately the electromagnet used in the experiments for this study did not provide a static field uniform through all space, but only a field uniform over a circular area about one inch in diameter. Also, in order to produce the required fields, the gap between the pole faces of the electromagnet was limited to a maximum of about one inch. Because of this the ferrite created a low reluctance path which distorted the field beyond that which would have occurred in a static field uniform through all space. That static field was measured as shown in the sketch (Fig. C-5) in a uniform portion of the field. This was necessary because of the physical size of the Gaussmeter probe and the probe holder. It was a useful and practical procedure since experimental results could be easily reproduced. The practical result was that the measured field (called the "applied" field, H_{app}) was usually less than the actual "external" field (H_{ext}) experienced by the ferrite and referred to in the theory (C. 4). That is, the ferrite concentrated the field so that the measurements were low. This trend was consistently followed in all the experiments. The actual differences between H_{ext} and H_{app} , as arrived at by a comparison of the predicted results for the experiments and the experiments themselves, was not great. Certainly, the differences were much less than the differences between the internal and external fields in Fig. C. 3.

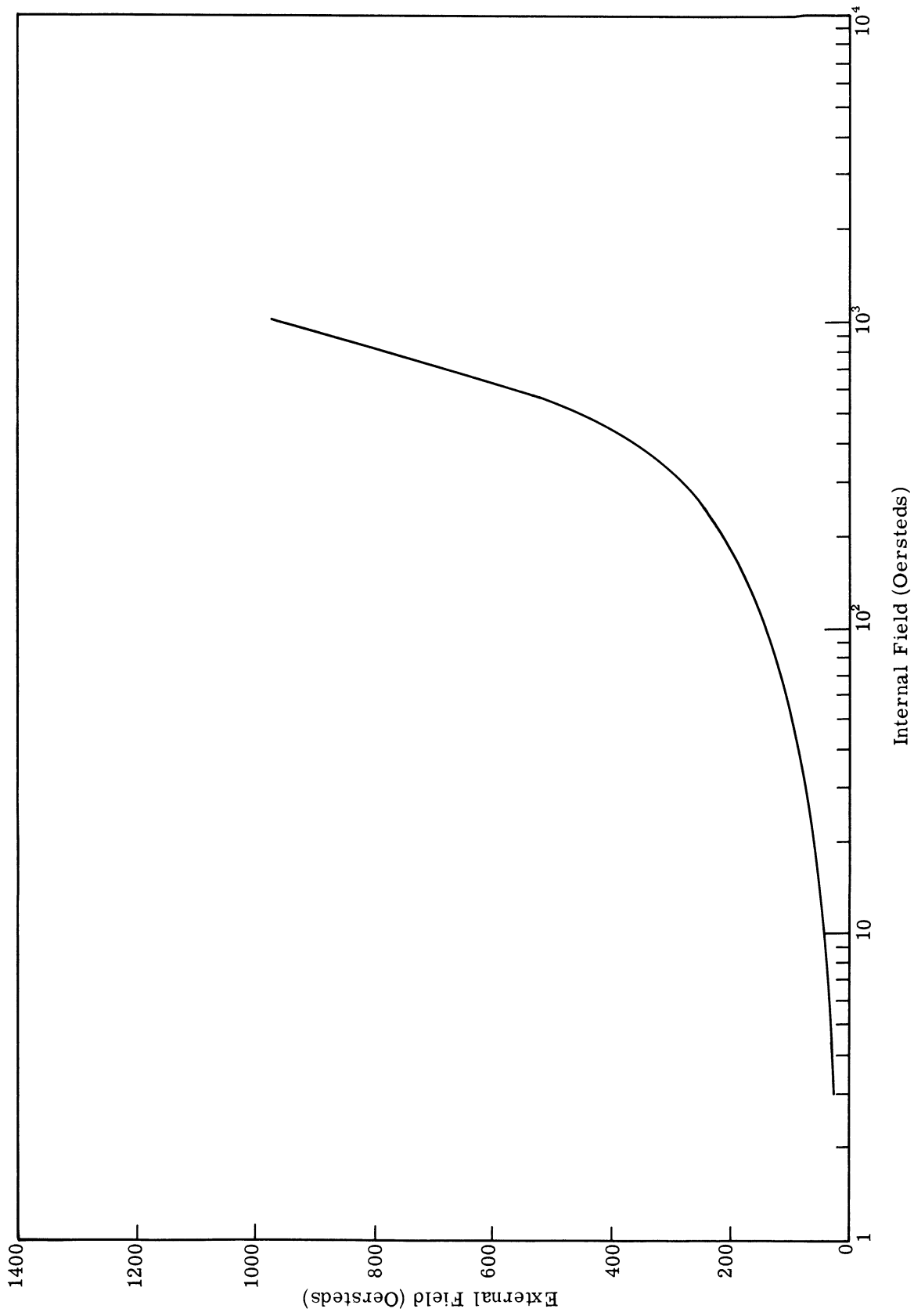
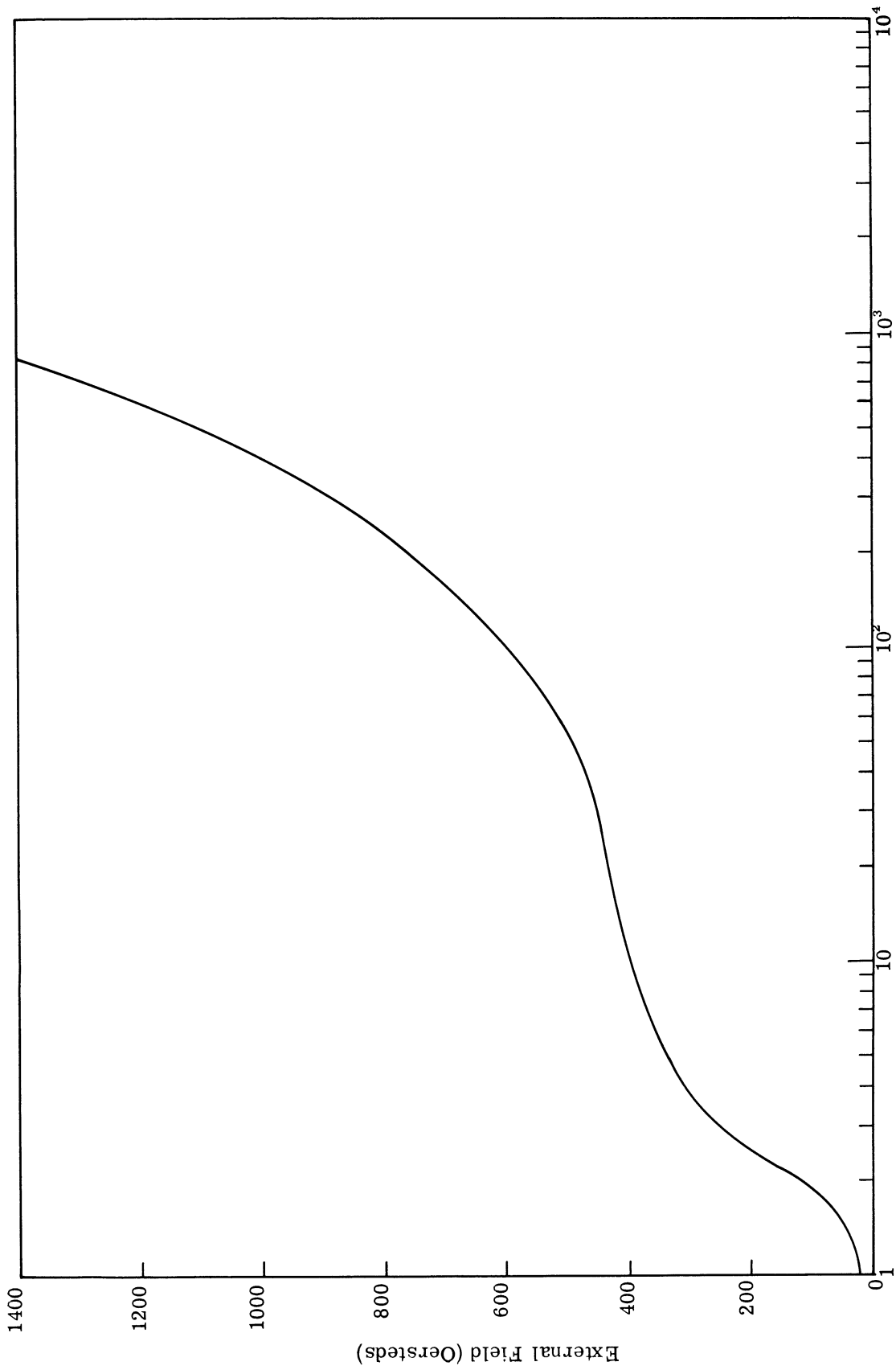


Fig. C. 3. (a) External field vs. internal field for two different demagnetizing factors. Diameter/length = .117, $N_z/4\pi = .02$, diameter = .0468".

Internal Field (Oersteds)

External Field (Oersteds)



Internal Field (Oersteds)

Fig. C. 3. (b) External field vs. internal field for two different demagnetizing factors. Diameter/length = .737, $N_z/4\pi = .26$, diameter = .295".

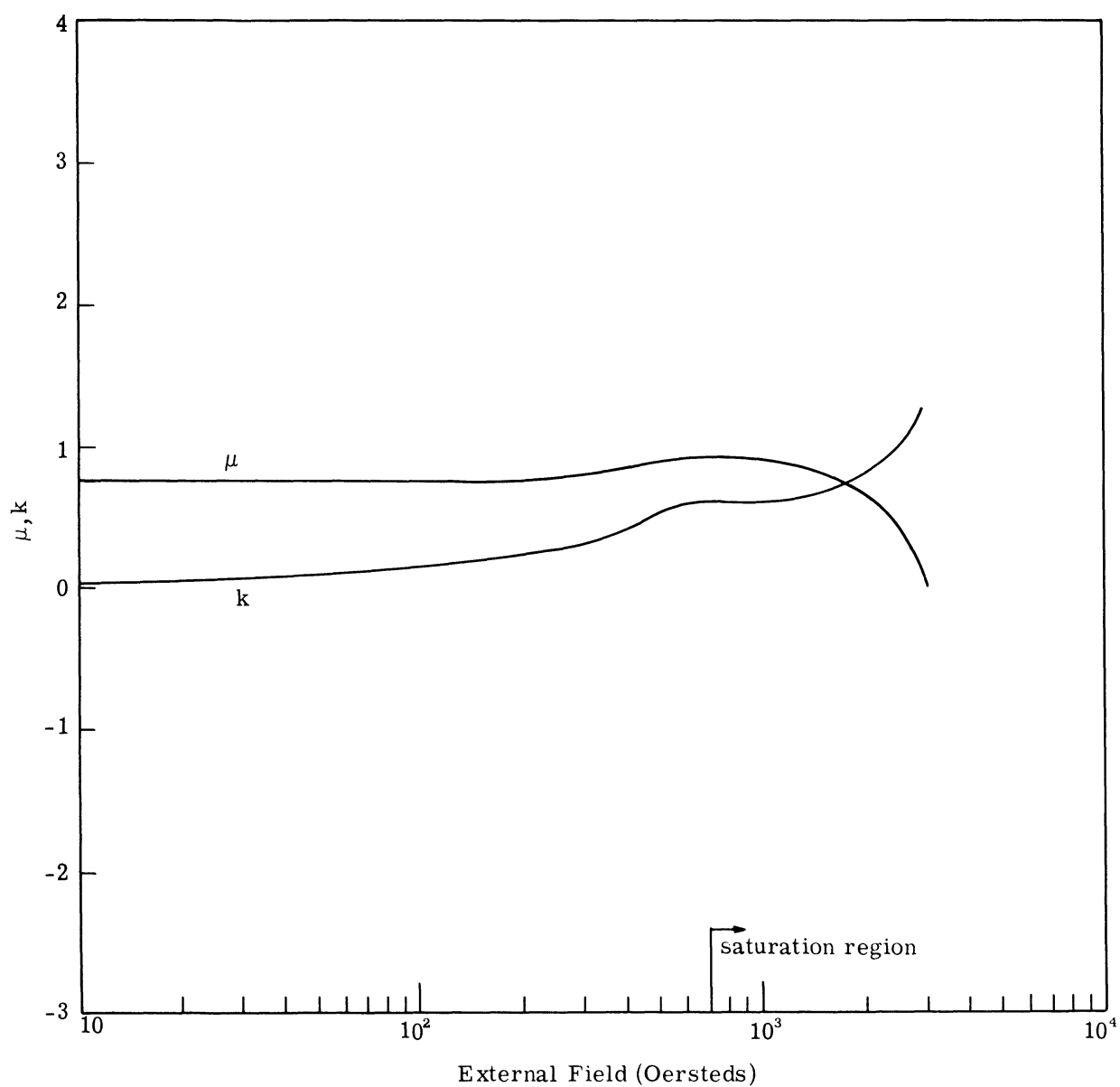


Fig. C.4. Permeability as a function of the external static field.
 Frequency = 10 Gc/sec, diameter/length = .737,
 $N_z/4\pi = .26$, diameter = .295".

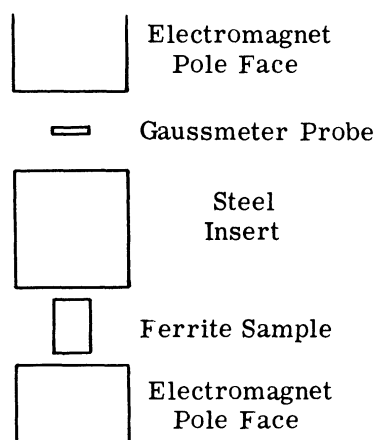


Fig. C. 5. Geometry for measurement of the applied field.

APPENDIX D

EVALUATION OF TERMS USED IN CHAPTER III

In Chapter III, Section 3.2, the evaluation of the terms $e^{-jnD} E_o(0)$ and $e^{jnD} e^{-j\ell D_o} G_1(0,0)$ was not completed. The methods used and the final results for the terms with indices -1, 0, +1 will be given in this appendix.

Evaluation of $e^{-jnD} E_o(0)$

From (3.15) we have

$$E_o = \sin \frac{\pi y}{a} e^{-\gamma_1 x} + \sum_{n=1}^{\infty} R_{1n} \sin \frac{n\pi y}{a} e^{\gamma_n x} \quad (3.15)$$

Recall that $e^{-jnD} E_o(0)$ means the operation

$$\left[\frac{1}{jk_o} \left(\frac{\partial}{\partial x'} - j \frac{\partial}{\partial y'} \right) \right]^n E_o$$

evaluated at the center of the circle. And the (x', y') coordinates refer to the system whose origin is the center of the circle (see Fig. D.1), i. e., $y = y' + c$, $x = x' - d$. The evaluation is now straightforward and the results are

$$e^{-j0D} E_o(0) = \sin \frac{\pi c}{a} e^{+\gamma_1 d} + \sum_{n=1}^{\infty} R_{1n} \sin \frac{n\pi c}{a} e^{-\gamma_n d} \quad (D-1a)$$

$$e^{\pm jD} E_o(0) = \frac{1}{jk_o} \left\{ -\gamma_1 \sin \frac{\pi c}{a} e^{+\gamma_1 d} + \sum_{n=1}^{\infty} R_{1n} \gamma_n \sin \frac{n\pi c}{a} e^{-\gamma_n d} \right. \\ \left. \pm j \left[\frac{\pi}{a} \cos \frac{\pi c}{a} e^{+\gamma_1 d} + \sum_{n=1}^{\infty} R_{1n} \frac{n\pi}{a} \cos \frac{n\pi c}{a} e^{-\gamma_n d} \right] \right\} \quad (D-1b)$$

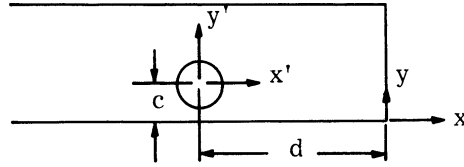


Fig. D. 1. Coordinate system for evaluation of terms from Chapter III.

For the case where the post is centered in the waveguide at $c = a/2$ these simplify to

$$e^{-j0D} E_o(0) = e^{\gamma_1 d} + \sum_{n=1}^{\infty} R_{1n} \sin \frac{n\pi}{2} e^{-\gamma_n d} \quad (\text{D-2a})$$

$$e^{\pm jD} E_o(0) = \frac{j\gamma_1}{k_o} e^{\gamma_1 d} - j \sum_{n=1}^{\infty} \frac{R_{1n}\gamma_n}{k_o} \sin \frac{n\pi}{2} e^{-\gamma_n d} \quad (\text{D-2b})$$

where R_{1n} was taken as zero for n even due to symmetry.

Evaluation of $e^{jnD} e^{-j\ell D_o} G_i(r|r_o)$

The terms will be evaluated here for the case of the centered post.

We have from (3. 48)

$$G_i(r|r_o) = bG(r|r_o) - G_{f.s.}(r|r_o) \quad (3. 48)$$

So, that

$$G_i(r|r_o) = \sum_{k=1}^{\infty} \frac{\sin \frac{k\pi y}{a} \sin \frac{k\pi y_o}{a} e^{-\gamma_k |x - x_o|}}{\gamma_k a} + \sum_{k=1}^{\infty} \sum_{m=1}^{\infty} \frac{R_{km}}{\gamma_k a} \sin \frac{k\pi y_o}{a} \sin \frac{m\pi y}{a} e^{\gamma_k x_o + \gamma_m x} + \frac{N_o(k_o |\bar{r} - \bar{r}_o|)}{4} \quad (\text{D-3})$$

To evaluate at $r = r_o = 0$, add and subtract the static Green's function for the empty matched waveguide problem. This gives

$$\begin{aligned}
G_i(r|r_o) &= \sum_{k=1}^{\infty} \sin \frac{k\pi y}{a} \sin \frac{k\pi y_o}{a} \left(\frac{e^{-\gamma_k |x-x_o|}}{\gamma_k a} - \frac{e^{-\frac{k\pi}{a} |x-x_o|}}{k\pi} \right) \\
&+ \sum_{k=1}^{\infty} \sum_{m=1}^{\infty} \frac{R_{km}}{\gamma_k a} \sin \frac{k\pi y}{a} \sin \frac{m\pi y_o}{a} e^{\gamma_k x_o + \gamma_m x} \\
&+ \sum_{k=1}^{\infty} \frac{\sin \frac{k\pi y}{a} \sin \frac{k\pi y_o}{a} e^{-\frac{k\pi}{a} |x-x_o|}}{k\pi} + \frac{N_o(k_o | \bar{r} - \bar{r}_o |)}{4}
\end{aligned} \tag{D-4}$$

The singularity at $x = x_o$, $y = y_o$ was thus removed from the first summation. The first term in (D-4) now converges approximately as the series of terms $1/k^2$. The singularity in the static Green's function at $x = x_o$, $y = y_o$ can be expressed analytically and it will cancel the singularity in the Neumann function as required to make $G_i(0|0)$ a finite number. The procedure used in finding the analytic form of the static Green's function follows.

$$\begin{aligned}
&\sum_{k=1}^{\infty} \frac{\sin \frac{k\pi y}{a} \sin \frac{k\pi y_o}{a} e^{-\frac{k\pi}{a} |x-x_o|}}{k\pi} \\
&= \sum_{k=1}^{\infty} \frac{1}{2\pi} \operatorname{Re} \left[\frac{e^{j \frac{k\pi}{a} (y' - y'_o) - \frac{k\pi}{a} |x' - x'_o|} - e^{j \frac{k\pi}{a} (y' + y'_o + a) - \frac{k\pi}{a} |x' - x'_o|}}{k\pi} \right]
\end{aligned}$$

Use the summation formula

$$\sum_{n=1}^{\infty} \frac{e^{jn x}}{n} = -\ell n(1 - e^{jx})$$

This sums to

$$\frac{1}{2\pi} \operatorname{Re} \left\{ -\ell n \left[1 - e^{j \frac{\pi}{a} (y' - y'_o) - \frac{\pi}{a} |x' - x'_o|} \right] + \ell n \left[1 + e^{j \frac{\pi}{a} (y' + y'_o) - \frac{\pi}{a} |x' - x'_o|} \right] \right\} \tag{D-5}$$

Taking the limit as $x'_o \rightarrow 0$, $y'_o \rightarrow 0$ and then the limit as $x' \rightarrow 0$, $y' \rightarrow 0$ gives for this term

$$\frac{1}{2\pi} \operatorname{Re} [-\ell n(1 - 1 - j \frac{\pi}{a} y' + \frac{\pi}{a} |x'|) + \ell n 2] = \frac{-\operatorname{Re}}{2\pi} [\ell n(\operatorname{re}^{j\alpha}) + \ell n 2] = -\frac{1}{2\pi} \ell n \left(\frac{\pi r}{2a} \right) \tag{D-6}$$

Also

$$\lim_{r \rightarrow 0, r_0 \rightarrow 0} \frac{N_0(k_0 |\bar{r} - \bar{r}_0|)}{4} = \lim_{r \rightarrow 0} \frac{1}{2\pi} \ell n \frac{\gamma' k_0 r}{2} \quad (D-7)$$

where

$$\gamma' = 1.781$$

The result is

$$G_i(0|0) = \sum_{k=1}^{\infty} \sin^2 \frac{k\pi}{2} \left(\frac{1}{\gamma_k a} - \frac{1}{k\pi} \right) + \sum_{k=1}^{\infty} \sum_{m=1}^{\infty} \frac{R_{km}}{\gamma_k a} \sin \frac{k\pi}{2} \sin \frac{m\pi}{2} e^{-(\gamma_k + \gamma_m)d} + \frac{1}{2\pi} \ell n \left(\frac{\gamma' k_0 a}{\pi} \right) \quad (D-8)$$

Similar derivations for the remaining operations give

$$e^{\pm jD} G_i(0|0) = e^{\pm jD_0} G_i(0|0) = \frac{1}{jk_0 a} \sum_{k=1}^{\infty} \sum_{m=1}^{\infty} R_{km} \sin \frac{m\pi}{2} \sin \frac{k\pi}{2} e^{-(\gamma_k + \gamma_m)d} \quad (D-9)$$

$$\begin{aligned} e^{jD} e^{-jD_0} G_i(0|0) &= e^{-jD} e^{jD_0} G_i(0|0) = - \sum_{k=1}^{\infty} \sin^2 \frac{k\pi}{2} \left(\frac{1}{\gamma_k a} - \frac{1}{k\pi} \right) - \sum_{k=1}^{\infty} \frac{(-1)^k}{k_0^2} \left[\frac{(k\pi)^2}{\gamma_k a^3} - \frac{k\pi}{a^2} - \frac{k_0^2}{2k\pi} \right] \\ &+ \frac{\pi}{4a^2 k_0^2} - \frac{1}{2\pi} \ell n \left(\frac{\gamma' k_0 a}{2\pi} \right) - \frac{1}{k_0^2} \sum_{k=1}^{\infty} \sum_{m=1}^{\infty} \frac{R_{km}}{\gamma_k a} \left(\gamma_k \gamma_m \sin \frac{k\pi}{2} \sin \frac{m\pi}{2} \right. \\ &\left. + \frac{k\pi}{a} \frac{m\pi}{a} \cos \frac{k\pi}{2} \cos \frac{m\pi}{2} \right) e^{-(\gamma_k + \gamma_m)d} \end{aligned} \quad (D-10)$$

$$\begin{aligned} e^{jD} e^{jD_0} G_i(0|0) &= e^{-jD} e^{-jD_0} G_i(0|0) = \sum_{k=1}^{\infty} \frac{1}{k_0^2} \left[\frac{(k\pi)^2}{\gamma_k a^3} - \frac{k\pi}{a^2} - \frac{k_0^2}{2k\pi} \right] - \sum_{k=1}^{\infty} \sin^2 \frac{k\pi}{2} \left(\frac{1}{\gamma_k a} - \frac{1}{k\pi} \right) \\ &- \frac{1}{2\pi} \ell n 2 - \frac{1}{k_0^2} \sum_{k=1}^{\infty} \sum_{m=1}^{\infty} \frac{R_{km}}{\gamma_k a} \left(\gamma_k \gamma_m \sin \frac{k\pi}{2} \sin \frac{m\pi}{2} \right. \\ &\left. - \frac{k\pi}{a} \frac{m\pi}{a} \cos \frac{k\pi}{2} \cos \frac{m\pi}{2} \right) e^{-(\gamma_k + \gamma_m)d} - \frac{\pi}{12k_0^2 a^2} \end{aligned} \quad (D-11)$$

APPENDIX E

REFLECTION COEFFICIENT FOR OBSTACLE PARTLY OUTSIDE OF APERTURE

In Chapter III, Section 3.1, the expression for the reflection coefficient was derived for the case of the obstacle inside the waveguide. In this appendix, (3.17) will be shown to be valid even if the obstacle extends partially into the free space region as in Fig. E.1.

E.1 The Integral Equation

The wave equation (3.9)

$$\nabla^2 \bar{E} + k_0^2 \bar{E} = -\bar{J} \quad (\text{E-1})$$

is still valid. The fictitious source current distribution (\bar{J}) now extends into the region $x > 0$. As before, \bar{J} is given by

$$\bar{J} = k_0^2 \chi_e \bar{E} - j\omega\mu_0 \nabla \times \vec{\chi}_m \bar{H}$$

We will consider only cases where the obstacle extends only a small distance outside the aperture. For these cases the assumption is made that inside the obstacle only the z-component of electric field exists and no z-component of magnetic field is present. Thus as in Chapter III, \bar{J} has only a z-component, i. e., $\bar{J} = J \bar{a}_z$. The solution to the wave equation can still be written as

$$\bar{E} = \int \vec{G}(r|r_0) \cdot \bar{J}(r_0) dv_0 + \bar{E}_0 \quad (\text{E-2})$$

where \bar{E}_0 is the field present when the obstacle is absent. The Green's function is the solution to the equation

$$\nabla^2 \vec{G} + k_0^2 \vec{G} = -\frac{1}{b} \vec{I} \delta(x - x_0) \delta(y - y_0) \quad (\text{E-3})$$

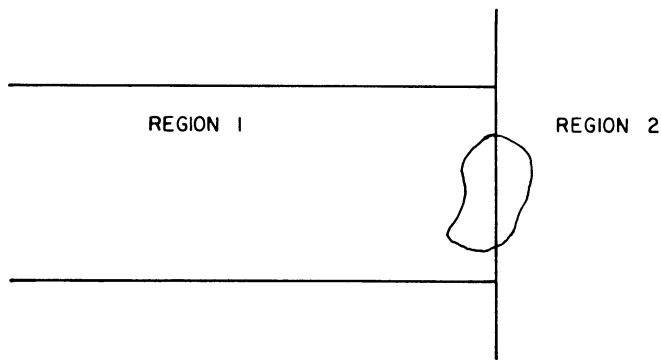
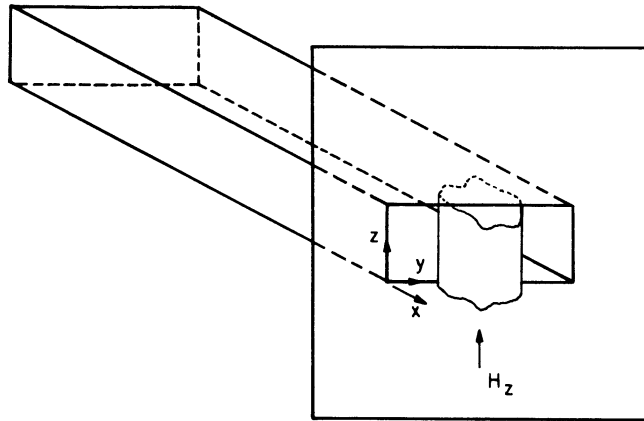


Fig. E. 1. Cylindrical ferrite obstacle in the aperture of a rectangular waveguide.

where \vec{G} has the same boundary conditions as the electric field \vec{E} .

$$\vec{n} \times \vec{G} = 0 \text{ on all metal walls}$$

\vec{G} is continuous at the waveguide aperture.

The components of the Green's function are again electric fields due to a line source of unit strength located at the point (x_0, y_0) , where now (x_0, y_0) can be outside the waveguide. This point is assumed to be close to the aperture for the derivation to follow. Region 1 will refer to the waveguide ($x < 0$), while Region 2 will refer to free space ($x > 0$). The Green's function consists of four different functions corresponding to the following cases:

1. Both source point (r_0) and field point (r) are inside the waveguide. Call this Green's function \vec{G}_{11} . The first subscript on \vec{G} refers to the field point and the second to the source point.

2. The source point (r_o) is in free space, and the field point (r) is in the waveguide. Call this solution \bar{G}_{12} .
3. The source point is in the waveguide and the field point is in free space. Call this solution \bar{G}_{21} .
4. The source point and the field point are both in free space. Call this solution \bar{G}_{22} .

In order to obtain an equation for the reflection coefficient, we evaluate the integral equation (E-2) in the waveguide as x approaches minus infinity. Since the field point for this evaluation is in Region 1, we need only the Green's functions \bar{G}_{11} and \bar{G}_{12} . The total Green's function can be written in terms of the step functions $u(x)$ and $u(x_o)$.

$$\bar{G} = \bar{G}_{11} u(-x_o) u(-x) + \bar{G}_{12} u(x_o) u(-x) + \bar{G}_{21} u(-x_o) u(x) + \bar{G}_{22} u(x_o) u(x) \quad (\text{E-4})$$

Then (E-3) becomes in component form

$$\nabla^2 \bar{G}_{11} + k_o^2 \bar{G}_{11} = -\bar{I} \delta(x - x_o) \delta(y - y_o) \quad (\text{E-5a})$$

$$\nabla^2 \bar{G}_{12} + k_o^2 \bar{G}_{12} = 0 \quad (\text{E-5b})$$

$$\nabla^2 \bar{G}_{21} + k_o^2 \bar{G}_{21} = 0 \quad (\text{E-5c})$$

$$\nabla^2 \bar{G}_{22} + k_o^2 \bar{G}_{22} = -\bar{I} \delta(x - x_o) \delta(y - y_o) \quad (\text{E-5d})$$

Since the components of \bar{G} represent the electric fields, they must satisfy continuity at the aperture. This condition is

$$\bar{G}_{11}(r|r_o) \Big|_{x=0} = \bar{G}_{21}(r|r_o) \Big|_{x=0} \quad (\text{E-6a})$$

$$\bar{G}_{22}(r|r_o) \Big|_{x=0} = \bar{G}_{12}(r|r_o) \Big|_{x=0} \quad (\text{E-6b})$$

As before, we assume for the two dimensional case that only the G_{zz} component of \bar{G} is needed. We can then drop the tensor notation.

G_{11} is given by (3.12),

$$G_{11} = \sum_{n=1}^{\infty} \frac{\sin \frac{n\pi y_o}{a}}{\gamma_n^{ab}} \left[\sin \frac{n\pi y}{a} e^{-\gamma_n |x - x_o|} + \sum_{m=1}^{\infty} R_{nm} \sin \frac{m\pi y}{a} e^{\gamma_n x_o} e^{\gamma_m x} \right] \quad (\text{E-7})$$

This is the electric field inside the waveguide due to a z-directed line source at (x_o, y_o) inside the waveguide. The electric field at the aperture due to this source will be needed and is (E-7) evaluated at $x = 0$.

$$G_{11} \Big|_{x=0} = \sum_{n=1}^{\infty} E_n(z, y) = \sum_{n=1}^{\infty} \frac{\sin \frac{n\pi y_o}{a}}{\gamma_n ab} \left[\sin \frac{n\pi y}{a} e^{\gamma_n x_o} + \sum_{m=1}^{\infty} R_{nm} \sin \frac{m\pi y}{a} e^{\gamma_n x_o} \right] \quad (\text{E-8})$$

From Appendix B, (B-7) and (B-5a) can be used to show that the z-component of electric field in the region $x > 0$ due to an aperture distribution $E_n(\xi, \eta)$ is given by

$$E^{(n)} = -\frac{1}{2\pi} \int_0^a \int_0^b E_n(\xi, \eta) \frac{\partial}{\partial x} \frac{e^{-jk_o r}}{r} d\xi d\eta \quad (\text{E-9})$$

where now,

$$r = [x^2 + (y-\eta)^2 + (z-\xi)^2]^{\frac{1}{2}}$$

Since $G_{21}(r|r_o)$ is the electric field due to a z-directed current element inside the waveguide, and since the aperture field distribution due to this current element is given by (E-8), G_{21} can be written immediately if the field point is in the region near the aperture.

$$G_{21}(r|r_o) = \sum_{n=1}^{\infty} E^{(n)} = -\frac{1}{2\pi} \sum_{n=1}^{\infty} \int_0^a \int_0^b \frac{\sin \frac{n\pi y_o}{a}}{\gamma_n ab} \left[\sin \frac{n\pi \eta}{a} e^{\gamma_n x_o} + \sum_{m=1}^{\infty} R_{nm} \sin \frac{m\pi \eta}{a} e^{\gamma_n x_o} \right] \frac{\partial}{\partial x} \left(\frac{e^{-jk_o r}}{r} \right) d\xi d\eta \quad (\text{E-10a})$$

Using reciprocity (3.13), $G_{12}(r|r_o) = G_{21}(r_o|r)$, we get

$$G_{12}(r|r_o) = -\frac{1}{2\pi} \sum_{n=1}^{\infty} \int_0^a \int_0^b \frac{\sin \frac{n\pi y}{a}}{\gamma_n ab} \left[\sin \frac{n\pi \eta}{a} e^{\gamma_n x} + \sum_{m=1}^{\infty} R_{nm} \sin \frac{m\pi \eta}{a} e^{\gamma_n x} \right] \frac{\partial}{\partial x_o} \left(\frac{e^{-jk_o r_o}}{r_o} \right) d\xi d\eta \quad (\text{E-10b})$$

This equation for G_{12} is valid when the field point (x, y) is anywhere inside the waveguide and when the source point (x_o, y_o) is near the aperture but outside the waveguide.

The evaluation of \vec{G}_{21} in the region away from the aperture is not required to obtain the reflection coefficient. Also \vec{G}_{22} , the electric field in free space due to a line source in free space in the z-direction, is not required for the evaluation of the reflection coefficient and will not be computed.

E.2 The Reflection Coefficient

As in Chapter III, Section 3.1.4, the reflection coefficient is found by assuming the form of \vec{E} in the integral equation (E-2) and taking the limit as the point of observation in the waveguide becomes very far from the obstacle, i. e., as $x \rightarrow -\infty$.

Using (3.15) and (3.16) for \vec{E} and \vec{E}_0 , we obtain,

$$\vec{E}_{x \rightarrow -\infty} = \sin \frac{\pi}{a} y \left(e^{-\gamma_1 x} + R_1 e^{+\gamma_1 x} \right) \quad (\text{E-14a})$$

$$\vec{E}_0_{x \rightarrow -\infty} = \sin \frac{\pi}{a} y \left(e^{-\gamma_1 x} + R_{11} e^{+\gamma_1 x} \right) \quad (\text{E-14b})$$

and, in the region $x < 0$

$$\int \vec{G}(r|r_0) \cdot \vec{J}(r_0) dv_0 = \int [\vec{G}_{11}(r|r_0) \cdot \vec{J}(r_0) u(-x_0) u(-x) + \vec{G}_{12}(r|r_0) \cdot \vec{J}(r_0) u(x_0) u(-x)] dv_0 \quad (\text{E-15})$$

Evaluating (E-15) as x approaches minus infinity gives,

$$\begin{aligned} \int \vec{G}(r|r_0) \cdot \vec{J}(r_0) dv_0 \Big|_{x \rightarrow -\infty} &= \int \left[\frac{\sin \frac{\pi y}{a} \sin \frac{\pi y_0}{a} e^{\gamma_1(x-x_0)}}{\gamma_1 ab} \right. \\ &+ \left. \sum_{n=1}^{\infty} \frac{R_{n1}}{\gamma_n ab} \sin \frac{\pi y}{a} \sin \frac{n\pi y_0}{a} e^{\gamma_n x_0} e^{\gamma_1 x} \right] \bar{a}_z \cdot \vec{J}(r_0) u(-x_0) u(-x) dv_0 \\ &+ \int \left\{ -\frac{1}{2\pi} \int_0^a \int_0^b \left[\frac{\sin \frac{\pi y}{a} \sin \frac{\pi \eta}{a} e^{\gamma_1 x}}{\gamma_1 ab} \right. \right. \\ &+ \left. \left. \sum_{m=1}^{\infty} \frac{R_{1m}}{\gamma_1 ab} \sin \frac{m\pi \eta}{a} e^{\gamma_1 x} \right] \frac{\partial}{\partial x_0} \left(\frac{e^{-jk_0 r_0}}{r_0} \right) d\xi d\eta \right\} \bar{a}_z \cdot \vec{J}(r_0) u(x_0) u(-x) dv_0 \quad (\text{E-16}) \end{aligned}$$

Using (3.15) evaluated at $x = 0$ for $E_n(\xi, \eta)$ in (E-9) gives the electric field outside the waveguide in the absence of the ferrite obstacle. The result is

$$\mathbf{E}_o(\mathbf{r}) = \frac{-1}{2\pi} \int_0^a \int_0^b \left[\sin \frac{\pi\eta}{a} + \sum_{n=1}^{\infty} R_{1n} \sin \frac{n\pi\eta}{a} \right] \frac{\partial}{\partial \mathbf{x}} \frac{e^{-jk_o r}}{r} d\xi d\eta$$

Using this equation and (3.14) in (E-16) then gives,

$$\begin{aligned} & \frac{\sin \frac{\pi y}{a} e^{\gamma_1 x}}{\gamma_1 ab} \int \bar{\mathbf{E}}_o(\mathbf{r}_o) u(-\mathbf{x}_o) u(-\mathbf{x}) \cdot \bar{\mathbf{J}}(\mathbf{r}_o) d\mathbf{v}_o + \frac{\sin \frac{\pi y}{a} e^{\gamma_1 x}}{\gamma_1 ab} \int \bar{\mathbf{E}}_o(\mathbf{r}_o) u(\mathbf{x}_o) u(-\mathbf{x}) \cdot \bar{\mathbf{J}}(\mathbf{r}_o) d\mathbf{v}_o \\ & = \frac{\sin \frac{\pi y}{a} e^{\gamma_1 x}}{\gamma_1 ab} \int \bar{\mathbf{E}}_o(\mathbf{r}_o) \cdot \bar{\mathbf{J}}(\mathbf{r}_o) d\mathbf{v}_o \end{aligned} \quad (\text{E-17})$$

Combining (E-14a), (E-14b) and (E-17) in the integral equation (E-2) gives the desired solution for the reflection coefficient.

$$R_1 = R_{11} + \frac{1}{\gamma_1 ab} \int \bar{\mathbf{E}}_o(\mathbf{r}_o) \cdot \bar{\mathbf{J}}(\mathbf{r}_o) d\mathbf{v}_o \quad (\text{E-18})$$

Thus (3.17) has been shown to be applicable even when the obstacle extends outside the waveguide. The construction of the variational expression (3.28) then follows exactly as in Chapter III with the same result. In addition, if the ferrite cylinder is circular and has its center inside the waveguide, the evaluation of the variational expression and the application of stationarity leads again to (3.59). Thus, even for the case of the cylinder actually in the aperture the analysis of Chapter III remains correct. This is true, at least within the approximations made concerning no z-dependent fields.

APPENDIX F

PLASMA CYLINDER - FERRITE CYLINDER DUALITY*

In Chapter II an analysis was made of the scattering of a plane wave by an infinitely long ferrite cylinder. The dual of this problem is the plasma cylinder with plane wave incidence as shown in Fig. F. 1. The plasma has a tensor permittivity of the form

$$\vec{\epsilon} = \begin{bmatrix} \epsilon_1 & -j\epsilon_2 & 0 \\ j\epsilon_2 & \epsilon_1 & 0 \\ 0 & 0 & \epsilon_3 \end{bmatrix} \quad (\text{F-1})$$

when magnetized in the z-direction. The components are given by

$$\epsilon_1 = 1 + \frac{\left(\frac{\omega_m}{\omega}\right)^2}{\left(\frac{\omega_0}{\omega}\right)^2 - 1} \quad (\text{F-2a})$$

$$\epsilon_2 = \frac{\left(\frac{\omega_m}{\omega}\right)^2 \frac{\omega_0}{\omega}}{\left(\frac{\omega_0}{\omega}\right)^2 - 1} \quad (\text{F-2b})$$

where

$$\omega_m = \left(\frac{Ne^2}{m\epsilon_0}\right)^{\frac{1}{2}}, \quad \text{plasma frequency}$$

$$\omega_0 = \frac{\mu_0 eH}{m}$$

$$N = \text{electron density}$$

$$e = \text{electron charge}$$

* A similar discussion of this duality was published by the author. ³⁴

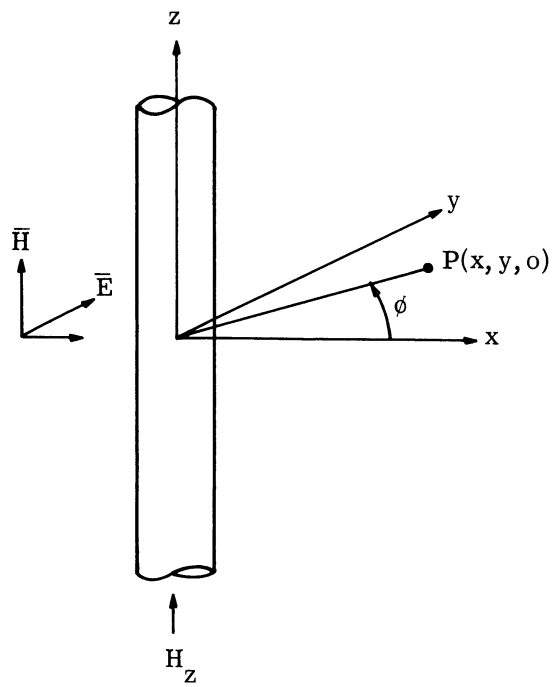


Fig. F. 1. A plane wave incident on an infinitely long, magnetized, plasma cylinder.

m = electron mass

H = applied magnetic field

Curves comparing the field and frequency dependence of the plasma permittivity and the ferrite permeability are shown in Fig. F. 2.

For the plasma, Maxwell's equations are (assuming $e^{+j\omega t}$ time dependence)

$$\nabla \times \vec{E} = - \frac{\partial \vec{B}}{\partial t} = -j\omega \mu_0 \vec{H} \quad (\text{F-3a})$$

$$\nabla \times \vec{H} = \frac{\partial \vec{D}}{\partial t} = j\omega \epsilon_0 \vec{\epsilon} \vec{E} \quad (\text{F-3b})$$

$$\nabla \cdot \vec{D} = 0 \quad (\text{F-3c})$$

$$\nabla \cdot \vec{B} = 0 \quad (\text{F-3d})$$

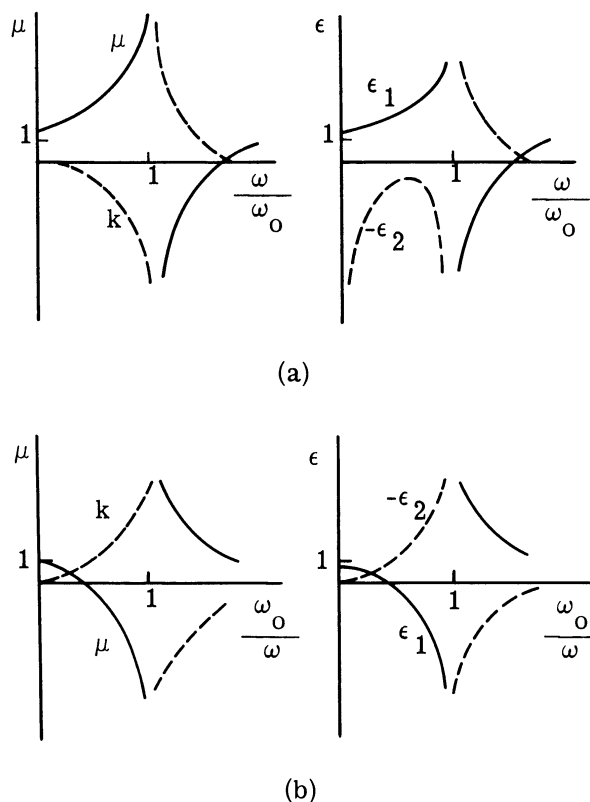


Fig. F. 2. Typical ferrite permeability and plasma permittivity curves. (a) Variations with increasing frequency. (b) Variations with increasing static field.

From (F-3b)

$$\vec{E} = \frac{1}{j\omega\epsilon_0} [\vec{\epsilon}]^{-1} \nabla \times \vec{H} \quad (\text{F-4})$$

where

$$[\vec{\epsilon}]^{-1} = \frac{1}{\epsilon_1^2 - \epsilon_2^2} \begin{bmatrix} \epsilon_1 & j\epsilon_2 & 0 \\ -j\epsilon_2 & \epsilon_1 & 0 \\ 0 & 0 & \frac{\epsilon_1^2 - \epsilon_2^2}{\epsilon_3} \end{bmatrix}$$

Since $\vec{H} = H_z \vec{a}_z$, we then obtain

$$\vec{E} = \frac{1}{j\omega\epsilon_0 (\epsilon_1^2 - \epsilon_2^2)} \begin{bmatrix} -j\epsilon_2 & \epsilon_1 \\ -\epsilon_1 & -j\epsilon_2 \end{bmatrix} \nabla H_z \quad (\text{F-5})$$

or, in rectangular coordinates

$$\mathbf{E}_x = \frac{1}{j\omega\epsilon_0(\epsilon_1^2 - \epsilon_2^2)} \left[\epsilon_1 \frac{\partial H_z}{\partial y} - j\epsilon_2 \frac{\partial H_z}{\partial x} \right] \quad (\text{F-6a})$$

$$\mathbf{E}_y = \frac{1}{j\omega\epsilon_0(\epsilon_1^2 - \epsilon_2^2)} \left[-j\epsilon_2 \frac{\partial H_z}{\partial y} - \epsilon_1 \frac{\partial H_z}{\partial x} \right] \quad (\text{F-6b})$$

From (F-3a)

$$\frac{\partial E_y}{\partial x} - \frac{\partial E_x}{\partial y} = -j\omega\mu_0 H_z \quad (\text{F-7})$$

In this equation, substitute (F-6) to obtain the wave equation for the plasma.

$$\nabla^2 H_z + k_3^2 H_z = 0 \quad (\text{F-8})$$

where

$$k_3^2 = \omega^2 \mu_0 \epsilon_0 \left(\frac{\epsilon_1^2 - \epsilon_2^2}{\epsilon_1} \right)$$

The boundary conditions are continuity of the tangential components of \vec{E} and \vec{H} .

Comparison of the wave equation (F-8), and equation (F-5) and the boundary conditions for the plasma problem with the similar equations in Chapter II for the ferrite cylinder reveals the following duality. The plasma solution can be obtained from the ferrite solution by replacing E_z with H_z , H_r with $-E_r$, H_ϕ with $-E_\phi$ and $\vec{\mu}$ with $\vec{\epsilon}$.

Since the components of the permittivity tensor and the ferrite permeability tensor are similar, we can then expect the plasma column to produce beam shifting also. A proposed design is shown in Fig. F.3. A plasma column is placed in the aperture of a rectangular waveguide, parallel to the broad wall. This structure is not the exact dual of the ferrite scanning antenna, since the incident fields (TE₁₀ mode) are no longer constant but vary over the cylinder axis coordinate. It might still be expected that this structure

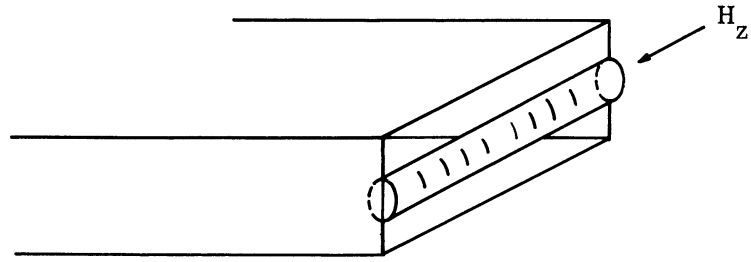


Fig. F.3. Plasma cylinder in the aperture of a rectangular waveguide.

will produce scanning, however.

A plasma scanning antenna could have several advantages over the ferrite antenna. Instead of varying the magnetic field, we can vary the electron density by a changing applied voltage. Faster scanning rates would probably be obtained by this method.

Samaddar³⁵ discussed the scattering of plane waves by an infinite gyrotropic cylinder. Both tensor permeability and permittivity were included. In his analysis of the results for the plasma case (i. e. , the case considered in this section) he mentioned the possibility of electronic scanning using the asymmetries in the far field phase angle. The only real addition this appendix makes to his report (which was entirely theoretical) is to suggest a practical model for achieving the scanning. However, this model was motivated by the duality with the ferrite cylinder derived here and the extensive experiments performed on the ferrite antenna proving its feasibility.

REFERENCES

1. H. E. J. B. du Bois, "On Magnetization in Strong Fields at Different Temperatures," Phil. Mag., Vol. 29, 1890, p. 293.
2. D. Polder, "On the Theory of Ferromagnetic Resonance," Phil. Mag., Vol. 40, 1949, pp. 99-115.
3. H. Shnitkin, "Survey of Electronically Scanned Antennas," Microwave J., Vol. 3, December 1960, pp. 67-72. Vol. 4, January 1961, pp. 57-64.
4. D. J. Angelakos, M. M. Korman, "Radiation from Ferrite Filled Apertures," Proc. IRE, Vol. 44, October 1956, pp. 1463-1468.
5. G. Tyras, G. Held, "Radiation from a Rectangular Waveguide Filled with Ferrite," IRE Trans. on Microwave Theory and Techniques, Vol. MTT-6, July 1958, pp. 268-277.
6. M. S. Wheeler, "Nonmechanical Beam Steering by Scattering from Ferrites," IRE Trans. on Microwave Theory and Techniques, Vol. MTT-6, January 1958, pp. 38-42.
7. R. S. Engelbrecht, U. S. Patent 3, 007, 165, October 31, 1961.
8. L. Lewin, Advanced Theory of Waveguides, Illife and Sons, Ltd., London, 1951.
9. P. S. Epstein, A. D. Berk, "Ferrite Post in a Rectangular Waveguide," J. Appl. Phys., Vol. 27, November 1956, pp. 1328-1335.
10. V. V. Nikol'skii, "A Transverse Ferrite Rod in a Rectangular Waveguide," Radio Eng. and Electronics, Vol. 3, No. 6, 1958, pp. 142-145.
11. W. Hauser, "On the Theory of Anisotropic Obstacles in Waveguides," Quart. J. Mech. and Appl. Math., Vol. 11, November 1958, pp. 427-437.
12. H. N. Chait, T. R. Curry, "Y Circulator," J. Appl. Phys., Supplement to Vol. 30, April 1959, pp. 152S-153S.
13. B. A. Auld, "The Synthesis of Symmetrical Waveguide Circulators," IRE Trans. on Microwave Theory and Techniques, Vol. MTT-7, April 1959, pp. 238-247.
14. H. Bosma, "On Stripline Y-Circulation at UHF," IEEE Trans. on Microwave Theory and Techniques, Vol. MTT-12, January 1964, pp. 61-72.
15. V. V. Nikol'skii, "The Simplest Case of Diffraction of a Plane Wave on a Gyrotropic Cylinder," Radio Eng. and Electronics, Vol. 3, No. 6, 1958, pp. 41-46.
16. W. H. Eggimann, "Scattering of a Plane on a Ferrite Cylinder at Normal Incidence," IRE Trans. on Microwave Theory and Techniques, Vol. MTT-8, July 1960, pp. 440-445.
17. J. A. Stratton, Electromagnetic Theory, McGraw-Hill Book Co., Inc., New York, New York, 1941.
18. W. K. H. Panofsky, M. Phillips, Classical Electricity and Magnetism, Addison-Wesley Publishing Co., Inc., Reading, Massachusetts, 1955.
19. J. C. Palais, "Radiation from a Ferrite Cylinder," J. Appl. Phys., Vol. 35, Part 2, March 1964, pp. 779-781.

REFERENCES (Cont.)

20. J. B. Davies, "An Analysis of the M-Port Symmetrical H-Plane Waveguide Junction with Central Ferrite Post," IRE Trans. on Microwave Theory and Techniques, Vol. MTT-10, November 1962, pp. 596-603.
21. J. Schwinger, "The Mathematical Analyses of Waveguide Discontinuities," (Unpublished notes).
22. R. E. Collin, Field Theory of Guided Waves, McGraw-Hill Book Co., Inc., New York, New York, 1960.
23. R. F. Harrington, A. T. Villeneuve, "Reciprocity Relationship for Gyrotropic Media," IRE Trans. on Microwave Theory and Techniques, Vol. 6, July 1958, pp. 308-310.
24. P. M. Morse, H. Feshbach, Methods of Theoretical Physics, Vol. 1, McGraw-Hill Book Co., Inc., New York, New York, 1953.
25. R. F. Soohoo, Theory and Application of Ferrites, Prentice Hall, Inc., Englewood Cliffs, New Jersey, 1960.
26. B. Lax, K. J. Button, Microwave Ferrites and Ferrimagnetics, McGraw-Hill Book Co., Inc., New York, New York, 1962.
27. N. G. Ponomarev, "Radiation Pattern of Sweeping-Beam Antennas," Radio Eng. and Electronic Phys., No. 6, June 1962, pp. 892-904.
28. J. Brown, J. Clark, "A Unique Solid-State Diplexer," IRE Trans. on Microwave Theory and Techniques, Vol. MTT-10, July 1962, p. 298.
29. L. Kint, E. Schanda, "A Microwave Quadruplexer," IEEE Trans. on Microwave Theory and Techniques, Vol. MTT-11, January 1963, pp. 90-92.
30. M. I. Skolnik, D. D. King, "Self-Phasing Array Antennas," IEEE Trans. on Antennas and Propagation, Vol. AP-12, March 1964, pp. 142-149.
31. G. I. Rado, Phys. Rev., Vol. 89, 1953, p. 529.
32. R. C. LeCraw, E. G. Spencer, "Tensor Permeabilities of Ferrites Below Magnetic Saturation," IRE National Convention Record, Part 5, 1956, pp. 66-74.
33. G. R. Jones, "Calculated Magnetic Fields in Ferrite Rods, Discs, and Slabs," DOFL Proj. 50350, TR-574, April 1958.
34. J. C. Palais, "Scattering From A Gyrotropic Cylinder," IEEE Trans. on Antennas and Propagation, Vol. AP-11, July 1963, p. 505.
35. S. N. Samaddar, "Scattering of Plane Waves from an Infinitely Long Cylinder of Anisotropic Materials at Oblique Incidence with an Application to an Electronic Scanning Antenna," Appl. Sci. Research, Vol. 10, Sec. B, 1963, pp. 385-411.

DISTRIBUTION LIST

- 1-2 Commanding Officer, U. S. Army Electronics Command, U. S. Army Electronics Laboratories, Fort Monmouth, New Jersey, Attn: Senior Scientist, Electronic Warfare Division.
- 3 Commanding General, U. S. Army Electronic Proving Ground, Fort Huachuca, Arizona, Attn: Director, Electronic Warfare Department
- 4 Commanding General, U. S. Army Materiel Command, Bldg. T-7, Washington 25, D. C. , Attn: AMCRD-DE-E-R
- 5 Commanding Officer, Signal Corps Electronics Research Unit, 9560th USASRU P. O. Box 205, Mountain View, California
- 6 U. S. Atomic Energy Commission, 1901 Constitution Avenue, N. W. , Washington 25, D. C. , Attn: Chief Librarian
- 7 Director, Central Intelligence Agency, 2430 E Street, N. W. , Washington 25, D. C. , Attn: OCD
- 8 U. S. Army Research Liaison Officer, MIT-Lincoln Laboratory, Lexington 73, Massachusetts
- 9 Commander, Air Force Systems Command, Andrews Air Force Base, Washington 25, D. C. , Attn: SCSE
- 10 Headquarters, USAF, Washington 25, D. C. , Attn: AFRDR
- 11 Commander, Aeronautical Systems Division, Wright-Patterson Air Force Base, Ohio, Attn: ASRNCC-1
- 12 Commander, Aeronautical Systems Division, Wright-Patterson Air Force Base, Ohio, Attn: ASAPRD
- 13 Commander, Aeronautical Systems Division, Wright-Patterson Air Force Base, Ohio, Attn: ASRN-CS
- 14 Commander, Aeronautical Systems Division, Wright-Patterson Air Force Base, Ohio, Attn: ASNP
- 15 Commander, Electronic Systems Division, L. G. Hanscom Field, Bedford, Massachusetts
- 16 Commander, Rome Air Development Center, Griffiss Air Force Base, New York, Attn: RAYLD
- 17 Commander, Air Proving Ground Center, Attn: ADJ/Technical Report Branch, Eglin Air Force Base, Florida
- 18 Chief of Naval Operations, EW Systems Branch, OP-35, Department of the Navy, Washington 25, D. C.

DISTRIBUTION LIST (Cont.)

Copy No.

- 19 Chief, Bureau of Ships, Code 691C, Department of the Navy, Washington 25, D. C.
- 20 Commander, Bu Naval Weapons Code RRRE-20, Department of the Navy, Washington 25, D. C.
- 21 Commander, Naval Ordnance Test Station, Inyokern, China Lake, California, Attn: Test Director - Code 30
- 22 Commander, Naval Air Missile Test Center, Point Mugu, California
- 23 Director, Naval Research Laboratory, Countermeasures Branch, Code 5430, Washington 25, D. C.
- 24 Director, Naval Research Laboratory, Washington 25, D. C., Attn: Code 2021, Washington 25, D. C.
- 25 Director, Air University Library, Maxwell Air Force Base, Alabama, Attn: CR-4987
- 26 Commanding Officer-Director, U. S. Navy Electronic Laboratory, San Diego 52, California
- 27 Commanding Officer, U. S. Naval Ordnance Laboratory, Silver Spring 19, Maryland
- 28-30 Chief, U. S. Army Security Agency, Arlington Hall Station, Arlington 12, Virginia, 22212 Attn:
2 Copies - IADEV
1 Copy - EW Div. IATOP
- 31 President, U. S. Army Defense Board, Headquarters, Fort Bliss, Texas
- 32 President, U. S. Army Airborne and Electronics Board, Fort Bragg, North Carolina
- 33 U. S. Army Anti-aircraft Artillery and Guided Missile School, Fort Bliss, Texas, Attn: ORL
- 34 Commander, USAF Security Service, San Antonio, Texas, Attn: CLR
- 35 Chief of Naval Research, Department of the Navy, Washington 25, D. C., Attn: Code 427
- 36 Commanding Officer, 52d U. S. Army Security Agency, Special Operations Command, Fort Huachuca, Arizona
- 37 President, U. S. Army Security Agency Board, Arlington Hall Station, Arlington 12, Virginia
- 38 The Research Analysis Corporation, McLean, Virginia, 22101 Attn: Document Control Officer
- 39-48 Headquarters, Defense Documentation Center, Cameron Station, Alexandria, Virginia

DISTRIBUTION LIST (Cont.)

Copy No.

49 Commanding Officer, U. S. Army Electronics Research and Development Laboratory, Fort Monmouth, New Jersey, Attn: U. S. Marine Corps Liaison Office, Code: SIGRA/SL-LNR

50 Director, Fort Monmouth Office, Communications-Electronics Combat Developments Agency, Building 410, Fort Monmouth, New Jersey

51-57 Commanding Officer, U. S. Army Electronics Command, U. S. Army Electronics Laboratories, Fort Monmouth, New Jersey, Attn:

1 Copy - Director of Research
1 Copy - Technical Documents Center - ADT/E
1 Copy - Chief, Special Devices Branch, Electronic Warfare Division
1 Copy - Chief, Advanced Techniques Branch, Electronic Warfare Division
1 Copy - Chief, Jamming and Deception Branch, Electronic Warfare Division
1 Copy - File Unit No. 2, Mail and Records, Electronic Warfare Division
1 Copy - Chief, Vulnerability Br., Electromagnetic Environment Division

58-59 Commanding Officer, U. S. Army Signal Missile Support Agency, White Sands, Missile Range, New Mexico, Attn: SIGWS-MEW and SIGWS-FC

60 Commanding Officer, U. S. Naval Air Development Center, Johnsville, Pennsylvania, Attn: Naval Air Development Center Library

61 Headquarters, Aeronautical Systems Division, Attn: ASRNCC-10, Wright-Patterson Air Force Base, Ohio

62 U. S. A. F. Project Rand, The Rand Corporation, 1700 Main Street, Santa Monica, California

63 Stanford Electronic Laboratories, Stanford University, Stanford, California

64 Director, National Security Agency, Fort George G. Meade, Maryland, Attn: RADE-1

65 Bureau of Naval Weapons Representative, Lockheed Missiles and Space Company, P. O. Box 504, Sunnyvale, California

66 Dr. B. F. Barton, Director, Cooley Electronics Laboratory, The University of Michigan, Ann Arbor, Michigan

67-77 Cooley Electronics Laboratory, The University of Michigan, Ann Arbor, Michigan

Above distribution is effected by Electronic Warfare Division, Surveillance Department, USAEL, Evans Area, Belmar, New Jersey. For further information contact Mr. I. O. Myers, Senior Scientist, Telephone 59-61252.

UNIVERSITY OF MICHIGAN



3 9015 03695 2219